To the Graduate Council:

I am submitting herewith a thesis written by Anne Robinson-Silber entitled "Long-Term Thermal Aging of Resistance Temperature Detectors." I have examined the final copy of this thesis for form and content and recommend that it be accepted in partial fulfillment of the requirements for the degree of Master of Science, with a major in Nuclear Engineering.

Belle R Upadhyaya

Belle R. Upadhyaya, Major Professor

We have read this thesis
and recommend its acceptance:

E. M. Katz

L. F. Miller

Accepted for the Council:

Associate Vice Chancellor and
Dean of The Graduate School

LONG-TERM THERMAL AGING OF RESISTANCE TEMPERATURE

A Thesis
Presented for the
Degree
Master of Science
The University of Tennessee, Knoxville

Anne E. Silber
May 1999

ABSTRACT

This thesis describes research concerning the characteristics of long-term aging of resistance temperature detectors and the development of life estimation techniques performed at The University of Tennessee. The objectives included the study of long-term thermal aging of resistance temperature detectors (RTDs) and the study of changes in several RTD parameters throughout the aging and degradation process. The study of long-term aging of thin-film design and wire wound element construction RTDs was performed at elevated and constant temperatures and with thermal cycling at elevated temperatures. A single manufacturer provided all of the RTDs used in this study. Variations in calibration parameters (α, δ and Ro from the Callendar-Van Dusen Equation), loop resistance, insulation resistance, sheath to lead voltage, compensating loop resistance, open circuit voltage, self-heating index, drift rates and life prediction of RTDs were periodically and continuously monitored. Relationships among these parameters were identified and established.

The RTD aging facility used was designed and constructed to include four high-temperature furnaces. These furnaces were used to carry out several RTD tests. All the RTD measurements were performed automatically using a data acquisition system with an expanded capability to acquire resistance measurements from up to eighty RTDs.

One of the tasks during this phase of the project was to establish the maximum temperatures at which the RTDs completely fail (either in the fail open mode or by indication of a non-physical behavior). These temperatures are in the range 600-700 °C for thin film RTDs and 800-900 °C for wire wound RTDs. Thermal cycling at elevated

temperatures indicated a stronger drift rate in resistance and a faster failure of RTDs. As the aging progressed, a strong correlation between the calibration parameter α (of the Callendar-Van Dusen equation) and the self-heating index (SHI) was also observed. This was further confirmed by an excellent linear fit between the two parameters with a small least-squares error variance. As the aging progressed, the drift rates changed with the temperature, and the resistance drift changed its rate of change to a negative value. The life prediction of RTDs was continued until the resistance value reached preset alarm and failure levels.

The possible correlation between the calibration parameter α and the self-heating index, when fully established may be used for on-line calibration verification of RTDs. This intelligence can be built into the transmitter for periodic and non-intrusive monitoring of industrial platinum resistance thermometers.

ACKNOWLEDGMENTS

I want to thank my committee members, Dr. E.M. Katz, Dr. L.F. Miller and committee chair/advisor Dr. B. R. Upadhyaya, Dr. H.L. Dodds, Head of the Nuclear Engineering Department at the University of Tennessee, for their comments and direction during this research project. I want to recognize Mr. Bob Shepard, Dr. Tom Kerlin and Mr. Paulo Ferreira of The University of Tennessee and Mr. R. M. Carroll of Oak Ridge National Laboratory for their invaluable guidance and suggestions during the course of the project. I would also like to recognize the industrial sponsor for the financial support and oversight of this project. In addition acknowledgement is due to Analysis and Measurement Services Corp., Knoxville, TN, for their assistance with RTD testing and calibration.

Many Thanks to Ralph Demeglio, Wesley Hooper and Scott Snowden for their assistance with manually shaving ice for the calibration baths throughout the two years of this project - Scott Snowden additional thanks for a great friendship throughout our engineering education. My husband Brian for the endless Friday nights I had to cancel plans and work, thanks for always understanding and helping - your support meant a lot. Finally my Lord and Savior Jesus Christ.

TABLE OF CONTENTS

Chapter **Page**

ABSTRACT ii

ACKNOWLEDGMENTS iv

1. INTRODUCTION 1

1.1 Background and Purpose of Research and Development 1

1.2 Summary of Technical Approach and General Features 2

1.3 Summary of Significant Results 3

2. RESISTANCE TEMPERATURE DETECTORS (RTDs) 5

2.1 Electrical Resistivity of Metals 5

2.2 Description of Typical Resistance Temperature Detectors 10

2.3 Common Causes of RTD Failure 14

3. RTD THERMAL AGING LABORATORY 19

3.1 General Test Laboratory Design 19

3.2 Description of Laboratory and Data Acquisition Equipment 19

3.2.1 Laboratory Equipment 21

3.2.2 Additional Calibration Equipment 28

3.2.3 Data Acquisition Equipment 29

3.3 Description of the Data Acquisition Program 32

3.4 Vibration Test System 34

4. TEST PROCEDURES FOR RESISTANCE TEMPERATURE DETECTORS

.....41

4.1 RTD Calibration Procedure.....41

4.1.1 Procedure for the 0°C temperature calibration.....42

4.1.2 Procedure for the 100°C temperature calibration.....43

4.1.3 Procedure for the 145°C temperature calibration.....44

4.1.4 Procedure for the 300°C temperature calibration.....46

4.1.5 Procedure for the 660°C temperature calibration.....47

4.2 Measurement of RTD Performance Parameters.....49

4.3 General RTD Thermal Aging Test Procedure.....52

4.4 Verification of Triple-Point Resistance of SPRTs.....55

5. CALIBRATION OF RESISTANCE TEMPERATURE DETECTORS AND UNCERTAINTY ANALYSIS.....57

5.1 Introduction.....57

5.2 The Callendar-Van Dusen Equation.....57

5.3 Calculation of Temperature from Resistance Measurement Using the SPRT

.....59

5.4 Determination of RTD Calibration Constants.....61

5.5 RTD Parameter Sensitivities and Calibration Uncertainties.....66

5.6 Uncertainty and Sensitivity Analysis.....66

5.7 RMS Value of the Fractional Error.....69

5.8 Uncertainty and Sensitivity Analysis Results including the RMS Value of the Fractional Error 70

6. DEVELOPMENT OF A SENSOR LIFE PREDICTION METHOD 80

6.1 Introduction 80

6.2 Time-to-Alarm and Time-to-Failure 81

6.3 Dynamic Prediction 83

6.4 Static Prediction 84

6.5 Weighted Least-Squares Method for Model Estimation 86

6.6 Confidence Analysis of Life Prediction 89

6.7 Determination of Relationships Among RTD Parameters by Correlation Analysis 92

6.8 Results of RTD Life Prediction 95

7. SUMMARY OF RTD THERMAL AGING STUDIES 101

7.1 Introduction 101

7.2 Tabular Summary of Ten Experimental Tests 101

7.3 General Comments About Furnace History Plots 102

7.3.1 General Comments About Test #1 104

7.3.2 General Comments About Test #2 104

7.3.3 General Comments About Test #3 105

7.3.4 General Comments About Test #4 105

7.3.5 General Comments About Test #5 106

7.3.6 General Comments About Test #6 106

7.3.7 General Comments About Test #7 107

7.3.8 General Comments About Test #8 108

7.3.9 General Comments About Test #9 109

7.3.10 General Comments About Test #10 110

7.3.11 General Comments About All Tests 110

8. SUMMARY OF DRIFT RATE CALCULATIONS 113

8.1 Introduction 113

8.2 Description of Drift Rate Calculations 113

8.3 Sample Drift Rate Calculation Results 114

8.4 Arrhenius Relationship Results 120

9. SUMMARY OF WEEKLY MONITORING OF RTDS 126

9.1 Introduction 126

9.2 Weekly Calibration Results 126

9.3 Results of Performance Parameter Monitoring 128

10. SELF-HEATING INDEX AND ITS CORRELATION TO RTD CALIBRATION PARAMETER 136

10.1 Introduction 136

10.2 Correlation Coefficient Calculation between Self-Heating Index and Alpha 137

10.3 Linear Fit Between Self-Heating Index and Alpha 138

10.4 Remarks on the Relationship Between Alpha and Self-Heating Index 140

10.5 Further Experimental Investigations 140

10.5.1 Additional Applied Current Values 144

10.5.2 Single Current or Two Current Comparison Measurements 148

10.5.3 In-Situ Measurements 151

11. CONCLUSIONS AND FUTURE WORK 161

11.1 Concluding Remarks 161

11.2 Recommendations for Future Research and Development 162

REFERENCES 164

APPENDICES 168

Appendix A 169

Appendix B 206

Appendix C 242

Appendix D 280

VITA 295

LIST OF FIGURES

2.1 Schematic arrangements of the atoms in one plane of a monovalent metal 6

2.2 Resistance vs. temperature for a platinum wire 7

2.3 Schematic variation of electrical resistivity of a metal with absolute temperature 9

2.4 Typical dimensions of Test RTDs 11

2.5 A 4-wire RTD circuit 13

2.6 A fully-supported, wire wound platinum RTD 15

2.7 Lead wire configurations of various temperature sensors 16

3.1 A schematic of the RTD testing laboratory 20

3.2 Geometry of the high temperature furnace 22

3.3 Alignment of the RTD holes for the first two furnaces 24

3.4 Alignment of the RTD holes for the third furnace 25

3.5 Software system flow diagram 35

3.6 Main program for long-term thermal aging program 36

3.7 Vibration test set up showing the shaker with the mount, vertical furnace and the RTD attachment 37

3.8 Details of RTD and accelerometer clamping devices and attachment to the shaker end nut 39

4.1 Schematic diagram of RTD end and lead wires 50

4.2 Schematic diagram of insulation resistance measurement....50

4.3 Schematic diagram of compensating loop resistance measurement....51

4.4 Schematic diagram of the open circuit voltage measurement....51

4.5 Diagram of the Self-Heating Index Measurement Configuration....52

4.6 Data recorded during triple-point check of SPRT....56

6.1 Definition of various degradation and performance parameters....82

6.2 Regression model diagram....83

6.3 Data window weighting functions used in model development....88

6.4 Upper and lower failure limits based on the uncertainty in slope and intercept..91

6.5 Upper and lower failure limits based on residual standard deviation....93

6.6 Resistance trend and time-to-failure plot for RTD #A-48 from Furnace #3....96

6.7 Resistance trend and time-to-failure plot for RTD #A-35 from Furnace #3....97

6.8 Resistance trend and time-to-failure plot for RTD #A-45 from Furnace #3....99

7.1 Plot of RTDs Exhibiting General Features....103

7.2 Thermal Cycling at 550-750 °C showing RTD Failure....109

8.1 Arrhenius relationship plot for all recorded drift rates.....122

8.2 Arrhenius relationship plot of drift rates for each RTD type and drift level....123

8.3 Thermometer Drift at Various Temperatures Arrhenius Plot.[16]....125

9.1 RTD B-5 Ro Trend....129

9.2 RTD A-74 Ro Trend....129

9.3 RTD B-5 Alpha Trend....130

9.4 RTD A-74 Alpha Trend....130

9.5 RTD B-5 Delta Trend 131

9.6 RTD A-74 Delta Trend 131

9.7 RTD B-5 Self-Heating Index (Ohms/Watt) Trend 134

9.8 RTD B-5 Self-Heating Index (mWatts/C) Trend 134

9.9 RTD A-74 Self-Heating Index (Ohms/Watt) Trend 135

9.10 RTD A-74 Self-Heating Index (mWatts/C) Trend 135

10.1 Self-Heating Index (Ω/W) versus Alpha Plot with Fitted Line for RTD A-74 141

10.2 Self-Heating Index (mW/C) versus Alpha Plot with Fitted Line for RTD A-74 141

10.3 Self-Heating Index (Ω/W) versus Alpha Plot with Fitted Line for RTD B-5 142

10.4 Self-Heating Index (mW/C) versus Alpha Plot with Fitted Line for RTD B-5 142

10.5 Individual Resistance Values Recorded 149

10.6 Bath Temperature Measurements 149

10.7 Plot of the In-situ Self Heating Index Measurements for RTD B-5 154

10.8 Plot of the In-situ Self Heating Index Measurements for RTD B-6 155

10.9 Plot of the In-situ Self Heating Index Measurements for RTD B-11 156

10.10 Plot of the In-situ Self Heating Index Measurements for RTD A-66 157

10.11 Plot of the In-situ Self Heating Index Measurements for RTD A-69 158

LIST OF TABLES

2.1 Summary of RTD Characteristics 12

4.1 Results of SPRT Triple-Point Temperature Resistance Measurements 55

5.1 Values of the coefficients D_0, D_1, . . ., D_9 in Equation (5.5) [7] 60

5.2 Summary of the Pre-test RTD Calibration Results 65

5.3 Averaged Calibration Values for New RTDs 71

5.4 Analysis Results for New RTD Average Values 71

5.5 Post-test Calibration Values for RTD A-1 72

5.6 Post-test Analysis Results for RTD A-1 72

5.7 Post-test Calibration Values for RTD A-2 73

5.8 Post-test Analysis Results for RTD A-2 73

5.9 Post-test Calibration Values for RTD A-3 74

5.10 Post-test Analysis Results for RTD A-3 74

5.11 Post-test Calibration Values for RTD A-4 75

5.12 Post-test Analysis Results for RTD A-4 75

5.13 Post-test Calibration Values for RTD A-5 76

5.14 Post-test Analysis Results for RTD A-5 76

5.15 Post-test Calibration Values for RTD A-6 77

5.16 Post-test Analysis Results for RTD A-6 77

5.17 Post-test Calibration Values for RTD A-7 78

5.18 Post-test Analysis Results for RTD A-7 78

5.19 Post-test Calibration Values for RTD A-8 79

5.20 Post-test Analysis Results for RTD A-8 79

6.1 Summary of RTDs life prediction obtained for RTDs #A-48, #A-35, #A-45 98

7.1 Summary of RTD Thermal Aging Tests 102

8.1 Sample Drift Rate Calculation Values 115

8.2 Summary of Average Drift Rates per Temperature 115

8.3 Summary of Minimal Drift Rates per Temperature and RTD Type 116

8.4 Summary of Increasing Drift Rates per Temperature and RTD Type 117

8.5 Summary of Appreciable Drift Rates per Temperature and RTD Type 118

8.6 Summary of Failure Drift Rates per Temperature and RTD Type 119

8.7 Average Slopes of Arrhenius Relationships for each RTD Type and Drift 124

9.1 RTDs used in Weekly Calibration Tests 127

10.1 Summary of Correlation Coefficient Calculations 139

10.2 Summary of RMS Error Associated with the Linear Fit 143

10.3 Possible RTD Degradations Causing a Relationship Between α and SHI 144

10.4 RTD A-209 Self-Heating Index Measurements and Correlation Coefficients 146

10.5 Summary of Correlation Coefficient Calculations (1 to 5 mA Applied Current) 147

10.6 Summary of RMS Error Associated with the Linear Fit (1 to 5 mA Applied Current) 148

10.7 Paired Resistance Value Comparison 150

10.8 Background Information for In-situ Measurement RTDs.....153

10.9 Self-Heating Index and Correlation Values for RTD B-5 154

10.10 Self-Heating Index and Correlation Values for RTD B-6 155

10.11 Self-Heating Index and Correlation Values for RTD B-11 156

10.12 Self-Heating Index and Correlation Values for RTD A-66 157

10.13 Self-Heating Index and Correlation Values for RTD A-69 158

LIST OF ACRONYMS

DVM Digital Voltmeter

GPIB General Purpose Interface Board

IPRT Industrial Platinum Resistance Thermometer

NIST National Institute of Standards and Technology

RMS Root Mean Square

RTD Resistance Temperature Detector

SHI Self Heating Index

SPRT Standard Platinum Resistance Thermometer

CHAPTER 1

INTRODUCTION

1.1 Background and Purpose of Research and Development

The study of long-term thermal aging of resistance temperature detectors (RTDs) and the characterization of its effect on calibration degradation and other RTD performance parameters were the objectives of this project started in October 1995. Systematic changes in the measured resistance of both thin film type and wire-wound type RTDs were observed. These trends were used for predicting the residual life of RTDs. The scope of the degradation research and development included the aging of RTDs with different aging mechanisms. Additional investigation was carried out to determine if a correlation between the RTD calibration parameters α or δ (from the Callendar-Van Dusen equation), and performance parameters such as the loop resistance, insulation resistance, sheath to lead voltage, compensating loop resistance, open circuit voltage, self-heating index and the resistance drift rate.

In order to establish the long-term thermal aging characteristics of RTDs and correlation among RTD parameters the following tasks were completed during this project.

- Long-term thermal aging of thin film and wire-wound RTDs and the determination of ultimate failure temperatures.
- Thermal aging of thin film and wire-wound RTDs with temperature cycling to determine if this further aggravates degradation.

- Trending of RTD parameters and establishing correlation among calibration parameters and other performance parameters.
- Life prediction of RTDs and root cause analysis of RTD degradation.

Several parameters, that indicate the degradation of RTDs including Callendar-Van Dusen equation parameters α, δ, and ice-point resistance (R_0), self-heating index (SHI), dissipation constant, insulation resistance, and sheath-to-lead voltage were monitored. The results obtained indicate a relationship (high correlation) between α and SHI. If this is true for all operating situations, then the SHI may be used as a parameter reflecting the validity of the RTD calibration. The results of RTD aging in this study and the development of simple but robust calibration trending and life prediction methods have demonstrated the potential feasibility of this technology for RTD monitoring, using externally measured parameters. The degree of degradation depends on individual RTDs and the length of continuous heat soak. The results are based on aggravated thermal aging at temperatures ranging between 400°C and 1000 °C and temperature cycling experiments with average temperatures of 500 °C and above with ±100 °C variation. The current system is capable of testing up to 80 RTDs simultaneously.

1.2 Summary of Technical Approach and General Features

The research and development project is a combined experimental and analytical approach for establishing the thermal aging characteristics of RTDs. The previous work in this area is limited, and the current combined project is probably the largest of its kind.

- Simultaneous aging of more than eighty RTDs and continuous data acquisition from four high-temperatures (up to 1,200 °C) tubular furnaces.
- Thermal aging studies on thin film and wire-wound RTDs at different furnace temperatures. These include temperature cycling with high mean temperatures.
- An automated data acquisition system for continuous measurement of four-wire RTD element resistance.
- Periodic calibration of RTDs and the measurement of performance parameters such as loop resistance, compensating loop resistance, open circuit voltage, sheath to lead voltage, self-heating index, dissipation constant, insulation resistance and drift rates.
- Development of correlation between the calibration parameter α (Callendar-Van Dusen equation) and the self-heating index.
- Life prediction of RTDs using the trends in the measured resistance.

1.3 Summary of Significant Results

The project at The University of Tennessee is unique in terms of its scope and usefulness of the project results to industry. The RTD testing laboratory is one of the best facilities available for testing industrial platinum resistance thermometers (IPRTs). The following is a summary of important results achieved through December 1997.

- Expansion of the RTD aging and testing laboratory to include four high-temperature furnace and the capability for continuous data acquisition from up to 80 RTDs.

- Life prediction of both thin film and wire-wound RTDs using the trends in the measured resistance. Consistent estimates of time-to-alarm and time-to-failure could be estimated with confidence levels for these parameters.
- A strong correlation between the self-heating index (SHI) and the RTD calibration parameter α has been observed. This correlation increases with the RTD aging. The relationship between the two parameters can be characterized by a linear fit with a small RMS error.
- The calibration parameter α decreases and the ice-point temperature increases with thermal aging.
- The RTD resistance drift rate ($\Delta R/\Delta t$) increases with increases in the furnace temperature.
- A theoretical uncertainty and sensitivity analysis of RTD resistance variation was performed as a function of uncertainties in the Callendar-Van Dusen equation.

CHAPTER 2

RESISTANCE TEMPERATURE DETECTORS (RTDs)

2.1 Electrical Resistivity of Metals

In metallic solids the atoms are arranged in a crystal structure with extremely small unit cell sizes. These unit cells are bound together by their outer valence electrons by metallic bonding [1]. The metallic bonds in solid metals make the free movement of the valence electrons possible since they are shared by many atoms and are not bound to any particular atom. The valence electrons at times form an electron charge cloud and at other times they are considered to be individual free electrons not associated with any particular atom (see Figure 2.1). The outer electrons are free to move between the positive-ion cores. At room temperature the positive ion cores have kinetic energy and vibrate about their lattice positions. With increasing temperature these ions vibrate with increasing amplitudes and their continuous interchange of energy between the ion cores and their valence electrons increases. In the presence of an applied electric potential the electrons attain a directed drift velocity which is proportional to the applied field but in the opposite direction. These changes, at the atomic level occurring with temperature changes, translate into changes in measurable properties of metallic solids.

The principle of operation of a resistance temperature detector (RTD) is based on the fact that the resistance of a metal changes with temperature. Figure 2.2 shows the

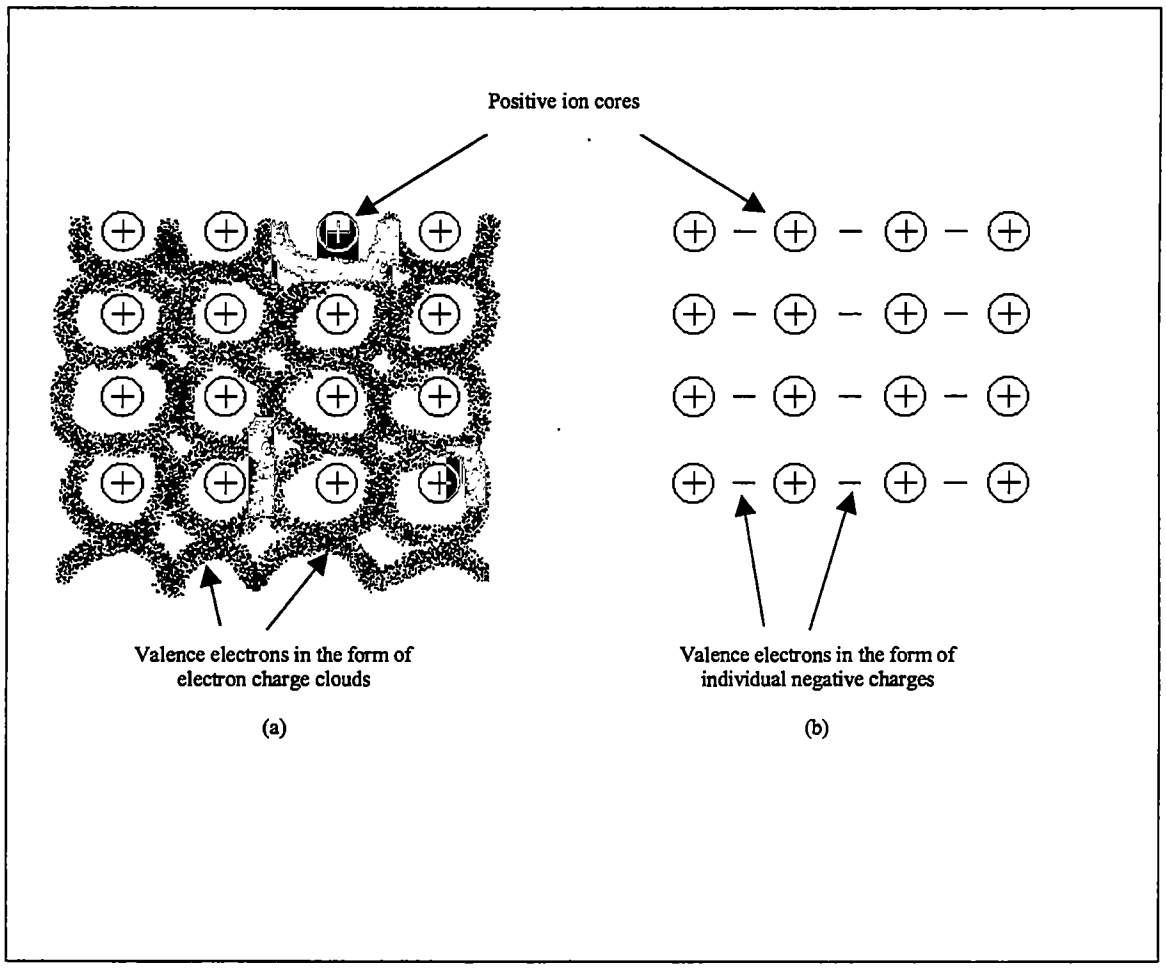


Figure 2.1. Schematic arrangements of the atoms in one plane of a monovalent metal. In (a) the valence electrons are pictured as an "electron gas," and in (b) the valence electrons are visualized as free electrons of unit charge. [1]

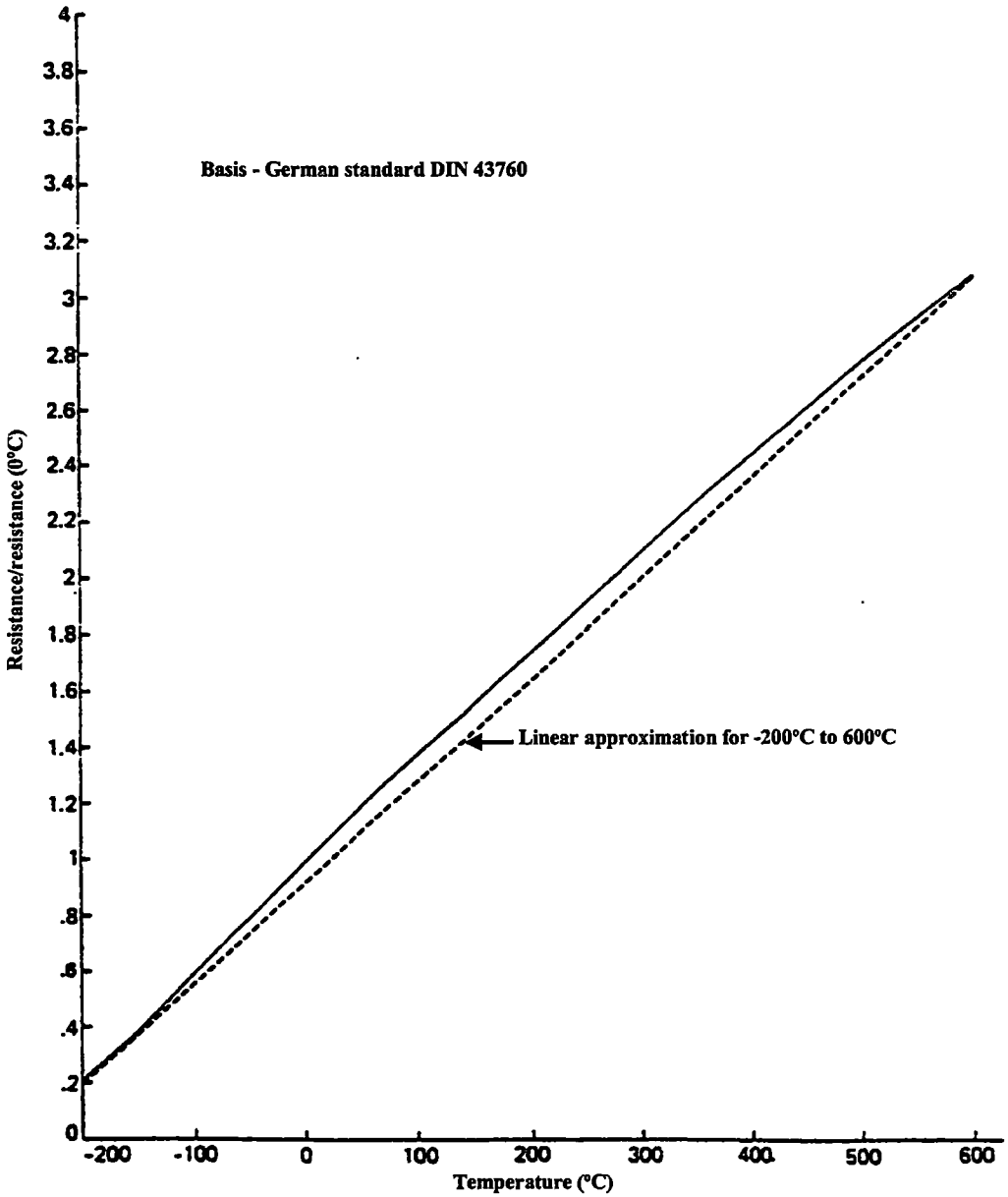


Figure 2.2. Resistance vs. temperature for platinum wire [2].

increase in resistance of a platinum wire as a function of temperature [2]. This resistance-temperature relationship is almost linear for Industrial Platinum Resistance Thermometers (IPRTs). At a given temperature, the resistance is proportional to the length and inversely proportional to the cross-sectional area.

$$R = \rho * \frac{L}{A} \tag{2.1}$$

where

R = Resistance (Ω)

ρ = Resistivity (Ω-cm)

L = Length (cm)

A = Cross-sectional area (cm^2).

The electrical resistivity of a pure metal can be approximated by the sum of two terms: a thermal component and a residual component as shown in Eq.(2.2),

$$\rho_{Total} = \rho_T + \rho_{ref}. \tag{2.2}$$

The thermal component arises from the vibration of the positive ion cores about their equilibrium positions in the metallic crystal lattice. As the temperature is increased, the ion cores vibrate more and more, and a large number of thermally excited elastic waves scatter conduction electrons and decrease the mean free paths and relaxation times between collisions. Thus the resistance to electron motion increases with temperature, and as the temperature is increased, the electrical resistivities of pure metals increase. The residual component of the electrical resistivity of pure metals is small and is caused by structural imperfections such as dislocations, grain boundaries, and impurity atoms

which scatter electrons. The residual component is almost independent of temperature and becomes significant only at low temperatures (see Figure 2.3).

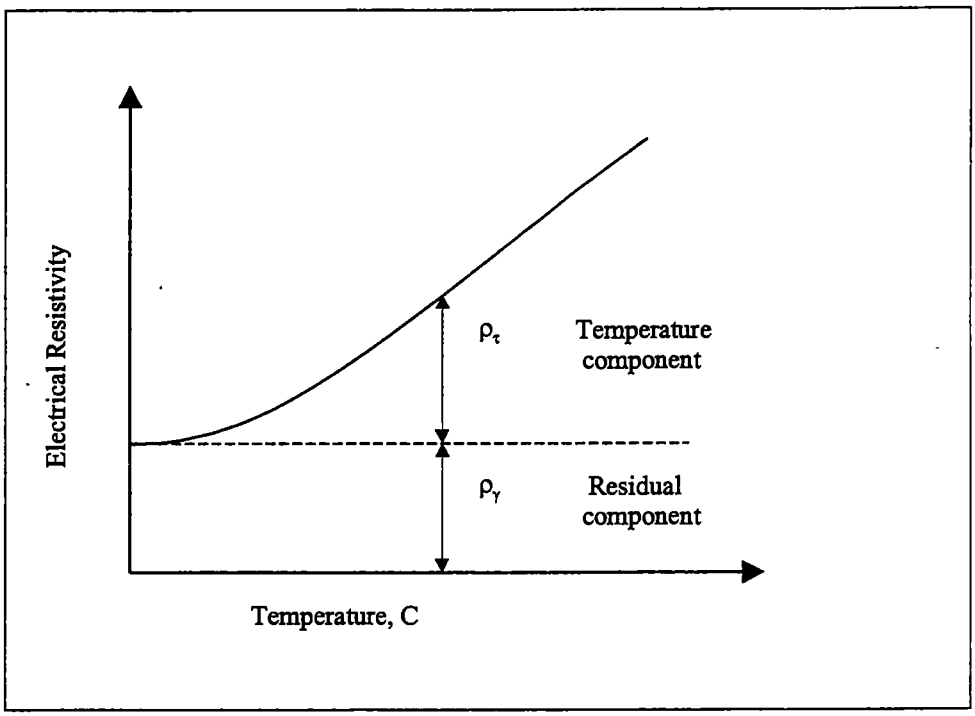


Figure 2.3. Schematic variation of electrical resistivity of a metal with absolute temperature. At higher temperatures the electrical resistivity is the sum of a residual component ρ, and a thermal component ρ_T.

For most metals at temperatures above about -200 °C, the electrical resistivity varies almost linearly with temperature. Thus the electrical resistance of many metals at

temperature T may be approximated by the equation

$$R(T) = R_0 (1 + \alpha T) \tag{2.3}$$

where R_0 = electrical resistance at 0 °C.

α = temperature coefficient of resistance ($^{\circ}C^{-1}$).

T = temperature of metal (°C).

When alloying elements are added to pure metals, they cause additional scattering of the conduction electrons and thus increase the electrical resistivity of pure metals. Thus, the migration of impurities into the platinum element of an RTD with thermal aging will cause increase in the resistance at a given temperature.

2.2 Description of Typical Resistance Temperature Detectors

A typical platinum RTD capsule sensor is shown in Figure 2.4. The RTD used in this study have the dimensions shown in the figure. The RTD material has the following properties [2]:

- high resistivity that permits fabrication of elements of practical dimensions,
- chemical inertness with respect to materials used for structural element, electrical insulation, and sheath and lead-wire materials,
- physical properties that permit strain-free fabrication in the form of wires and thin films,
- a large temperature coefficient of resistance that is large enough to provide easy measurement of resistance changes when temperature changes.

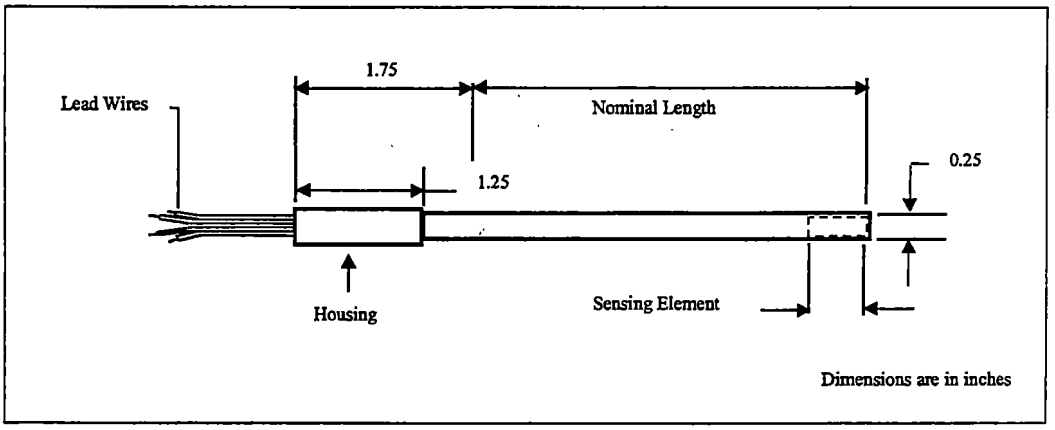


Figure 2.4. Typical Test RTD.

The temperature coefficient of resistance is defined as

$$\alpha = (R_{100} - R_0)/100R_0 \ (^{\circ}C)^{-1} \tag{2.4}$$

where R_{100} = resistance at 100 °C,

R_0 = resistance at 0 °C.

Table 2.1 shows the design specifications of the RTDs used in this study. All of the RTD measurements employed the four-wire configuration that removes the lead-wire effects. This approach also does not require a Wheatstone bridge for resistance measurement as shown in Figure 2.5. In this method, a constant current power source is connected to two of the RTD leads. The voltage drop across the RTD is measured at the other two leads. The voltage drop is independent of lead wire effects [3].

Table 2.1 Summary of RTD Characteristics

RTD Type	Wire-Wound	Thin Film
Average Length	10.75 inches or 270.3 mm	10.75 inches or 270.3 mm
Average Diameter	.25 inch or 6mm	.25 inch or 6mm
Average Weight	62g	55g
Sheath Material	Inconel®	316 SST
Sensing Element	Platinum single-element	Thin film platinum
Lead wire	Teflon-insulated nickel-coated, 22-gauge stranded copper wire	Teflon-insulated nickel-coated, 22-gauge stranded copper wire
Ice Point Resistance	100 Ω	100 Ω
Temperature Range	-200 to 400 °C	-50 to 400 °C
Insulation Resistance	500 * 10^6 Ω measured at 100 Vdc at room temp	100 * 10^6 Ω measured at 100 Vdc at room temp
Response Time Self Heating Index	60 mW to cause 1°C change in water flowing at 3 ft/sec.	25 mW to cause 1°C change in water flowing at 3 ft/sec.

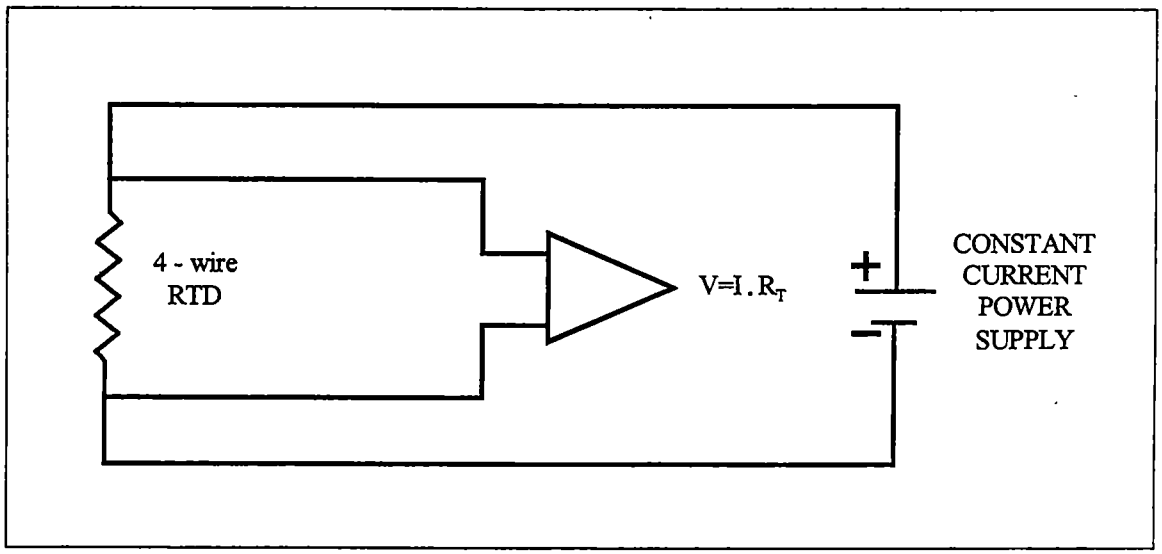


Figure 2.5. A 4-wire RTD circuit [3].

The basic construction of a thin film RTD consists of encapsulating a precision thin-film platinum element in a 316 SST sheath. The platinum element and internal lead wires are firmly secured within the capsule by highly compacted aluminum oxide. The compaction process is accomplished by a unique centrifuge method of manufacturing. The technique provides a homogeneous (voidless) compaction throughout the sensor capsule that assures superior insulation resistance under most vibration environments. For humid environments a moisture-proof seal is provided where the Teflon insulated external lead wires exit the sensor housing [3].

Wire-wound RTDs are constructed with fully supported elements. The platinum wire is wound around an insulating mandrel and encapsulated in a 316 SST sheath. The

construction features are similar to those of thin film RTDs. A typical single-element wire-wound RTD is shown in Figure 2.6. The lead wires are made of Teflon-insulated, nickel-coated, 22-gauge stranded copper wire. Each sensor is subjected to a resistance accuracy test at 0 °C and a rear seal integrity test [3]. The lead seal is capable of withstanding 100% relative humidity. The lead wire configurations of various temperature sensors are shown in Figure 2.7 [3].

2.3 Common Causes of Failure of RTDs

A review of failure modes of resistance temperature detectors (RTDs) was conducted based primarily on the NUREG report [4]. The following causes and effects of RTD failures were identified.

1. Mechanical shock -- any flexing in the interior wire causes work-hardening of the wire and therefore causes an increase in the resistance of the RTD.

2. Vibration -- any flexing in the interior wire causes work-hardening of the wire and therefore causes an increase in the resistance of the RTD.

3. Thermal deformation -- this is caused by the differential expansion of the wire and the substrate. This effect is usually divided into two separate categories of elastic deformation (hysteresis) and plastic deformation (work hardening). These deformations result from the different expansion coefficients of the wire and substrate. An example of how thermal deformation effects an RTD is that the thermal

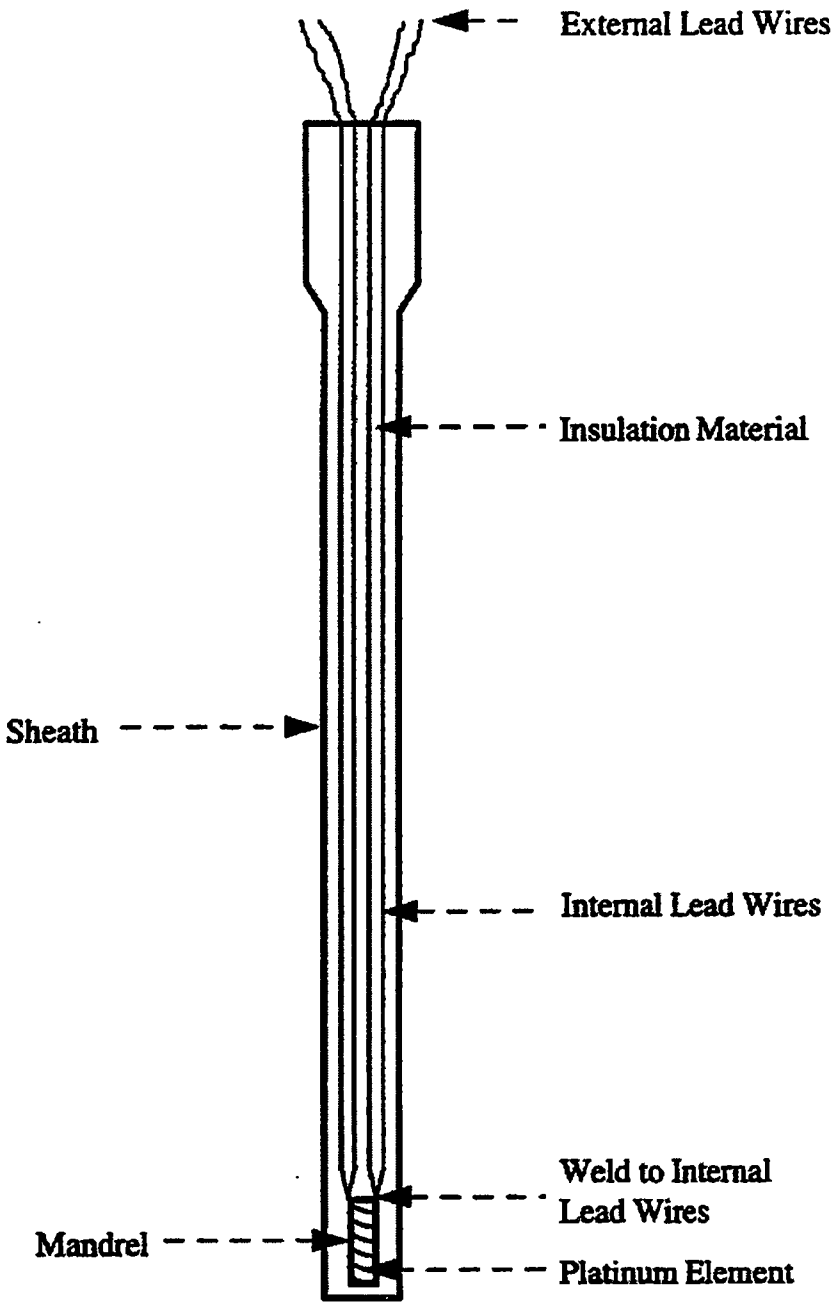


Figure 2.6. A fully-supported, wire-wound platinum RTD.

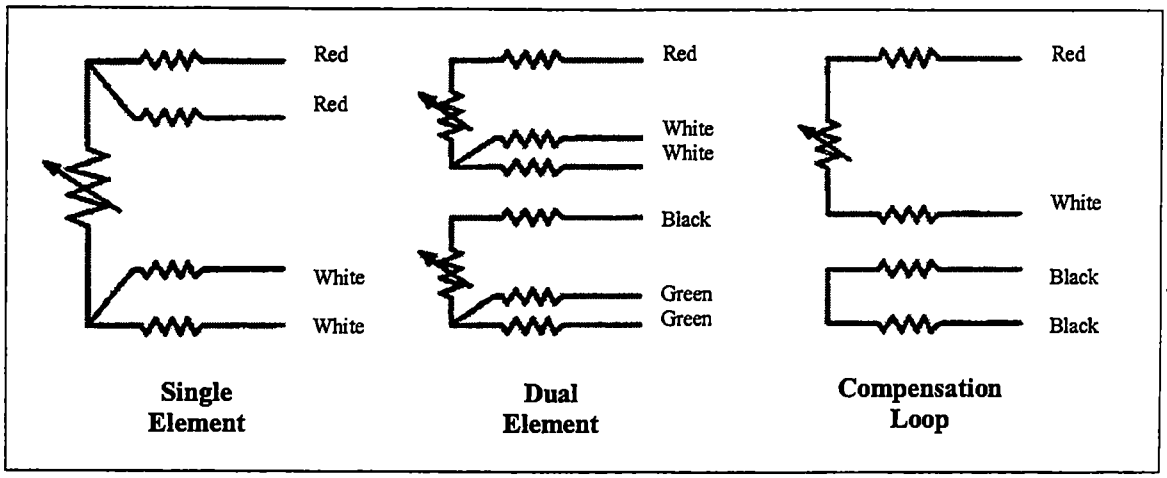


Figure 2.7. Lead wire configurations of various temperature sensors.

effects can cause temporary changes in the wire and it can cause permanent deformation to the crystalline structure.

4. Thermal effects on lead wires -- just as the RTD wire expands so do the lead wires and they are likewise susceptible to the same structural dislocations (in this study this was compensated for by using a four-wire measurement technique).

5. Grain growth -- increase in the material grain size due to prolonged exposure to a high temperature environment. Effect upon resistance is still undefined.

6. Contamination -- in any high temperature environment it is possible to obtain impurities in a metal and in an RTD that can cause an increase/decrease in resistance.

7. Oxidation of the platinum -- due to oxygen in the internal RTD environment oxidation can occur. This reaction would reduce the cross-sectional area of the platinum wire, therefore increasing resistance.

8. Leakage/insulation degradation -- if any decrease occurs in the insulation surrounding the sensing element (either due to high temperature exposure or to moisture at low temperature) then all of the current might not be flowing through the element and then heat could cause error in the resistance measurement (namely a decrease at high temperatures).

Similar to the listing above for RTD failure, there are several factors that cause calibration drifts in industrial platinum resistance thermometers (IPRTs). Some of these factors are [5]

- Annealing of fabrication-produced work hardening
- Production of work hardening by process vibration
- Production of work hardening by thermal cycling
- Thermoelectric effects in internal lead wires
- Increase in grain size by exposure to high temperatures and chemical effects
- Chemical contamination of platinum wire
- Oxidation of platinum wire
- Electrical insulating shunting
- Changes in measuring system alignment.

RTDs used in this study were oxidized to stabilize the capsule's internal atmosphere when subjected to elevated temperature applications. When an oxidized product is subjected to a high temperature application, further oxidation does not occur inside the capsule. As a result, the internal oxygen is not depleted, and the atmosphere does not turn into a reducing environment. Platinum needs oxygen to remain stable. Oxidation during the production process helps to maintain free oxygen in the capsule when the capsule is in the customer's application.

From the above discussion, the lack of oxygen during production of the study RTDs could result in a reducing atmosphere in the sheath during the heat soak. All free oxygen would quickly be combined with free metals until free oxygen no longer exists in the internal atmosphere. This reducing atmosphere could accelerate the contamination of the platinum. The results of The University of Tennessee tests at 660 °C show that the R_o values generally increase and alpha values (Callendar equation) decrease from their respective nominal values for study RTDs. The cause of this behavior might be due to the contamination of the platinum at higher temperatures.

CHAPTER 3

RTD THERMAL AGING LABORATORY

This chapter describes the laboratory for RTD thermal aging experiments and associated tests. First an overview of the laboratory is given, and then the equipment setup and data acquisition software are explained.

3.1 General Test Laboratory Design

There are several components in the laboratory, calibration and data acquisition system. The experimental environments are established using several high temperature, test and calibration furnaces. The data acquisition system consists of an IBM compatible personal computer, an HP3497A data acquisition and control unit, an HP3456A digital multimeter and patch panels. The experimental equipment and their interface configuration are shown in Figure 3.1

3.2 Description of Laboratory and Data Acquisition Equipment

The task of setting up the equipment and the measurement system is very critical and considerable time has been spent in ensuring the high quality of information acquired from the test system. Each component described had several tests completed for it to insure that the measurements recorded were accurate. A brief summary of each verification test is included with each equipment description or functional group description.

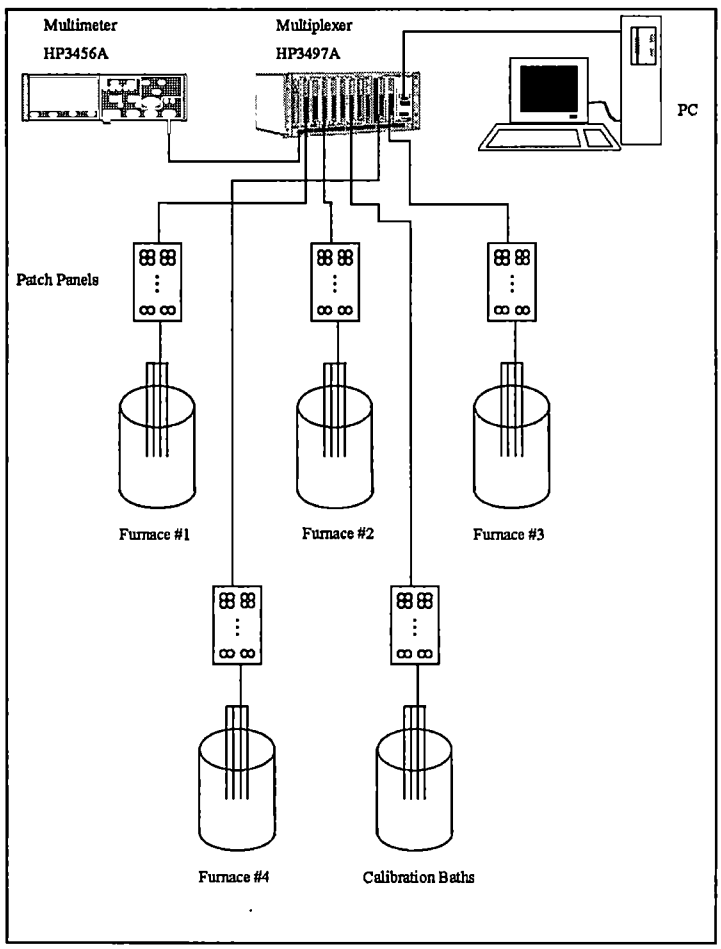


Figure 3.1. A schematic of the RTD testing laboratory.

3.2.1 Laboratory Equipment

High Temperature Furnace: Four tubular furnaces (series 3110) from Applied Test Systems with Barber Coleman series 15 controllers are used for continuous testing of RTDs. Each furnace has a simple one temperature control system, employing a Type S thermocouple side mounted into each furnace, and is rated to a maximum temperature of 1200°C. The control thermocouples in the furnaces are type-S thermocouples, which minimize the effect of controller drift. These thermocouples have a maximum range of 0-1450 °C, with a standard error of 1.5 °C at 660 °C. The tests are carried out ranging from 400°C to 900°C. A drawing of the furnaces is given in Figure 3.2. The furnaces were vertical in orientation with each furnace placed upright on a level platform and the RTDs being inserted from the top. The outer diameter of the furnaces was approximately sixteen inches, and the inner area available for use with an approximate six inch diameter. The interior of the furnaces were filled with first a support cylinder and then a stainless steel equalizing block both with approximate outer diameters of 4 inches. The final piece to each furnace was the top end cap, which inserted two inches into the furnace and sat one inch above the top of the furnace. The RTDs were inserted through the top end cap and into the equalizing block. The RTDs rested on the top end cap with approximately an inch, the RTD end cap, exposed to the room environment. This then left approximately three inches of the RTD in the top end cap, approximately three inches exposed to the internal air environment of the furnace and the final remaining approximate three inches of the RTD, including the sensing element, inserted into the equalizing block. The holes in the equalizing block and the end cap were drilled to match the same pattern. Three

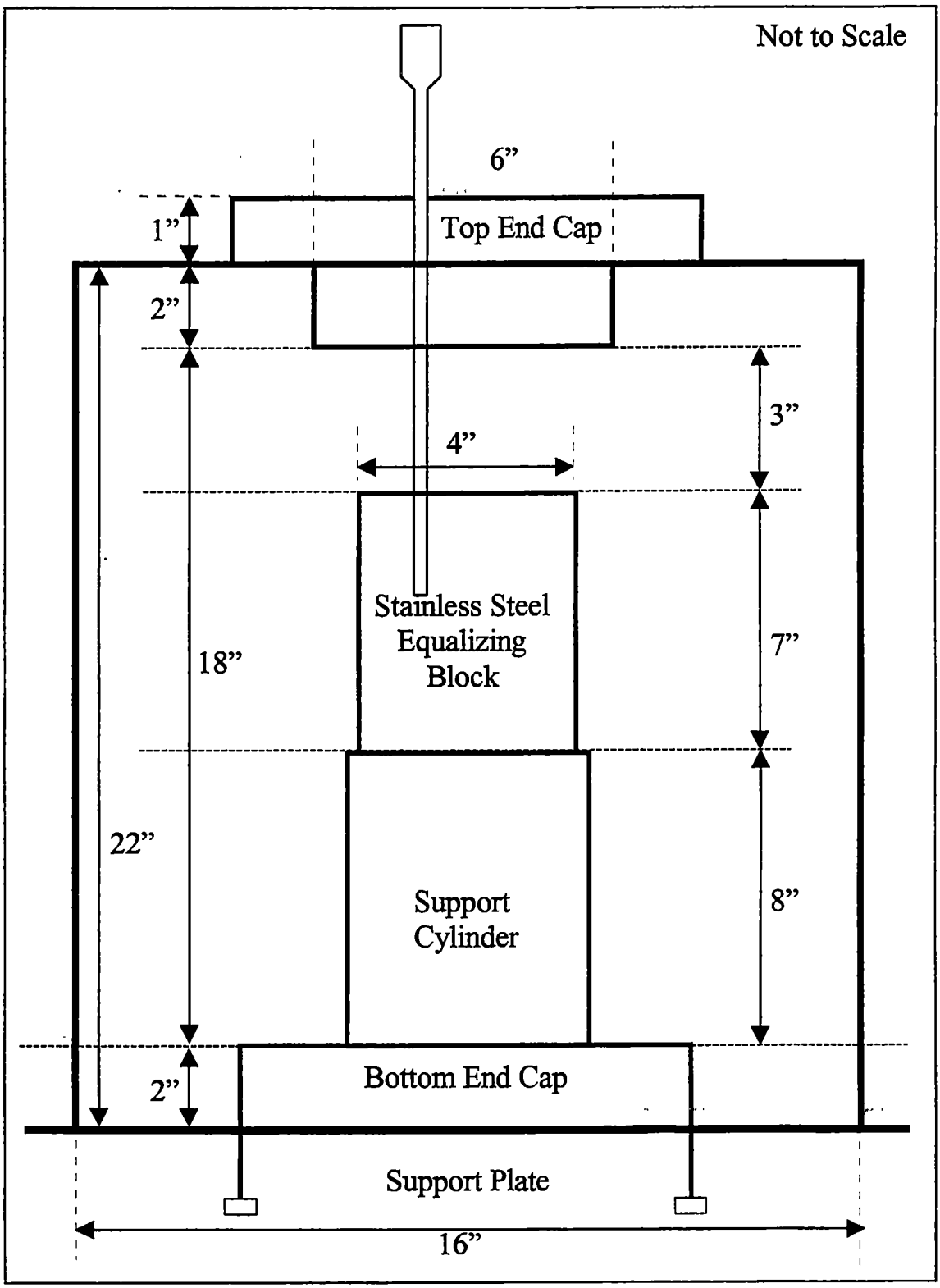


Figure 3.2. Geometry of the high temperature furnaces.

furnaces have 20 RTD holes (Figure 3.3), whereas one furnace has 12 RTD holes (Figure 3.4) thus yielding a total capacity of 72 RTDs for the high temperature ATS furnaces. The furnaces for the temperature ranges they could achieve were considerable compact and well insulated. Throughout the experiments, with additional insulation added around the RTDs after they were fully inserted, very little temperature fluctuation was experienced.

Several tests of the accuracy of the temperatures produced in the high temperature furnaces were performed at the start of each test and at several periods during each test. A calibrated SPRT and an additional Type S thermocouple were both used to test the furnace temperatures. One of the sensor locations was intentionally left open in each of the constant temperature experiments in order to be able to investigate the furnace temperature at any time using either the SPRT or the Type S thermocouple for an independent temperature measurement. Generally the SPRT was used when the furnaces were brought up in temperature so that the calibration of the RTDs could be completed at 300 °C and 400 °C or 660 °C (or the final temperature of the furnace could be reached and verified). Once the SPRT was removed the sheath for the bare wire type S thermocouple was inserted to reduce the temperature fluctuations from the open test position. The type S thermocouple was periodically used to check the furnace temperatures by slowly being inserted in each of the sheaths of the furnaces and the temperature recorded using a distilled ice water bath for ice point compensation and an HP 3456A Multimeter for measuring the voltage.

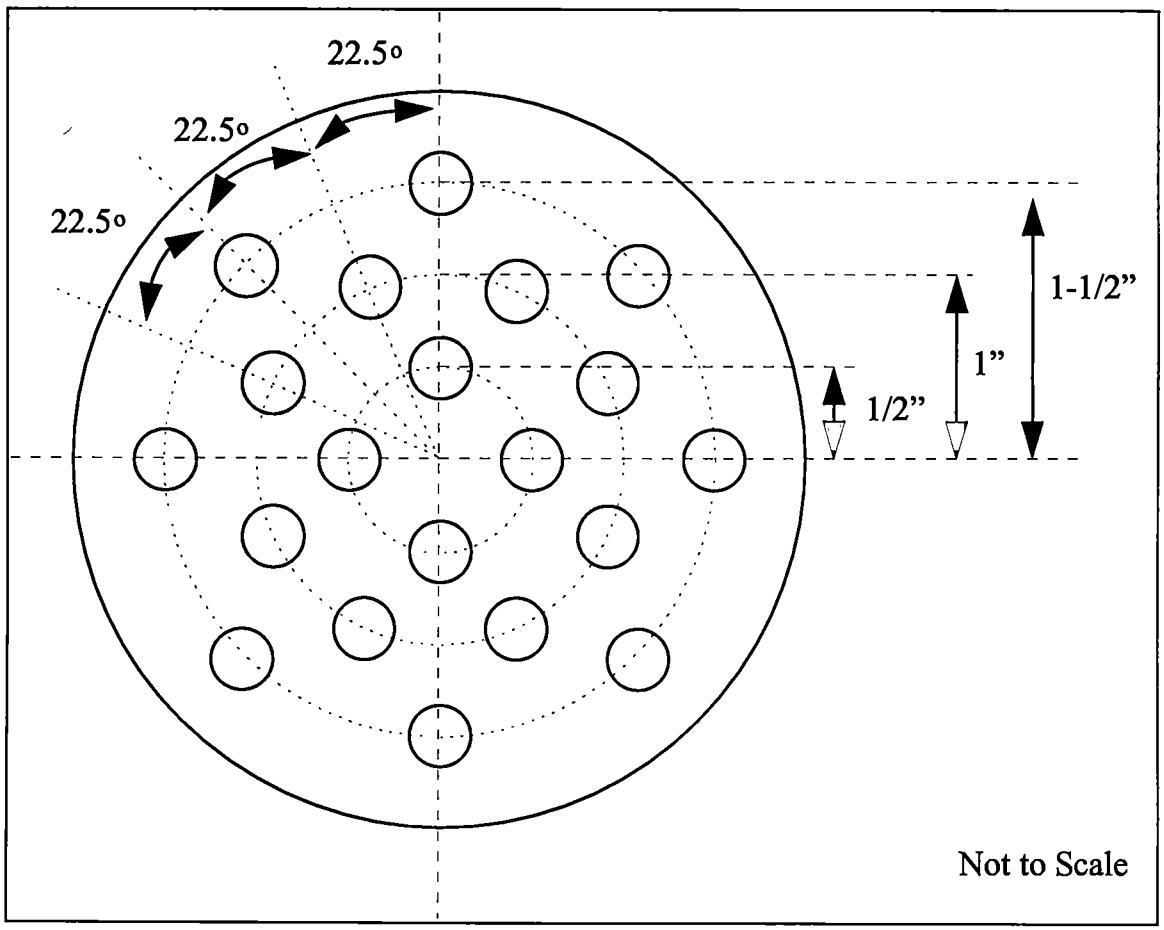


Figure 3.3. Alignment of the RTD holes for the first two furnaces.

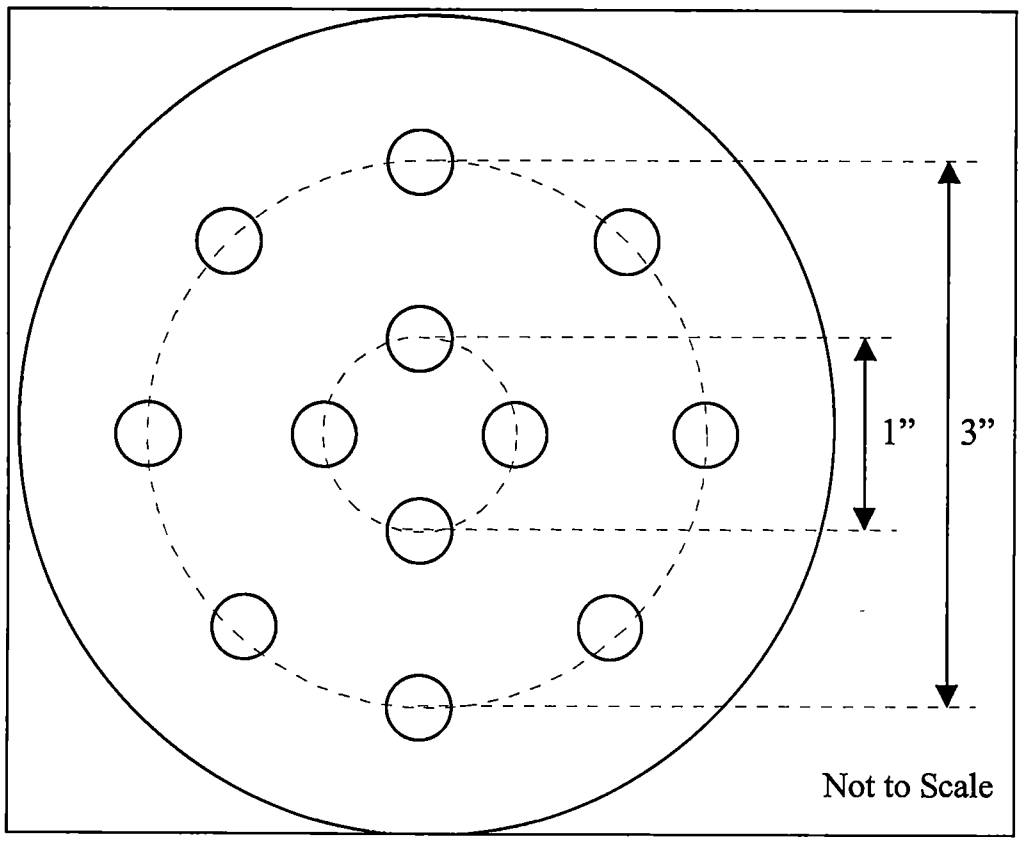


Figure 3.4. Alignment of the RTD holes for the third furnace.

Calibration Baths: The calibration of the RTDs were made at four temperatures: 660 °C or 400 °C, 300 °C or 145 °C, 100 °C and 0 °C. The high temperature furnaces described above were used for the higher temperatures (660 °C, 400 °C and 300 °C) and oil baths are used for the 100 and 145 °C temperatures. The oil calibration baths were performed in two different types of oil baths. The 0 °C calibration point was performed using crushed ice produced from tap water in a Rosemount Temperature Calibration Bath Model 911A2C S/N 409 with Rosemount Temperature Controller. The 100 °C calibration point was performed in a Rosemount Temperature Calibration Bath Model 910AB2 S/N 1393, stirred oil bath with Rosemount Temperature Controller using Dow Corning 200 fluid. The 145 °C calibration point was performed in a NESLAB EXACAL EX-250HT high temperature stirred oil bath with NESLAB EXACAL High Temperature Controller/readout using Dow Corning 210H fluid. A stainless steel equalizing block is used to provide uniform temperature field for all the RTDs in the 145 °C oil bath. The RTD sensing end is inserted up to a depth of 3 inches into the block.

For each of the calibration baths accuracy of the bath temperature was maintained by adequate heat-up or cool-down times and additionally was monitored continuously by the SPRT. The SPRT was used during the calibration to monitor the bath temperatures. The SPRT was inserted in each bath with the RTDs and was monitored by the data acquisition system just like the RTDs. This insured the accurate bath temperature was recorded at the beginning of each set of measurements recorded. The SPRT was always attached as the first sensor to be queried by the measurement system therefore it was easy for the bath

temperature fluctuations during the first 25 SPRT measurements to be monitored. If the fluctuations were too great, the calibration halted before the first data point was recorded. This allowed for tending to the calibration baths if there was a difficulty and eventually determination of approximate stabilization or wait times from sensor entry in the medium to calibration data recording.

Additional Test Furnaces and Baths: Over the course of the study several additional furnaces and baths were used for various additional shorter term tests. The first of these is a tubular furnace that was used at the beginning of the project prior to receipt of the ATS furnaces. That furnace was on loan to the project from Oak Ridge National Laboratories. This furnace was a considerable smaller horizontal tubular furnace. This furnace provided the capability of testing eight RTDs simultaneously at up to 660 °C. The furnace was controlled using a single Type S thermocouple and a controller also provided by Oak Ridge National Laboratories. The only test performed using this furnace was Test #1, which will be described in depth in following chapters. The second of these furnaces was another tubular furnace, this was also a horizontal furnace but the test setup, described later, required it be modified to function as a vertical furnace. This furnace was provided by the Nuclear Engineering Department from a previous project. This furnace was used to a maximum temperature of 400 °C and was controlled by a Type K thermocouple and controller also provided by the University of Tennessee. The furnace was used in only one test, the vibration testing which will be described in following chapters as Test #10. The final additional bath used was a 30 °C stirred water

bath. This bath was used on a weekly basis as the medium in which the majority of the performance parameter readings were taken. This bath is a Rosemount Temperature Calibration Bath Model 911A20, this bath was filled with tap water and the stirrer, heaters, and controller maintained the bath temperature. One additional test was performed using this bath in addition to the regular use it received from the calibration procedures. This test was a very short-term test to verify the sheath to lead voltage readings, it will be briefly described in a later chapter.

3.2.2 Additional Calibration Equipment

There are two additional pieces of equipment that are used during sensor calibration in addition to the laboratory equipment listed above and the data acquisition equipment to be listed in the following section.

Digital Voltmeter/Multimeter: The additional HP 3456A multimeter is used during the calibration of the RTDs to verify that each individual bath has stabilized in temperature. This task is accomplished by temporarily connecting the SPRT to this additional DVM and monitoring the temperature/resistance readings until they appear stable. This multimeter is also used during the performance parameter measurements. The measurements for insulation resistance, sheath-to-lead voltage, loop resistance, compensating loop resistance, open circuit voltage and self heating index are completed using this multimeter. It was also used for all of the in-situ measurements, including self-heating index and thermocouple measurements.

Current Source: A Keithly Model 220 programmable current source was also used during the performance parameter measurements. The current source was used to supply the required mA of current to the individual RTDs for the self-heating index measurements.

3.2.3 Data Acquisition Equipment

Computer: Personal computer with an Intel 80386 processor and 16 Mbytes of RAM. This PC controls all the programmable devices through an internal GPIB interface. It performs the following tasks:

a) Sets the external devices for a given experimental configuration.

b) Controls the multiplexer during calibration and long-term testing.

c) Reads and records RTD resistance values measured by the digital voltmeter.

d) Calculates the standard deviation of recorded measurements.

e) Stores RTDs resistances and standard deviation along with date and time information for retrieval and archiving.

The initial configuration tests on the computer, computer connections and software consisted of testing the ability of the computer program to set the external devices initially from any configuration and then change that configuration with each sensor being tested. There were no additional tests performed on the computer to insure any

additional functionality beyond the configuration and initial full system tests. The initial full system tests consisted of running the system with dummy resistance values attached to ends of the extension wires, which would be attached to the RTDs in actual operation. This testing, for the computer, provided ample opportunity to see the control of the multiplexer and multimeter during calibration and standard testing, reading and recording of resistances, calculation of the standard deviation and the data storage, marking with date and time and retrieval capabilities.

Multiplexer: The primary task of this device (HP3497A) in this experiment is to switch data acquisition channels. The computer software controls the multiplexer unit. The multiplexer is made up of several cards, which are inserted in the back of unit. Each of the cards has a removable connector box where the twisted pair cables are attached. The multiplexer has all of the card slots currently full. The capacity of this unit is increased to its maximum 100 channels. Since two channels are used for a 4-wire Ohm measurement, the system is capable of testing up to 50 RTDs.

Extender: The HP 3498A Data Acquistion Extender functions similarly to the multiplexer. The extender, as its name implies, increases the number of channels that can be monitored. The extender can increase the number of channels up to 100 RTDs. Currently 80 RTDs can be monitored with card slots still available to increase capacity.

Digital Voltmeter/Multimeter: The HP 3456A multimeter reads the multiplexer output, i.e. the RTD resistance for the desired channel at a given time. The computer also controls the multimeter and therefore the computer reads and records the RTD resistance values from the multimeter.

Patch Panel: The patch panel is used to interface test RTDs to the multiplexer through cables. The patch panels were designed to connect the test subjects to the test equipment. The patch panels are simple aluminum boxes approximately 12 inches long by 4 inches wide by 3 inches high. In construction, 40 screw-in connector plug receptacles were inserted in the boxes and soldered to a flat cable connected to a twisted pair cable connector also screwed into the box. The twisted pair connector could then be attached to the twisted pair cables that had been attached to the multiplexer card connector boxes, and the RTDs, through copper extension wires, could be connected to the connector plug receptacles. This completed the flow path for the data connections.

The measurement system as a whole had considerable tests performed as well as on each component to insure the accuracy of the data produced. The continuity of each of the 280 cables connecting the RTDs to the patch panels was individually checked prior to being placed in service. The continuity of each patch panel was checked three times. The first check of the patch panel was that of the patch panel alone and required continuity tests of the extension wire plug-in receptacles to the twisted pair cable connection. The second check of the patch panel included the extension wires that connected to the RTDs and

required a continuity test of the alligator clips at the end of the wires to the twisted pair cable connection. The third test of the patch panel included the twisted pair cables that connect to the multiplexer and extender. The third test required a continuity test of the extension wire plug in receptacles to the twisted pair cable termination points in the multiplexer/extender plug-in boxes. These three tests insured that the connections were correct and unbroken through the path from each of the individual RTD extension wires to the point of final termination inside the multiplexer/extender plug-in boxes. Two calibrated standard resistance boxes were used to check the accuracy of each measurement made by the multimeter through the system. It was during these checks completed on each new multiplexer card that it was discovered that the new cards have an offset caused by several jumpers on the multiplexer/extender cards. These jumpers were removed and the system read and recorded the calibrated standard resistors perfectly. All aspects of the measurement and data acquisition system were tested and verified before the system was placed in service.

3.3 Description of the Data Acquisition Program

A computer program was developed for data acquisition, calibration and long-term testing. The platform used for this program is the commercial software LabVIEW. The program performs all functions of the data acquisition. The program performs the following tasks:

1) Set up of the digital voltmeter and multiplexer for calibration or long-term testing.

2) Control of the multiplexer and switching of channels to perform data acquisition for up to eighty RTDs in the calibration baths and long term testing furnaces. As a part of switching channels a time delay feature was added. Initially there were several spikes in the data from the voltmeter prior to the multiplexer closing the channel to the RTD. The user can set the data acquisition interval at any desired value.

3) Acquisition of the data from the digital voltmeter through the GPIB interface.

4) Computation of statistical parameters such as the mean value and standard deviation from 25 consecutive measurements of the RTDs under test. If the standard deviation is within a threshold limit, the data are recorded into a file. If the standard deviation is outside the threshold limit, the process is repeated for the same RTD and a new set of measurements evaluated. This procedure is repeated for a maximum of 3 measurement sets. The final value is recorded even if the standard deviation is exceeded during the third measurement

5) The mean value and standard deviation are recorded for each RTD measurement. At the end of the measurements in a furnace the date and time are also written to the file. The program then completes any other furnaces indicated to be on line and waits until the time interval elapses again.

Figure 3.5 shows a simplified block diagram of how the program operates. Figure 3.6 shows the main screen of the calibration and long-term testing program.

3.4 Vibration Test System for RTDs

The purpose of this test module is to determine the effects of mechanical vibration on RTD calibration drift. Mechanical shock and vibration can damage the sensing element, insulation packing and other components of an RTD. The combination of temperature and vibration may result in the rearrangement of the insulation material. Previous studies have shown that with a vibration frequency of 20 Hz and amplitude of 3 mm, there was no noticeable drift in RTD calibration at a test temperature of 320 °C [4]. Mechanical vibration may cause more degradation in RTD response time than result in calibration drifts.

The shaker system, shown in Figure 3.7, is used to subject an RTD to vibrations at a specified frequency, acceleration and displacement. The system used in this project is manufactured by Labworks, Inc., Costa Mesa, California. The three major components are: the electrodynamic shaker (Model ET-132-203), the sine servo controller (Model SC-121), and the power amplifier (Model PA-119). The sine servo controller and the power amplifier are housed in a single unit. The electrodynamic shaker may be mounted in a variety of configurations. The shaker includes a mounting base.

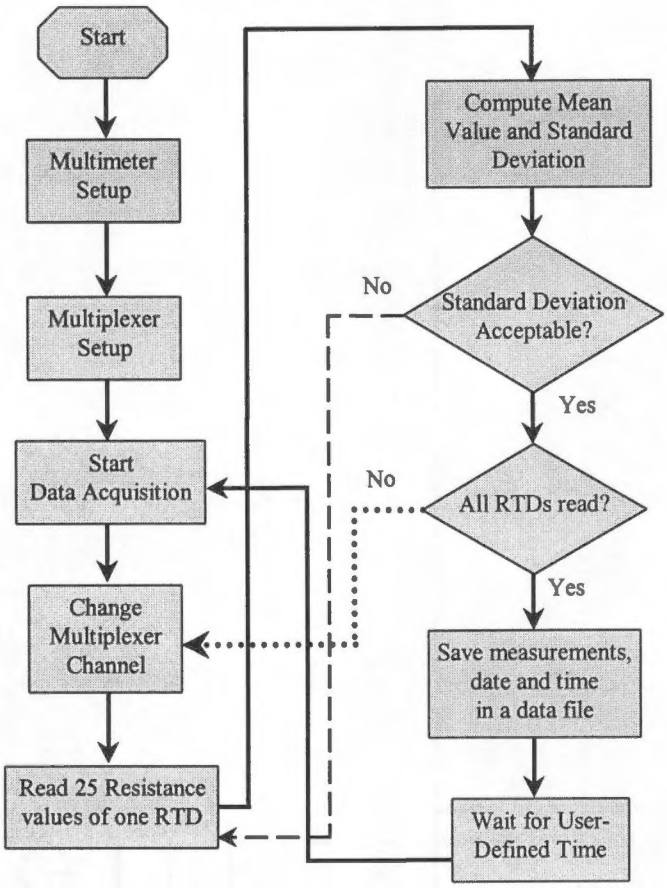


Figure 3.5. Software system flow diagram.

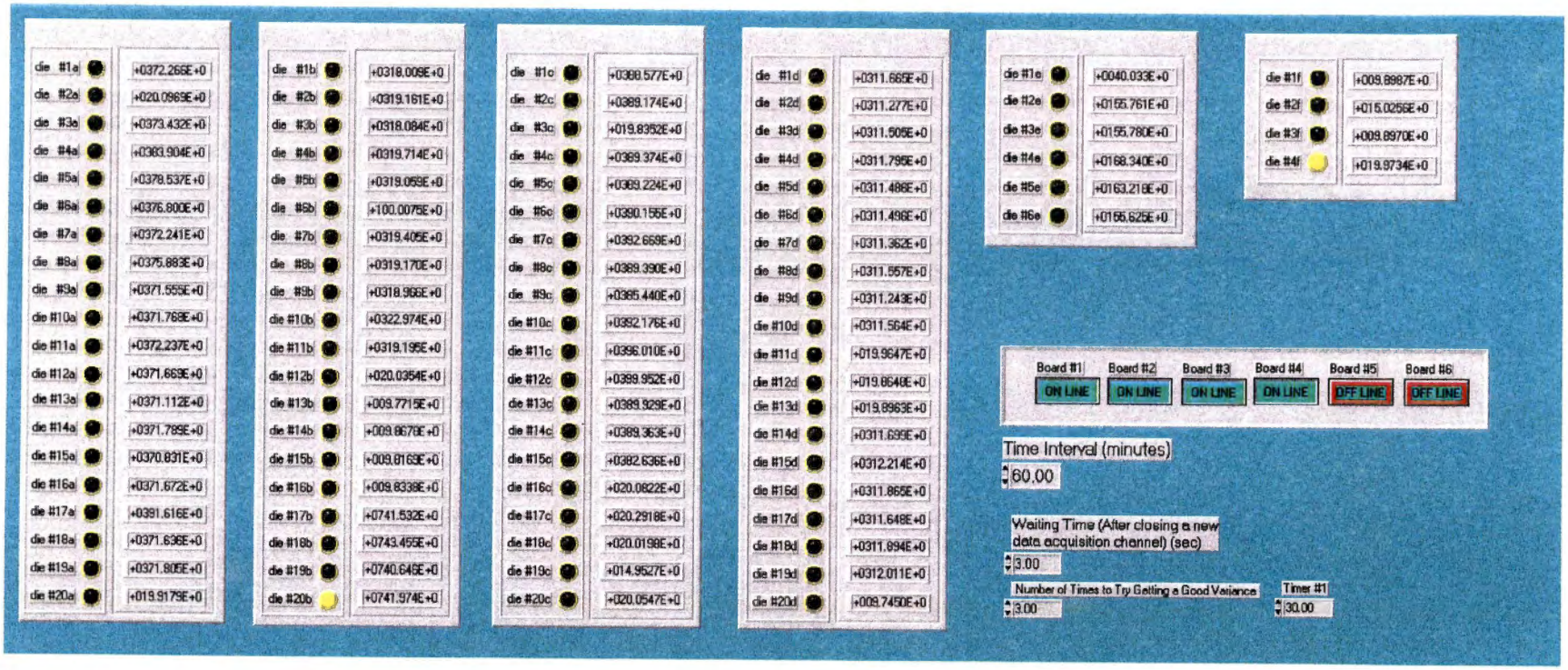


Figure 3.6. Main screen for long-term thermal aging program.



Figure 3.7. Vibration test set up showing the shaker with the mount, vertical furnace and the RTD attachment.

Two components were fabricated in order to use this shaker for the current application. One is a support stand that would allow the shaker to be mounted vertically above a furnace. The support has to be stable against vibration and should isolate the shaker vibration from the furnace and other devices. The second component is a device for securing the RTD to the shaker, along with a feedback accelerometer that supplies the shaker control system with information about the shaker output. This allows for a precise operation of the shaker.

A simple and stable tripod skeleton was fabricated, composed of 2-inch angle irons, welded together, with rubber footpads for vibration isolation. An aluminum mounting plate is bolted to the top of the exoskeleton to provide a solid, yet a light foundation for the shaker. Holes were drilled in the aluminum plate to attach the shaker mounting pad. This allows for a variety of angles and positions for the shaker orientation, if necessary.

The shaker has a mounting nut for attaching equipment to be tested. Since the shaker has limitations on mass and acceleration (in the axis of vibration and in off-axis applications), the RTD and the accelerometer mounting device must be as lightweight as possible, with minimal offset between the axis of vibration and the mass center. With these two constraints, a simple device was designed composing of two parts: a threaded bolt that matched the shaker's mounting nut and a small clamp (see Figure 3.8). The threaded bolt is made of stainless steel. The bolt length was adjusted to match the height

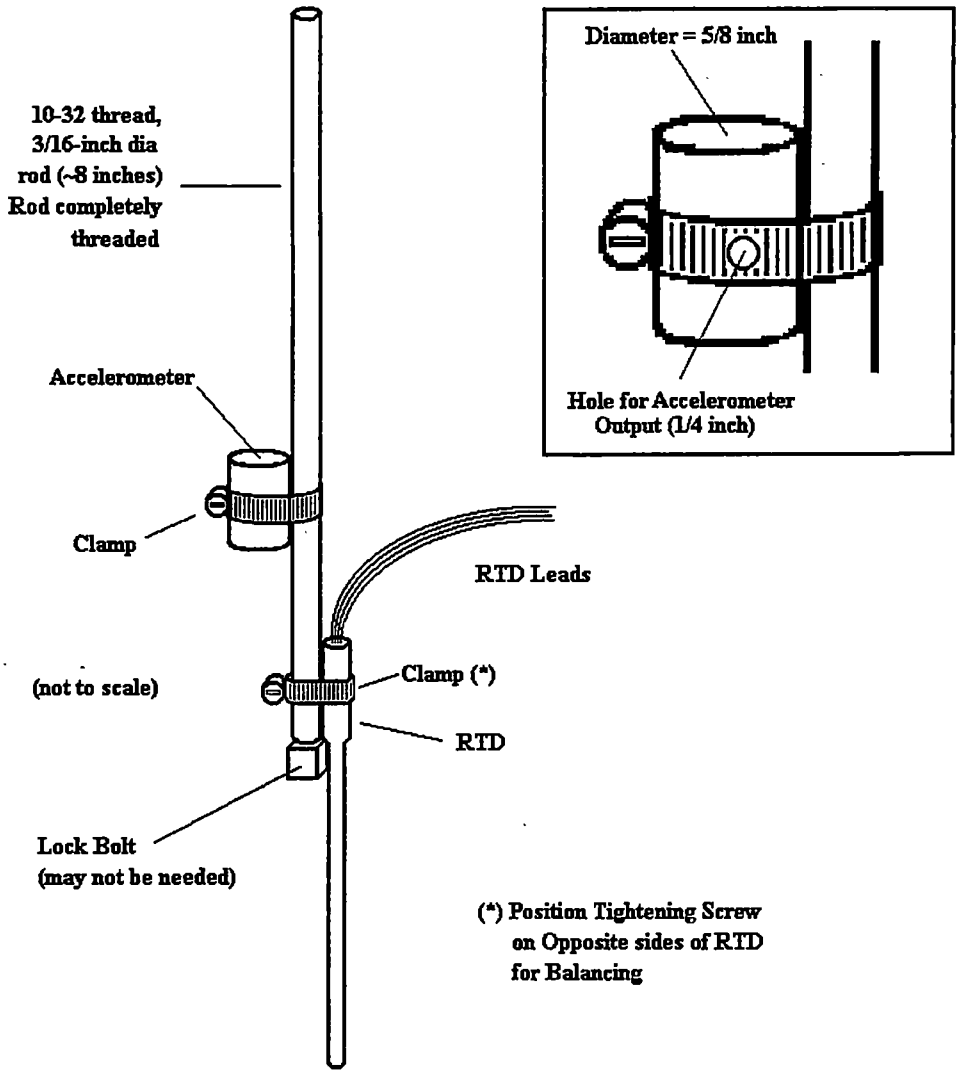


Figure 3.8. Details of RTD and accelerometer clamping devices and attachment to the shaker end nut.

of the furnace and the shaker end. Care was exercised to make the bolt as short as possible so that the major portion of the mass to be attached to it is close to the mounting end of the shaker. This resulted in a stable system, along with a minimal mass.

The alignment of the accelerometer along the axis of vibration is necessary for accurate readings of the accelerometer. One of the clamps was modified to accommodate the accelerometer's output connection. This modification of the accelerometer clamp provides a rigid and accurate alignment with respect to the shaker axis. For accurate vibration reading the RTD should have the same mounting characteristics as the accelerometer. The test RTD and the temperature control RTD are inserted into the vertical furnace through a ceramic plug placed on the furnace top. This plug provides proper guides for the RTDs and also minimizes heat loss from the furnace.

The RTDs are being vibrated at a frequency of 100 Hz, with RMS amplitude of 0.3 mm and at a furnace temperature of 400 °C. The limitations on the acceleration and mass are expressed by the equation

$$F = m * a \tag{3.1}$$

where F = maximum allowable force, equal to 4.5 lbf for sinusoidal vibration (for the shaker model used in these tests),

m = load mass (lbm) = (specimen mass + fixture mass + armature mass),

a = maximum programmed (or desired) acceleration (ft/sec^2).

These constraints limit the amplitude of motion for a given frequency of vibration.

CHAPTER 4

TEST PROCEDURES FOR RESISTANCE TEMPERATURE DETECTORS

This chapter describes the procedures used for the various tests performed on RTDs. These include

a) calibration of RTDs at 0, 100, 145, 300 and 400 °C,

b) measurement of RTD performance parameters such as various loop resistances, insulation resistance, open circuit voltage and the self-heating index,

c) RTD thermal aging procedure.

4.1 RTD Calibration Procedure

For the study RTDs were calibrated at 0, 100, 145, 300 and 400 °C. The 0 °C point was determined using crushed ice and a Rosemount Temperature Calibration Bath Model 911A2C S/N 409. The 100 °C point was determined using Dow Corning 200 Fluid and a Rosemount Temperature Calibration Bath Model 910AB2 S/N 1393. The 145 °C point was determined using Dow Corning 210H fluid and a NESLAB EXACAL High Temperature Bath Controller/readout EX -250HT. The 300 and 400 °C points were determined using the ATS furnaces.

4.1.1 Procedure for the 0 °C temperature calibration

1. Prepare a container of water and place it in a refrigerator at least one day prior to preparation of ice bath.
2. Select the RTDs for calibration, inspect/clean and place in a convenient place.
3. Clean the interior of the calibration bath, bowl and utensils.
4. Set up the ice shaver, and remove the ice from freezer.
5. Crush the ice using the ice shaver, and transfer the ice to the calibration bath until the bath is full.
6. Fill the calibration bath with water until a homogeneous water/ice mixture is achieved (usually the addition of more ice is required).
7. Turn on the stirring/pumping system in the calibration bath.
8. Allow the bath temperature to stabilize then check the bath for uniformity (ensure that the ice is not floating on a region of water).
9. Insert the SPRT into the ice bath to the same depth as the RTDs and insert the first batch of five RTDs.
10. Connect the RTDs to the extension wires of the calibration patch panel.
11. Stop the data acquisition system and change the configuration from the long-term aging patch panels to the calibration patch panel.
12. Open the data storage file and insert a line of text depicting the test being performed, the RTD numbers in the order in which the SPRT and RTDs are connected.
13. Verify the connections of the wires by a test run of the data acquisition system.

14. Connect the SPRT to an additional DVM to have continuous monitoring of the SPRT resistance values.
15. Monitor the output resistance of the SPRT until it reaches a stable reading.
16. Remove the secondary DVM, reconnect the SPRT to the patch panel and begin data acquisition system which will take 25 resistance measurements, average them, check standard deviation, and record the information to a file.
17. Repeat the data acquisition two additional times.
18. Remove the extension wire connections from the five RTDs and remove the RTDs from the bath.
19. Replace the RTDs with the next five to be calibrated at zero degrees Celsius and repeat steps 10 to 19.

4.1.2 Procedure for the 100 °C temperature calibration

1. Select the RTDs for calibration inspect/clean and place in a convenient place.
2. Check the calibration bath for appropriate oil level and if necessary add more oil to sufficiently cover the heating elements.
3. Turn on heaters and the stirring/pumping system in the calibration bath.
4. Allow the bath temperature to stabilize then check the bath for uniformity.
5. Insert the SPRT to the same depth as the RTDs and insert the first batch of five RTDs.
6. Connect the RTDs to the extension wires of the calibration patch panel.

7. Stop the data acquisition system and change the configuration from the long-term aging patch panels to the calibration patch panel.
8. Open the data storage file and insert a line of text depicting the test being performed, the RTD numbers and the order in which the SPRT and RTDs are connected.
9. Verify the connections of the wires by a test run of the data acquisition system.
10. Connect the SPRT to an additional DVM to have continuous monitoring of the SPRT resistance values.
11. Monitor the output resistance of the SPRT until it reaches a stable reading.
12. Remove the secondary DVM, reconnect the SPRT to the patch panel and begin data acquisition system which will take 25 resistance measurements, average them, check standard deviation, and record the information to a file.
13. Repeat the data acquisition two additional times.
14. Remove the extension wire connections from the five RTDs and remove the RTDs from the bath.
15. Replace the RTDs with the next five to be calibrated at 100 °C and repeat steps 5 to 15.

4.1.3 Procedure for the 145°C temperature calibration

1. Select the RTDs for calibration inspect/clean and place in a convenient place.
2. Check the calibration bath for appropriate oil level and if necessary add more oil to sufficiently cover the heating elements.

3. Turn on heaters and the stirring/pumping system in the calibration bath and set the controller temperature to 130 °C. Once the indicated temperature reaches 130 °C, increase the controller temperature to 145 °C. This minimizes overshoot and the possibility of vaporizing and of the Dow Corning Fluid.
4. Allow the bath temperature to stabilize then check the bath for uniformity.
5. Insert the SPRT to the same depth as the RTDs and insert the first batch of five RTDs.
6. Connect the RTDs to the extension wires of the calibration patch panel.
7. Stop the data acquisition system and change the configuration from the long-term aging patch panels to the calibration patch panel.
8. Open the data storage file and insert a line of text depicting the test being performed, the RTD numbers and the order in which the SPRT and RTDs are connected.
9. Verify the connections of the wires by a test run of the data acquisition system.
10. Connect the SPRT to an additional DVM to have continuous monitoring of the SPRT resistance values.
11. Monitor the output resistance of the SPRT until it reaches a stable reading.
12. Remove the secondary DVM, reconnect the SPRT to the patch panel and begin data acquisition system which will take 25 resistance measurements, average them, check standard deviation, and record the information to a file.
13. Repeat the data acquisition two additional times.
14. Remove the extension wire connections from the five RTDs and remove the RTDs from the bath.

15. Replace the RTDs with the next five to be calibrated at 145 °C and repeat steps 5 to 15.

4.1.4 Procedure for the 300 °C temperature calibration

1. Select the RTDs for calibration inspect/clean and place in a convenient place.
2. Check the furnace for ambient temperature and alignment of the end cap relative to the equalizing block.
3. Position the RTDs in the furnace in a uniform manner.
4. Connect the extension wires from the patch panel to the individual RTD leads.
5. Insert the SPRT to the same depth as the RTDs make similar connections.
6. Place the insulation material around the tops of the RTDs to minimize thermal leakage from the furnace.
7. Stop the data acquisition system and change the configuration to include the furnace being used for calibration.
8. Open the data storage file and insert a line of text depicting the test being performed, the RTD numbers in the order in which the SPRT and RTDs are connected.
9. Verify the connections of the wires by a test run of the data acquisition system.
10. Connect the SPRT to an additional DVM to have continuous monitoring of the SPRT resistance values.
11. Change the set point of the furnace to 300 °C and allow the thermocouple in the furnace to reach and stabilize at that temperature before proceeding. This is usually done overnight.

12. Monitor and verify that the output resistance of the SPRT has reached a stable reading.
13. Remove the secondary DVM, reconnect the SPRT to the patch panel and begin data acquisition system which will take 25 resistance measurements, average them, check standard deviation, and record the information to a file.
14. Repeat the data acquisition two additional times.
15. If no additional calibration point is required, turn off the furnace and wait for it to cool.
16. Remove the extension wire connections from the RTDs and remove the RTDs from the furnace.
17. If needed replace the RTDs with the next batch to be calibrated at 300 °C and repeat steps 3 to 17.

4.1.5 Procedure for the 660 °C temperature calibration

(This calibration is usually completed immediately following step 14 in the above described procedure for 300 °C calibration. In that case this procedure should begin at step 11.)

1. Select the RTDs for calibration inspect/clean and place in a convenient place.
2. Check the furnace for ambient temperature and alignment of the end cap relative to the equalizing block.
3. Position the RTDs in the furnace in a uniform manner.

4. Connect the extension wires from the patch panel to the individual RTD leads.
5. Insert the SPRT to the same depth as the RTDs and make similar connections.
6. Place the insulation material around the top of the RTDs to minimize thermal leakage from the furnace.
7. Stop the data acquisition system and change the configuration to include furnace being used for calibration.
8. Open the data storage file and insert a line of text depicting the test being performed, the RTD numbers and the order in which the SPRT and RTDs are connected.
9. Verify the connections of the wires by a test run of the data acquisition system.
10. Connect the SPRT to an additional DVM to have continuous monitoring of the SPRT resistance values.
11. Change the set point of the furnace by 100 °C increments and allow the thermocouple in the furnace to reach and stabilize at that temperature before proceeding. This pattern is followed up to 500 °C.
12. Upon reaching 500 °C reduce the step increment to 50 °C.
13. Upon reaching 600 °C reduce the step increment to 10 °C.
14. At 650 °C reduce the step increment to 1 °C, and the furnace is slowly moved up to the final temperature of 660 °C.
15. Monitor and verify that the output resistance of the SPRT has reached a stable reading.

16. Remove the secondary DVM, reconnect the SPRT to the patch panel and begin data acquisition system which will take 25 resistance measurements, average them, check standard deviation, and record the information to a file.
17. Repeat the data acquisition two additional times.
18. If no additional calibration point is required, turn off the furnace and wait for it to cool.
19. Remove the extension wire connections from the RTDs and remove the RTDs from the furnace.
20. If needed replace the RTDs with the next batch to be calibrated at 660 °C and repeat steps 3 to 20.

4.2 Measurement of RTD Performance Parameters

To assist in the determination of the failure and the mode of failure for the thermally aged resistance temperature detectors several performance parameters are being monitored. These performance parameters include loop resistance, insulation resistance, sheath to lead voltage, compensating loop resistance, open circuit voltage, and self-heating index. All of these measurements were recorded in a 30°C stirred water bath.

The loop resistance is the resistance measurement of the element and the leads uncompensated - a basic two-wire measurement. The loop resistance consists of four resistance measurements. Using the lead wire designations prescribed in Figure 4.1, the measurements are A to C, A to D, B to C, and B to D.

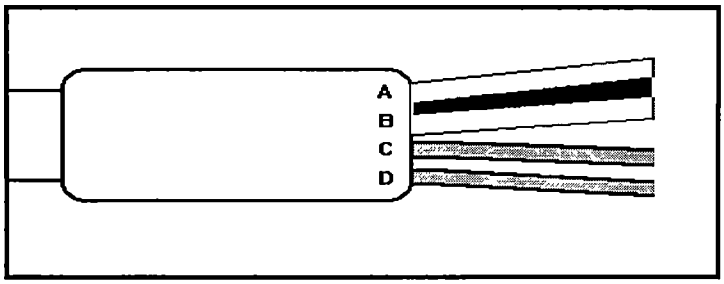


Figure 4.1 Diagram of RTD end and lead wires

The insulation resistance is the resistance measurement of the insulation material. This measurement is made between each of the four leads and the sheath. The measurement sequence, following Figure 4.2, would be sheath to A, sheath to B, sheath to C and sheath to D.

The sheath to lead voltage is the voltage measurement across the insulation. This measurement is made between each of the four leads and the sheath. The measurement sequence, following Figure 4.2, would be sheath to A, sheath to B, sheath to C and sheath to D.

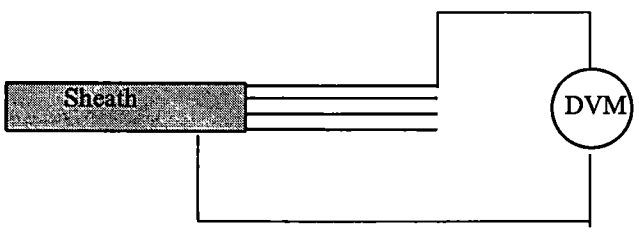


Figure 4.2 Diagram of insulation resistance measurement

The compensating loop resistance is the resistance of the lead wires. In a four-wire measurement of the resistance, the contribution of the lead wires is removed. An additional parameter of the RTD status is the compensating loop resistance. The measurement is made by reading the resistance of the circuit made by two lead wires attached to the same side of the RTD element (following Figure 4.3, A to B and C to D).

The open circuit voltage is a measure of the EMF across the element. This parameter is evaluated as the difference in the resistance measurements if the leads in the measurement are reversed. To record this parameter the four-wire resistance is recorded, the leads reversed and the resistance is again recorded. The true resistance reading would be the average of the two recorded values. The difference in the readings will be compared before and after thermal testing (see Figure 4.4).

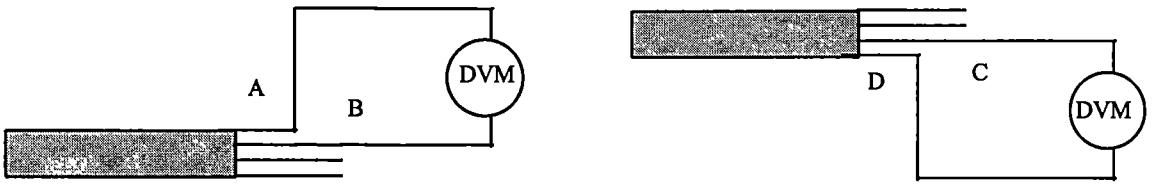


Figure 4.3 Diagram of compensating loop resistance measurement

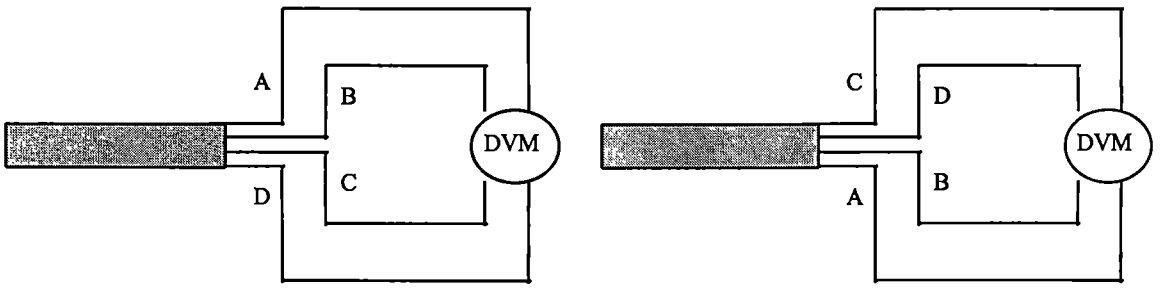


Figure 4.4 Diagram of the open circuit voltage measurement

The self-heating index is the ratio that relates the heating of the RTD to the current applied. To determine this parameter the bath temperature is noted and a set current (1 mA) is applied to the RTD through two of the leads (A and D) and the voltage is read through the other two leads (B and C). The current is then increased to 10 mA and the voltage (once it has settled) is read through the other two leads. Likewise the readings at 20 mA, 30 mA and 40 mA are obtained. These readings are then exported to Excel and are used to compute the self-heating index for the RTD (see Figure 4.5). Additional later scope growth of testing included the incremental steps of 2, 3, 4 and 5 mA being added between the 1 and 10 mA applied current measurements.

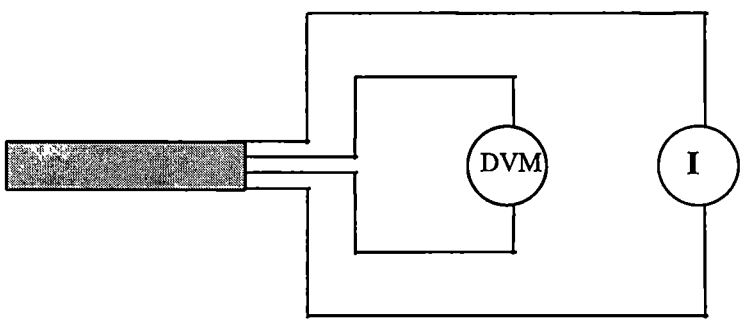


Figure 4.5 Diagram of the Self-Heating Index Measurement Configuration

4.3 General RTD Thermal Aging Test Procedure

In this study four high temperature furnaces were used to investigate the thermal aging of RTDs at elevated temperatures. A total of 101 wire-wound RTDs were tested in accordance with this study. Of the total 99 were tested in humidity and vibration-free environments, with a single RTD undergoing a vibration test and a single RTD

undergoing a humidity test. An additional 18 thin film RTDs were also tested in humidity and vibration free environments. The procedure for these thermal aging studies are outlined below.

Upon receipt of the RTDs they are carefully inspected, their serial number verified with the shipping order, a tag number assigned to them and a numerical tag attached to each RTD. The RTD is then stored in a cabinet until it is removed for testing.

First, each RTD is prepared for testing by an initial calibration to determine the specific pretest calibration parameters for that RTD. After the previously described calibration has been completed, the RTD is then measured for the pretest performance parameters. These data points are all recorded and stored for future comparison with post-test values and parameters.

Once all of the data points have been recorded, each RTD is then placed in position in the furnace. Each RTD is carefully attached to the corresponding extension cables for its assigned position in the data acquisition order. Each connection is tested by an initial data acquisition test prior to the test start.

With the system fully connected the set point of the furnace is slowly ramped by 100 °C step increments. The step intervals are approximately fifteen minutes after furnace air temperature stabilization. Due to the obvious need to reduce the amount of

overshoot that the furnace would experience during fast ramping, the rate of increase is reduced as the desired set point is approached. When the furnace temperature is within 160 °C of the final desired set point, the step increment is reduced to 50 °C. When the furnace temperature reaches within 60 °C of the desired set point the step interval is reduced to 10 °C. Finally, when the furnace temperature is within 10 °C of the desired set point the increment is reduced to 1 °C. This process facilitates reaching the final desired temperature with minimal overshoot and continuous monitoring by personnel while it is heating.

Once the furnace is brought to the desired set point, the controller, connections and RTDs remain untouched until the furnace is brought down in temperature, additional testing is done or problems occur. An additional type S thermocouple was used to test the furnace temperature to assure continuity, and weekly calibration of several RTDs was performed to track the calibration constants and performance parameters through the aging process.

Regular operation of the system consists of the RTD resistance measurements being taken by the LabView data acquisition program hourly, and the weekly collection and transfer of the data to another computer for analysis and trending.

At the end of the testing cycle for a batch of RTDs the furnace is reduced in temperature to facilitate calibration point measurements, and then completely cooled to

room temperature. The RTDs are then removed from the furnace and additional calibration points are measured and the performance parameters are determined.

4.4 Verification of Triple-Point Resistance of SPRTs

A Rosemount Aerospace Standard Platinum Resistance Thermometer (SPRT) is being used as a standard for temperature measurement during calibration. The SPRT (Model 162CE, Serial No. 2702) was originally calibrated by Rosemount Aerospace in September 1995. In order to ensure the SPRT calibration for continuous use, we requested Analysis and Measurement Services (AMS) Corp., Knoxville, TN to verify the triple-point temperature resistance of this SPRT. AMS performed the triple-point verification at no cost. The results of these tests are presented in Table 4.1 and Figure 4.6. The variation in the triple-point resistance with time of experiment is plotted. Except for a few spurious spikes in the data, the triple-point resistance is well within the NIST requirements for SPRTs. Based on this result we decided not to recalibrate the SPRT.

Table 4.1 Results of SPRT* Triple-Point Temperature Resistance Measurements

Average Resistance	25.57666
Standard Deviation	4.24E-05
Maximum Resistance	25.57675
Minimum Resistance	25.57663

*Model 162CE, Serial No. 2702

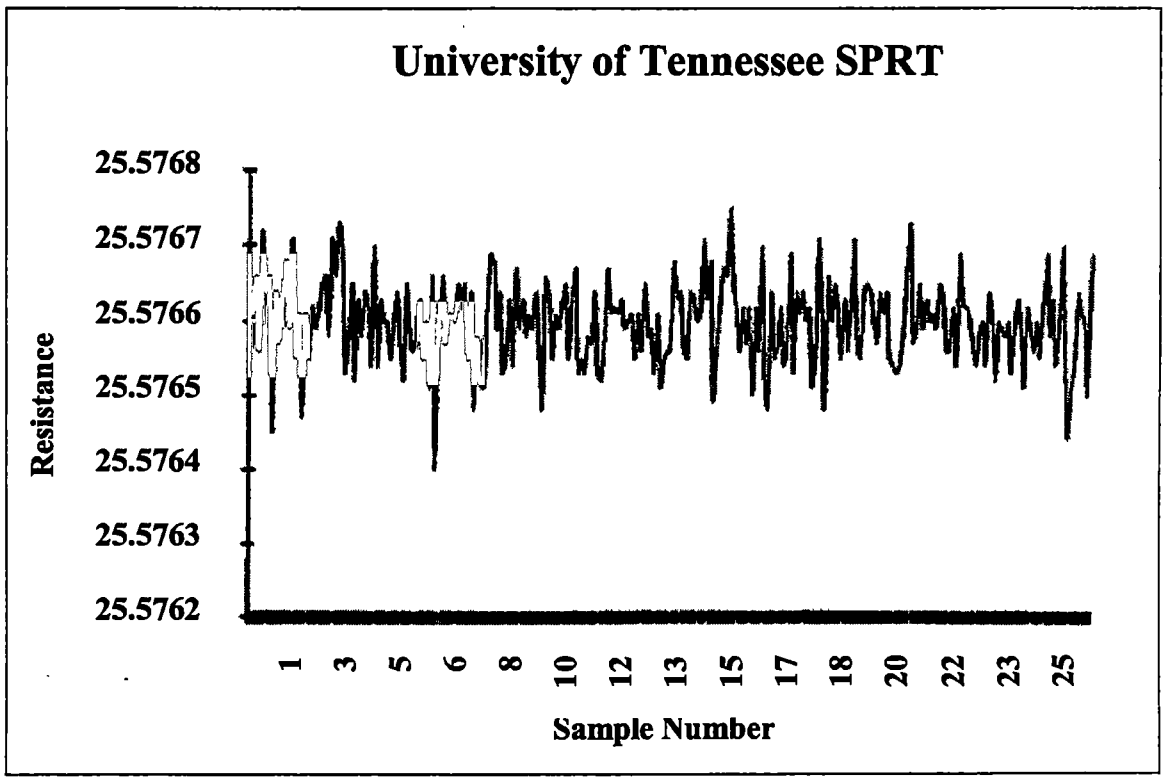


Figure 4.6. Data recorded during triple-point check of SPRT.

CHAPTER 5

CALIBRATION OF RESISTANCE TEMPERATURE DETECTORS AND UNCERTAINTY ANALYSIS

5.1 Introduction

As described in Chapter 2, there are several factors that cause calibration drifts in industrial platinum resistance thermometers (IPRTs). This chapter presents the calibration analysis of RTDs using the Callendar-Van Dusen equation relating RTD resistance and temperature, as well as the uncertainties in the resistance-temperature relationship as a function of Callendar equation parameters and ice-point resistance. The calibration uses the International Temperature Scale of 1990 (ITS-90) (see Ref. [7]) to relate the measured resistance to actual temperature. A Standard Platinum Resistance Thermometer (SPRT), manufactured by Rosemount Aerospace was used in the calibration of all test RTDs. All the relevant equations for converting SPRT resistance to temperature values are described. Most of the material was taken from Ref. [5, 7] and the Rosemount Aerospace Calibration Report [8] for Model 162CE SPRT. To complete the description of RTD calibration, some results of early studies are given in this chapter.

5.2 The Callendar-Van Dusen Equation

RTD resistance and temperature are related to each other by the Callendar-Van Dusen equation given by [2]

$$R(t)=R_0\left\{1+\alpha\left[t-\delta\left(\frac{t}{100}\right)\left(\frac{t}{100}-1\right)-\beta\left(\frac{t}{100}-1\right)\left(\frac{t}{100}\right)^3\right]\right\} \qquad (5.1)$$

where

R(t)	=	Resistance at temperature t, Ω.
R_o	=	Resistance at temperature 0 °C.
t	=	Temperature, °C.
α, β, δ	=	Calibration constants.
β	=	0 for t > 0 °C.

In RTD calibration, R(t) is the measured resistance and t is the actual temperature measured by the SPRT. Since the calibration and testing are performed at temperatures above 0 °C, the second-order version of Equation (5.1), the Callendar equation, is used. This is given by

$$R(t)=R_o\left\{1+\alpha\left[t-\delta\left(\frac{t}{100}\right)\left(\frac{t}{100}-1\right)\right]\right\} \qquad t\geq 0. \qquad (5.2)$$

The calibration curve for a platinum RTD is then given by a second order polynomial in temperatures above 0 °C:

$$R(t)=R_o(1+At+Bt^2) \qquad t\geq 0. \qquad (5.3)$$

The parameters (α,δ) and (A, B) are related to each other by the following relationships.

$$A=\alpha\left(1+\frac{\delta}{100}\right) \qquad B=-\alpha(\delta)(10^{-4}) \tag{5.4 a}$$

$$\alpha=A+100B \qquad \delta=\frac{-10^{4}B}{(A+100B)}. \tag{5.4 b}$$

In this study the recent calibration points correspond to 0, 100 and 145 °C. The measurement of R_o corresponds to a temperature of approximately 0.01 °C.

The measurements at 100 °C and 145 °C are made in oil baths. The measurements at 300 and 660 °C are made using the high-temperature tubular furnace. Equation (5.3), a second order polynomial representation, is used for fitting the calibration data: resistance vs. temperature.

5.3 Calculation of Temperature from Resistance Measurement Using the SPRT

The following set of equations are used to calculate the temperatures from the resistances measured by the SPRT. Based on the ITS-90 temperature scale, the temperature in Kelvin is given by [7]

$$T=273.15+D_o+\sum_{i=1}^{9} D_i\left[\frac{W_r(T)-2.64}{1.64}\right]^i. \tag{5.5}$$

The values of the constants (D_0, D_1, . . ., D_9) are given in Table 5.1. Temperature in °C is obtained as

$$t = T - 273.15 \tag{5.6}$$

Table 5.1. Values of the coefficients $D_0, D_1, \ldots, D_9$ in Equation (5.5) [7]

Constant or Coefficient	Value
D_0	439.932 854
D_1	472.418 020
D_2	37.684 494
D_3	7.472 018
D_4	2.920 828
D_5	0.005 184
D_6	-0.963 864
D_7	-0.188 732
D_8	0.191 203
D_9	0.049 025

The reference function $W_r(T)$ is defined by ITS-90 by the equation

$$W(T) = W_r(T) + \Delta W \tag{5.7}$$

where

$W(T) = R(T)/R(273.16)$ (5.8)

$R(T)$ = SPRT resistance at T, Ω

$R(273.16)$ = SPRT resistance at 273.16K, the triple point temperature of water.

$R(273.16) = 25.56885$ Ω, For the Rosemont Aerospace Model 162CE SPRT.

$$\Delta W = a_7 [W(T) -1] + b_7 [W(T) -1]^2 + c_7 [W(T) -1)]^3 \tag{5.9}$$

for $T > 273.15$ K.

$a_7 = -6.1993440D-04$

$b_7 = 3.0189916D-04$

$c_7 = -9.9433090D-05$

With the previous definitions the reference function is given by

$$W_r(T) = W(T) - \Delta W. \tag{5.10}$$

Relationships in Equations (5.8), (5.9) and (5.10) are used to calculate $W_r(T)$, which is then substituted in Equation (5.5) to determine the temperature measured by the SPRT.

5.4 Determination of RTD Calibration Constants

For each RTD (after the aging test) the values of resistances at temperatures 0, 100, 145°C are determined. The SPRT is used to determine the exact temperature values. The measured resistance R(t) is expressed as a function of the temperature (obtained from the SPRT) using the second order relationship

$$R(t) = R_0 (1 + At + Bt^2). \tag{5.11}$$

These models are developed for each of the post-test RTDs as

$$R_i(t) = R_{oi} (1 + A_i t + B_i t^2), \; i = 1, 2, ..., n \tag{5.12}$$

where n is the number of RTDs tested. The parameters (R_{oi}, A_i, B_i) are estimated using a least squares fit. The uncertainties in the parameters (A, B) are also estimated.

The least-squares estimation of parameters (R_o, A, B) and their variances are now described. Rewrite Equation (5.11) in the form

$$R(t) = a + bt + ct^2 + \varepsilon$$

$$a = R_0,\ b = AR_0,\ C = BR_0 \tag{5.13}$$

where ε is a random model error. The parameters (a, b, c) are estimated such that the sum of the squared errors at various calibration temperatures $\{t_i, i = 1, 2, .., N\}$ is minimized.

This is written as

$$\min_{(a,b,c)} \sum_{i=1}^{N} \left\{ y(t_i) - a - bt_i - ct_i^{\,2} \right\}^2 . \tag{5.14}$$

In the current experiment the temperature-resistance values near 0, 100, 145 and 300 °C are used. The temperature near 660 °C has a larger conversion error and is not used in the Callendar equation fit.

For N temperature (calibration) points $t_1, t_2, ..., t_N$, Equation (5.13) is written as

$$\begin{bmatrix} y(t_1) \\ y(t_2) \\ \bullet \\ \bullet \\ \bullet \\ y(t_3) \end{bmatrix} = \begin{bmatrix} 1 & t_1 & t_1^2 \\ 1 & t_2 & t_2^2 \\ \bullet & \bullet & \bullet \\ \bullet & \bullet & \bullet \\ \bullet & \bullet & \bullet \\ 1 & t_3 & t_3^2 \end{bmatrix} \begin{bmatrix} a \\ b \\ c \end{bmatrix} + \begin{bmatrix} \varepsilon_1 \\ \varepsilon_2 \\ \bullet \\ \bullet \\ \bullet \\ \varepsilon_3 \end{bmatrix} . \tag{5.15}$$

In a compact matrix notation the above has the form

$$\underline{y} = X \begin{bmatrix} a \\ b \\ c \end{bmatrix} + \underline{\varepsilon} \ . \tag{5.16}$$

The least-squares estimate of the parameter is given by

$$\underline{\beta}=\begin{bmatrix}a\\b\\c\end{bmatrix}=(X^TX)^{-1}X^T\underline{Y}. \tag{5.17}$$

The error variance σ_ε^2 is now calculated as

$$\sigma_3^2=\frac{1}{3}\sum_{i=1}^{3}\left[y(t_i)-a-bt_j-ct_j^2\right]^2 \quad . \tag{5.18}$$

The error covariance matrix of $\underline{\beta}$ is [11]

$$\sum_{\beta} =\sigma_\varepsilon^2(X^TX)^{-1} \quad . \tag{5.19}$$

Note that when N=3, the least squares, fit has $\sigma_\varepsilon = 0$. From the above, the standard deviations of the estimates of a, b and c are the square root of the diagonal elements of $\sum_{\beta}$. Denote these by $\sigma_a, \sigma_b \text{ and } \sigma_c$ respectively. From these we can calculate $\sigma_{Ro}, \sigma_A \text{ and } \sigma_B$.

The variances of the parameters α and δ in the Callendar equation may be computed from the relationships

$$\alpha = A + 100B \tag{5.20a}$$

$$\delta = \frac{-10^4 B}{(A+100B)} \tag{5.20b}$$

Thus

$$\Delta\alpha = \frac{\partial\alpha}{\partial A}\Delta A + \frac{\partial\alpha}{\partial B}\Delta B \tag{5.21a}$$

and

$$\Delta\delta = \frac{\partial\delta}{\partial A}\Delta A + \frac{\partial\delta}{\partial B}\Delta B \tag{5.21b}$$

From Equations (5.20) and (5.21)

$$\Delta\alpha = \Delta A + 100\Delta B$$

or

$$\sigma_\alpha^2 = \sigma_A^2 + 10^4\,\sigma_B^2 \tag{5.22}$$

Similarly

$$\Delta\delta = \frac{10^4 B}{(A+100B)^2}\Delta A - \frac{10^4}{(A+100B)^2}\Delta B$$

$$\sigma_\delta^2 = \frac{10^8}{(A+100B)^4}\left\{B^2\,\sigma_A^2 + A^2\,\sigma_B^2\right\} \tag{5.23}$$

The cross terms are neglected in Equation (5.23).

A summary of the results of pre-test RTDs is given in Table 5.2. The α value is also approximated using

$$\alpha = \frac{R(t_2) - R(t_1)}{R(t_1)(t_2 - t_1)} \tag{5.24}$$

The temperature t_1 is close to 0 °C, and t_2 is close to 100 °C. Note that the α value determined from the simple slope calculation is very close to the α calculated from the Callendar equation.

Table 5.2 Summary of the Pre-test RTD Calibration Results

RTD #	Ro	A	B	Alpha	delta	Two Point α
A-33	99.99127	0.003866	-4.9E-07	0.003816	1.2952	0.003854
A-34	99.99026	0.003889	-5.2E-07	0.003837	1.356998	0.003854
A-35	100.0054	0.003908	-5.5E-07	0.003854	1.424377	0.003855
A-36	99.96079	0.003894	-5.3E-07	0.003841	1.377744	0.003853
A-37	99.981	0.003884	-5.2E-07	0.003832	1.354516	0.00385
A-38	99.95265	0.00388	-5.1E-07	0.003828	1.335623	0.003852
A-39	99.96295	0.003879	-5E-07	0.003828	1.318699	0.003854
A-40	99.99014	0.003876	-5.1E-07	0.003826	1.321847	0.00385
A-41	99.95125	0.003873	-5E-07	0.003823	1.306026	0.003853
A-42	99.97058	0.003883	-5.1E-07	0.003832	1.338032	0.003853
A-43	99.98484	0.003897	-5.3E-07	0.003844	1.389838	0.003852
A-44	99.96237	0.003894	-5.3E-07	0.003841	1.376982	0.003854
A-45	99.94885	0.00389	-5.2E-07	0.003839	1.349622	0.003852
A-46	99.94265	0.003895	-5.3E-07	0.003842	1.384844	0.003855
A-47	99.92173	0.003882	-5.1E-07	0.003831	1.332532	0.003856
A-48	99.95516	0.003887	-5.2E-07	0.003836	1.344947	0.003855
A-49	99.95768	0.003869	-4.9E-07	0.003819	1.287778	0.003855

5.5 RTD Parameter Sensitivities and Calibration Uncertainties

This section provides a discussion of the uncertainties in measured resistances as a function of uncertainties in calibration constants and temperature and their sensitivity coefficients. This procedure, similar to that discussed in Refs [9,10], provides information about how the various factors propagate their errors to the resistance - temperature relationship. The uncertainly analysis provides an expression for $\Delta R/R(t)$ where ΔR is the variation in the resistance at temperature t. This may be expressed either using the second-order polynomial form

$$R(t) = R_0 (1 + At + Bt^2) \tag{5.25}$$

or the Callendar equation

$$R(t) = R_0 \left\{ 1 + \alpha \left[t - \delta \left(\frac{t}{100} \right) \left(\frac{t}{100} - 1 \right) \right] \right\} \tag{5.26}$$

Both the procedures are presented with results from actual measurements.

5.6 Uncertainty and Sensitivity Analysis

Expressions are developed for $\Delta R/R(t)$ using the second-order relationship between resistance and temperature. The fractional variation in R(t) is expressed as a function of the sensitivity coefficients defined for each of the parameters (A, B, R_0) in Equation (5.25) or (α, δ, R_0) in Equation (5.26).

Using Equation (5.1) the variation in R(t) is given by

$$\Delta R=\left(\frac{\partial R}{\partial t}\right)\Delta t+\left(\frac{\partial R}{\partial A}\right)\Delta A+\left(\frac{\partial R}{\partial B}\right)\Delta B+\left(\frac{\partial R}{\partial R_0}\right)\Delta R_0 \qquad (5.27)$$

Evaluate the partial differentials using Equation (5.25) and divide both sides of Equation (5.27) by R. This gives

$$\frac{\Delta R}{R}=\frac{R_0}{R}(At+2Bt^2)\cdot\left[\frac{\Delta t}{t}\right]+\frac{R_0 At}{R}\left[\frac{\Delta A}{A}\right]+\frac{R_0 Bt^2}{R}\cdot\left[\frac{\Delta B}{B}\right]+\frac{\Delta R_0}{R_0} \qquad (5.28)$$

In Equation (5.28) the coefficients of the fractional variations in each of the parameters are the corresponding sensitivity functions. These may be summarized as follows [10].

S_t^R = $\frac{R_0}{R}$ (At + 2Bt^2), sensitivity of R on t,

S_A^R = $\frac{R_0 At}{R}$, sensitivity of R on A,

S_B^R = $\frac{R_0 Bt^2}{R}$, sensitivity of R on B,

$S_{R_0}^R$ = 1, sensitivity of R on R_0.

Thus, the fractional uncertainty in R is given by

$$\frac{\Delta R}{R}=S_t^R\left[\frac{\Delta t}{t}\right]+S_A^R\left[\frac{\Delta A}{A}\right]+S_B^R\left[\frac{\Delta B}{B}\right]+S_{R_0}^R\left[\frac{\Delta R_0}{R_0}\right] \qquad (5.29)$$

Uncertainty expressions similar to Equations (5.28) and (5.29) may be derived using the Callendar Equation (5.26).

$$R(t)=R_0\left\{1+\alpha\left[t-\delta\left(\frac{t}{100}\right)\left(\frac{t}{100}-1\right)\right]\right\} \tag{5.26}$$

In this case the fractional uncertainty in R(t) is expressed in terms of the uncertainties in the coefficients α, δ and the resistance R_0. From Equation (5.26) the fractional uncertainty in R is given by

$$\frac{\Delta R}{R}=\frac{R_0}{R}\left(\frac{\alpha\delta t}{100}\right)\left\{\left[\frac{100+\delta}{\delta}-\frac{2t}{100}\right]\frac{\Delta t}{t}+\left[\frac{100+\delta}{\delta}-\frac{t}{100}\right]\frac{\Delta\alpha}{\alpha}+\left[1-\frac{t}{100}\right]\frac{\Delta\delta}{\delta}\right\}+\frac{\Delta R}{R_0}. \tag{5.30}$$

The fractional uncertainty in R as a function of the uncertainties in the parameters of the Callendar equation is given by

$$\frac{\Delta R}{R}=S_t^R\left[\frac{\Delta t}{t}\right]+S_\alpha^R\left[\frac{\Delta\alpha}{\alpha}\right]+S_\delta^R\left[\frac{\Delta\delta}{\delta}\right]+S_{R_0}^R\left[\frac{\Delta R_0}{R_0}\right] \tag{5.31}$$

where

$$S_t^R=\frac{R_0}{R}\left(\frac{\alpha\delta t}{100}\right)\left[\frac{100+\delta}{\delta}-\frac{2t}{100}\right]$$

$$S_\alpha^R=\frac{R_0}{R}\left(\frac{\alpha\delta t}{100}\right)\left[\frac{100+\delta}{\delta}-\frac{t}{100}\right]$$

$$S_\delta^R=\frac{R_0}{R}\left(\frac{\alpha\delta t}{100}\right)\left[1-\frac{t}{100}\right]$$

$$S_{R_0}^R=1.$$

Knowing the sensitivity coefficients, the error in R may be calculated for any temperature t. The values of α and δ are substituted in terms of A and B using Equation (5.27).

5.7 RMS Value of the Fractional Error

If it is assumed that the individual error terms in either Equation (5.29) or Equation (5.31) are independent of each other, the root-mean-squared (RMS) fractional error in $\Delta R/R$ may be calculated as follows:

$$\text{RMS}_{\Delta R/R} = \left\{ \left(S_t^R \frac{\Delta t}{t} \right)^2 + \left(S_A^R \frac{\Delta A}{A} \right)^2 + \left(S_B^R \frac{\Delta B}{B} \right)^2 + \left(S_{R_o}^R \frac{\Delta R_o}{R_o} \right)^2 \right\}^{1/2} \quad (5.32)$$

$$\text{RMS}_{\Delta R/R} = \left\{ \left(S_t^R \frac{\Delta t}{t} \right)^2 + \left(S_\alpha^R \frac{\Delta \alpha}{\alpha} \right)^2 + \left(S_\delta^R \frac{\Delta \delta}{\delta} \right)^2 + \left(S_{R_o}^R \frac{\Delta R_o}{R_o} \right)^2 \right\}^{1/2} \quad (5.33)$$

$\Delta\alpha$ and $\Delta\delta$ are calculated from the relationships in Equations (5.4),

$$\Delta\alpha = \frac{\partial \alpha}{\alpha \text{A}} \Delta\text{A} + \frac{\partial \alpha}{\partial \text{B}} \cdot \Delta\text{B} \quad (5.34)$$

Using Equation (5.27)

$$\Delta\alpha = \Delta\text{A} + 100\Delta\text{B} \quad (5.35)$$

Similarly,

$$\Delta\alpha = \frac{\partial \delta}{\partial \text{A}} \Delta\text{A} + \frac{\partial \delta}{\partial \text{B}} \Delta\text{B} \quad (5.36)$$

$$\Delta\delta = \frac{10^4\ \text{B}}{(\text{A}+100\text{B})^2} \cdot \Delta\text{A} - \frac{10^4\ \text{A}}{(\text{A}+100\text{B})^2} \Delta\text{B} \quad (5.37)$$

$\Delta\alpha$ and $\Delta\delta$ are calculated knowing A, B, ΔA and ΔB.

5.8 Uncertainty and Sensitivity Analysis Results including the RMS Value of the Fractional Error

The results provided in this section were determined using the calculation procedures provided in Sections 5.6 and 5.7. The sensitivities are calculated using assumed uncertainties assembled from calibration calculations and standard deviations recorded during calibrations. Tables 5.3 and 5.4 provide the averaged raw data values and the results of the calculations for new wire-wound RTDs. Tables 5.5 through 5.20 provide the post-test raw data values and the calculation results for RTDs A-1 through A-8. These wire-wound RTDs were the subjects of Test #1, a thermal soak test conducted at 660 °C for 57 days. In this test several of the RTDs drifted, some minimally and two considerably, specifically A-1 and A-6. This drift is easily identified by noting the increased Ro calibration value in the tables provided. These drifts can also be seen in the long-term thermal aging resistance plot, Figure A-1 in Appendix A. As well as the increase in Ro as the RTDs drifted similar changes were seen in the sensitivity, uncertainty and RMS values. The sensitivity of R on t, R on δ and R on B appear to decrease, where at the same time, the sensitivity of R on A and R on α do not show an obvious pattern of increasing or decreasing through all temperatures and drift rates. The post-test fractional uncertainties appear to increase with the amount of drift. The post-test RMS values as well appear to increase with the amount of drift the RTD experienced.

Table 5.3 Averaged Calibration Values for New RTDs

Average Values:	
Ro	99.96644633
delta Ro	0.001934716
A	0.003885097
delta A	1.66859E-05
B	-5.1632E-07
delta B	2.73868E-08
alpha	0.003833465
delta alpha	1.94246E-05
delta	1.346800212
delta delta	-0.00029578
T1	98.6820057
deltaT1	0.002814895
T2	311.2305747
delta T2	0.014863713
T3	663.0675923
deltaT3	0.233546394

Table 5.4 Analysis Results for New RTD Average Values

Sensitivity Analysis					Average New RTD	
Based on A and B Values						
	Sensitivity of R on T	Sensitivity of R on A	Sensitivity Of R on B	Sensitivity of R on Ro	Fractional Uncertainty (based on A and B)	RMS Values
T1	0.270480	0.277765	-0.003643	1	0.001413	0.001209
T2	0.513921	0.560269	-0.023174		0.003679	0.002702
T3	0.633596	0.769153	-0.067778		0.007141	0.004887
Based on Alpha and Delta						
	Sensitivity of R on T	Sensitivity of R on α	Sensitivity Of R on δ	Sensitivity of R on Ro	Fractional Uncertainty (based on α and δ)	RMS Values
T1	0.270480	0.274122	4.865E-05	1	0.001416	0.001389
T2	0.513923	0.537096	-0.015727		0.002769	0.002722
T3	0.633604	0.701378	-0.057553		0.003809	0.003561

Table 5.5 Post-test Calibration Values for RTD A-1

RTD #1 Values:	
Ro	104.4579
delta Ro	0.000201
A	0.003999
delta A	0.0002
B	-9.5E-07
delta B	3.34E-07
alpha	0.003904
delta alpha	0.000234
delta	2.443558
delta delta	-0.00382
T1	98.70266
deltaT1	0.002815
T2	298.715
delta T2	0.013476
T3	651.5313
deltaT3	0.213378

Table 5.6 Post-test Analysis Results for RTD A-1

Sensitivity Analysis					RTD #1	
Based on A and B Values						
	Sensitivity of R on T	Sensitivity of R on A	Sensitivity of R on B	Sensitivity of R on Ro	Fractional Uncertainty (based on A and B)	RMS Values
T1	0.275961	0.289597	-0.00682	1	0.016899	0.014697
T2	0.482946	0.563204	-0.04013		0.042276	0.031509
T3	0.561387	0.814568	-0.12659		0.085295	0.060233
Based on Alpha and Delta						
	Sensitivity of R on T	Sensitivity of R on α	Sensitivity of R on δ	Sensitivity of R on Ro	Fractional Uncertainty (based on α and δ)	RMS Values
T1	0.275961	0.282779	8.96E-05	1	0.016936	0.016926
T2	0.482946	0.523075	-0.0267		0.031374	0.031309
T3	0.561387	0.687977	-0.10716		0.041532	0.04118

Table 5.7 Post-test Calibration Values for RTD A-2

RTD #2 Values:	
Ro	101.2435
delta Ro	0.000201
A	0.004099
delta A	0.000186
B	-9.5E-07
delta B	3.1E-07
alpha	0.004004
delta alpha	0.000217
delta	2.372081
delta delta	-0.00353
T1	98.70266
deltaT1	0.002815
T2	298.715
delta T2	0.013476
T3	651.5313
deltaT3	0.213378

Table 5.8 Post-test Analysis Results for RTD A-2

Sensitivity Analysis					RTD #2	
Based on A and B Values						
	Sensitivity of R on T	Sensitivity of R on A	Sensitivity of R on B	Sensitivity of R on Ro	Fractional Uncertainty (based on A and B)	RMS Values
T1	0.280882	0.294346	-0.00673	1	0.015554	0.013526
T2	0.490568	0.569389	-0.03941		0.038703	0.028844
T3	0.570874	0.817795	-0.12346		0.077559	0.054756
Based on Alpha and Delta						
	Sensitivity of R on T	Sensitivity of R on α	Sensitivity of R on δ	Sensitivity of R on Ro	Fractional Uncertainty (based on α and δ)	RMS Values
T1	0.280882	0.287614	8.85E-05	1	0.015587	0.015577
T2	0.490568	0.529978	-0.02622		0.028767	0.028704
T3	0.570874	0.694334	-0.10451		0.03795	0.037606

Table 5.9 Post-test Calibration Values for RTD A-3

RTD #3 Values:	
Ro	100.8425
delta Ro	0.000201
A	0.004121
delta A	0.000186
B	-9.6E-07
delta B	3.11E-07
alpha	0.004025
delta alpha	0.000217
delta	2.380123
delta delta	-0.00354
T1	98.69481
deltaT1	0.002815
T2	298.715
delta T2	0.013476
T3	651.5313
deltaT3	0.213378

Table 5.10 Post-test Analysis Results for RTD A-3

Sensitivity Analysis				RTD #3		
Based on A and B Values						
	Sensitivity of R on T	Sensitivity of R on A	Sensitivity of R on B	Sensitivity of R on Ro	Fractional Uncertainty (based on A and B)	RMS Values
T1	0.281906	0.295464	-0.00678	1	0.015563	0.013535
T2	0.491593	0.570883	-0.03964		0.038682	0.028829
T3	0.571218	0.819462	-0.12412		0.077472	0.054695
Based on Alpha and Delta						
	Sensitivity of R on T	Sensitivity of R on α	Sensitivity of R on δ	Sensitivity of R on Ro	Fractional Uncertainty (based on α and δ)	RMS Values
T1	0.281906	0.288685	8.97E-05	1	0.015597	0.015587
T2	0.491593	0.531238	-0.02637		0.028747	0.028684
T3	0.571218	0.69534	-0.10507		0.037889	0.037545

Table 5.11 Post-test Calibration Values for RTD A-4

RTD #4 Values:	
Ro	100.8797
delta Ro	0.000201
A	0.004137
delta A	0.000145
B	-9.9E-07
delta B	2.41E-07
alpha	0.004038
delta alpha	0.000169
delta	2.442937
delta delta	-0.00276
T1	98.69481
deltaT1	0.002815
T2	298.715
delta T2	0.013476
T3	651.5313
deltaT3	0.213378

Table 5.12 Post-test Analysis Results for RTD A-4

Sensitivity Analysis					RTD #4	
Based on A and B Values						
	Sensitivity of R on T	Sensitivity of R on A	Sensitivity of R on B	Sensitivity of R on Ro	Fractional Uncertainty (based on A and B)	RMS Values
T1	0.281432	0.295334	-0.00695	1	0.012043	0.010471
T2	0.491489	0.573144	-0.04083		0.030063	0.022401
T3	0.567236	0.822962	-0.12786		0.060258	0.042513
Based on Alpha and Delta						
	Sensitivity of R on T	Sensitivity of R on α	Sensitivity of R on δ	Sensitivity of R on Ro	Fractional Uncertainty (based on α and δ)	RMS Values
T1	0.281432	0.288383	9.19E-05	1	0.012069	0.012059
T2	0.491489	0.532317	-0.02716		0.022314	0.022259
T3	0.567236	0.695099	-0.10824		0.029376	0.029067

Table 5.13 Post-test Calibration Values for RTD A-5

RTD #5 Values:	
Ro	101.1852
delta Ro	0.000185
A	0.004118
delta A	0.000194
B	-9.7E-07
delta B	3.23E-07
alpha	0.004021
delta alpha	0.000226
delta	2.406234
delta delta	-0.00369
T1	98.69481
deltaT1	0.002815
T2	298.715
delta T2	0.013476
T3	651.5313
deltaT3	0.213378

Table 5.14 Post-test Analysis Results for RTD A-5

Sensitivity Analysis					RTD #5	
Based on A and B Values						
	Sensitivity of R on T	Sensitivity of R on A	Sensitivity of R on B	Sensitivity of R on Ro	Fractional Uncertainty (based on A and B)	RMS Values
T1	0.281801	0.295506	-0.00685	1	0.016206	0.014095
T2	0.490678	0.570806	-0.04006		0.04027	0.030012
T3	0.569196	0.82038	-0.12559		0.080746	0.057012
Based on Alpha and Delta						
	Sensitivity of R on T	Sensitivity of R on α	Sensitivity of R on δ	Sensitivity of R on Ro	Fractional Uncertainty (based on α and δ)	RMS Values
T1	0.281801	0.288654	9.06E-05	1	0.016242	0.016232
T2	0.490678	0.530742	-0.02665		0.02991	0.029845
T3	0.569196	0.694788	-0.10632		0.039421	0.039071

Table 5.15 Post-test Calibration Values for RTD A-6

RTD #6 Values:	
Ro	110.546
delta Ro	0.000185
A	0.003809
delta A	0.000195
B	-9.3E-07
delta B	3.26E-07
alpha	0.003717
delta alpha	0.000228
delta	2.494174
delta delta	-0.00373
T1	98.69481
deltaT1	0.002815
T2	298.715
delta T2	0.013476
T3	651.5313
deltaT3	0.213378

Table 5.16 Post-test Analysis Results for RTD A-6

Sensitivity Analysis					RTD #6	
Based on A and B Values						
	Sensitivity of R on T	Sensitivity of R on A	Sensitivity of R on B	Sensitivity of R on Ro	Fractional Uncertainty (based on A and B)	RMS Values
T1	0.266088	0.279514	-0.00671	1	0.016704	0.014529
T2	0.470591	0.550645	-0.04003		0.042332	0.031551
T3	0.549131	0.804113	-0.12749		0.08623	0.060898
Based on Alpha and Delta						
	Sensitivity of R on T	Sensitivity of R on α	Sensitivity of R on δ	Sensitivity of R on Ro	Fractional Uncertainty (based on α and δ)	RMS Values
T1	0.266088	0.272801	8.88E-05	1	0.016741	0.016732
T2	0.470591	0.510618	-0.02663		0.031381	0.031318
T3	0.549131	0.676622	-0.10792		0.041843	0.0415

Table 5.17 Post-test Calibration Values for RTD A-7

RTD #7 Values:	
Ro	100.9819
delta Ro	0.000185
A	0.004132
delta A	0.000195
B	-9.8E-07
delta B	3.25E-07
alpha	0.004034
delta alpha	0.000228
delta	2.430335
delta delta	-0.00371
T1	98.69481
deltaT1	0.002815
T2	298.715
delta T2	0.013476
T3	651.5313
deltaT3	0.213378

Table 5.18 Post-test Analysis Results for RTD A-7

Sensitivity Analysis					RTD #7	
Based on A and B Values						
	Sensitivity of R on T	Sensitivity of R on A	Sensitivity of R on B	Sensitivity of R on Ro	Fractional Uncertainty (based on A and B)	RMS Values
T1	0.282408	0.296285	-0.00694	1	0.016295	0.014172
T2	0.490867	0.57194	-0.04054		0.040463	0.030157
T3	0.568039	0.822261	-0.12711		0.081158	0.057304
Based on Alpha and Delta						
	Sensitivity of R on T	Sensitivity of R on α	Sensitivity of R on δ	Sensitivity of R on Ro	Fractional Uncertainty (based on α and δ)	RMS Values
T1	0.282408	0.289346	9.18E-05	1	0.01633	0.016321
T2	0.490867	0.531403	-0.02697		0.030039	0.029974
T3	0.568039	0.69515	-0.1076		0.039562	0.039211

Table 5.19 Post-test Calibration Values for RTD A-8

RTD #8 Values:	
Ro	101.7002
delta Ro	0.000185
A	0.004096
delta A	0.000196
B	-9.7E-07
delta B	3.26E-07
alpha	0.004
delta alpha	0.000228
delta	2.41328
delta delta	-0.00372
T1	98.69481
deltaT1	0.002815
T2	298.715
delta T2	0.013476
T3	651.5313
deltaT3	0.213378

Table 5.20 Post-test Analysis Results for RTD A-8

Sensitivity Analysis				RTD #8		
Based on A and B Values						
	Sensitivity of R on T	Sensitivity of R on A	Sensitivity Of R on B	Sensitivity of R on Ro	Fractional Uncertainty (based on A and B)	RMS Values
T1	0.280757	0.294453	-0.00685	1	0.016389	0.014254
T2	0.48927	0.569435	-0.04008		0.040771	0.030386
T3	0.567772	0.819361	-0.12579		0.081843	0.057789
Based on Alpha and Delta						
	Sensitivity of R on T	Sensitivity of R on α	Sensitivity Of R on δ	Sensitivity of R on Ro	Fractional Uncertainty (based on α and δ)	RMS Values
T1	0.280757	0.287605	9.06E-05	1	0.016424	0.016415
T2	0.48927	0.529352	-0.02666		0.030277	0.030212
T3	0.567772	0.693566	-0.10649		0.039937	0.039585

CHAPTER 6

DEVELOPMENT OF A SENSOR LIFE PREDICTION METHOD

6.1 Introduction

The trending of resistance-time characteristic and the prediction of remaining calibration lifetime of RTDs is presented in this chapter [17]. Modeling of drift behavior may be performed using two different approaches. The first approach is to build single or multiple-step-ahead predictors (dynamic prediction) that do not require the overall trend of the RTD drift during its lifetime. However, these models are not easy to use for determining future values since they always require previous measurements. The second approach is to assume a general form for the drift behavior and then fit the parameters of the model using the measurements (static prediction). The disadvantage of the latter is that the drift behavior may change with time. This problem may be overcome by updating the model as more data become available. This piecewise linear adaptive modeling was used in this research.

The effectiveness of sensor drift data usage was improved by utilizing a large data window. The influence of current versus old data in this window was balanced by a weighted least-squares method. A large data window provides a more robust overall behavior of model fitting compared to a smaller data window. The data weighting is useful in weighting the current data more than the past data. Different forms of weighting

functions were tried to determine the best and simplest one to implement (with little subjectivity).

A confidence analysis of life prediction was developed for linear models. This provides lower and upper bounds for the estimated lifetime and uses the model prediction error and the standard deviations of model parameters.

6.2 Time-to-Alarm and Time-to-Failure

Two of the important parameters that define a trend towards degradation and eventual sensor failure are the *alarm limit* and the *failure limit*. Associated with these two parameters, two important time points are defined: "time-to-alarm" and "time-to-failure." These failure parameters are defined in Figure 6.1. The alarm limit indicates the value of a parameter beyond which the sensor is in continuous degradation and its reliability decreases. The failure limit defines the value of the parameter beyond which the sensor's function is unreliable and not acceptable. These limits have to be set according to the manufacturer-defined accuracy and the process in which the RTDs are used. No attempt has been made in defining these limits. The time interval between the current lifetime and the time at which the selected degradation parameter reaches the failure limit is called the *residual life of the detector*. The purpose of this research is to develop simple and robust methods for the estimation of these parameters associated with life prediction.

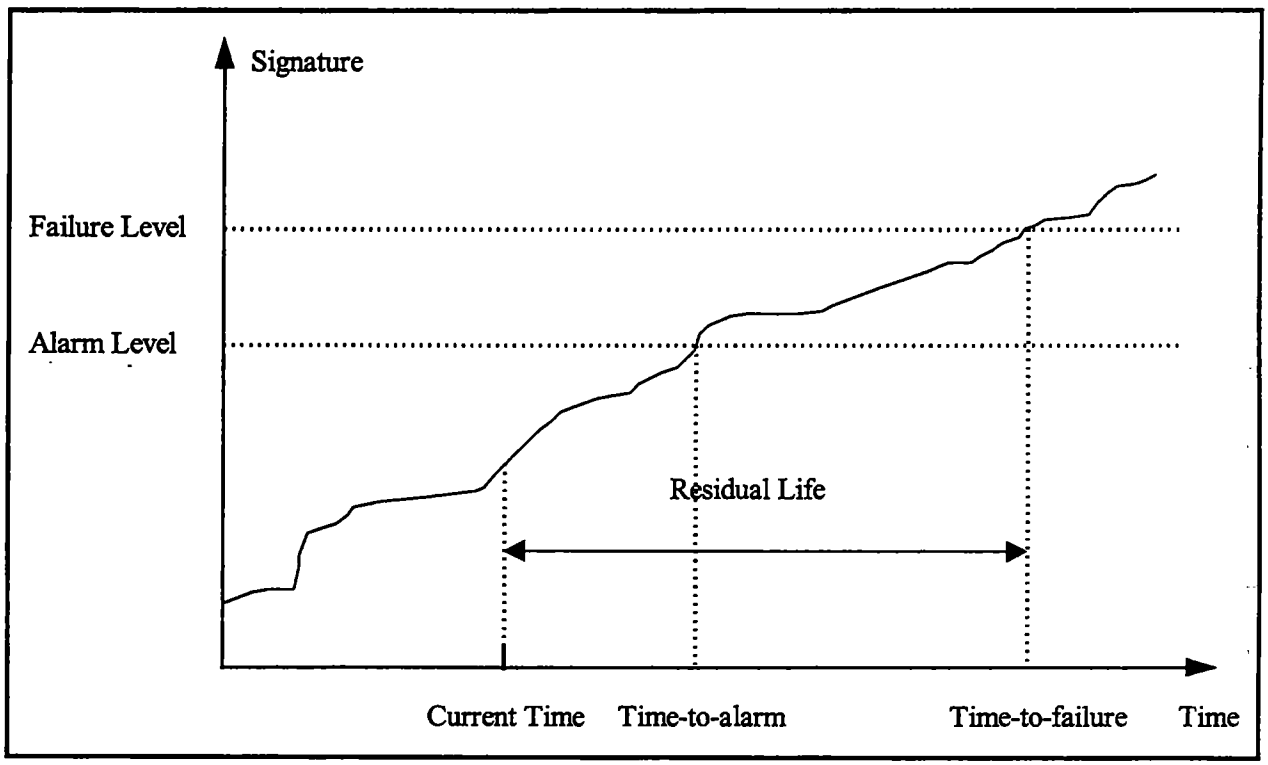


Figure 6.1. Definition of various degradation and performance parameters.

6.3 Dynamic Prediction

Regression Models

In this approach, the current life of the component is expressed as a linear combination of the present and some previous resistance measurements. This model (Figure 6.2) is given by

$$L(k) = \sum_{i=0}^{n} \beta_i R(k-i) + \varepsilon(k)$$

$$L(k) = \beta_0 R(k) + \beta_1 R(k-1) + \ldots + \beta_n R(k-n) + \varepsilon(k) \tag{6.1}$$

where *L(k)* is the lifetime of RTD at time step *k*, *R* is resistance, ε is the random error, *n* is the model order, and $\{\beta_i\}$ are model coefficients.

This model may then be used to predict the next resistance value using the measurements, along with the lifetime as in the following expression.

$$\hat{R}(k) = \frac{1}{\beta_0}\{L(k) - \beta_1 R(k-1) - \beta_2 R(k-2) - \ldots - \beta_n R(k-n)\} \tag{6.2}$$

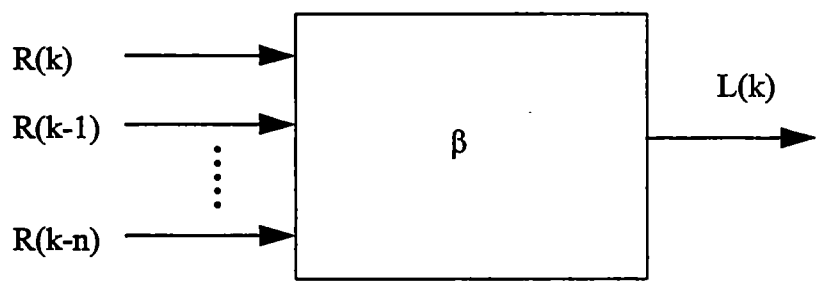


Figure 6.2. Regression model diagram.

6.4 Static Prediction

Initial testing of the wire-wound RTDs indicated that the resistance behavior of these RTDs shows a monotonically increasing trend that may be modeled by a linear relationship. This form of modeling is not only suitable for data fitting, but also a very effective approach for predicting future values. This method is very effective in extrapolating to alarm and failure limits. The modeling should be performed in a piecewise manner. If dynamic models that incorporate one-step-ahead or multi-step-ahead predictions are used, only the next step or next few steps may be estimated since future measurements are not available. Using the estimated values recursively for measured values is an alternative to dynamic models, however this decreases the quality of the answer since the error will be accumulated at each step.

The form of the piecewise linear model that uses only resistance is defined as

$$R(t) = \alpha t + \beta + \varepsilon \tag{6.3}$$

where t is the total lifetime (from the start of test), $R(t)$ is the resistance measurement at time t, α is the slope of the line, β is the intercept of the line, and ε is the random measurement error. Routine least-squares method is used for fitting slope and intercept. The model is used for estimation and has the form

$$\hat{R}(t) = \hat{\alpha} t + \hat{\beta} \tag{6.4}$$

where the "hat" denotes an estimated parameter or variable.

Model fitting and life estimation were performed daily, by shifting the data window. First a window size for fitting the model is established through a visual analysis of data. A block of data the size of that window is used to fit the model. This model is used for extrapolation to estimate the time that alarm and failure limits will be reached. This procedure is repeated every day when new data points are available. After fixing the length of the data window, the window is shifted by one day (or by a specified time interval) after acquiring additional data. A new model is fit and is used for extrapolating the resistance values to pre-defined alarm and failure limits. This approach avoids any local variations in the data, thus eliminating bias effects.

The parameters α and β are estimated using a least-square method. Let $\{R(t_i), i = 1, 2, ..., N\}$ be the RTD resistance value, at time instants $\{t_i, i=1, 2, ..., N\}$. The number of points N indicates the data points used in the fit. Estimate α and β such that the criterion function

$$J = \sum_{i=1}^{N} [R(t_i) - \alpha t_i - \beta]^2 \tag{6.5}$$

is minimized. This leads to

$$\frac{\partial J}{\partial \alpha} = 0 \; and \; \frac{\partial J}{\partial \beta} = 0. \tag{6.6}$$

Solving for α and β

$$\hat{\alpha}=\frac{N\sum_{i=1}^{N}R(t_i)t_i-\sum_{i=1}^{N}R_i\sum_{i=1}^{N}t_i}{N\sum_{i=1}^{N}t_i^2-\left(\sum_{i=1}^{N}t_i\right)^2} \tag{6.7}$$

$$\hat{\beta}=\frac{\sum_{i=1}^{N}R_i\sum_{i=1}^{N}t_i^2-\sum_{i=1}^{N}R_it_i\sum_{i=1}^{N}t_i}{N\sum_{i=1}^{N}t_i^2-\left(\sum_{i=1}^{N}t_i\right)^2} \tag{6.8}$$

$\hat{\alpha}$ and $\hat{\beta}$ may be computed very quickly for the given data points. As a result, the computational overhead is minimal for on-line updating of the model and new data becomes available.

Remarks: It is important to note that the data trend may not always be increasing or decreasing. If an increasing trend is expected, then α changes sign, this may indicate a temporary aberration of data and this behavior must be tagged. If both increasing and decreasing trends are expected, then the life prediction routine must extrapolate the trend to appropriate alarm or failure levels (either greater or less than the nominal sensor output).

6.5 Weighted Least-Squares Method for Model Estimation

In order to minimize strong dependence on current data and to improve the robustness of the overall model fit, a large data window could be used with appropriate

weighting. The weighting function is used to "forget" the old data in a systematic fashion. The weighted least-squares criterion is defined as:

$$J=\sum_{i=1}^{N} w_i(R(t_i)-\alpha t_i-\beta)^2 \tag{6.9}$$

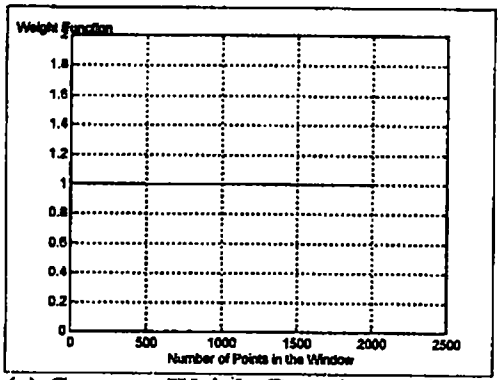
The parameters α and β are estimated such that J is minimized. $\{w_i, _i=1, 2, ..., N\}$ is a sequence of weights and they generally increase in a nondecreasing form. Several examples of weighting functional are shown in Figure 6.3. Starting from the first data point to the current data point these are

1. Constant: $w_i = 1$ for all i.
2. Linear: $w_i = 0$ for i=1

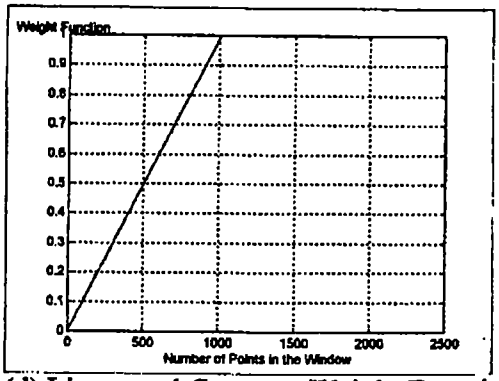
   $w_i = 1$ for i=N
3. Exponential: $w_i = e^{-(N-i)}$
4. Sigmoidal: $w_i = \dfrac{1}{1+e^{-\beta i}}$
5. Semi-sigmoidal (see Figure 6.3(f))
6. Linear and constant

The weighted least-squares minimization gives

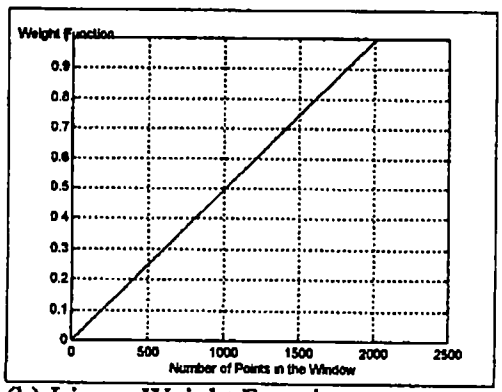
$$\frac{\partial J}{\partial \alpha}=0 \text{ and } \frac{\partial J}{\partial \beta}=0$$



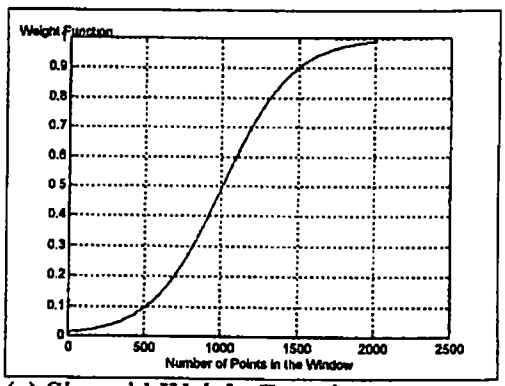
(a) Constant Weight Function (w's = 1)



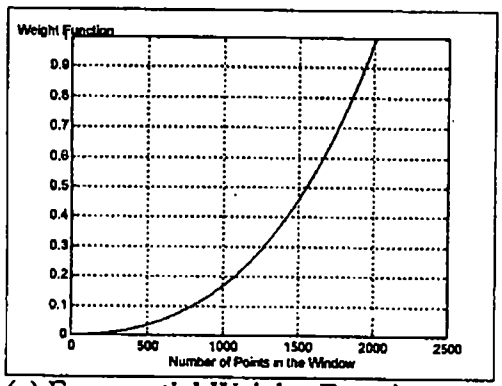
(d) Linear and Constant Weight Functions.



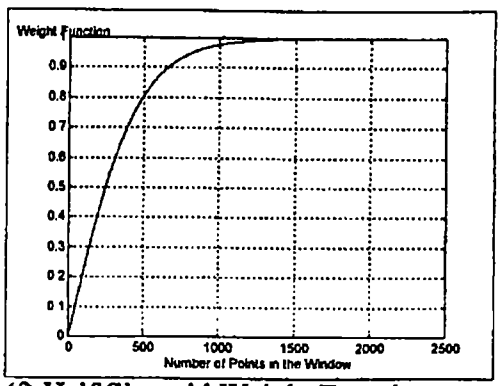
(b) Linear Weight Function.



(e) Sigmoid Weight Function.



(c) Exponential Weights Function.



(f) Half Sigmoid Weight Function.

Figure 6.3. Data window weighting functions w_i used in model development.

Solve for the estimates $\hat{\alpha}$ and $\hat{\beta}$.

$$\hat{\alpha} = \frac{\Sigma w_i R_i t_i - \Sigma w_i t_i \Sigma w_i R_i}{\Sigma w_i t_i^2 \Sigma w_i - (\Sigma w_i t_i)^2} \tag{6.10}$$

$$\hat{\beta} = \frac{\Sigma w_i t_i^2 \Sigma w_i R_i - \Sigma w_i R_i \Sigma w_i t_i}{\Sigma w_i t_i^2 \Sigma w_i - (\Sigma w_i t_i)^2} \tag{6.11}$$

The results of implementing this improved approach are presented in Section 6.8.

6.6 Confidence Analysis of Life Prediction

In any estimation study, the confidence in the results is as important as the results (due to inherent errors in the modeling). Confidence intervals for static regression models are addressed in this section.

If the random error component, ε, in the model (Equation 6.3) is uncorrelated and is distributed normally with mean zero and variance σ^2, then variances of the estimates for the slope and the intercept may be evaluated as follows.

$$\sigma_{\hat{\alpha}}^2 = \frac{\sigma^2}{\sum_{i=1}^{n} (t_i - \bar{t})^2} \tag{6.12}$$

$$\sigma_{\hat{\beta}}^2 = \sigma^2 \left(\frac{1}{n} + \frac{\bar{t}^2}{\sum_{i=1}^{n} (t_i - \bar{t})^2} \right) \tag{6.13}$$

where $\bar{t}$ is the mean time of the regression, n is the total number of points used in regression, and σ^2 is the error variance, which is evaluated using the residual sum of squares,

$$\sigma^2 = \frac{\sum_{i=1}^{n}[R(t) - \hat{R}(t)]^2}{n-1}. \tag{6.14}$$

Then the 99 percent confidence intervals on the estimated slope and intercept may be assessed as

$$\hat{\alpha} \pm c\sigma_{\alpha}^2$$
$$\hat{\beta} \pm c\sigma_{\beta}^2$$

where c is equal to 2.576 from the t-distribution tables. Lower bounds on the slope and intercept are used to obtain a lower curve that is used to evaluate the upper limit for estimated failure time, and upper bounds for the slope and the intercept are used to obtain a lower limit for estimated failure time (Figure 6.4).

This methodology produced unacceptably small confidence intervals. This indicated that the random errors in the resistance measurements are either correlated or not normally distributed. Therefore, an empirical confidence interval method, which is based on the portion of the variance that is not explained by the model, was implemented. In this method, the error standard deviation is evaluated as in Equation (6.14), and three

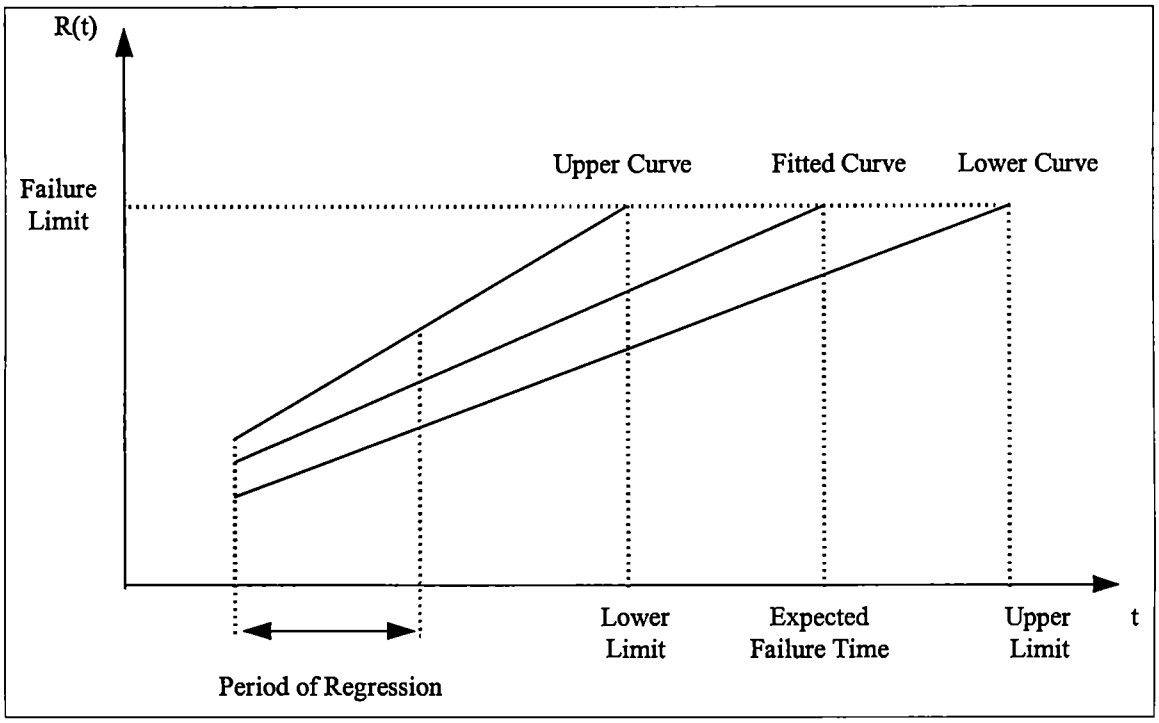


Figure 6.4. Upper and lower failure limits based on the uncertainty in slope and intercept.

times this deviation around the failure limit is used to obtain upper and lower failure time limits (Figure 6.5).

6.7 Determination of Relationships Among RTD Parameters by Correlation Analysis

A simple, first approach for establishing possible relationships among RTD parameters is to calculate correlation coefficients between any two quantities. Some quantities are direct in-situ measurements such as RTD resistance, self-heating index, insulation resistance, etc. Others are calculated parameters and include Callendar-Van Dusen equation parameters such as R_o, α and δ, and rate of change of some of the measurements. An example of the latter is dR/dt, rate of change of RTD resistance.

If a correlation between an externally measured (in-situ) parameter and a calibration parameter is established, then it may be possible to trend the in-situ measurement in lieu of calibration parameters. Such a relationship would result in a significant improvement in monitoring RTD calibration drifts. The correlation coefficient between any two variables $\{X_i\}$ and $\{Y_i\}$ is calculated as

$$\gamma_{xy} = \frac{\sum_{i=1}^{n} (x_i - \bar{x})(y_i - \bar{y})}{\left\{ \sum_{i=1}^{n} (x_i - \bar{x})^2 \sum_{i=1}^{n} (y_i - \bar{y})^2 \right\}^{1/2}} \qquad (6.15)$$

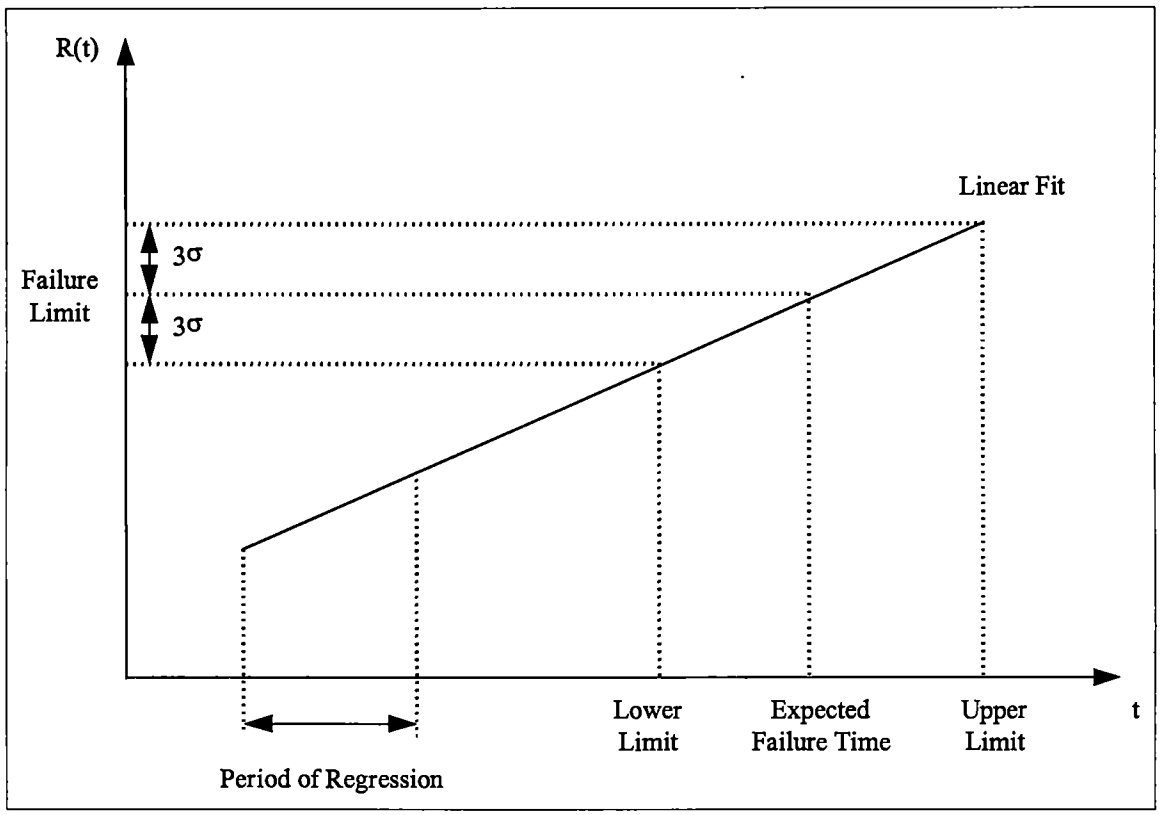


Figure 6.5. Upper and lower failure limits based on residual standard deviation.

where $\bar{x}$ and $\bar{y}$ are mean values of $\{x_i\}$ and $\{y_i\}$, respectively. Generally, $-1 \leq \gamma_{xy} \leq 1$. A value of $\gamma_{xy} = \pm 1$ indicates a direct linear relationship between X and Y of the form

$$y = ax + b \tag{6.16}$$

A value of $|\gamma_{xy}| < 1$ indicates a partial but definite relationship between the two variables. The correlation coefficient can be calculated for a large population of RTDs (static estimation) or can be calculated for the same RTD as a function of time (time-dependent estimation).

The application of this approach is demonstrated in Chapter 10 using the calibration parameter α and the self-heating index. The ultimate goal is to develop a relationship of the form

$$\alpha = f\ (R,\ dR / dt,\ SHI,\ \ldots) \tag{6.17}$$

where α is a function of RTD resistance (R), its rate of change (dR/dt), self-heating index (SHI), and others. A linear equation of the form

$$\alpha = a * (SHI) + b \tag{6.18}$$

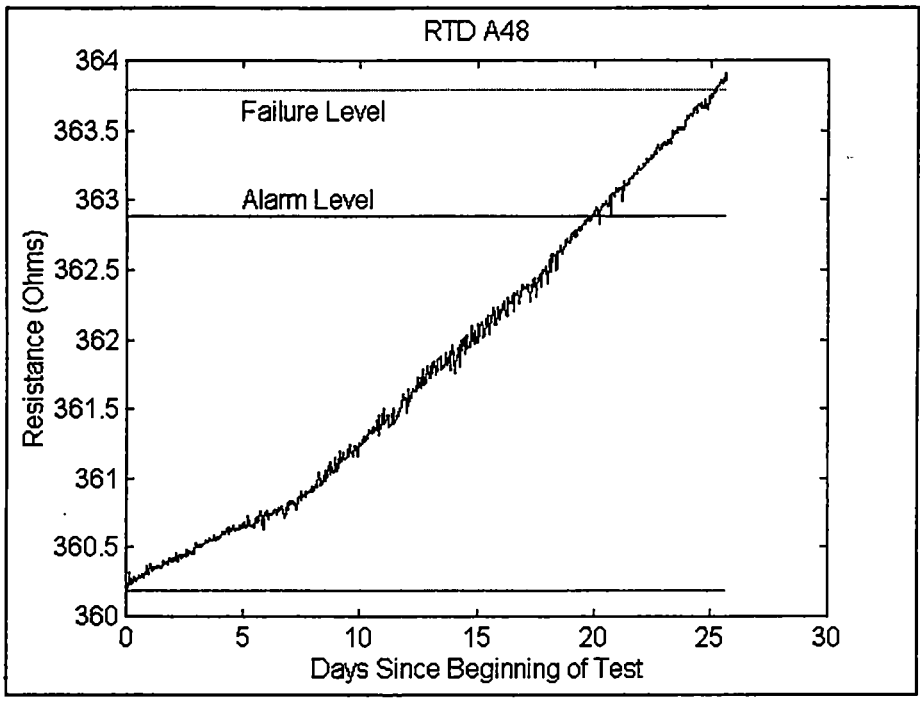
provides an excellent fit to the data for cases when a strong relationship exists between the calibration parameter α and the self-heating index, SHI. This is a more general approach for relating the two variables, because it avoids the bias caused by the mean

value of the variables. If necessary, this linear fit may be generalized to the case of a second order equation.

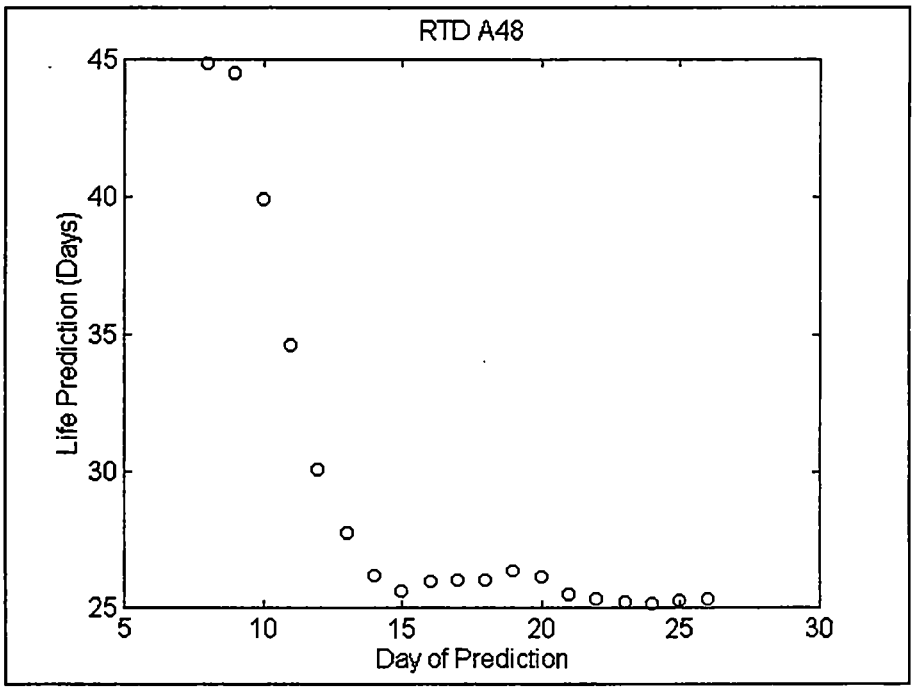
6.8 Results of RTD Life Prediction

A few examples of estimating the lifetime of test RTDs are presented in this section. The life prediction was made using the trends in the measured RTD resistance. There are cases where clear monotonic trends were not seen in the resistance behavior. The prediction was made using a linear regression fit to the resistance data as a function of time. The alarm and failure levels were set arbitrarily at 0.75% and 1.0% of the nominal resistance value at the given temperature. The results from resistance trending of three wire-wound RTDs are presented. A half-sigmoidal window of size 7-days was used in all of the resistance trend fitting.

Figure 6.6a shows a plot of the measured resistance versus time for RTD #A-48 at a furnace temperature of 750 °C. The failure level prediction with time (day of prediction) is shown in Figure 6.6b. The predicted failure time is about 25 days. A behavior seen often in the thermal aging of RTDs is shown in the resistance plot for RTD #A-35, at a temperature of 750 °C (see Figure 6.7a). The resistance, after reaching a maximum value, starts decreasing and shows somewhat an erratic behavior. In this case the trend did not cross the failure level. The life prediction indicates a failure time between 15 and 20 days (Figure 6.7b). It is interesting to note that the resistance trend had reached a maximum in this time interval and had started to decrease. The slope of

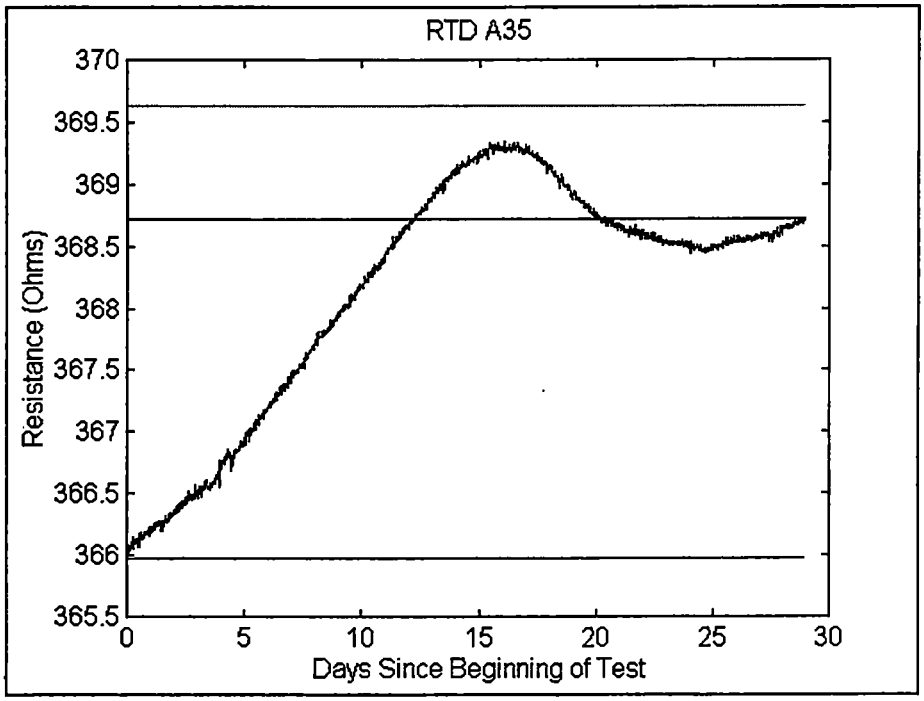


a. Resistance trend of RTD #A-48 (wire-wound) from Furnace #3.

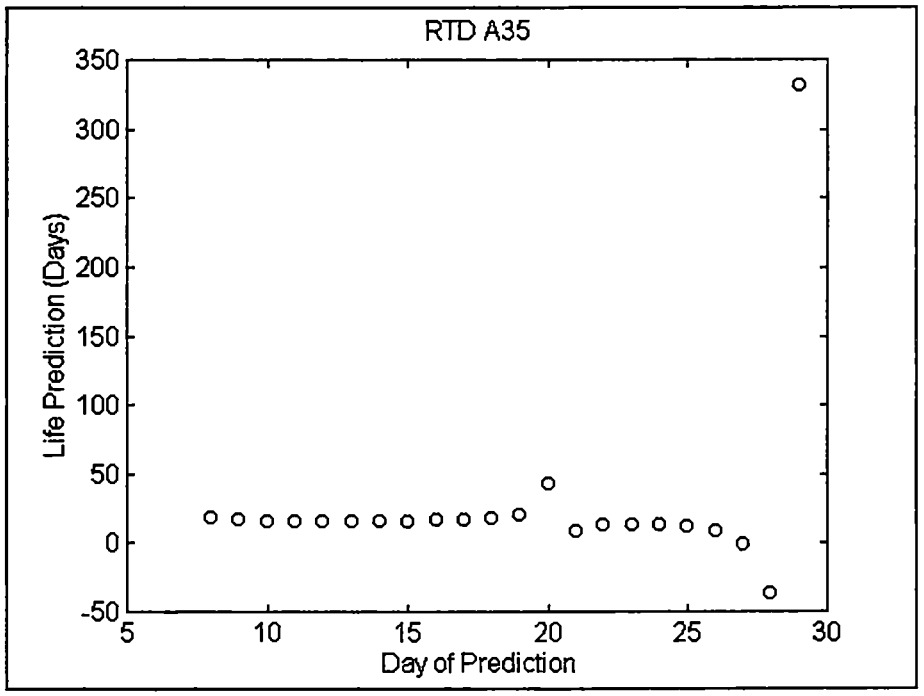


b. Time-to-failure (days) of RTD #A-48 (wire-wound) as a function of prediction point, using 7-day data window.

Figure 6.6 Resistance trend and time-to-failure plot for RTD #A-48 from Furnace #3.



a. Resistance trend of RTD #A-35 (wire-wound) from Furnace #3.



b. Time-to-failure (days) of RTD #A-35 (wire-wound) as a function of prediction point, using 7-day data window.

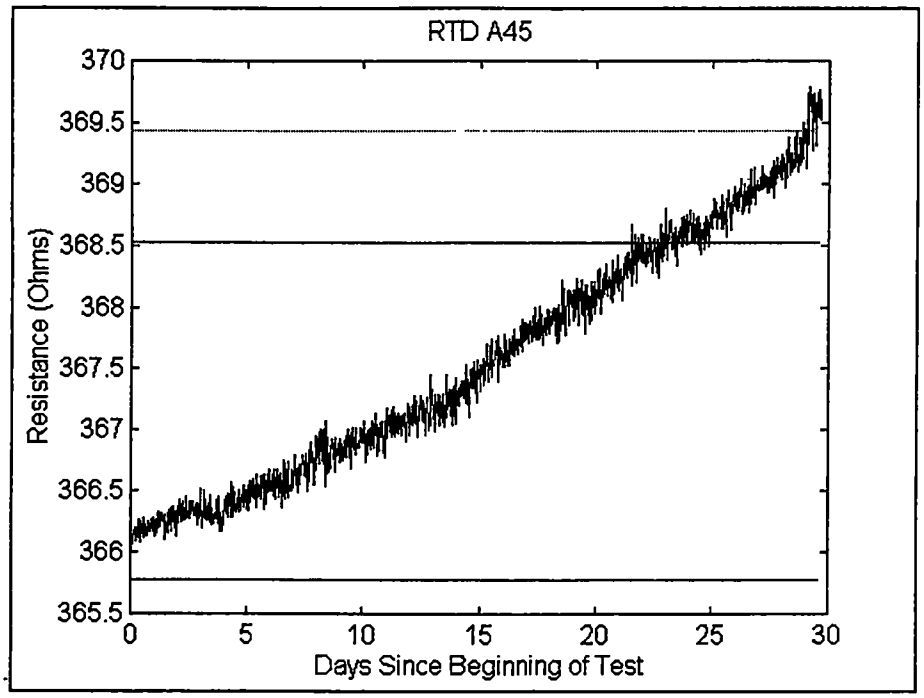
Figure 6.7 Resistance trend and time-to-failure plot for RTD #A-35 from Furnace #3.

the linear fit becomes negative at a certain point and life prediction has no real meaning beyond this value. When an RTD shows this form of behavior the RTD is considered as failed and no longer functional. Another example of resistance trending and life prediction is shown in Figures 6.8a and 6.8b for RTD #A-45. This RTD exhibits a higher noise level, but the life prediction is consistent. Table 6.1 summarizes the values presented in those Figures.

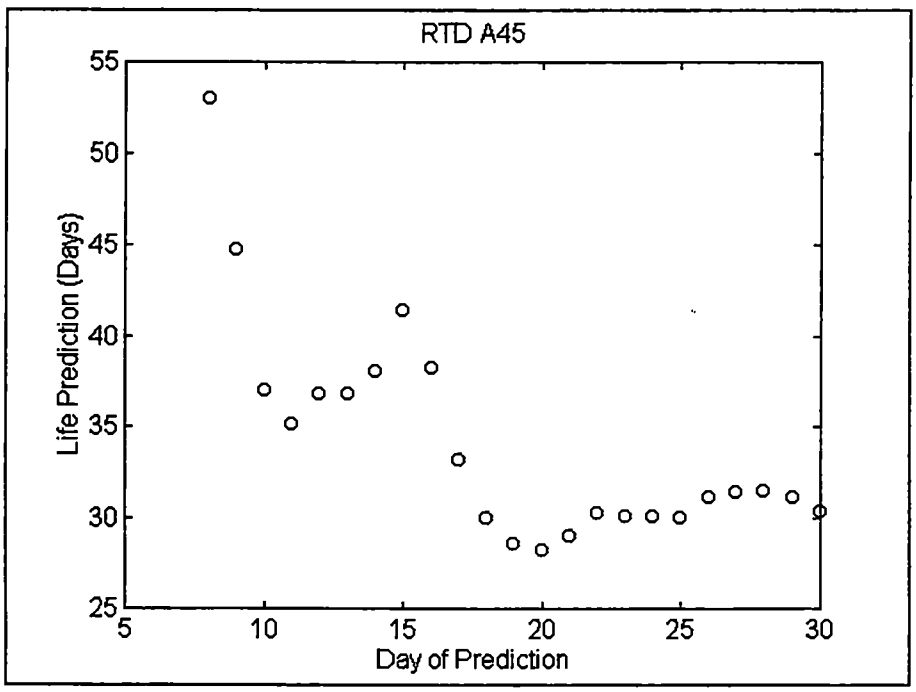
Table 6.1. Summary of RTD life prediction obtained for RTDs #A-48, #A-35 and #A-45.

RTD Number	Life Prediction Time	Confidence Interval	Starting failure day
RTD #A-48	25.2	24.6 – 25.8	25.1
RTD #A-35	15.9	15.7 – 16.1	15.8
RTD #A-45	31.1	29.4 – 32.8	29.5

All of the three case studies indicate that the measured resistance may be used to estimate the remaining useful life of these RTDs, and detect their decalibration even when the resistance-time trend is not monotonic. The self-heating index shows a systematic and continuous trend from the start of the thermal aging (presented later in Chapters 9 and 10), with its trend increasing at higher temperatures. This parameter may also be considered as a possible candidate for life prediction of RTDs. It has been noted that in



a. Resistance trend of RTD #A-45 (wire-wound) from Furnace #3.



b. Time-to-failure (days) of RTD #A-45 (wire-wound) as a function of prediction point, using 7-day data window.

Figure 6.8 Resistance trend and time-to-failure plot for RTD #A-45 from Furnace #3.

cases where the measured resistance remains unchanged, the self-heating index changes steadily.

It should also be noted that the self-heating index parameter seems to show a systematic and continuous trend from the beginning of thermal aging, with its trend increasing at higher temperatures. This parameter may be considered as a possible candidate for life prediction of RTDs. It has been observed that in cases where the measured resistance remains unchanged, the self-heating index changes steadily.

CHAPTER 7

SUMMARY OF RTD THERMAL AGING STUDIES

7.1 Introduction

This chapter presents the results from all of the long-term thermal aging tests performed on wire-wound type and thin film type RTDs. The results from these studies include the large database constructed from the recorded thermal aging data, observations about each individual test and comparisons between tests. The database is an assembly of the individual resistance measurements taken periodically for each RTD during each test. This database information consists of the data recorded during ten individual tests performed using the five furnaces and laboratory equipment described in Chapter 3.

7.2 Tabular Summary of Ten Experimental Tests

The ten individual experiments that have been conducted in support of this research effort are summarized in Table 7.1. The RTD unique identifiers signify wire wound construction if they begin with A and thin film construction if they begin with B. The plots of all the RTD resistance measurements are presented in Appendix A, Figures A.1 – A.36.

The test types presented in the table include soak, maximum temperature, thermal cycling and vibration. A soak test is a constant temperature soak where the RTDs are tested at a single temperature level or several constant temperature steps. A maximum

Table 7.1 Summary of RTD Thermal Aging Tests

Test Number	RTD List	Furnace Number	Temperature History	Test Duration (days)	Test Type
1	A1-A8	OR-1	660	57	Soak
2	A9-A20	ATS-1	660	98	Soak
3	A21-A32	ATS-2	660	122	Soak
4	A33-A49	ATS-3	660, 700, 725, 750, 775, 800 & 850	525	Soak
5	A50-A60	ATS-1	500	151	Soak
6	A50-A64, B12-B15	ATS-1	600, 700, 800 & 900	52	Maximum Temperature
7	B1-B11	ATS-2	400, 450, 500, 525, 550, 575, 600 & 625	441	Soak
8	A65-A70, A204-A213 & B38-B40	ATS-4	550, 575, & 600	273	Soak
9	A71-A89	ATS-1	500-700, 550-750, & 575-775	223	Thermal cycling
10	A199	OR-2	450	326	Vibration

temperature test includes rapid step increases in temperature to determine maximum usable RTD temperature. A thermal cycling test approximates more closely a process in which the temperature varies over a 200°C range in approximately 9 hours. The vibration test approximates more closely a process in which the sensor sees constant vibration throughout testing; the induced vibration maintained approximately 3.5g and 100 Hz.

7.3 General Comments about Furnace History Plots

General features appearing in all plots:

Sudden jumps or 'spikes', caused by physical movement of individual RTD being tested, by other RTDs being removed from bath causing a temperature transient, or by data acquisition equipment changes, appear as sudden skips between two or more consecutively recorded data points. These can be either increases or decreases.

Heatup/temperature increase curve, caused by the slower heatup rate of the equalizing block in each furnace, appears as a slope at the beginning of each temperature step increase.

Both of these features are evident in Figure 7.1.

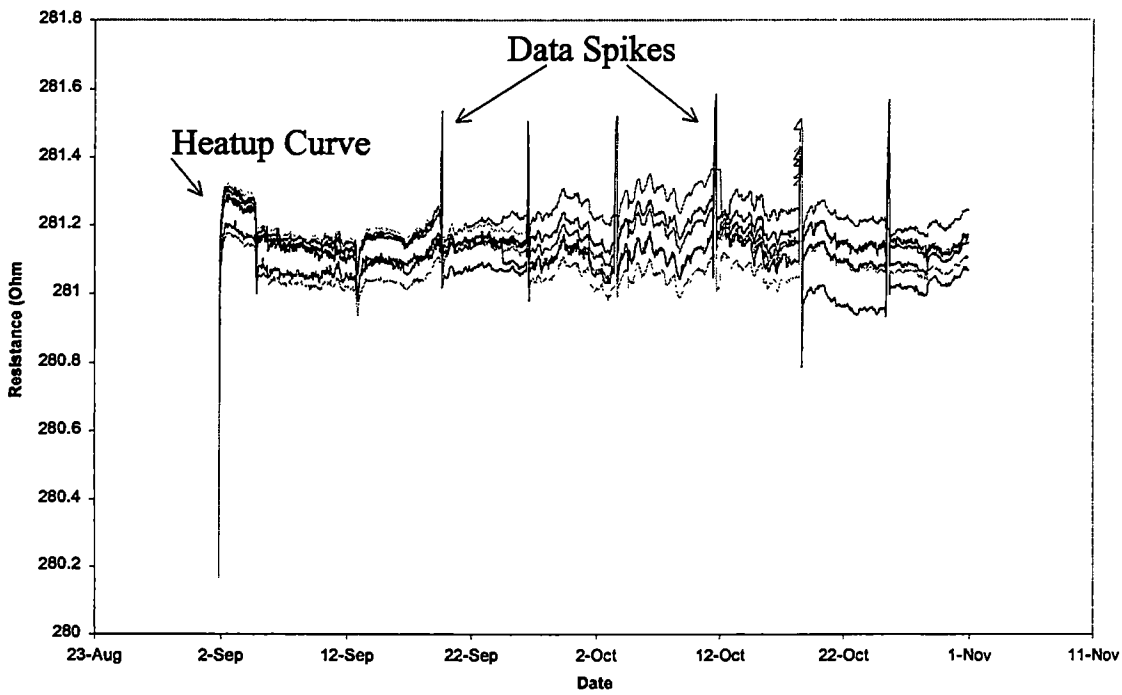


Figure 7.1 Plot of RTDs Exhibiting General Features

7.3.1 General Comments About Test #1 {Figure A-1}

Test #1 was performed on wire-wound RTDs in a horizontal tube furnace on loan to the project from Oak Ridge National Laboratory. The temperature setting was 660°C. During the 57 days of the test one RTD began drifting early. Around the middle of the test the majority of the RTDs began a general upward resistance drift behavior. Near the end of the test duration a second RTD drifted away from the general RTD population.

7.3.2 General Comments About Test #2 {Figure A-2}

Test #2 was performed in the vertical ATS furnace #1 on wire-wound RTDs. The temperature setting was 660°C. During the 98 days of testing all of the RTDs in this furnace exhibited some resistance drift. Initially, the RTDs in test #2 showed an increase in the resistance with time. This characteristic changed after about 30 days into the test and the majority of the RTDs either leveled off or began decreasing. Due to factors external to the test, namely changes in the data acquisition system, there were notable jumps in the data just before the decreases in the resistance initiated. This raises an unanswerable question about the cause of the decreases in resistance. In support of the decreases being natural phenomenon and not all due to data acquisition system changes, two observations must be pointed out. Several RTDs did not begin to decrease until almost a month after the data acquisition system changes. One RTD had absolutely no change in slope and continued to increase throughout the timeframe the other RTDs decreased.

7.3.3 General Comments About Test #3 {Figure A-3}

Test #3 was performed in ATS furnace #2 on wire-wound RTDs. The temperature setting was 660°C. During the 122 days of testing the RTDs showed a mixed behavior of increasing and decreasing resistances, with the final behavior showing stable RTD resistance values.

7.3.4 General Comments About Test #4 {Figures A-4 to A-11}

Test #4 was performed in ATS furnace #3 on wire-wound RTDs. The temperature setting was initially 660°C. During the two hundred and eighty days of testing at 660°C an appreciable drift was noted in only one RTD. The next temperature was achieved by a step increase to 700°C. During the forty-seven days of testing at 700°C, in addition to the single RTD noted as drifting previously, one RTD began drifting above the majority of RTDs. The next temperature step was to 725°C. During the fifty-one days at this stable temperature, the two RTDs previously drifting continued to drift and an additional RTD started showing a similar behavior. The next temperature step was to 750°C. During the thirty-two days at this temperature no new RTDs appreciably began drifting, but of the three already drifting one showed a significant increase in drift rate surpassing the resistance value of the RTD that began drifting first at 660°C. The next temperature step was to 775°C. During the sixty-two days at this temperature setting all of the RTDs in the furnace exhibited some amount of drift. Many of the RTDs, at random intervals, began reproducing the negative drift rate previously seen in Test #2. The next temperature step was to 800°C. During the thirty-five days at this temperature

setting all of the remaining RTDs initially followed the behavior they exhibited in the previous step. One of the RTDs began to show the decrease in resistance value after increasing for a considerable length of time. It is important to note that all of the RTDs previously showing the negative drift rate continue that behavior even after a step change in temperature. This temperature step supports that the RTDs do not return to a positive drift rate once they have initiated a negative drift rate. The last test temperature was 850°C. The duration of this test was 19 days. At this temperature further examples of initiation of drift and negative drift can be observed.

7.3.5 General Comments About Test #5 {Figure A-12}

Test #5 was performed in ATS furnace #1. This test was conducted on wire-wound RTDs at 500°C. The duration of the test was 151 days. There was not an appreciable drift seen in any of the RTDs from this test. The RTDs did exhibit some spread from the initial closeness of all of the resistance values, but nothing significant enough to label as appreciable drift.

7.3.6 General Comments About Test #6 {Figures A-13 to A-17}

Test #6 was performed in ATS furnace #1. This test was conducted on wire-wound and thin film RTDs at initially 600°C. During the seven days at the 600°C temperature setting the four thin film RTDs exhibited extreme positive drift. The next chosen temperature step was 700°C. During the three days at this temperature, the thin film RTDs continued to drift, two continuing positive drift and two initiating a negative

drift which inexplicably recovered to a positive drift. Also at the 700°C temperature setting the wire-wound RTDs began to show some spread in their values. The next temperature step was to 800°C. During the four days at this temperature the thin film RTDs failed catastrophically by the measurement circuit opening. The wire-wound RTDs at this temperature began to appreciably drift. The next temperature step was to 900°C. During the thirty-three days at this temperature all of the RTDs exhibited extreme drift rates, many ending in a catastrophic failure. Several of the RTDs experienced sudden downward drops in resistance possibly associated with short-circuiting of the RTD windings. Several of the RTDs continued to have resistance reading throughout the duration of the testing but these readings became as extreme as a 1000 Ohm resistance reading.

7.3.7 General Comments About Test #7 {Figures A-18 to A-26}

Test #7 was performed in ATS furnace #2 on thin film RTDs. The initial temperature set point was 400°C. For the one hundred and ninety-three day duration at 400°C there is no visible drift rate to be reported. The next temperature step to 450°C, which had a duration of forty-nine days, similarly has no visible drift rate to report. The next temperature step to 500°C, for a duration of twenty-one days, finds the RTDs beginning to spread without appreciable drift. The next temperature step of 525°C was maintained for nineteen days. At 525°C all of the RTDs begin a general increasing drift rate. Three of the RTDs separate and show appreciable drift. During the seventy-four days at the next temperature step of 550°C, the three already drifting RTDs continue to

drift. Those RTDs are then joined by a fourth RTD that surpasses their high resistance readings. The next temperature step is to 575°C for a duration of thirty-one days. At this temperature all of the RTDs are greatly spread apart and most exhibit some increment of drift. Two of the RTDs show the negative turn in their drift rate. The next temperature setting of 600°C, for thirty-three days, shows the two negative drift rates continue, many positive drift rates increase and many new negative drift rates initiate. The final temperature setting of 625°C, maintained for nineteen days, shows many of the same behaviors as the previous temperature setting with both increasing and decreasing drift rates present.

7.3.8 General Comments About Test #8 {Figures A-27 to A-30}

Test #8 was performed in ATS furnace #4 on thin film and wire wound RTDs. The initial test temperature setting was 550°C. This temperature was maintained for one hundred and sixty days. This temperature allowed for the appreciable positive drift of the three thin film RTDs. The gaps in the data are associated with the sending of these RTDs for additional testing. The second test temperature setting was 575°C for a duration of forty-four days. Similarly, here the thin film RTDs continued to drift and the wire-wound RTDs did not. The third test temperature setting was 600°C for a duration of fifty-two days. At this temperature the thin film RTDs began to show the negative drift rate after only a few days of continued testing. The wire-wound RTDs at this temperature still remain without appreciable drift.

7.3.9 General Comments About Test #9 {Figures A-31 to A-34}

Test #9 was performed in ATS furnace #1 on wire-wound RTDs. The test is not a thermal soak or constant temperature test, this test is a temperature cycling or process simulation test. This initial test cycled between 500°C and 700°C. This temperature range for the duration of seventy-three days showed a noticeable amount of drift in only a few of the RTDs. The second temperature range tested was from 550°C to 750°C. This test, for its duration of forty-one days produced drift in several RTDs, one RTD to the point of a catastrophic failure. Figure 7.2 shows this segment of the testing, including the failure of the drifting RTD. The third test temperature range was set for 575°C to 775°C. This test had a duration of eighty-three days. This test temperature range did not produce any additional catastrophic failures but has produced appreciable drift in many of the test RTDs.

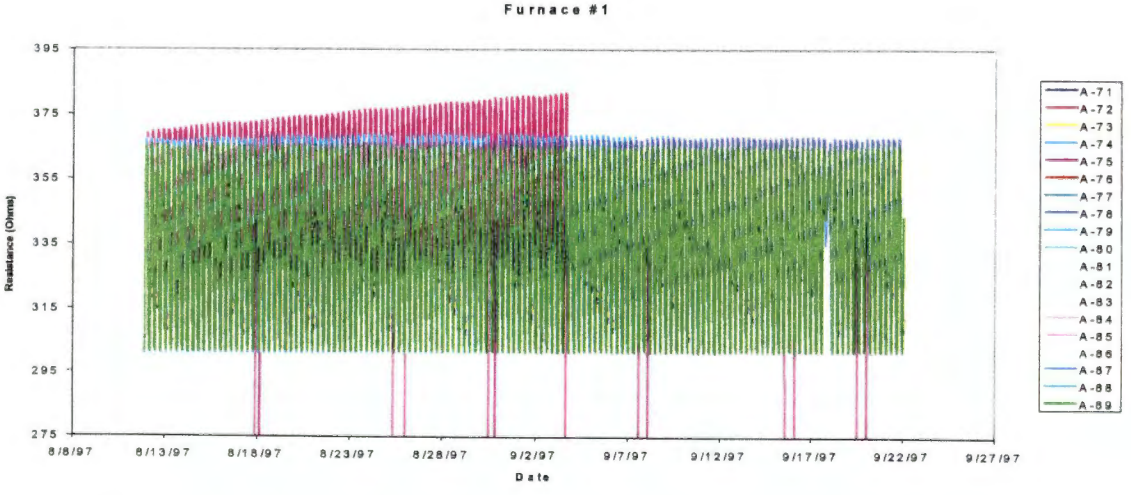


Figure 7.2 Thermal Cycling at 550-750 °C showing RTD Failure

7.3.10 General Comments About Test #10 {Figure A-35}

Test #10 was performed in a tubular furnace previously acquired by The University of Tennessee. This test was designed to monitor the effect of vibration on the resistance drift of an RTD. The vibration induced in the RTD was at a frequency of 100 Hz with an RMS vertical displacement of 0.3 mm. The test temperature was 450°C and a single wire-wound RTD was connected to the vibration equipment for testing. This test showed no appreciable drift in the RTD over the 326 days duration of the test.

7.3.11 General Comments About All Tests

In this study two of the tests were to approximate process changes and the effects on the RTDs. These two tests were the vibration test and the thermal cycling test. In comparison the vibration test, though limited in scope, did not induce additional drift beyond what was seen in similar constant thermal soak tests. The thermal cycling test by contrast showed much faster drift initiation and failure of drifting RTDs. This shows that for the RTDs tested, the process changes in temperature are much more difficult on the sensors than the process vibration that was induced in this project.

The thermal soak tests, though each different in temperature, time and application, had certain general behaviors that should be presented. The general behavior seen in all of the tests can very readily be described but not as easily explained. These are the observations related to the RTD behavior during the long-term thermal aging tests.

Initially, once a suitably high enough temperature is reached, a very limited number of sensors begin to drift. The RTDs were all received in batches of five RTDs at one-week intervals. This helped to insure a single manufacturing defect would not skew the study results. There was not a pattern visible in the tests related to the early drifts that show any manufacturing group defect. The initial drift appears to be random, in that, the early drifts might indicate a single sensor problem or defect.

The next observation is that at some point for all of the RTD groups there appeared to be a burn in time over which the RTDs did not appear to appreciable drift but settle out into a more spread out pattern. This spread occurred in each of the test. This spread appears to be attributable to an internal equalization process that is occurring in the RTDs.

After a considerable amount of time or increase in temperature the majority group of RTDs began to drift. Since this is occurring in the majority of the population at similar time or temperature frames, it again appears to be a change in the internal RTD. These drifts, in contrast to the individual RTDs described earlier, appear to affect the group within reason as a whole. This would then lead to the questions of what is internally affecting the RTDs. Unfortunately any destructive analysis of the RTDs was beyond the scope, and budget, of this project.

The final comment is related to the decreases noted in several of the tests. This decrease, though initially believed to be an operator error, appears to be significant in the behavior of the RTDs. Several of the RTDs experienced this decrease at similar time and temperature settings and others just prior to catastrophic failure. Again, this decrease in several RTDs at similar time or temperature frames would obviously indicate an internal change in the RTD. Due to the confines of this research, this could not be completely investigated but rightly deserves future study.

CHAPTER 8

SUMMARY OF DRIFT RATE CALCULATIONS

8.1 Introduction

This chapter presents the results of the drift rate calculations. The results in this chapter will be presented as the drift rates of individual RTDs at various temperatures and at different levels of degradation. The degradations are described by the actual numerical drift rate value and a description of the RTD condition related to the initiation or continuation of drift and the temperature level at which that drift occurred. The Arrhenius relationship is used to represent the drift rate as a function of temperature (K) and comparison with other IPRTs and other test results.

8.2 Description of Drift Rate Calculations

The drift rate of each individual RTD is calculated by determining the slope of the consecutive resistance measurements versus time. For analysis, the individual furnace and test data files are divided into temperature set point subsections. The data from each RTD at each temperature set point is analyzed, and from observation, the RTDs with appreciable drift are noted. The remainder of test RTDs are evaluated for a general drift rate value. The notably drifting RTDs are then analyzed and continuation of drift or the initial point of drift are determined. For the RTDs continuing previously initiated drift, the rate is calculated and compared to previous values. For the RTDs initiating drift the data set to be analyzed is reduced to remove values prior to the initial point of drift. From

this initial point of drift to the end of the temperature set, the drift rate is calculated and recorded. At extreme temperatures, drift in individual RTDs is also evaluated for negative drift rate components. The sections of negative drift after the failure of the sensor are removed prior to the calculation of the continuing drift rate. When the drift became completely negative the negative drift rate was recorded.

8.3 Sample Drift Rate Calculation Results

Table 8.1 presents drift rate calculation results for selected test RTDs. The RTDs presented are from Test #4. The RTDs are all wire-wound RTDs and have been tested in furnace #3 for the total duration of the test. The drift rates are presented in units of Ohms per 1000 hours. The drift rates at the initiation of drift seem to be distinct for each individual RTD. As can be seen in RTD A-44 the drift rates generally increase as time and temperature increase. RTD A-47 shows another common behavior characteristic that a decrease in the positive drift rate occurs just prior to the initiation of a negative drift rate. RTDs A-48 and A-49 were removed from the test furnace prior to the 800 °C temperature set point. Table 8.2 provides a summary of average drift rates per temperature. Tables 8.3 through 8.6 provide average drift rates per RTD condition description. The full statistics of the drift rates are provided in the tables in Appendix C.

The general observations that seem to be common to the majority of the RTDs tested include the following. The initiation of drift is apparently a product of manufacturing anomalies due to the fact it is individual to each RTD. Initially a few

Table 8.1 Sample Drift Rate Calculation Values

Temperature ☆	A-44 *	A-47 *	A-48 *	A-49 *
660	7.900	(2.309)	(3.463)	(2.338)
700	8.181	(1.147)	(1.897)	(-0.170)
725	19.100	27.388	38.385	(1.531)
750	29.831	19.221	152.383	22.448
775	53.386	-44.121	233.466	58.347
800	75.571	-42.436	N/A	N/A

☆ Temperature in degree Celsius

* Drift Rate in Ohms per 1000 hours

Table 8.2 Summary of Average Drift Rates per Temperature

All RTD Drift:	
Temperature in °C	Drift Rate in Ohms per 1000 hours
400	-0.86943
450	-1.52033
500	-2.35019
525	11.2957
550	6.442786
575	16.00431
600	65.33487
625	48.33636
660	25.57034
700	293.7146
725	7.024921
750	16.9936
775	44.4329
800	13269.03
850	132.3701
900	10789.98

Table 8.3 Summary of Minimal Drift Rates per Temperature and RTD Type

Average RTD Drift:			
wire-wound		thin film	
Temperature in °C	Drift Rate in Ohms per 1000 hours	Temperature in °C	Drift Rate in Ohms per 1000 hours
400	N/A	400	-0.86943
450	0.813803	450	-1.73252
500	0.000291	500	-4.70067
525	N/A	525	2.457466
550	0.069555	550	1.875956
575	9.193385	575	-0.89321
600	-2.18737	600	-0.45689
625	N/A	625	10.93456
660	3.300392	660	N/A
700	-0.6543	700	N/A
725	1.972601	725	N/A
750	3.708025	750	N/A
775	6.176005	775	N/A
800	N/A	800	N/A
850	N/A	850	N/A
900	N/A	900	N/A

Table 8.4 Summary of Increasing Drift Rates per Temperature and RTD Type

Increasing Drift:			
wire-wound		thin film	
Temperature in °C	Drift Rate in Ohms per 1000 hours	Temperature in °C	Drift Rate in Ohms per 1000 hours
400	N/A	400	N/A
450	N/A	450	N/A
500	N/A	500	N/A
525	N/A	525	11.13743
550	N/A	550	10.4879
575	N/A	575	8.658282
600	N/A	600	10.24985
625	N/A	625	N/A
660	9.532075	660	N/A
700	8.180523	700	N/A
725	8.906921	725	N/A
750	9.309536	750	N/A
775	11.78363	775	N/A
800	11.55803	800	N/A
850	36.28622	850	N/A
900	N/A	900	N/A

Table 8.5 Summary of Appreciable Drift Rates per Temperature and RTD Type

Appreciable Drifts:			
wire-wound		thin film	
Temperature in °C	Drift Rate in Ohms per 1000 hours	Temperature in °C	Drift Rate in Ohms per 1000 hours
400	N/A	400	N/A
450	N/A	450	N/A
500	N/A	500	N/A
525	N/A	525	29.36785
550	N/A	550	223.6137
575	N/A	575	72.39249
600	N/A	600	378.5553
625	N/A	625	25.7994
660	59.74948	660	N/A
700	64.41923	700	2402.432
725	28.29097	725	N/A
750	68.22048	750	N/A
775	54.92619	775	N/A
800	3115.421	800	N/A
850	422.9434	850	N/A
900	2137.122	900	N/A

Table 8.6 Summary of Failure Drift Rates per Temperature and RTD Type

Failure Drifts:			
wire-wound		thin film	
Temperature in °C	Drift Rate in Ohms per 1000 hours	Temperature in °C	Drift Rate in Ohms per 1000 hours
400	N/A	400	N/A
450	N/A	450	N/A
500	N/A	500	N/A
525	N/A	525	N/A
550	N/A	550	13.59108
575	N/A	575	30.1958
600	N/A	600	221.3551
625	N/A	625	N/A
660	N/A	660	N/A
700	N/A	700	N/A
725	N/A	725	N/A
750	19.22083	750	N/A
775	131.1899	775	N/A
800	82.17953	800	97721.05
850	N/A	850	N/A
900	13936.48	900	N/A

RTDs would begin to drift while the majority stays in a larger group with minimal, if any, drift. Once drift initiates it was not observed to stop or reverse throughout the remaining RTD life. In general the RTD drift increased with temperature as well as additional RTDs initiating drift. At the apparent end of RTD useful life an initiation of a negative drift rate often occurred. A slight decrease in positive drift rate was seen in several RTDs just prior to this initiation of negative drift. For all practical purposes no RTDs recovered from the initiation of the negative drift rate, and several opened, or had a physical failure, shortly following the initiation of negative drift rate.

8.4 Arrhenius Relationship Results

Savante August Arrhenius found that the rate of many chemical reactions as a function of temperature could be expressed by a relationship [2]. The Arrhenius relationship, though initially applied to chemical reaction rates, is an interesting tool for examining changes in organic materials brought about by thermal stresses. The Arrhenius rate equation is as follows:

$$\text{Rate of Reaction} = Ce^{-Q/RT} \tag{8.1}$$

where

Q = activation energy, J/mol or cal/mol

R = molar gas constant

= 8.314 J/(mol·K) or 1.987 cal/(mol·K)

T = temperature, K

C = rate constant, independent of temperature.[2]

This equation is translated into a simplified form applicable to RTDs:

$$\text{Rate} = Ae^{-B/T} \tag{8.2}$$

where

A and B = constants

Rate = rate of change of chosen monitored characteristic.

By taking the logarithm (base 10) of equation (8.2) it becomes [12]

$$\log(\text{Rate}) = a_o - b_o/T. \tag{8.3}$$

It is assumed that $a_o = 0$ and $b_o = -1$, therefore the equation becomes

$$\log(\text{Resistance Change/Time}) = 1/T. \tag{8.4}$$

Equation (8.4) was used in the Arrhenius evaluation of the experimentally determined drift rates. The Resistance Change/Time is represented as the drift rate, or change in resistance (Ohms) per 1000 hours. The T, or Temperature is the temperature at which the drift rate was recorded in Kelvin. Figure 8.1 is a plot of the Arrhenius relationship results for all of the RTD drift witnessed during this research. In figure 8.1, the individual points are the Arrhenius calculated points for the average drift rate calculated at a given temperature. The line has been fitted to the individual data points to represent the trend in the recorded data.

Further breakdown of the Arrhenius relationship for RTD drift rate was completed. The drift rate data was divided by RTD type and level of RTD drift. The

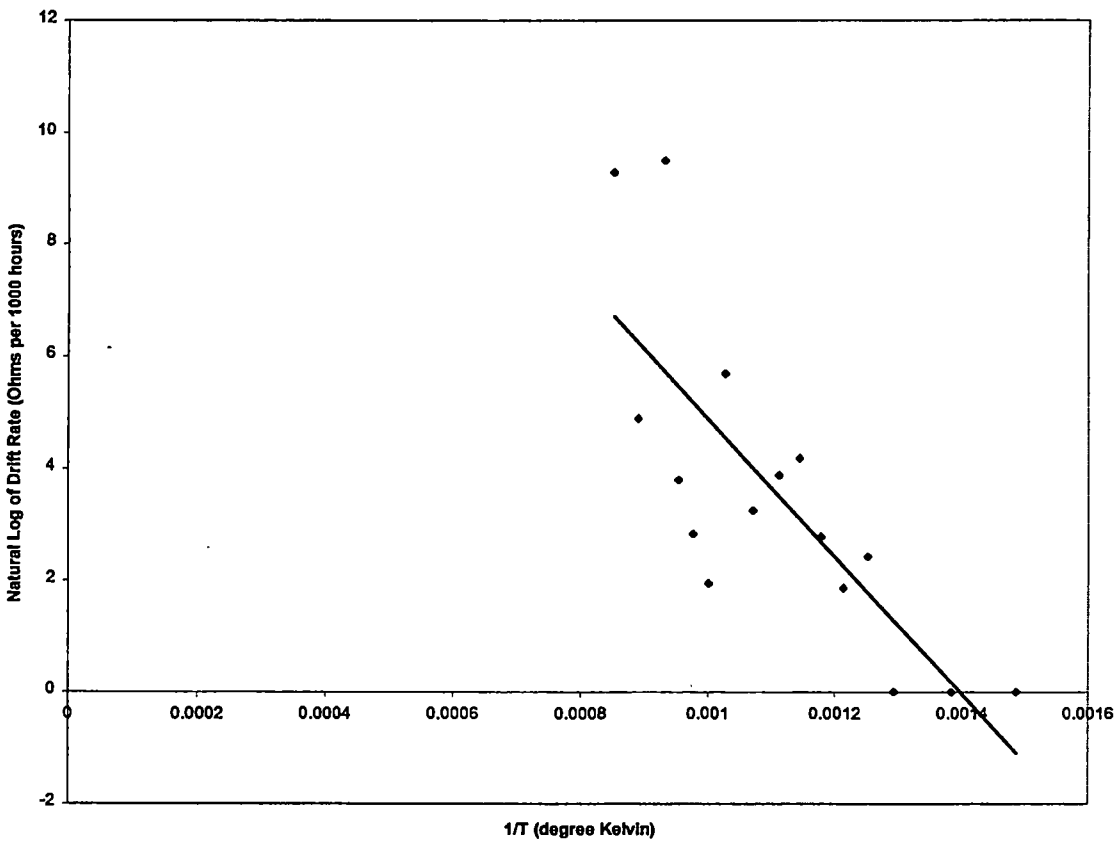


Figure 8.1. Arrhenius relationship plot for all recorded drift rates.

divided data sets were then analyzed using the Arrhenius relationship. Figure 8.2 shows the results of this analysis. The results appear to be grouped more by RTD type than by amount of drift. This apparent RTD type grouping would be expected since the chemical mechanism of degradation would be more type specific.

Linear line fits were also completed for the data groupings in Figure 8.2. The slope of each of the fitted lines is provided in Table 8.7.

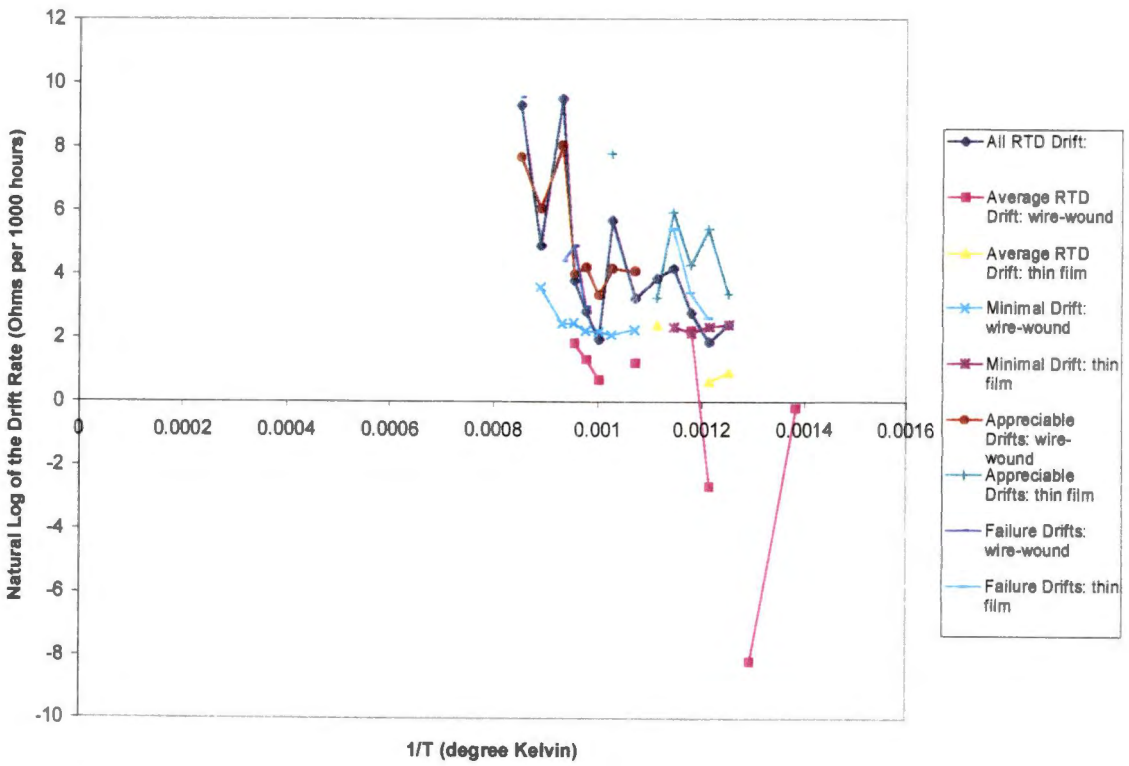


Figure 8.2. Arrhenius relationship plot of drift rates for each RTD type and drift level.

Table 8.7. Average Slopes of Arrhenius Relationships for each RTD Type and Drift

All RTD Drift:	Average RTD Drift: wire-wound	Average RTD Drift: thin film	Minimal Drift: wire-wound	Minimal Drift: thin film	Appreciable Drifts: wire-wound	Appreciable Drifts: thin film	Failure Drifts: wire-wound	Failure Drifts: thin film
-12842	-12406	-12077	-6413	1266	-18924	-13912	-51048	-39930

The Arrhenius relationship technique is not novel to the life prediction field, or to the specific application of RTDs. R. L. Shepard has completed considerable compilation of data in this area.[16] The short summary of this data set can be seen in Figure 8.3. This figure shows the general premise that there is a common band of drift rates for all RTDs and thermocouples.

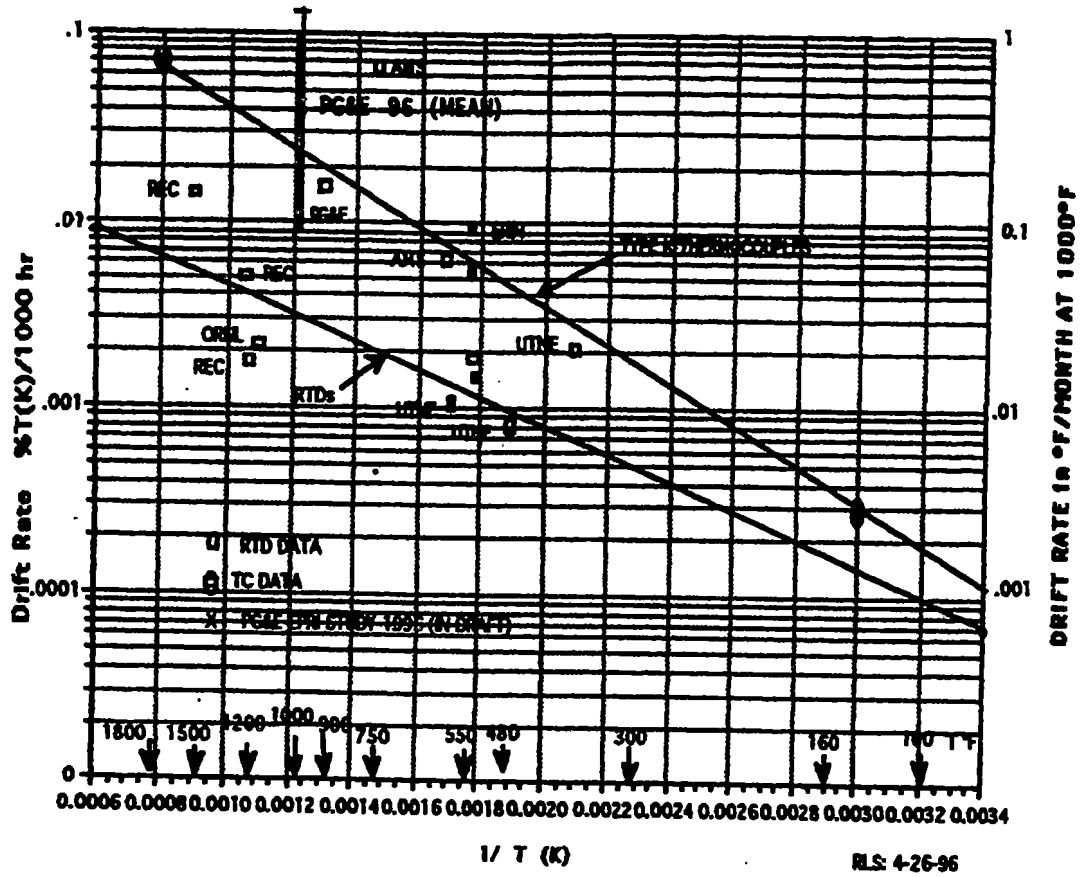


Figure 8.3. Thermometer Drift at Various Temperatures Arrhenius Plot.[16]

CHAPTER 9

SUMMARY OF WEEKLY MONITORING OF RTDS

9.1 Introduction

This chapter presents the results of the weekly calibration, performance parameter measurement and analysis. The results in this chapter are presented as the trends in the data that were monitored during the test duration. The weekly calibrations were performed using the data acquisition system described earlier and three temperature baths 0°C, 100°C and 145°C. The monitored results of the calibrations included Ro, α and δ as defined in the Callendar-Van Dusen equation relating resistance and temperature. The performance parameter measurements require the use of the HP digital multimeter, the Kiethley current source and a 30°C stirred water bath. The monitored results of the performance parameter measurements include the loop resistance, the insulation resistance, the sheath-to-lead voltage, the compensating loop resistance, the open circuit voltage, and the self-heating index.

9.2 Weekly Calibration Results

Between five and fifteen RTDs were removed weekly from the ten long-term tests for the purpose of calibration and RTD performance parameter trending. The RTDs and the tests they were involved in are listed in Table 9.1.

Table 9.1 RTDs used in Weekly Calibration Tests

RTD Number	Test Number	Number of Data Points
A-51	5	22
A-57	5	22
B-5	7	61
B-6	7	58
B-11	7	12
A-66	8	35
A-67	8	35
A-69	8	29
A-70	8	29
A-209	8	29
A-74	9	29
A-75	9	29
A-87	9	3
A-199	10	47

The plot of the trended values of Ro, α and δ for each of the RTDs listed above is presented in Appendix B. Series - A refer to wire-wound constructed RTDs and series - B refer to thin film constructed RTDs.

The plots of the ice-point resistance (Ro) for the individual RTDs are similar to the two examples provided in Figures 9.1 and 9.2. The Ro values over the period of the testing, both for the overall long-term tests and the weekly calibrations, increased as the RTDs drifted from their original calibration.

The plots of the calibration parameter α, for the individual RTDs are similar to the two examples provided in Figures 9.3 and 9.4. The trended alpha values for both the thin film and wire-wound RTDs decreased as the RTDs drifted from their original calibration. It can also be noted that several of the large jumps in the alpha parameter plots correspond to increases in the furnace temperature.

The plots of the calibration parameter δ, for the individual RTDs are similar to the two examples provided in Figures 9.5 and 9.6. The trended delta values showed no appreciable trend over the duration of testing. The delta values appear to be more random and erratic in nature. This is to be expected since the delta calibration constant is essentially a correction factor for the non-linearity of the resistance versus temperature relationship.

9.3 Results of Performance Parameter Monitoring

In addition to the weekly calibrations, while the RTDs were removed from the furnaces, the measurements for the loop resistance, the insulation resistance, the sheath-to-lead voltage, the compensating loop resistance, open circuit voltage, and self-heating

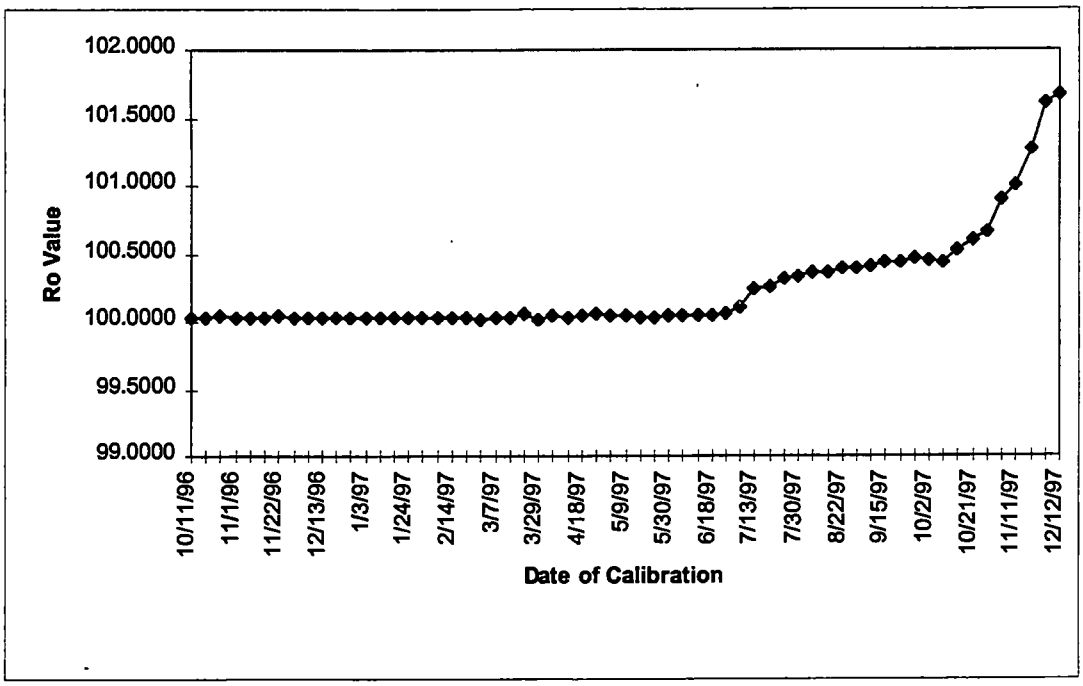


Figure 9.1 · RTD B-5 Ro Trend.

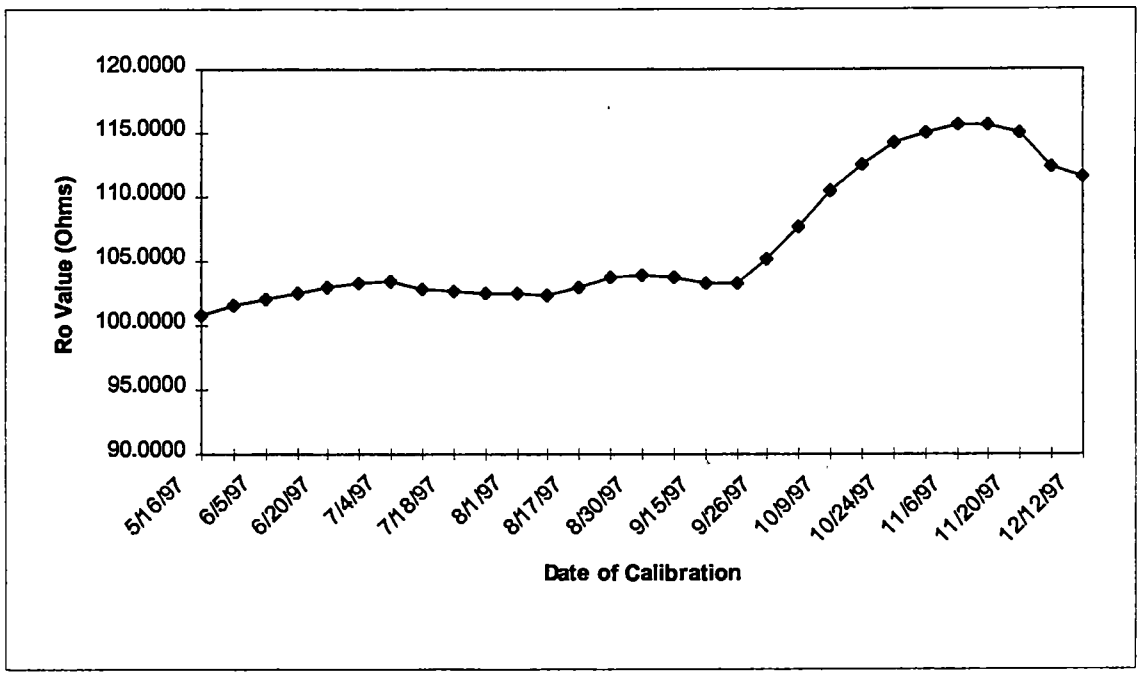


Figure 9.2 RTD A-74 Ro Trend.

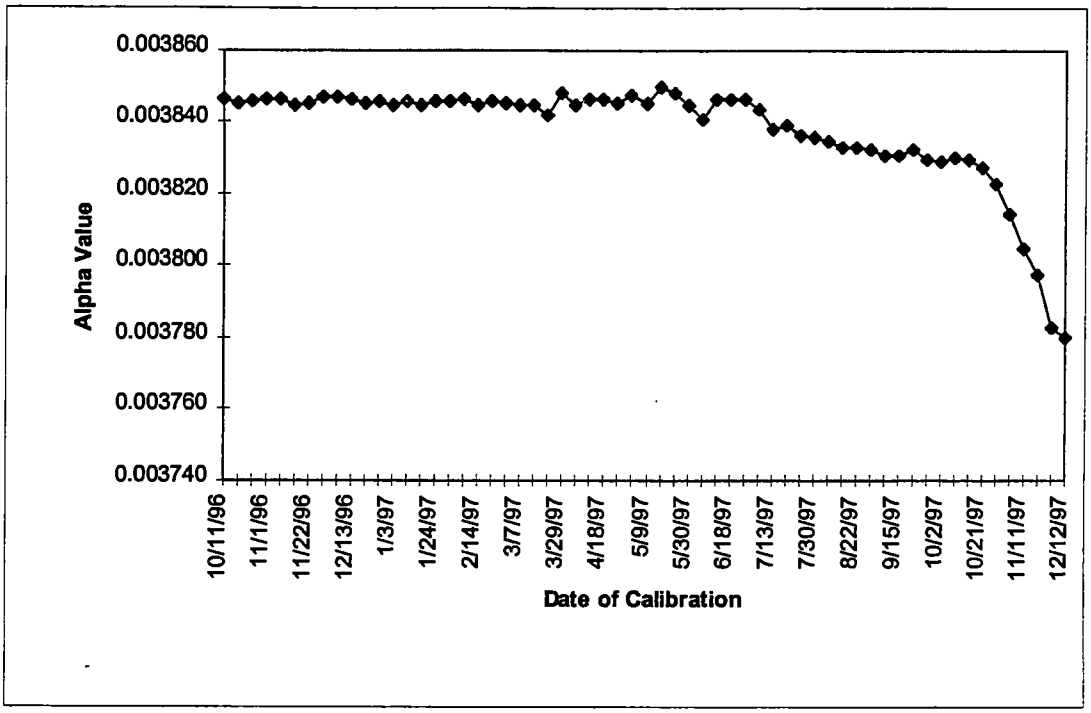


Figure 9.3 RTD B-5 Alpha Trend.

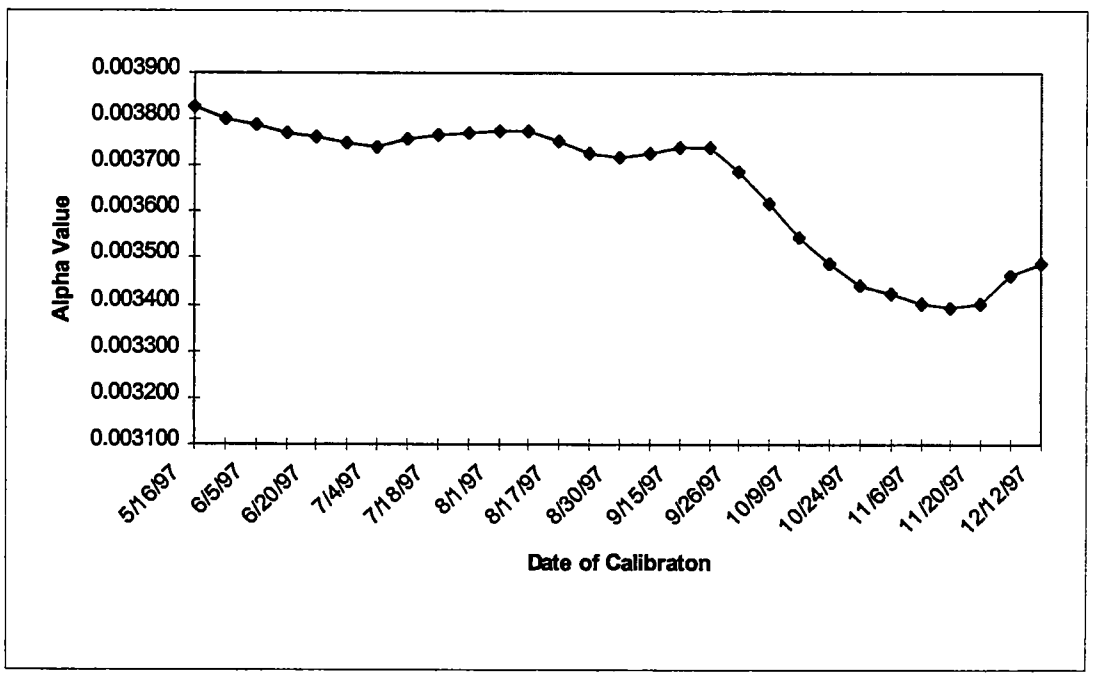


Figure 9.4 RTD A-74 Alpha Trend.

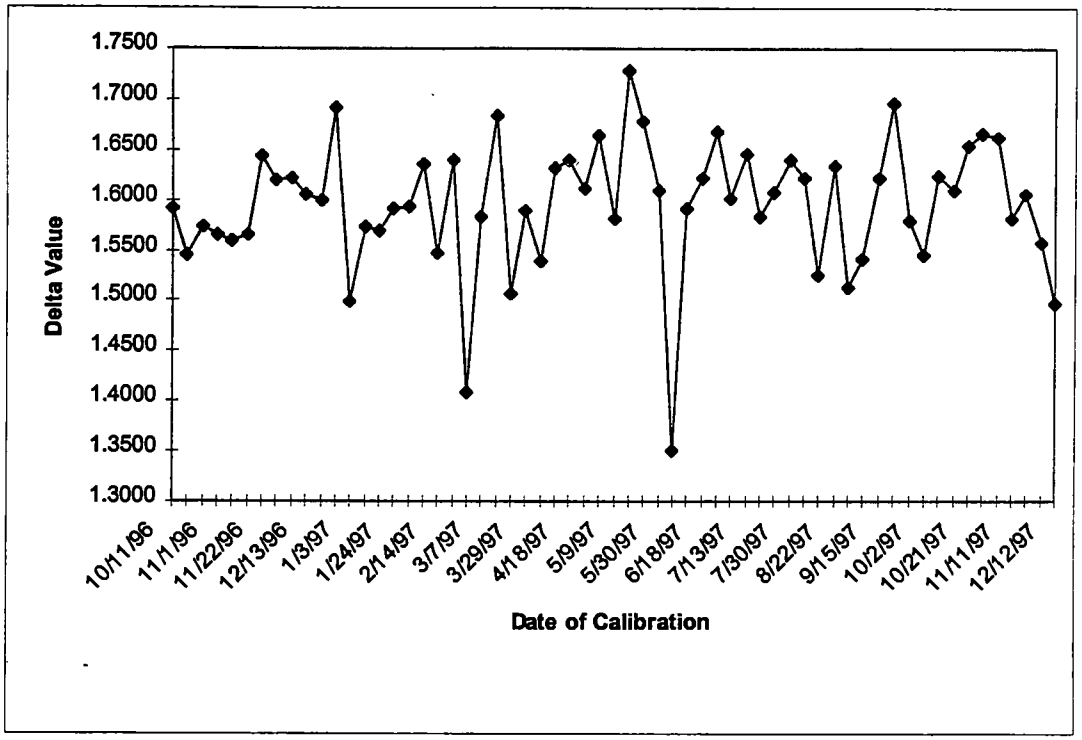


Figure 9.5 RTD B-5 Delta Trend.

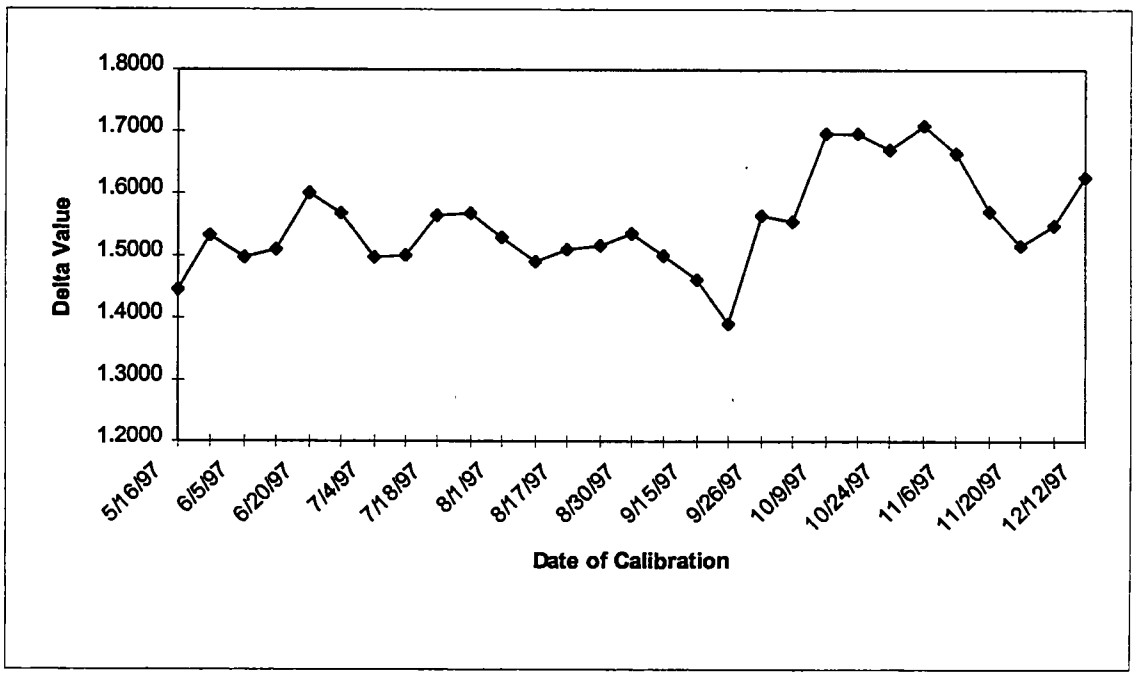


Figure 9.6 RTD A-74 Delta Trend.

index were taken. These measurements were recorded into an Excel database for each of the RTDs and the values were trended over time.

For the insulation resistance and the sheath-to-lead voltage measurements, there was not a noted or recorded trend throughout the measured values. This is somewhat dependent on the limitations in the equipment used to determine the recorded values. In the case of the insulation resistance the multimeter used was not able to differentiate resistance readings greater than three GigaOhms. For the sheath to lead voltages, the lack of water or a similar medium in the system caused unstable readings for the RTDs unless there was a problem with the integrity of the RTD sheath or end cap. This was tested to insure the readings were correct by the only destructive test performed in this study. A single RTD, A-200 a wire-wound RTD, was calibrated including the performance parameters, removed from the test population, drilled through the sheath into the insulating material and water intrusion encouraged. Once the RTD was thoroughly saturated it was again calibrated including performance parameters. The second set of performance parameter measurements produced discernable measurements for the sheath to lead voltage. This proved the theory that the test RTDs have no discernable sheath to lead voltage because there is no medium for the Galvanic Action, which the water in RTD A-200 provided. The RTD was maintained in the 30°C stirred water bath for several weeks and recalibrated additional times to provide an experimental basis for the lack of sheath to lead voltage for the test RTDs.

For the loop resistance, compensating loop resistance, and open circuit voltage measurements, the medium temperature caused considerable deviations in the readings. These measurements, though not adding much additional information, did follow the deviation that was noted in the Ro measurements on a week-to-week basis.

For the self-heating index measurements, in contrast to the other performance parameters, a trend began to surface early in the testing. This trend appears to be independent of the localized small changes in temperature that seem to strongly dominate the other performance parameters. In examining the calculated self-heating index values it appears that the degradation can be noted prior to a change in the standard Ro and α values were observed.

The trended values of the self-heating index (Ω/W), and dissipation constant (mW/°C), for each of the weekly monitored RTDs are recorded in Appendix B. Typical examples of the thin film and wire-wound RTD self-heating index plots are provided below (Figures 9.7, 9.8, 9.9, 9.10). The two forms of the self-heating index exhibit opposite behavior through the trending. The *Ohms per Watt* form of the self-heating index increases steadily throughout the duration of the long-term test.. The *milliWatt per degree Celsius* form of the self-heating index, or dissipation constant, decreases steadily throughout the duration of the long-term tests.

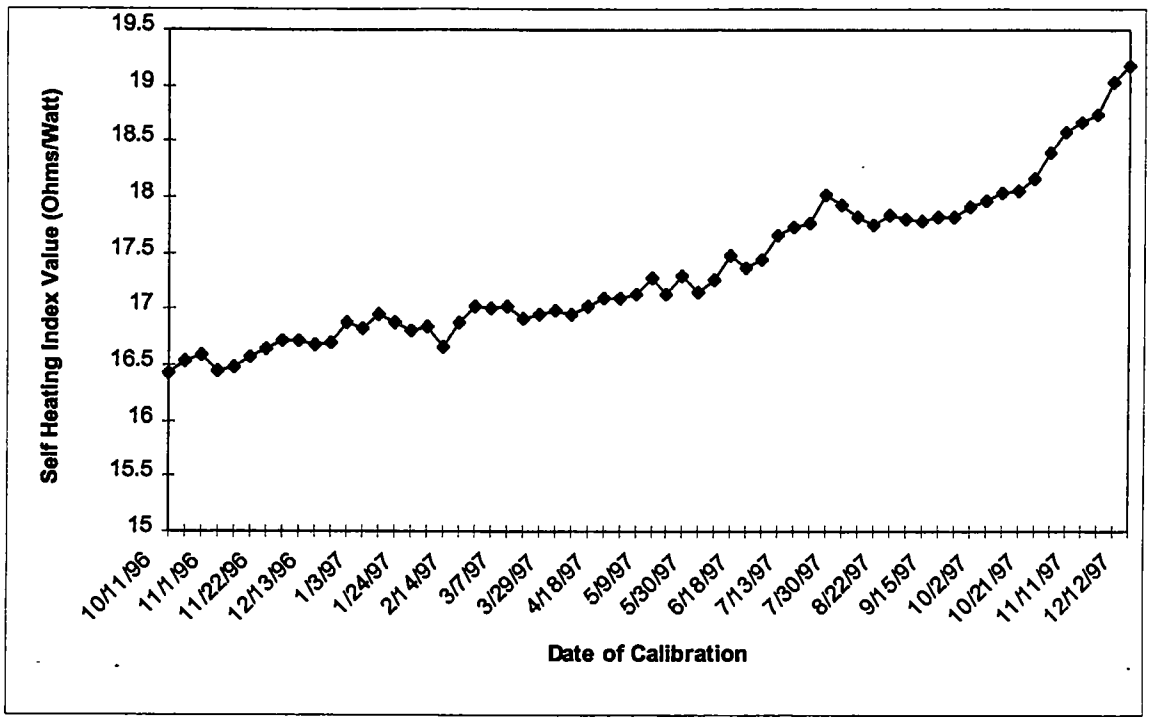


Figure 9.7 RTD B-5 Self-Heating Index (Ohms/Watt) Trend.

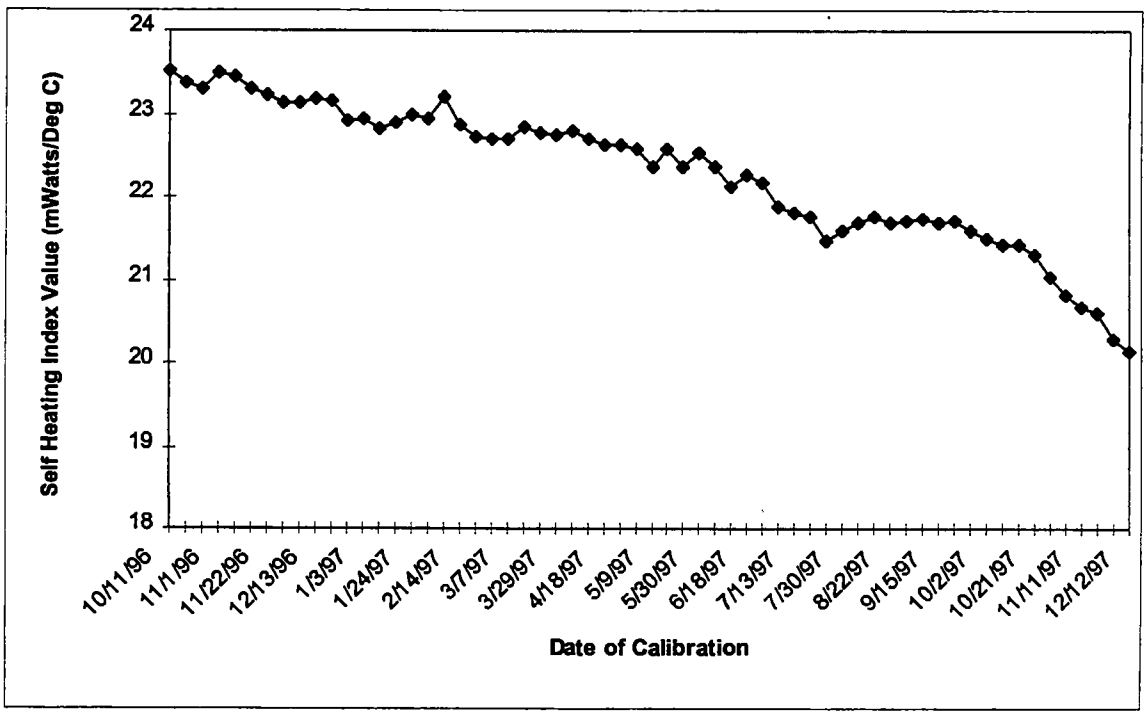


Figure 9.8 RTD B-5 Self-Heating Index (mWatts/°C) Trend.

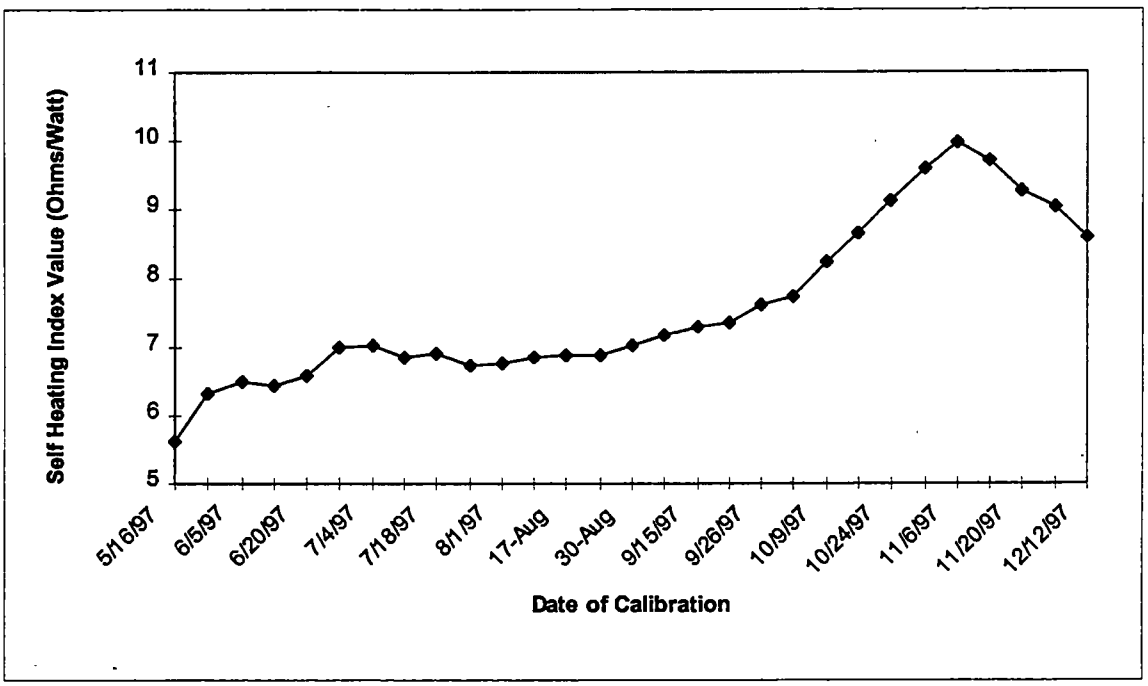


Figure 9.9 RTD A-74 Self-Heating Index (Ohms/Watt) Trend.

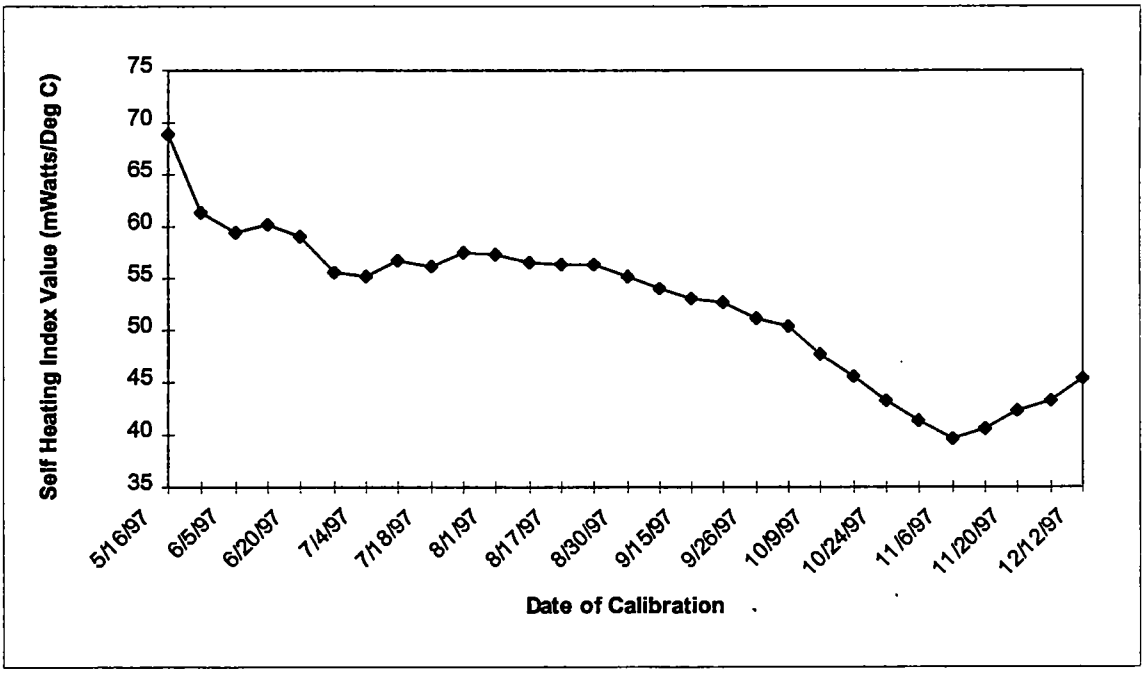


Figure 9.10 RTD A-74 Self-Heating Index (mWatts/°C) Trend.

CHAPTER 10

SELF-HEATING INDEX AND ITS CORRELATION TO RTD CALIBRATION PARAMETERS

10.1 Introduction

This chapter presents the results of the calculations made on the self-heating index measurements. The self-heating index, as described at the end of Chapter 9, is calculated by two calculational methods, which are again described further in this chapter. The results in this chapter will be presented as the summary of the different calculation techniques and experimental investigations into the relationship observed between the self-heating index and the calibration constant alpha. The two primary calculation techniques employed include a correlation coefficient and a linear fit. The additional experimental investigation consisted of three endeavors to further describe and explore the relationship between the self-heating index and alpha. The three additional investigations include the use of 2, 3, 4 and 5 milliAmperes of applied current, in-situ measurements, and an approach of monitoring an individual reading or a pair of readings rather than the more traditional four or five readings.

The self-heating index, as the name implies, is a measure of the internal heating of the sensor or a measure of the heat transfer characteristics of the sensor. The self-heating index was monitored using two calculational methods as described earlier. The first calculation provided a self-heating index in units of *Ohms per Watt*. This index is a

measure of the change in resistance per amount of applied power to the sensor. The second calculation provides a self-heating index in units of *milliWatts per degree Celsius*. This self-heating index is more of a measure of the amount of applied power required to cause a change of one-degree Celsius in the sensor temperature measurement. The *milliWatt per degree Celsius* self-heating index, or dissipation constant, also requires the use of the calibration constant alpha for calculation of the temperature in degrees Celsius. This use of the calibration constant alpha in the calculation of the self-heating index artificially inflates both the correlation and the linear fit between those values.

10.2 Correlation Coefficient Calculation between Self-Heating Index and Alpha

The correlation coefficient is a measure of how well the changes in the self-heating index values are reflected in the calibration constant alpha and vice versa. As can be seen in the plots from the weekly calibrations, the self-heating index and alpha have related trends. The correlation coefficient provides a numerical quantity to quantify and evaluate the relationship between the self-heating index and alpha. The correlation coefficient is calculated as

$$\rho = \frac{\sum \Delta\alpha \, \Delta(\mathrm{SHI})}{\left(\sum(\Delta\alpha)^2 \sum(\Delta\mathrm{SHI})^2\right)^{(1/2)}} \qquad (10.1)$$

where

$-1 \le \rho \le 1$

$\Delta\alpha = \alpha(i) - \alpha(\text{average})$

$\Delta\mathrm{SHI} = \mathrm{SHI}(i) - \mathrm{SHI}(\text{average})$.

The evaluation of the coefficient produced from the above equation is related to its range. At both ends of the range, +1 and -1, the relationship between alpha and the self-heating index is said to be perfect. A perfect relationship means that the changes in one value are directly translated as changes in the other. The relationship can be expressed as either positive or negative. A positive correlation coefficient means that an increase in one value is likewise seen as an increase in the other value. A negative correlation coefficient expresses that the changes are inversely related or that the positive change in one value is seen in the other value as a negative change. At the center of the range of values is zero, which is defined as the lack of any relationship between alpha and the self-heating index. The possible values range between zero and ±1 representing all levels of possible correlation from none (0) to perfect correlation (±1). The correlation coefficient defined in Equation (10.1) is a reflection of the linear relationship between any two parameters. A low correlation does not necessarily indicate a non-relationship between them. The results of the correlation coefficient calculations are presented in Table 10.1. In the table, SHI1 denotes the self-heating index in units of Ohms per Watt, and SHI2 denotes the self-heating index in units of milliWatts per degree Celsius.

10.3 Linear Fit Between Self-Heating Index and Alpha

In order to describe the observed relationship in more detail a linear fit for the self-heating index and alpha values were used. A least-squares linear regression was performed on the data sets and RMS error statistics were calculated to establish the value of the fit. The use of this linear regression avoids the need of using an average parameter

Table 10.1 Summary of Correlation Coefficient Calculations between α and SHI.

RTD #	Test #	ρ(SHI1)	ρ(SHI2)	# of pts.
A-51	5	-0.632	0.635	19
A-57	5	-0.054	0.073	19
B-5	7	-0.873	0.857	61
*B-5	7	-0.951	0.947	31
B-6	7	-0.927	0.915	57
*B-6	7	-0.918	0.941	27
B-11	7	-0.922	0.895	12
A-66	8	-0.089	0.118	35
A-67	8	-0.725	0.726	35
A-69	8	-0.814	0.812	29
A-70	8	0.044	-0.006	29
A-209	8	-0.455	0.491	29
A-74	9	-0.978	0.953	29
A-75	9	-0.967	0.950	29
A-87	9	-0.758	0.979	3
A-199	10	0.264	-0.258	43

SHI1: Ohms/Watt

SHI2: mWatts/°C

value. Figures 10.1, 10.2, 10.3 and 10.4 are examples of the linear fit and Table 10.2 contains the associated RMS error information. Additional plots of the linear fits between the self-heating index and alpha are provided for each RTD tested in Appendix D.

10.4 Remarks on the Relationship Between α and Self-Heating Index

The alpha parameter is one of two calibration parameters in the Callendar-Van Duesen equation, and is used to mathematically approximate the observed resistance versus temperature relationship. The self-heating index is a measure of the heat transfer characteristic of the RTD. The relationship appears to resemble that of two symptoms of a common cause. The possible causes hypothesized are listed in Table 10.3. Due to the scope and financial restraints of this project, destructive examination could not be conducted to further investigate the true cause of the alpha and self-heating index relationship.

10.5 Further Experimental Investigations

From the results seen in the previous sections additional questions arose related to the relationship between the self-heating index and alpha. A limited number of these questions could be explored within the scope of this project. The first of these questions is concerned with the applied current values; specifically, the goal to determine if smaller applied current values would produce the same relationship. This was possible to be incorporated into the current study. For a limited number of RTDs additional

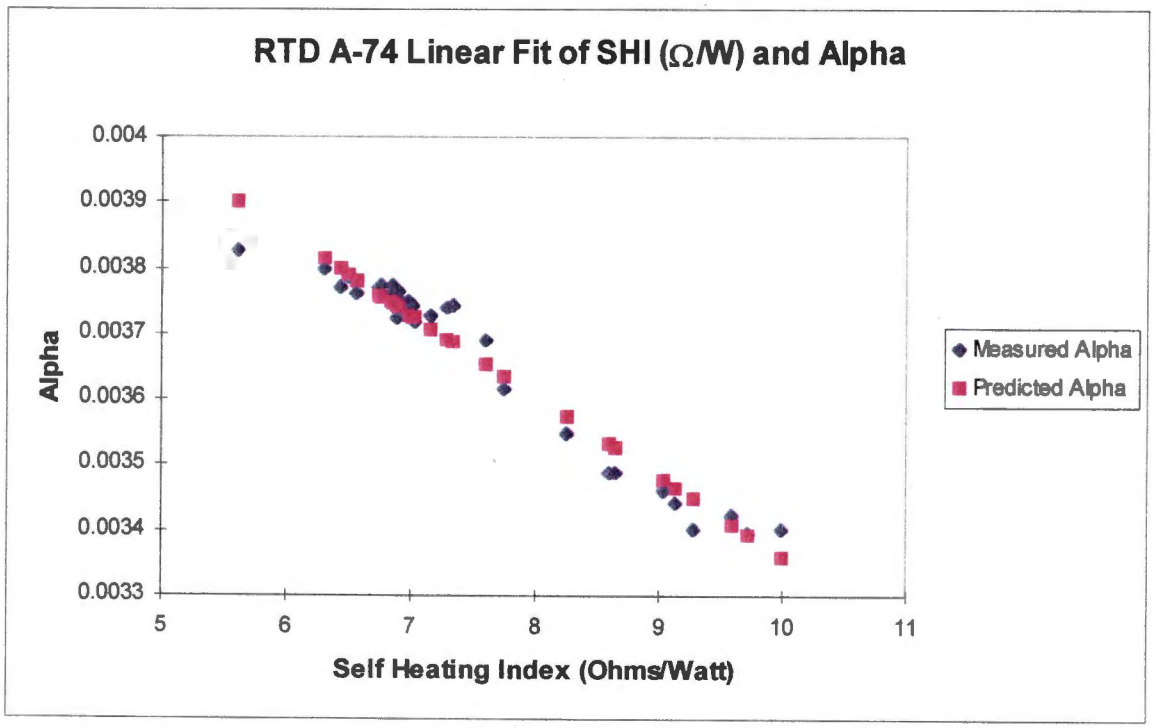


Figure 10.1 Self-Heating Index (Ω/W) versus Alpha Plot with Fitted Line for RTD A-74

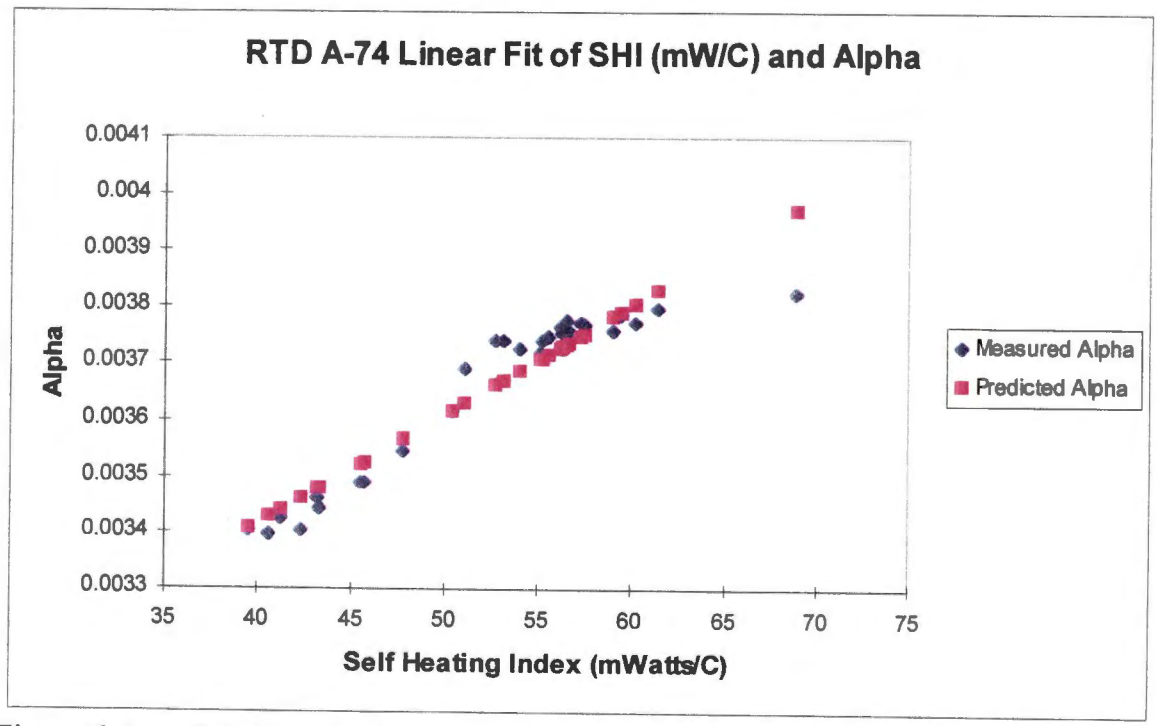


Figure 10.2 Self-Heating Index (mW/C) versus Alpha Plot with Fitted Line for RTD A-74

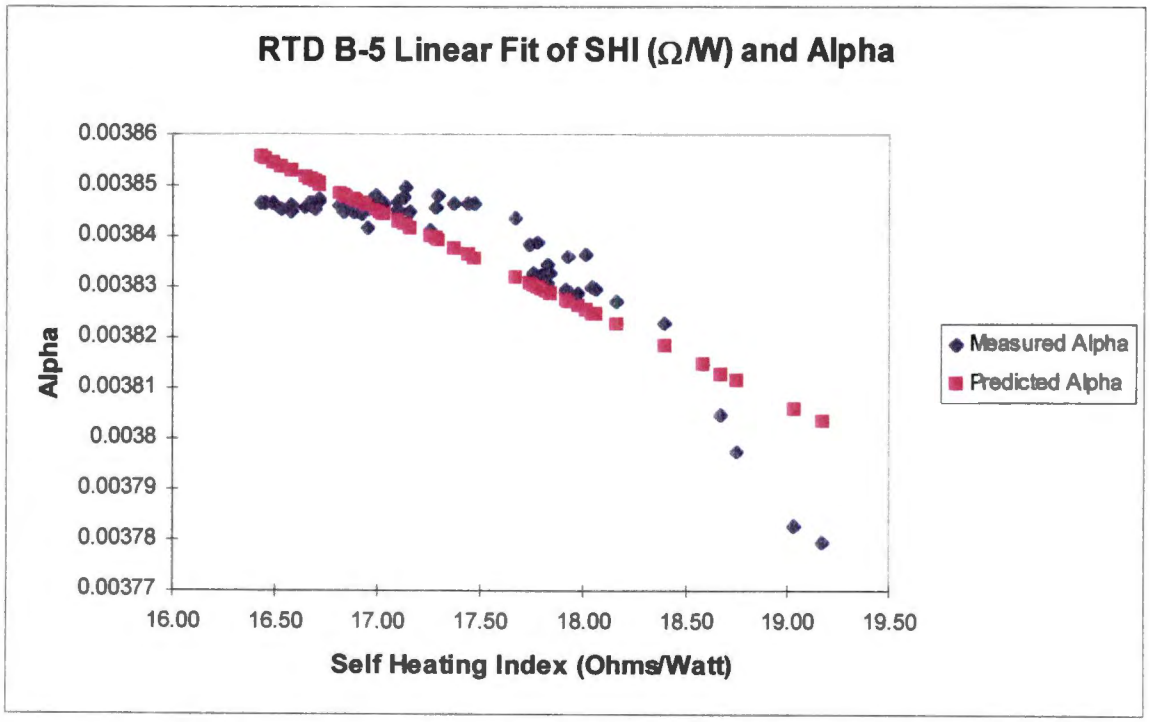


Figure 10.3 Self-Heating Index (Ω/W) versus Alpha Plot with Fitted Line for RTD B-5

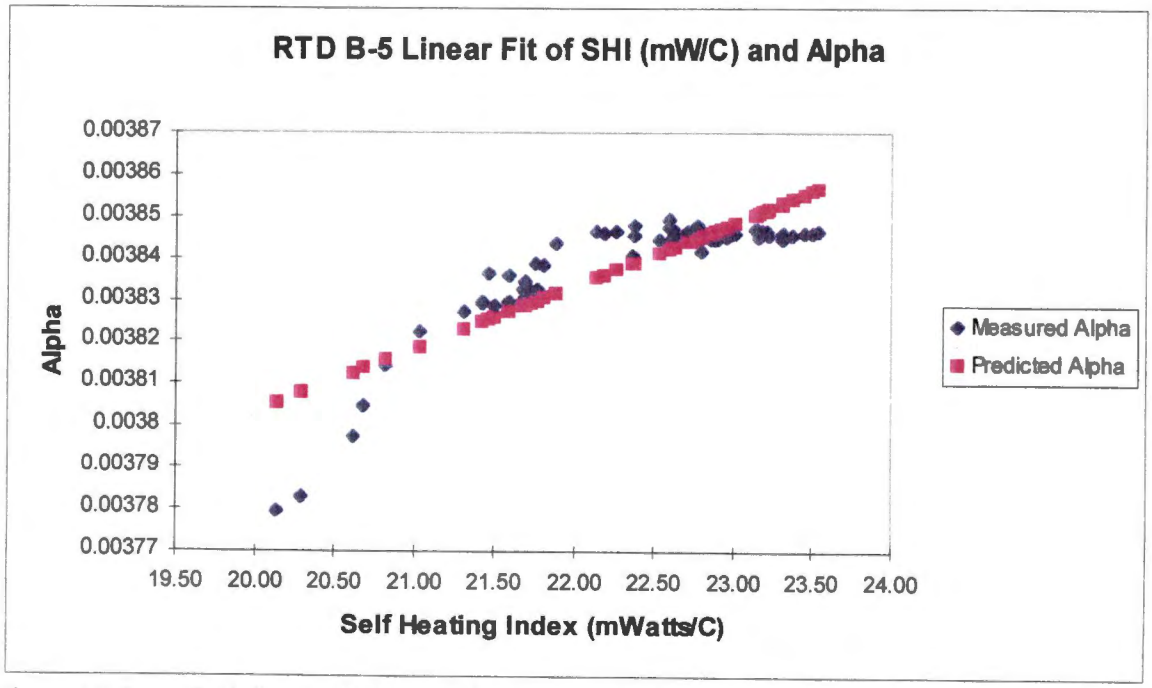


Figure 10.4 Self-Heating Index (mW/C) versus Alpha Plot with Fitted Line for RTD B-5

Table 10.2 Summary of RMS Error Associated with the Linear Fit

RTD Number	RMS Error SHI (Ω/W)	RMS Error SHI (mW/C)	Number of points
A-51	0.02%	0.02%	19
A-57	0.04%	0.04%	19
B-5	0.19%	0.20%	61
*B-5	0.15%	0.15%	31
B-6	0.23%	0.25%	57
*B-6	0.29%	0.24%	27
B-11	0.24%	0.28%	12
A-66	0.05%	0.05%	35
A-67	0.06%	0.06%	35
A-69	0.03%	0.03%	29
A-70	0.10%	0.10%	29
A-209	0.08%	0.08%	29
A-74	0.83%	1.21%	29
A-75	0.55%	0.67%	29
A-87	0.92%	0.28%	3
A-199	0.05%	0.05%	43

Table 10.3 Possible RTD Degradations Causing a Relationship Between α and SHI

Gaps between Element and Insulation	Grain Growth
Insulation Property Changes	Creep
Platinum Impurities	Contamination
Platinum Migration	Oxygen Depletion

measurements were recorded with 2 mA, 3 mA, 4 mA and 5 mA applied current values. The results are described in Section 10.5.1. Arising from the same line of questioning, the second additional experiment also involved the lower applied current values. This experiment involved different calculational techniques to reduce the number of required data points recorded and additional calculations required. Further description and results are provided in Section 10.5.2. The final additional experiment investigated the application of the self-heating index measurements in a more process like environment. This experiment involved recording the self-heating index values with the RTDs still in the high temperature furnaces. This study is further described and the results are provided in Section 10.5.3.

10.5.1 Additional Applied Current Values

To further understand the relationship between alpha and the self-heating index and to explore other properties of the self-heating index, the performance parameter

measurements were expanded to include the addition of 2 mA, 3 mA, 4 mA and 5 mA applied current values. The values were used in the calculation of the self-heating index.

RTD A-209 used in this study has a minimal drift rate, but has the largest number of recorded additional applied current values. For the statistical benefits of a larger number of data points, RTD A-209 will be used to describe this experiment. Three self-heating index values were calculated for comparison. The first self-heating index values were calculated using the 1 mA, 2 mA, 3 mA, 4 mA, 5 mA, 10 mA, 20 mA, 30 mA and 40 mA applied current values. The second self-heating index values were calculated using the 1 mA, 2 mA, 3 mA, 4 mA and 5 mA applied current values. The third self-heating index values were calculated using the 10 mA, 20 mA, 30 mA and 40 mA applied current values. A listing of these values for RTD A-209 is given in Table 10.4.

The correlation coefficient values were included at the bottom of the table to assist in comparisons between the provided calculation methods. It can be seen that for both the Ohms per Watt and milliWatt per degree Celsius measurements the 1 through 40 mA and the 1 through 5 mA values do not correlate as well with the recorded alpha values. The Ohm per Watt self-heating index values for the 1 through 40 mA and the 1 through 5 mA calculations are showing a correlation of the opposite sign as seen in the majority of the standard correlations. The sign change signifies that they follow more closely as a direct comparison than as a mirror comparison. As Table 10.4 shows, the best correlations to alpha for RTD A-209, are provided by the calculations done using the

Table 10.4 RTD A-209 Self-Heating Index Measurements and Correlation Coefficients

Date of Calibration	Alpha	(Ω/W) 1 to 40 mA	(Ω/W) 1 to 5 mA	(Ω/W) 10 to 40 mA	(mW/C) 1 to 40 mA	(mW/C) 1 to 5 mA	(mW/C) 10 to 40 mA
5/16/97	0.003841	4.878	20.306	4.795	78.850	9.079	80.573
5/30/97	0.003841	4.890	22.348	4.804	78.573	8.175	80.414
6/5/97	0.003841	5.031	20.547	4.952	76.495	9.403	78.023
6/13/97	0.003841	4.903	19.883	4.838	78.466	9.149	79.836
6/20/97	0.00384	5.011	22.689	4.930	76.679	8.197	78.335
6/26/97	0.003839	5.032	21.392	4.953	76.365	8.862	77.929
7/4/97	0.003839	5.020	21.314	4.944	76.555	9.171	78.057
7/13/97	0.003841	5.052	23.296	4.954	76.086	8.659	77.972
7/18/97	0.003828	5.175	21.773	5.090	73.978	9.263	75.504
7/25/97	0.003838	5.063	21.352	4.983	75.952	8.926	77.501
8/1/97	0.003837	4.983	22.331	4.903	77.042	8.076	78.709
8/10/97	0.003838	5.212	20.657	5.132	73.846	9.517	75.269
8/17/97	0.003838	5.147	23.722	5.050	74.692	8.622	76.487
8/25/97	0.003837	5.051	23.643	4.968	76.049	7.812	77.734
8/30/97	0.003837	5.069	21.647	5.000	75.880	8.276	77.279
9/7/97	0.003837	5.040	21.475	4.968	76.296	8.358	77.755
9/15/97	0.003836	4.986	22.054	4.915	77.075	8.581	78.549
9/19/97	0.003835	5.006	22.512	4.928	76.835	8.141	78.333
9/26/97	0.003838	5.037	18.769	4.953	76.408	10.388	78.070
10/2/97	0.003835	5.135	22.442	5.048	74.868	8.674	76.511
10/9/97	0.003835	5.150	20.133	5.071	74.738	9.737	76.166
10/17/97	0.003836	5.137	23.332	5.066	74.861	8.134	76.276
10/24/97	0.003834	5.082	23.078	5.014	75.580	8.092	76.993
10/30/97	0.003834	5.067	23.129	4.992	75.808	7.799	77.354
11/6/97	0.003834	5.077	24.915	4.999	75.653	7.707	77.278
11/13/97	0.003833	2.287	-80.919	4.908	5.782	-0.033	78.608
11/20/97	0.003831	4.950	22.157	4.878	77.487	7.732	79.063
12/4/97	0.003831	5.107	23.152	5.029	75.204	7.970	76.756
12/12/97	0.003834	5.106	22.881	5.028	75.269	7.746	76.855
Correlation Coefficient	N/A	0.116	0.168	-0.455	0.237	0.297	0.491

10 through 40 mA applied current values for both the Ohm per Watt and milliWatt per degree Celsius calculations.

Tables 10.5 and 10.6 provide the correlation coefficients and RMS errors for the complete set of RTDs included in the additional applied current study. Again for the RTDs with known degradation and minimal needed points, a possible pattern appears to be immerging. There are several RTDs, as can be seen in the tables, that do not follow this reasoning. There is not sufficient data in the seven RTDs tested and seventy-six points recorded to draw any conclusive results. The data does not conclusively rule out the possibility that the lower applied current values may hold significant information about the RTDs, but cannot independently support the claim either.

Table 10.5 Summary of Correlation Coefficient Calculations (1 to 5 mA Applied Current)

RTD #	Test #	ρ(SHI1)	ρ(SHI2)	# of pts.
B-5	7	-0.884	0.723	6
B-6	7	-0.961	0.527	4
B-11	7	-0.122	0.258	8
A-209	8	0.168	0.297	29
A-74	9	-0.663	0.434	13
☆A-74	9	-0.780	0.642	12
A-75	9	-0.716	0.405	13
☆A-75	9	-0.851	0.702	12
A-87	9	0.993	-0.930	3

☆ = one bad data point removed – possibly due to inaccurate data recording or not following procedure

Table 10.6 Summary of RMS Error Associated with the Linear Fit (1 to 5 mA Applied Current)

RTD Number	RMS Error SHI (Ω/W)	RMS Error SHI (mW/C)	Number of points
B-5	0.31%	0.46%	6
B-6	0.14%	0.43%	4
B-11	0.57%	0.66%	8
A-209	0.09%	0.08%	29
A-74	2.68%	3.22%	13
A-75	1.22%	1.60%	13
A-87	0.17%	0.52%	3

10.5.2 Single Current or Two Current Comparison Measurements

An additional issue arose about the possibility of calculating an approximation of the self-heating index that would also mirror the changes in alpha but require less data points, therefore less data acquisition and less data analysis. The methodologies investigated included the tracking of a single resistance value for a set applied current. As can be seen in Figure 10.5 the tracking of any of the individual resistance values would result in a value that mostly follows the medium temperature (Figure 10.6). The next analysis centers on the use of any two of the low current values to approximate the self-heating index and the relationship with alpha. From the plots of the low current values the applied current values of 1 mA, 2 mA and 5 mA were chosen. The self-heating index values for the 1 mA and 5 mA values and the 2 mA and 5 mA values were calculated and are provided in Table 10.7. The correlation coefficients for each of these data sets were calculated and compared to those of the other partial and complete data sets. Table 10.7 and Table 10.4 show the values used in these comparisons. Although

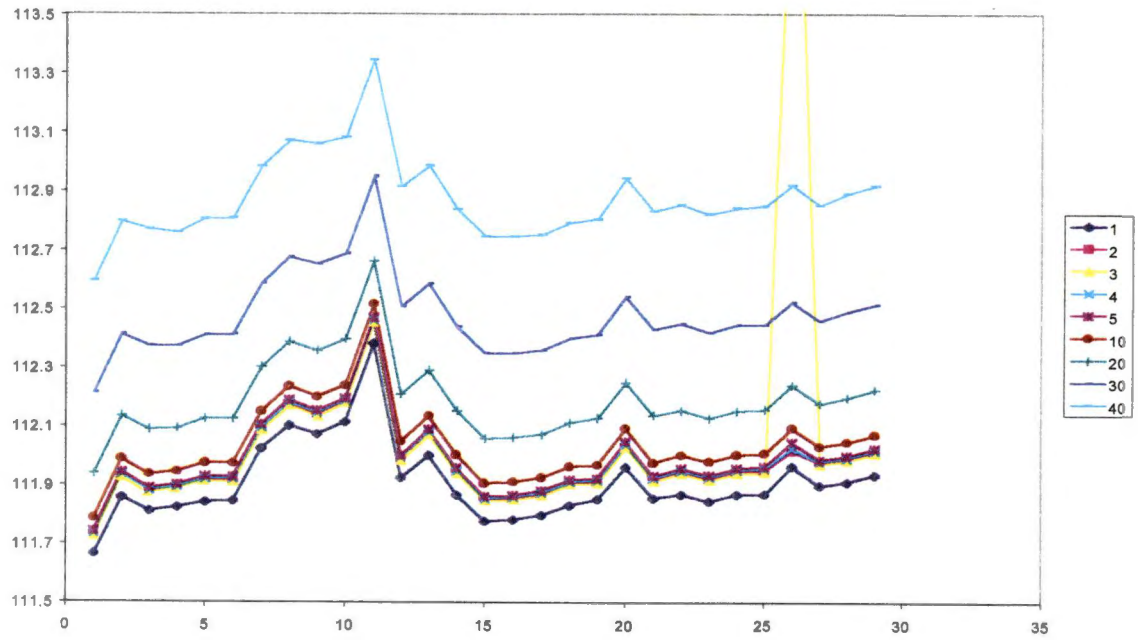


Figure 10.5 Individual Resistance Values Recorded

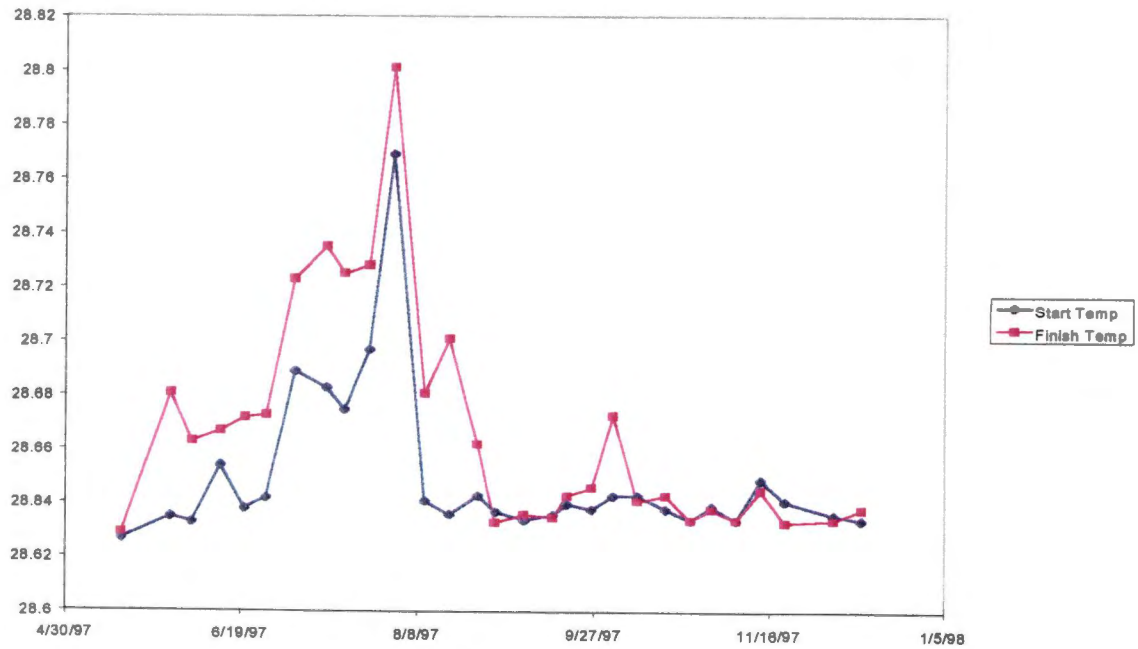


Figure 10.6 Bath Temperature Measurements

Table 10.7 Paired Resistance Value Comparison

Date	Alpha	SHI (Ω/W) 1 mA and 5mA	SHI (Ω/W) 2 mA and 5mA
5/16/97	0.003841	0.034	0.247
5/30/97	0.003841	0.031	0.224
6/5/97	0.003841	0.034	0.196
6/13/97	0.003841	0.035	0.247
6/20/97	0.00384	0.031	0.196
6/26/97	0.003839	0.033	0.214
7/4/97	0.003839	0.033	0.188
7/13/97	0.003841	0.031	0.157
7/18/97	0.003828	0.033	0.174
7/25/97	0.003838	0.033	0.196
8/1/97	0.003837	0.031	0.225
8/10/97	0.003838	0.035	0.205
8/17/97	0.003838	0.031	0.147
8/25/97	0.003837	0.030	0.196
8/30/97	0.003837	0.032	0.235
9/7/97	0.003837	0.032	0.247
9/15/97	0.003836	0.032	0.204
9/19/97	0.003835	0.031	0.204
9/26/97	0.003838	0.038	0.224
10/2/97	0.003835	0.032	0.174
10/9/97	0.003835	0.035	0.204
10/17/97	0.003836	0.030	0.181
10/24/97	0.003834	0.031	0.196
10/30/97	0.003834	0.030	0.235
11/6/97	0.003834	0.029	0.174
11/13/97	0.003833	0.033	0.078
11/20/97	0.003831	0.031	0.294
12/4/97	0.003831	0.030	0.196
12/12/97	0.003834	0.030	0.248
Correlation Coefficient	N/A	0.298	0.090

the 1 mA and 5 mA calculation actually provided a better positive correlation than the 1 through 5 mA calculation provided, both, by comparison to other values throughout the study, should have been negative. In actuality, the 10 mA through 40 mA calculation still had a better absolute correlation to alpha than either of the paired comparisons. It can be seen that the best information for the relation of alpha and the self-heating index is contained in the 10 mA, 20 mA, 30 mA and 40 mA applied current values.

10.5.3 In-Situ Measurements

The performance parameter measurements were all recorded during calibration conditions. In order to gain more information about the self-heating index, its relation to temperature conditions, and its application for predicting alpha, in-situ measurements were taken on five RTDs. In-situ measurements are measurements taken with the RTD remaining in the process environment. Five RTDs were included in this study. The procedure requires the removal of the data acquisition connections and attachment of the DVM and current source used in the standard performance parameter monitoring. Use of the same equipment and the same procedures should assist in the consistency of data. It had to be assumed that the temperature in the furnace at each time of in-situ data acquisition was the same. The applied currents used in the in-situ measurements included 1 mA, 2 mA, 3 mA, 4 mA, 5 mA, 10 mA, 20 mA, 30 mA and 40 mA values.

From the in-situ measurements several values were calculated and several behaviors observed. The calculated values similar to the performance parameter

calculations included three self-heating index values. Since these calculations were completed without the removal of the RTDs for calibration, an accurate calibration constant alpha value is not known. The lack of an accurate calibration constant alpha value makes the calculation of the self-heating index in the *milliWatts per degree Celsius* form impossible or extremely inaccurate at best. The three calculated self-heating indices are all in the *Ohms per Watt* form and are again related to the applied current values. The first self-heating index values are based on all of the recorded values from 1 mA applied to 40 mA applied. The second self-heating index values are based on the recorded values from the 1 mA to 5 mA applied current range. The third self-heating index values are based on the recorded values from the 10 mA to 40 mA applied current ranges. The observed behaviors included spikes noted in the furnace data plots (Figures A-24 and A-25) occurring at the same time period as the in-situ measurements. These spikes are possibly due to the heating in the RTD that occurs during the in-situ self-heating index measurements.

The five RTDs included in the brief study each have characteristics and history that need to be considered. The vital information for each of the RTDs is provided in Table 10.8. These RTDs were chosen to give additional insight into the characteristics of the in-situ measurements. The test group included both types of RTDs, and RTDs at different stages appreciable drift. RTDs were chosen with no appreciable drift, not much appreciable drift and considerable drift. RTDs without excellent correlation statistics were also chosen so that as the test progressed, if the correlation improved, an in depth

Table 10.8 Background Information for In-situ Measurement RTDs

RTD #	RTD Type	Test Number	Resistance Trend Characteristics from Long-Term Tests	Overall SHI (Ω/W) Correlation
B-5	Thin Film	7	Not Much Drift	-0.87
B-6	Thin Film	7	A Small but Noticeable Amount	-0.93
B-11	Thin Film	7	Largest Drift for Furnace	-0.92
A-66	Wire-Wound	8	Not Much Drift	-0.09
A-69	Wire-Wound	8	Not Much Drift	-0.81

look at how this is seen in the in-situ measurements could also be performed. Only a limited number of data points could be collected prior to completion of this study, therefore, this comparison could not reach its potential. Additionally the temperatures in the two furnaces were increased across the duration of the in-situ testing. Both furnaces began the in-situ testing at 575°C. Between the 10/21/97 measurements and the 10/27/97 measurements both furnaces were increased to 600°C. Between the 11/17/97 and 12/3/97 measurements, Test #7 was increased again to 625°C. Figures 10.7 through 10.11 and Tables 10.9 through 10.13 provide the results of the in-situ calculations.

From the data provided in Tables 10.9 through 10.13 and Figures 10.7 through 10.11 several observations can be made.

The first observation is that the calibration correlation coefficients are generally closer to ±1 than the in-situ values calculated for the same number of points and date of measurements. Of the in-situ values, the 1 through 40 and the 10 through 40 calibrations appear to be the most similar to the calibration calculations.

Table 10.9 Self-Heating Index and Correlation Values for RTD B-5

In-situ Date	Alpha Date	Calibration Alpha	Calibration SHI (Ω/W)	In-situ SHI 1 to 40	In-situ SHI 1 to 5	In-situ SHI 10 to 40
10/10/97	10/8/97	0.00383	18.04287	26.14795	39.02505	26.2439
10/20/97	10/21/97	0.003827	18.15726	26.30801	38.80256	26.38981
10/27/97	10/28/97	0.003823	18.38998	26.20689	40.66985	26.25021
11/4/97	11/4/97	0.003815	18.57674	26.32259	35.87696	26.36534
11/10/97	11/11/97	0.003805	18.66761	26.3791	39.31871	26.41102
11/17/97	11/19/97	0.003798	18.74447	26.1751	34.45386	26.21443
12/3/97	12/4/97	0.003783	19.02946	26.01334	37.92854	26.01479
RTD B-5	Correlations:		-0.96941	0.443696	0.435445	0.61024

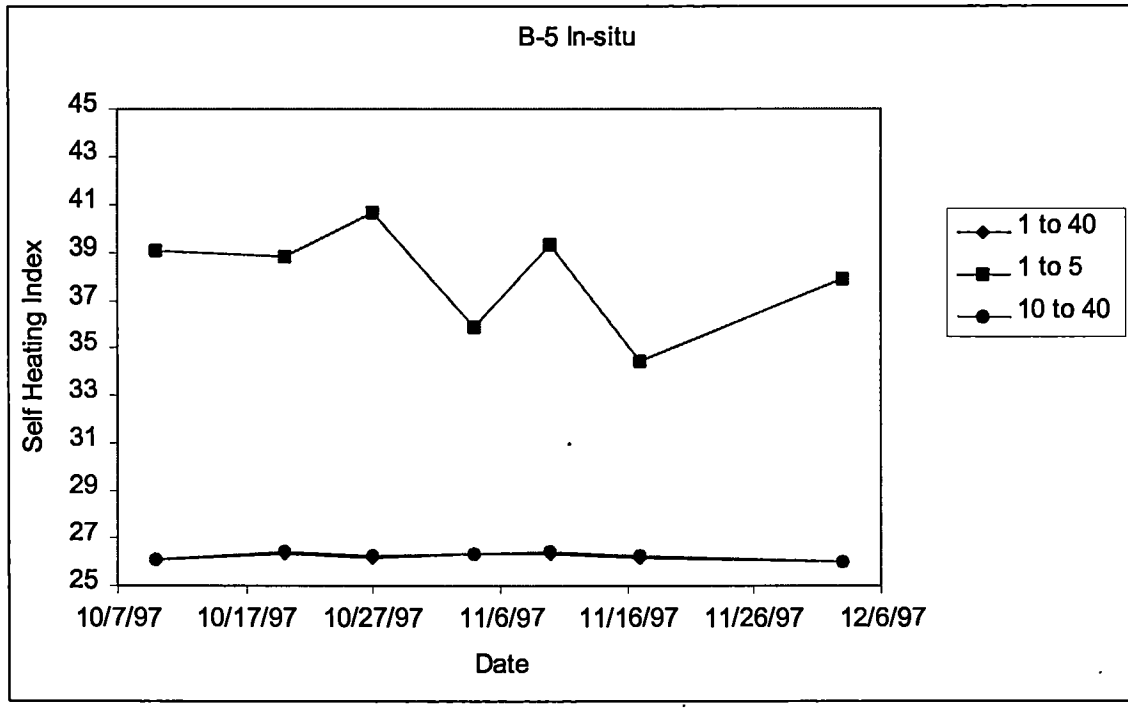


Figure 10.7 Plot of the In-situ Self Heating Index Measurements for RTD B-5

Table 10.10 Self-Heating Index and Correlation Values for RTD B-6

In-situ Date	Alpha Date	Calibration Alpha	Calibration SHI (Ω/W)	In-situ SHI 1 to 40	In-situ SHI 1 to 5	In-situ SHI 10 to 40
10/10/97	10/8/97	0.003795	15.78102	25.33209	42.38937	25.50727
10/20/97	10/21/97	0.00378	15.97986	24.20476	44.40978	24.42467
10/27/97	10/28/97	0.003758	18.88607	27.54108	51.11078	28.30561
11/4/97	11/4/97	0.003755	19.04721	26.57525	31.19389	26.77808
11/10/97	11/11/97	0.00375	N/A	27.60426	50.07168	27.7509
RTD B-6	Correlations:		-0.95834	-0.81022	-0.10382	-0.78828

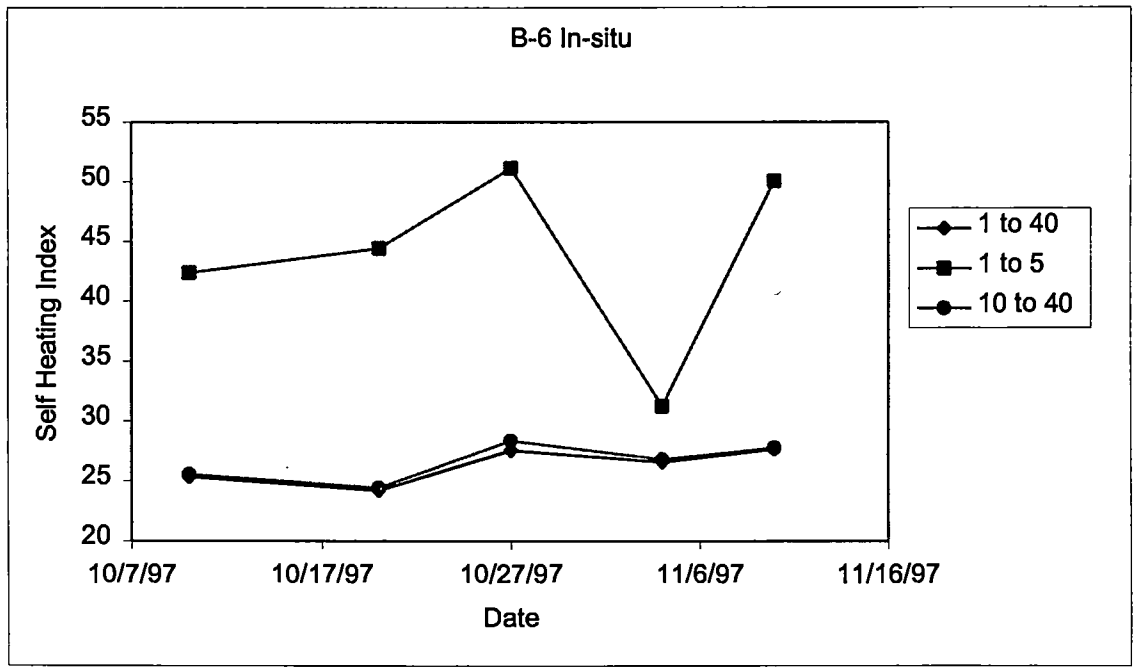


Figure 10.8 Plot of the In-situ Self Heating Index Measurements for RTD B-6

Table 10.11 Self-Heating Index and Correlation Values for RTD B-11

In-situ Date	Alpha Date	Calibration Alpha	Calibration SHI (Ω/W)	In-situ SHI 1 to 40	In-situ SHI 1 to 5	In-situ SHI 10 to 40
10/10/97	10/8/97	0.003831	18.66564	25.41222	40.315	25.50159
10/20/97	10/21/97	0.003844	19.12827	26.99441	44.89816	27.04285
10/27/97	10/28/97	0.00384	19.14272	27.80282	45.11237	28.01426
11/4/97	11/4/97	0.003838	19.1504	26.25698	51.14945	26.30878
11/10/97	11/11/97	0.003838	19.3217	27.26835	41.14015	27.29114
11/17/97	11/19/97	0.003831	19.39459	26.03306	44.49501	25.89716
12/3/97	12/4/97	0.003795	21.65394	28.6716	48.01517	28.56775
RTD B-11	Correlations:		-0.91641	-0.51332	-0.24445	-0.45258

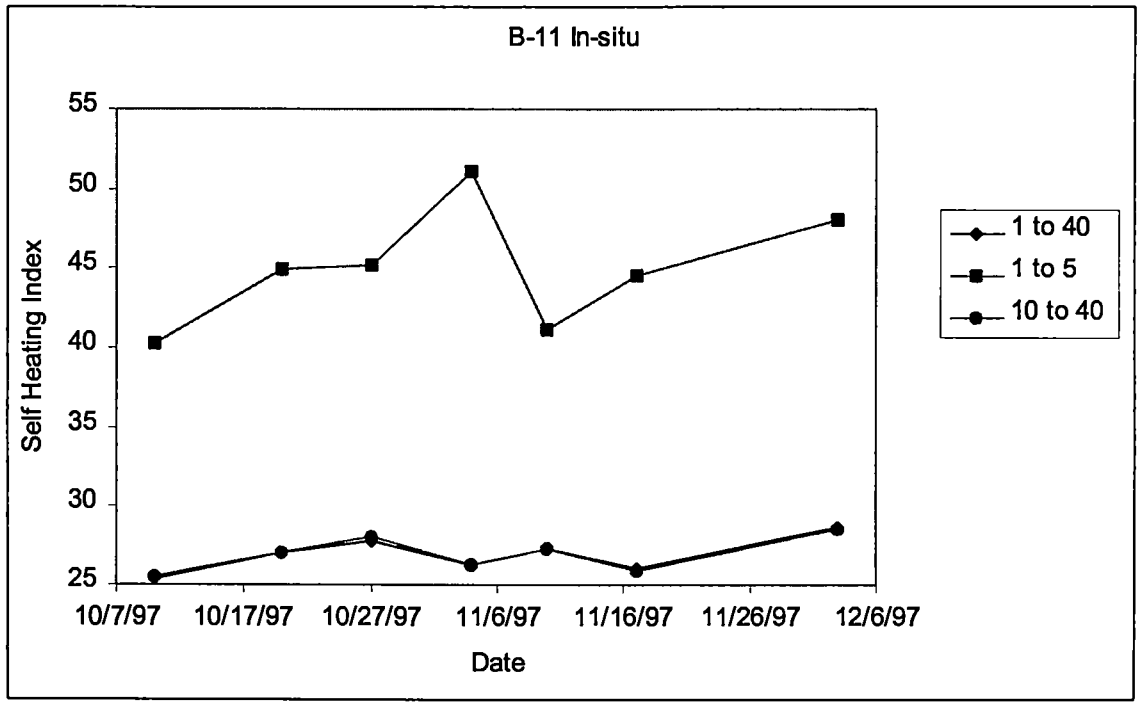


Figure 10.9 Plot of the In-situ Self Heating Index Measurements for RTD B-11

Table 10.12 Self-Heating Index and Correlation Values for RTD A-66

In-situ Date	Alpha Date	Calibration Alpha	Calibration SHI (Ω/W)	In-situ SHI 1 to 40	In-situ SHI 1 to 5	In-situ SHI 10 to 40
10/13/97	10/14/97	0.003842	5.580353	7.427632	23.97828	7.442216
10/21/97	10/21/97	0.003843	5.587017	7.597483	25.64674	7.580418
10/28/97	10/28/97	0.003842	5.564701	7.493069	23.65273	7.4457
11/4/97	11/4/97	0.00384	5.615153	7.32852	22.75208	7.375422
11/10/97	11/11/97	0.003839	5.689259	7.392343	23.7733	7.421131
11/17/97	11/19/97	0.003838	5.639276	7.339891	15.20846	7.373547
12/3/97	12/4/97	0.003836	5.540254	7.608075	23.24803	7.631478
RTD A-66	Correlations:		-0.18585	0.1857	0.51129	-0.0128

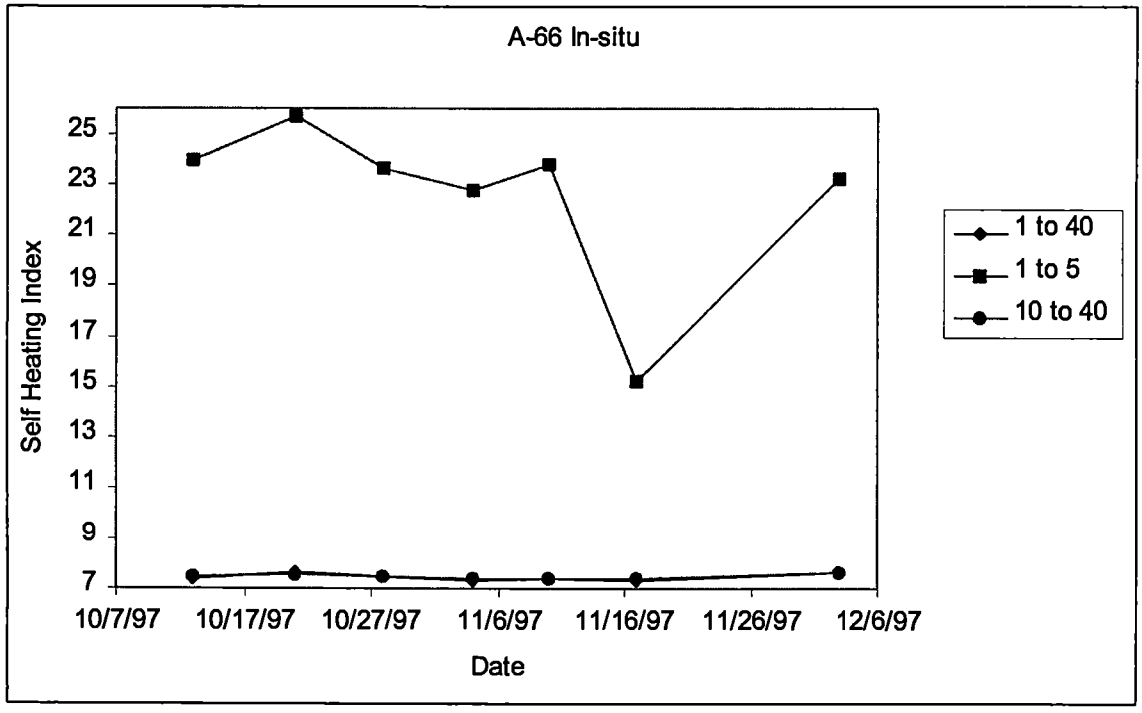


Figure 10.10 Plot of the In-situ Self Heating Index Measurements for RTD A-66

Table 10.13 Self-Heating Index and Correlation Values for RTD A-69

In-situ Date	Alpha Date	Calibration Alpha	Calibration SHI (Ω/W)	In-situ SHI 1 to 40	In-situ SHI 1 to 5	In-situ SHI 10 to 40
10/13/97	10/17/97	0.003843	5.893637	7.780927	20.00558	7.809189
10/21/97	10/24/97	0.003843	6.131411	8.501638	16.8623	8.554139
10/28/97	10/30/97	0.003843	6.182949	7.539403	20.8215	7.53454
11/4/97	11/6/97	0.003843	6.207843	7.846841	20.73038	7.895144
11/10/97	11/13/97	0.003842	6.066393	7.713555	22.23345	7.734649
11/17/97	11/20/97	0.00384	6.027186	7.59477	22.39968	7.606896
12/3/97	12/4/97	0.003841	6.096408	7.769572	19.94887	7.809617
RTD A-69	Correlations:		0.186412	0.357955	-0.4956	0.351329

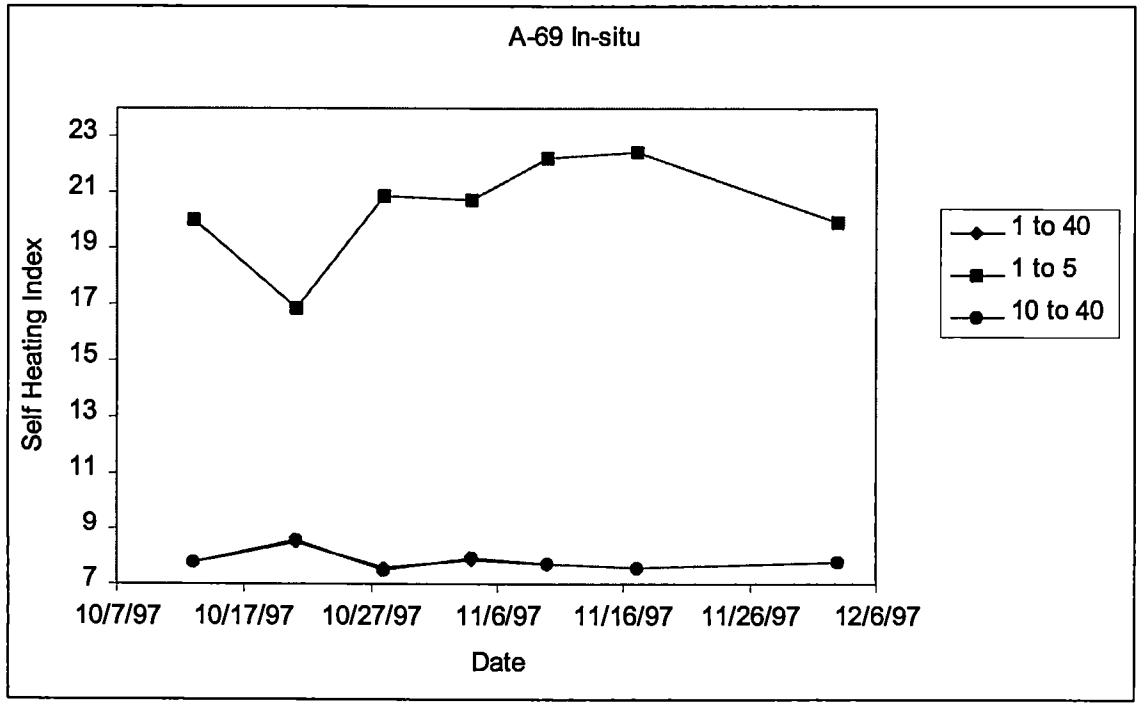


Figure 10.11 Plot of the In-situ Self Heating Index Measurements for RTD A-69

The in-situ correlations may be skewed in this study due to the lack of a concurrent alpha measurement. Effort was made to provide closely coinciding measurements, but some alpha measurements were not available within two days of the in-situ self-heating index measurements. This time inconsistency may be insignificant over the life of a process RTD, but in an accelerated aging test the alpha measurement changes over several days may effect correlation results.

The final observation is that the in-situ self-heating index measurements did not respond as the calibration self-heating index measurements generally responded to furnace temperature changes. The calibration measurements ordinarily showed a shift in overall value at each temperature step. The in-situ measurements have no definitive changes at any of the furnace temperature increases, even though several of the individual measurements showed very defined shifts in value. These shifts may be muted by the disjoined alpha values discussed above, or may be insignificant in contribution to the overall calculations considering other applied current measurements saw no significant change.

The in-situ measurements provided useful information into the dynamics of process environment and self-heating indices. The additional study, as seen earlier in the calibration measurements, showed improved correlation results for the two RTDs noted in Table 10.8 as notable drift. Though the limited number of data points recorded does

not provide ample justification for any conclusion, there is justification for additional study into the dynamics of the in-situ self-heating index measurement and alpha.

CHAPTER 11

CONCLUSIONS AND FUTURE WORK

11.1 Concluding Remarks

The primary goal of the thesis research was to study the changes in RTD calibration and performance characteristics as a function of accelerated thermal aging. A new state-of-the-art RTD testing laboratory was developed as part of this project. The aging studies were performed using thin-film and wire-wound RTDs. The laboratory has the capability for continuous, uninterrupted data acquisition from up to ninety RTDs. A method for the life prediction of RTDs using trends in the measured resistance was developed and applied successfully to the aging data. The following are the major conclusions of this research.

- The aging of RTDs at high temperatures results in a decrease in the calibration constant α (Callendar-Van Dusen equation) and an increase in the ice point resistance R_0. These changes are consistent with the expected behavior of these RTDs.
- A high correlation (correlation coefficients greater than 0.8) between the calibration parameter α and the self-heating index (SHI) was observed. This conclusion is derived from results of tests from both thin film and wire-wound RTDs.
- The self-heating index shows a consistent trend throughout the thermal aging experiment.

- Thermal aging with temperature cycling causes a faster degradation of RTDs compared to those with constant temperature aging with the same mean furnace temperature.
- A new algorithm was developed for estimating the remaining calibration lifetime of RTDs using resistance-time trends. The predictions of time-to-alarm and time-to-failure are consistent with the observed alarm and failure times.
- *Ultimate failure temperatures* of RTDs were established by continuously increasing the furnace temperatures until the RTDs either failed open or started to show erratic behavior. This maximum temperature is in the range 600-700 °C for thin film type RTDs and in the range 800-900 °C for wire-wound type RTDs.

The correlation between the calibration constant and the self-heating index, when fully established may be used on-line for verifying the calibration status of RTDs. This intelligence can be built into the transmitter.

11.2 Recommendations for Future Research and Development

The study of thermal aging of RTDs should continue in order to build up an extensive database and to establish a high confidence in the correlation among RTD performance parameters. The following are the major tasks that should be carried out in future research:

- Continuation of the thermal aging of RTDs at constant temperature and under temperature cycling conditions. A large database should be established in order to

focus on the relationship between calibration constant alpha and performance parameters such as the self-heating index and the resistance drift rate.

- Further investigation into the in-situ self-heating index and how well this parameter is related to the calibration constant alpha. Additionally further investigation into how the measurements in the self-heating index change relative to medium temperature may provide useful insight.
- Additional investigation into the reduction in applied current to determine the self-heating index. This reduction in applied current has the benefit of more widespread application of a self-heating index if proven effective.
- Destructive testing of the RTDs including micrographic structural analysis should be completed. The mechanism behind the relationship between the self-heating index and the calibration coefficient alpha is inherent to the RTD mechanics. The way to definitively determine this mechanism is to structurally examine a new and several degraded and failed RTDs.
- Broadening of the scope to include several manufactures of RTDs and thermocouples. Investigation should be completed to determine if the characteristics noted here are applicable only to the sensors tested in this study, or if the characteristics seen are common to RTDs made by most of the sensor manufacturers.

REFERENCES

REFERENCES

1. W.F. Smith, "Principles of Materials Science and Engineering," McGraw-Hill, New York, Chapter 5, 1996.

2. T.W. Kerlin and R.L. Shepard, "Industrial Temperature Measurement," Instrument Society of America, 1982.

3. Rosemount Measurement, "Temperature Sensors, Assemblies and Accessories," PDS2654A00, September 1995.

4. H.M. Hashemian, D.D. Beverly, D.W. Mitchell and K.M. Petersen, "Aging of Nuclear Plant Resistance Temperature Detectors," NUREG/CR-5560, June 1990.

5. R.L. Shepard, "Calibration of Industrial Platinum Resistance Thermometers," ASTM Monograph on Resistance Temperature Detectors (to be published), 1997.

6. D.H. Rossi, Private Communication, Rosemount Measurement Division, Fisher-Rosemount, June 1996.

7. B.W. Magnum and G.T. Furukawa, "Guidelines for Realizing the International Temperature Scale of 1990 (ITS-90)," NIST Technical Note 1265, U.S. Dept. of Commerce, August 1990.

8. Rosemount Aerospace, "Report of Calibration: Standard Platinum Resistance Thermometer," September 1995.

9. T.W. Kerlin and E.M. Katz, "Temperature Measurement in the 1990s," InTech, pp 40-43, August 1990.

10. B.R. Upadhyaya and T.W. Kerlin, "Estimation of Response Time Characteristics of Platinum Resistance Thermometers by the Noise Analysis Technique," ISA Transactions, Vol. 29, No. 4, pp 21-38, 1978.

11. P.H. Myers, "Classical and Modern Regression with Applications," PWS-SENT Publishing Co., Boston, 1990.

12. B.R. Upadhyaya, B. Raychaudhuri, J.E. Banks and M. Naghedolfeizi, "Monitoring and Prognosis of Plant Components," P/PM Technology, Vol. 7, No. 6, pp 43-49, December 1994.

13. "Standard Test Methods for Testing Industrial Resistance Thermometers," ASTM Standard E-644-91, pp 317-335, 1991.

14. J.V. Nicholas and D.R. White, "Traceable Temperatures," John Wiley, New York, 1994.

15. T.W. Kerlin et al, "Uncertainty in Temperature Measurements with Industrial Platinum Resistance Thermometers," Proc. IMEKO XI, Houston October 1988.

16. R.L. Shepard et al, "Advanced Thermetrics for Fossil Power Plant Process Improvement," Pres. ISA POWID/EPRI Controls and Instrumentation Conference, Baltimore, June 1996.

17. B.R. Upadhyaya, A.E. Silber, P.B.S. Ferreira, M.S. Hammond, "Long-Term Aging Of Temperature Detectors And Validation Of Distributed Sensors," Research Report, University of Tennessee, December 1997.

APPENDICIES

Appendix A

Plots of all RTD resistance measurements for all included tests.

Table A.1, provided below, serves as the index for the figures included in this appendix. A complete plot is included for each numbered test, as well as an individual plot for each tested temperature step.

Table A.1 Summary of RTD Thermal Aging Tests

Test Number	RTD List	Furnace Number	Temperature History	Test Duration (days)	Test Type
1	A1-A8	OR-1	660	57	Soak
2	A9-A20	ATS-1	660	98	Soak
3	A21-A32	ATS-2	660	122 days	Soak
4	A33-A49	ATS-3	660, 700, 725, 750, 775, 800 & 850	525	Soak
5	A50-A60	ATS-1	500	151	Soak
6	A50-A64, B12-B15	ATS-1	600, 700, 800 & 900	52	Maximum Temperature
7	B1-B11	ATS-2	400, 450, 500, 525, 550, 575, 600 & 625	441	Soak
8	A65-A70, A204-A213 & B38-B40	ATS-4	550, 575, & 600	273	Soak
9	A71-A89	ATS-1	500-700, 550-750, & 575-775	223	Thermal cycling
10	A199	OR-2	450	326	Vibration

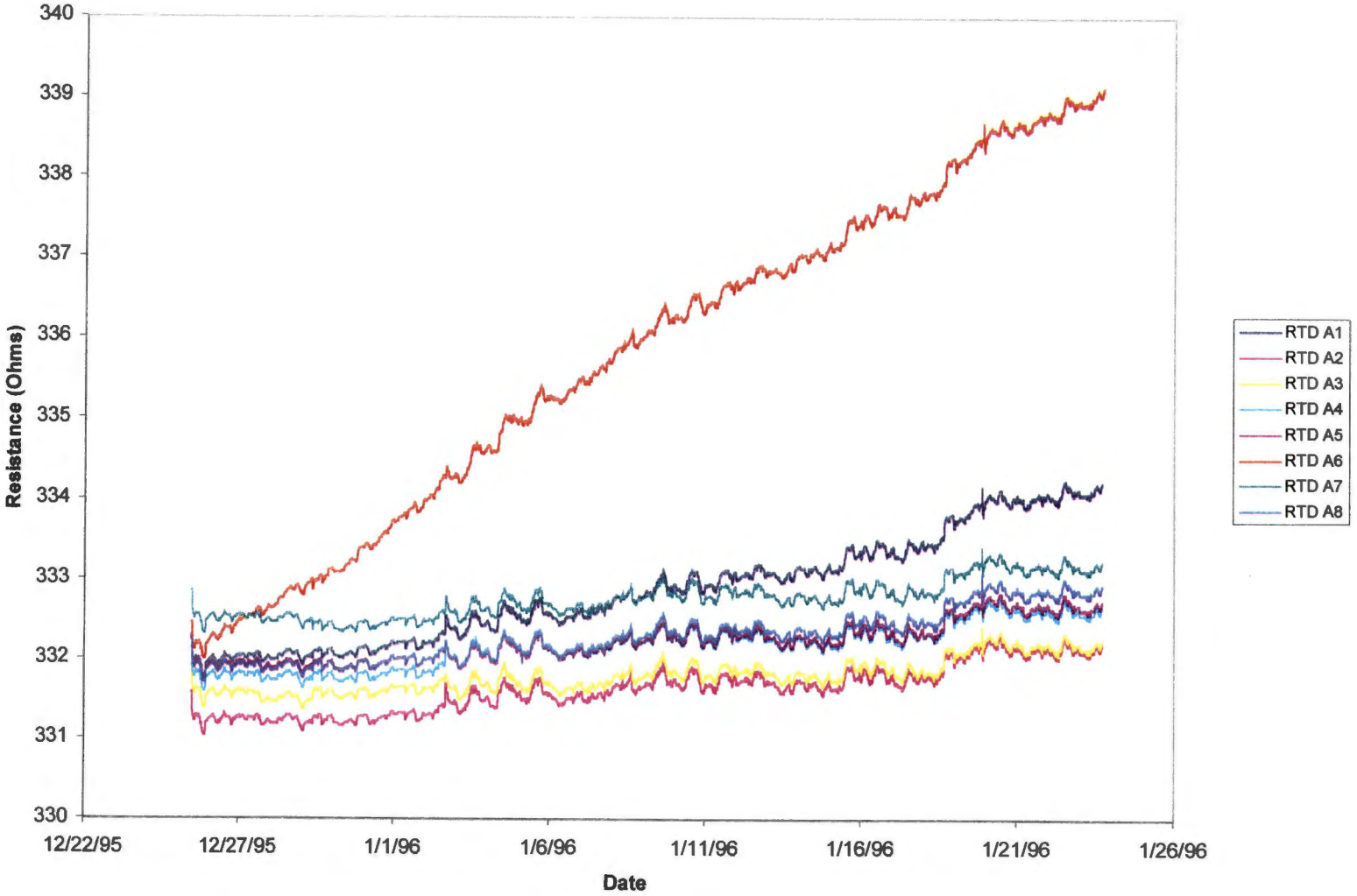


Figure A-1. Test #1 660 °C

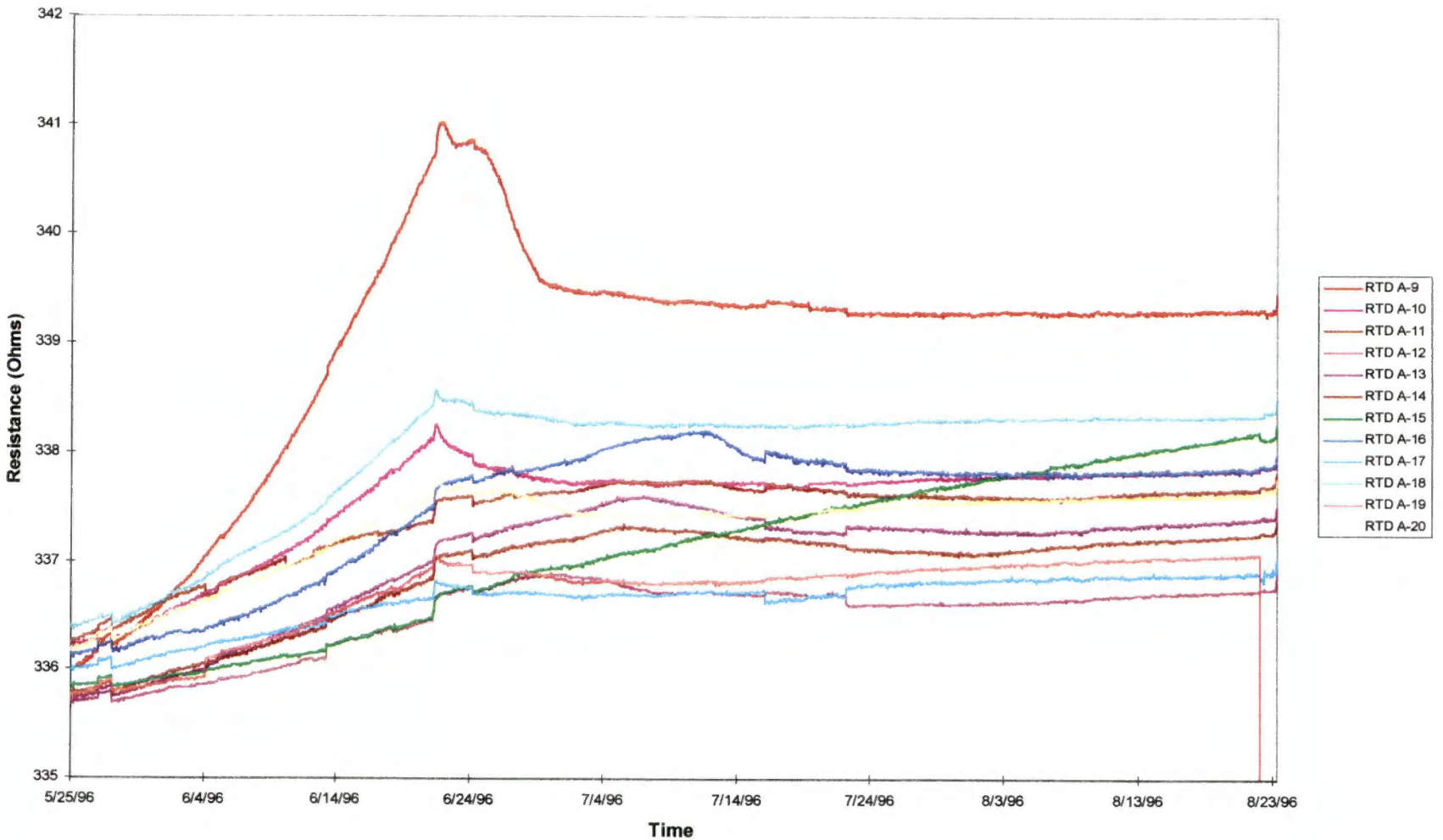


Figure A-2. Test #2 at 660 °C

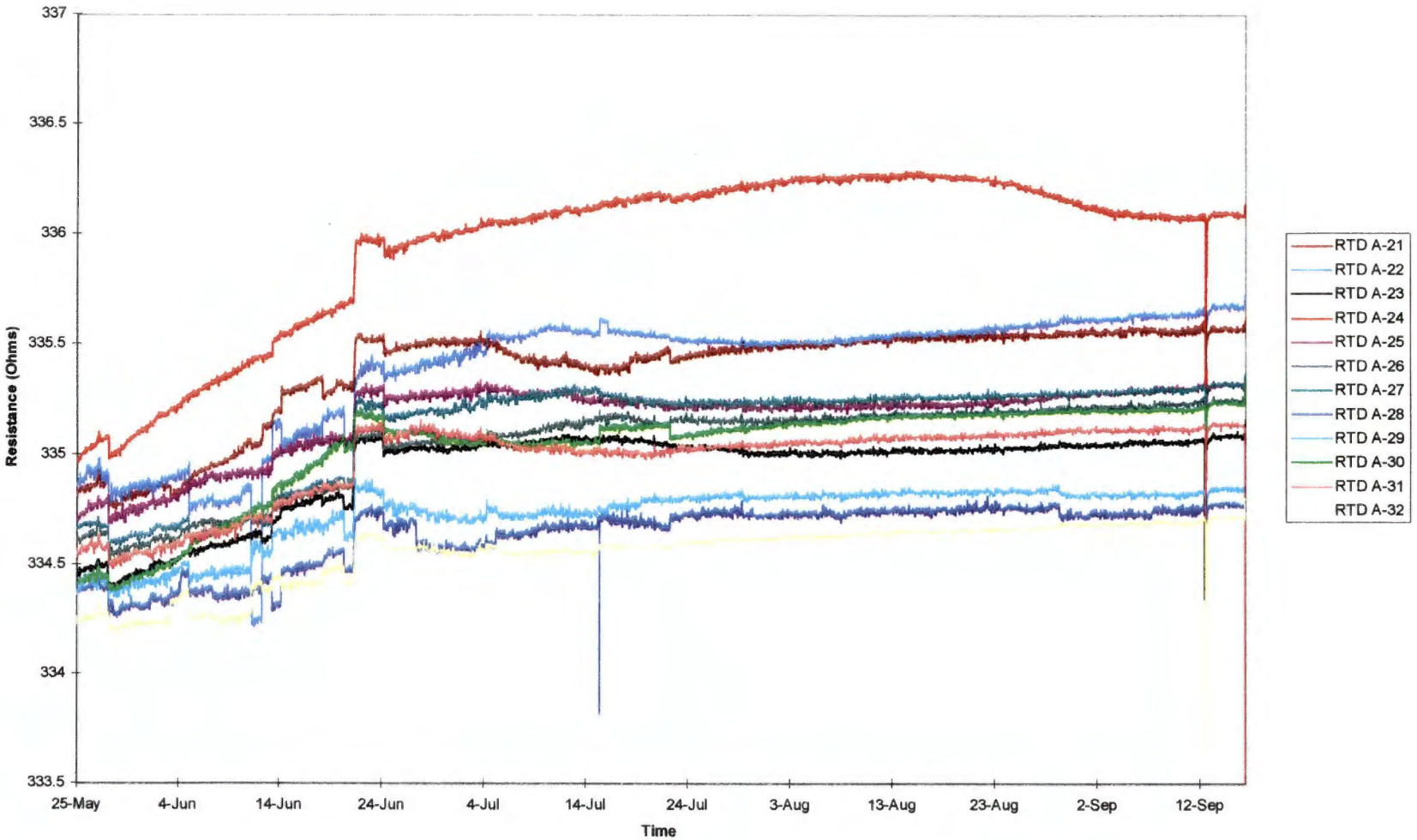


Figure A-3. Test #3 660 °C

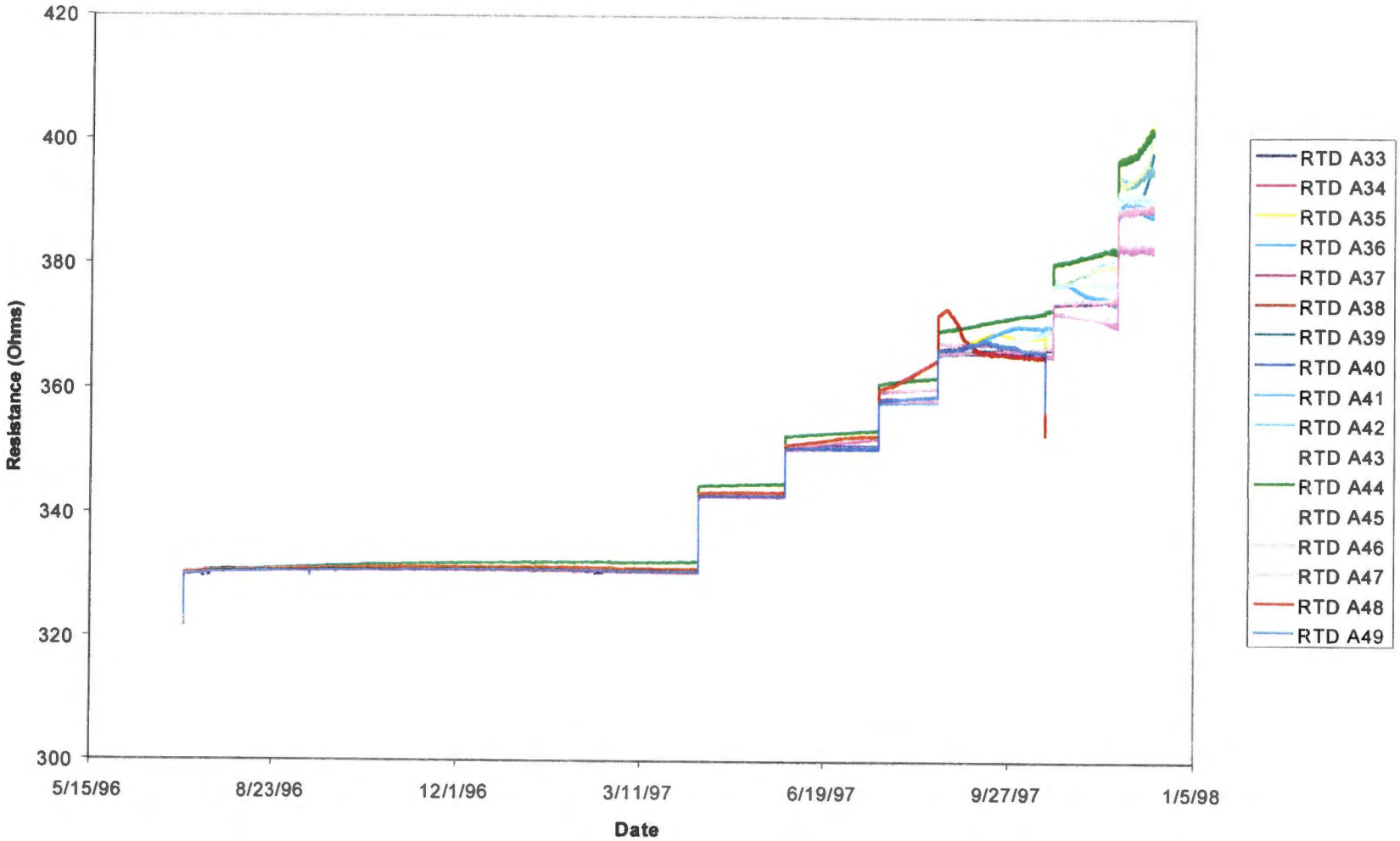


Figure A-4. Test #4 Full Temperature Plot

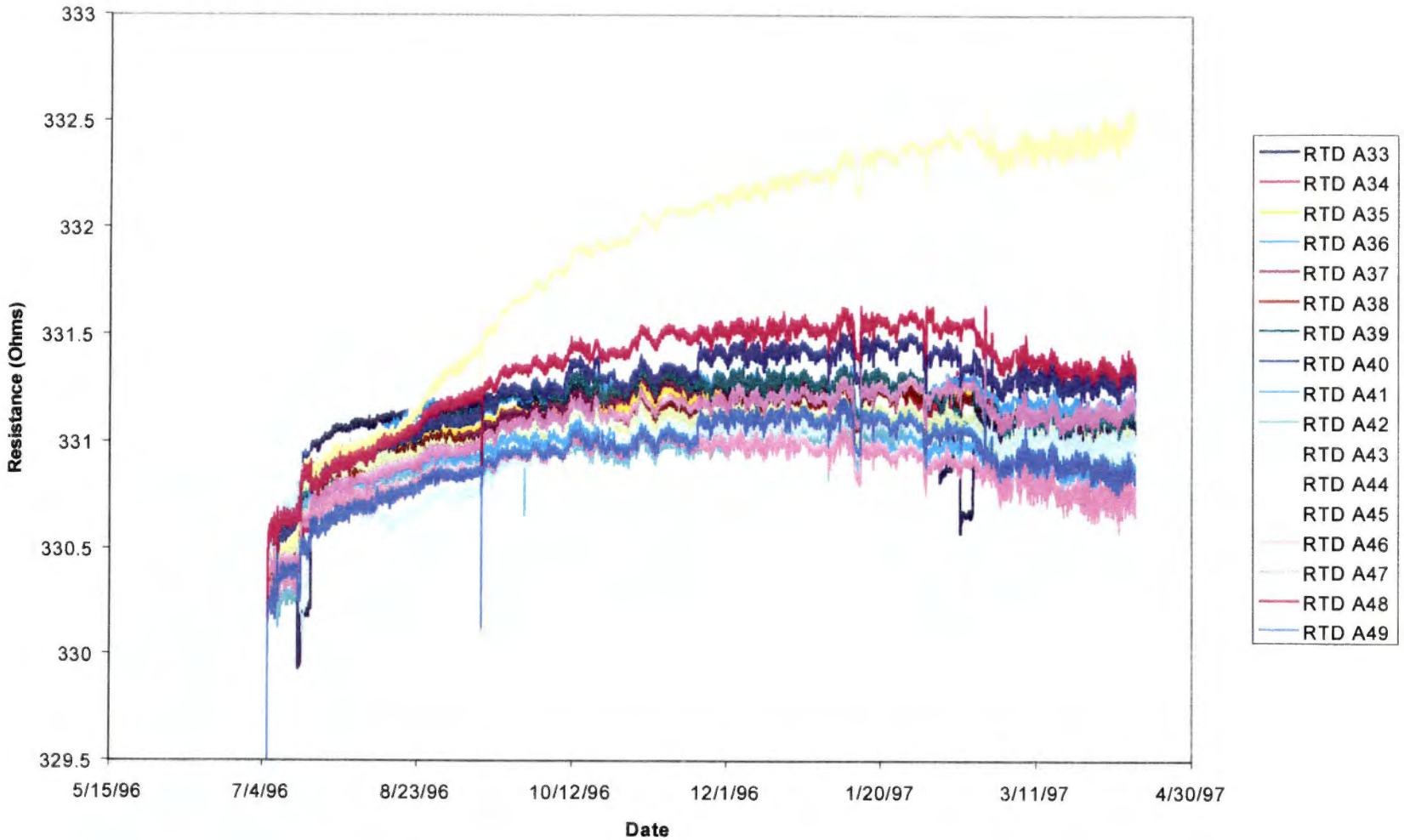


Figure A-5. Test #4 660 °C

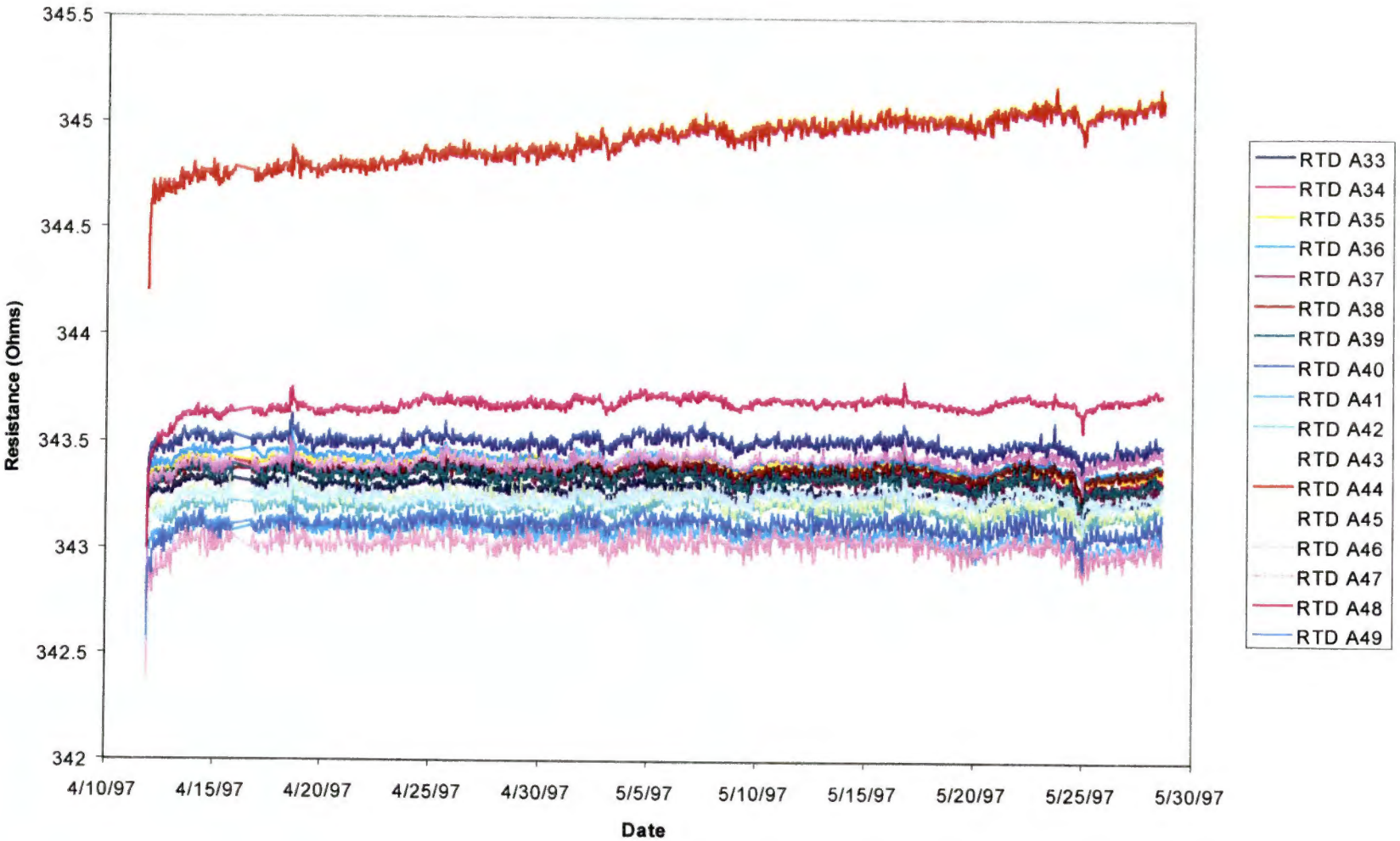


Figure A-6. Test #4 700 °C

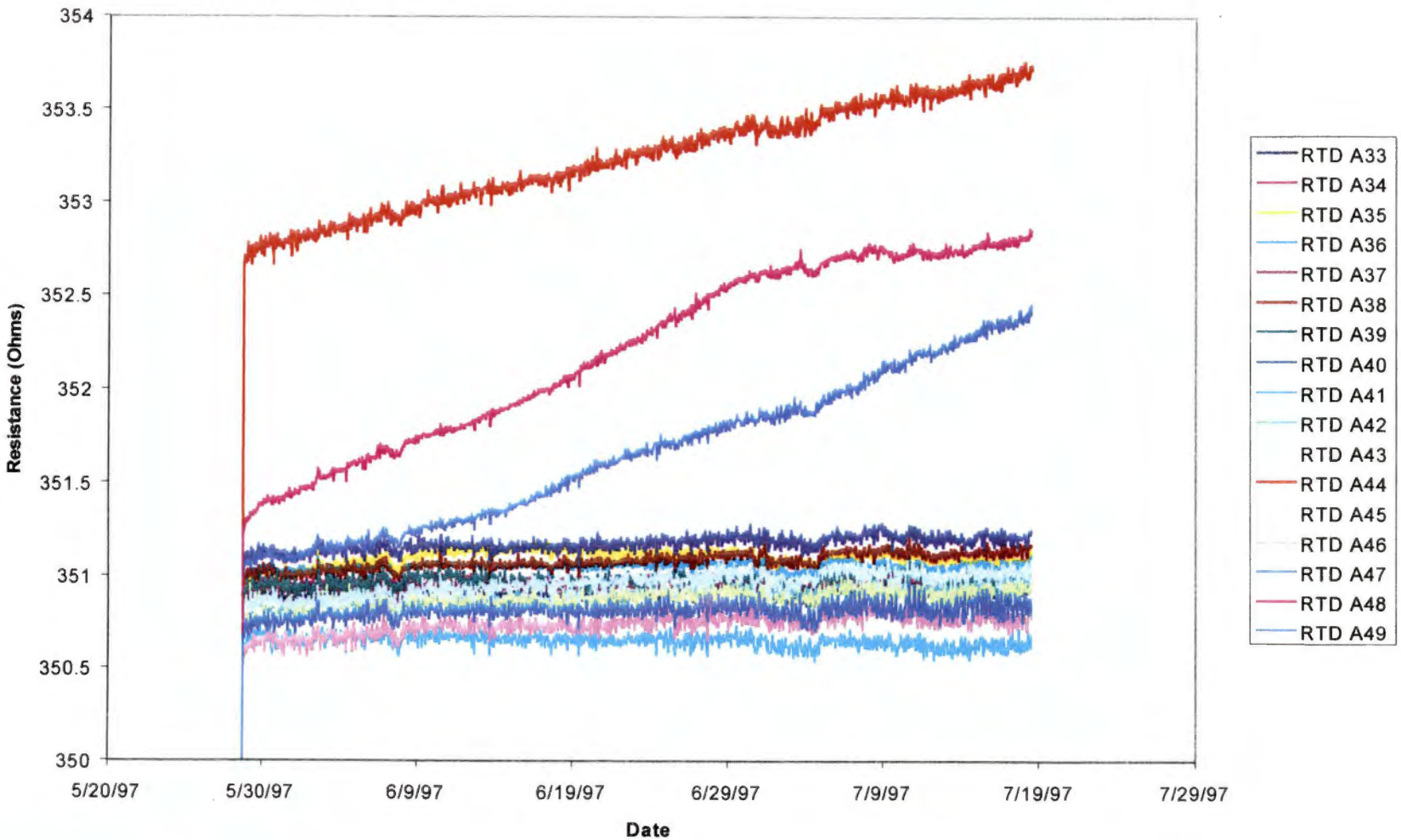


Figure A-7. Test #4 725 °C

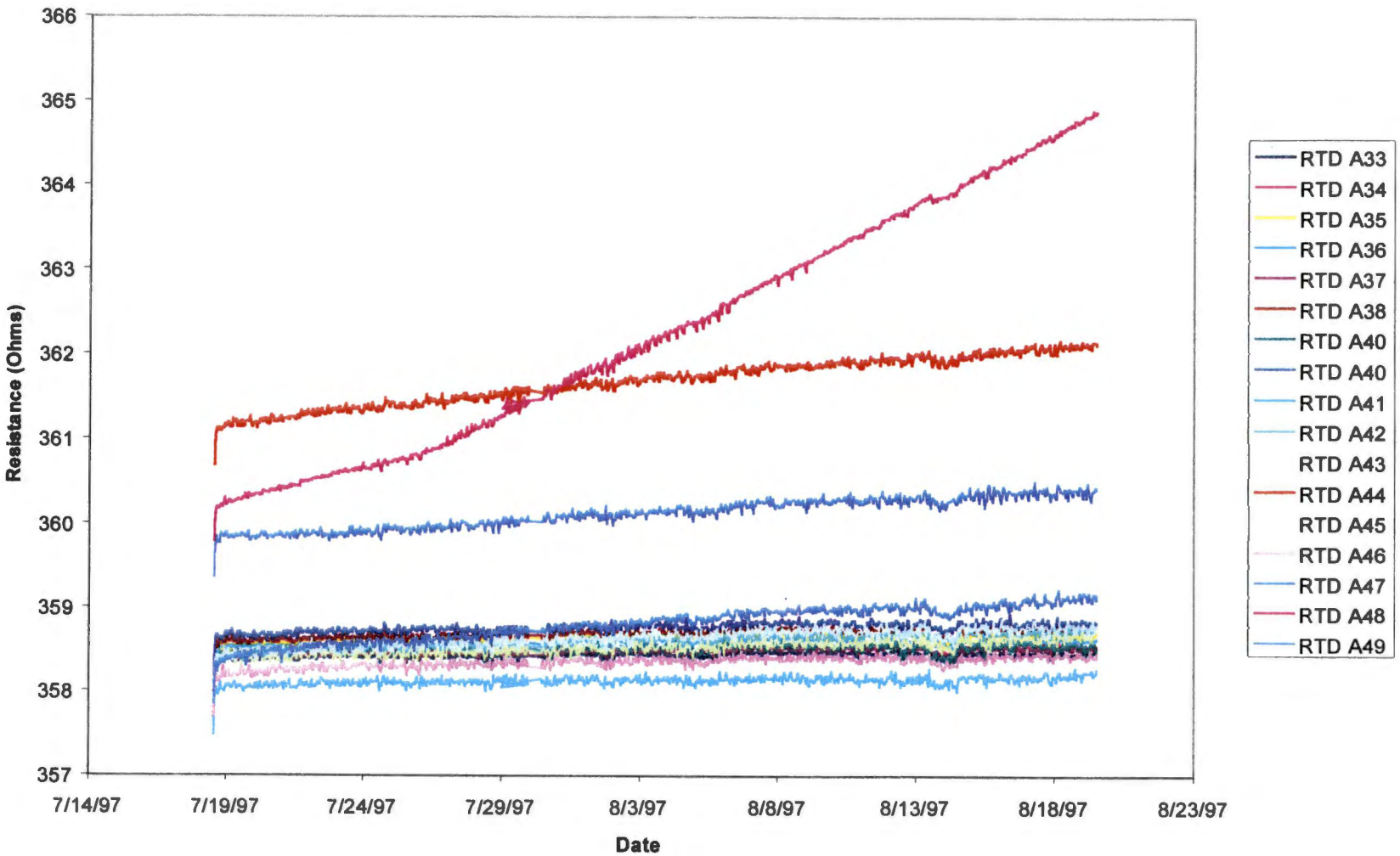


Figure A-8. Test #4 750 ℃

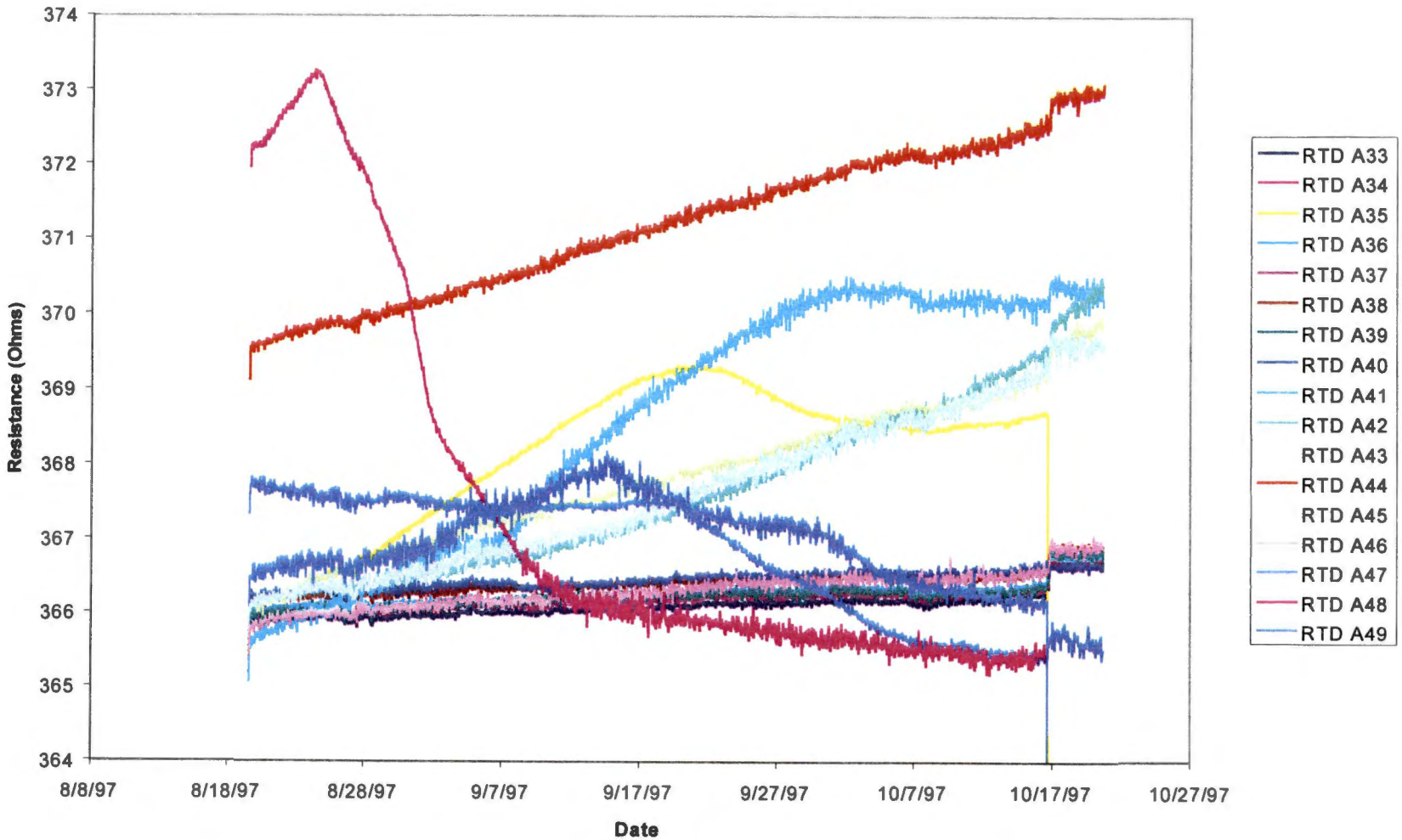


Figure A-9. Test #4 775 °C

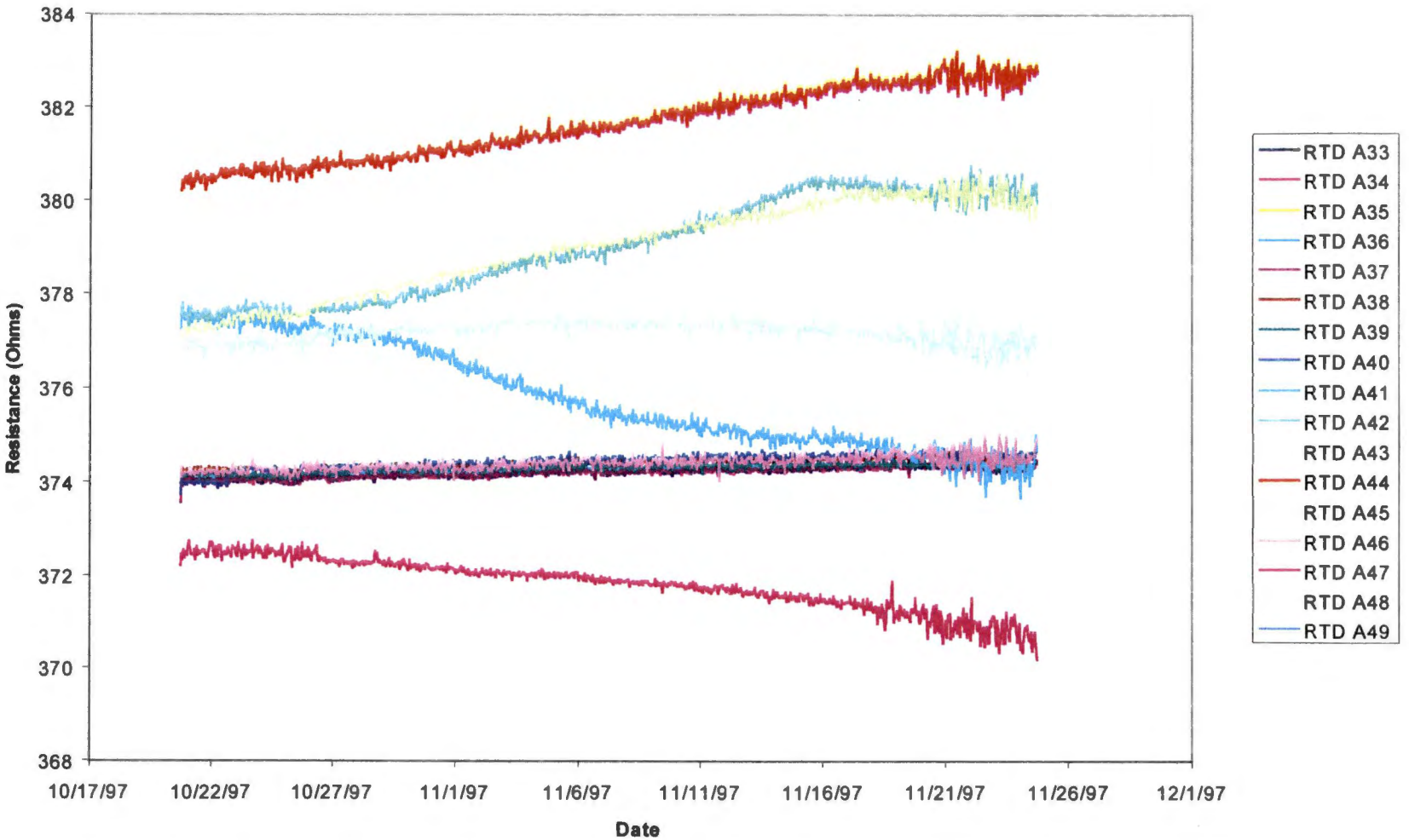


Figure A-10. Test #4 800 °C

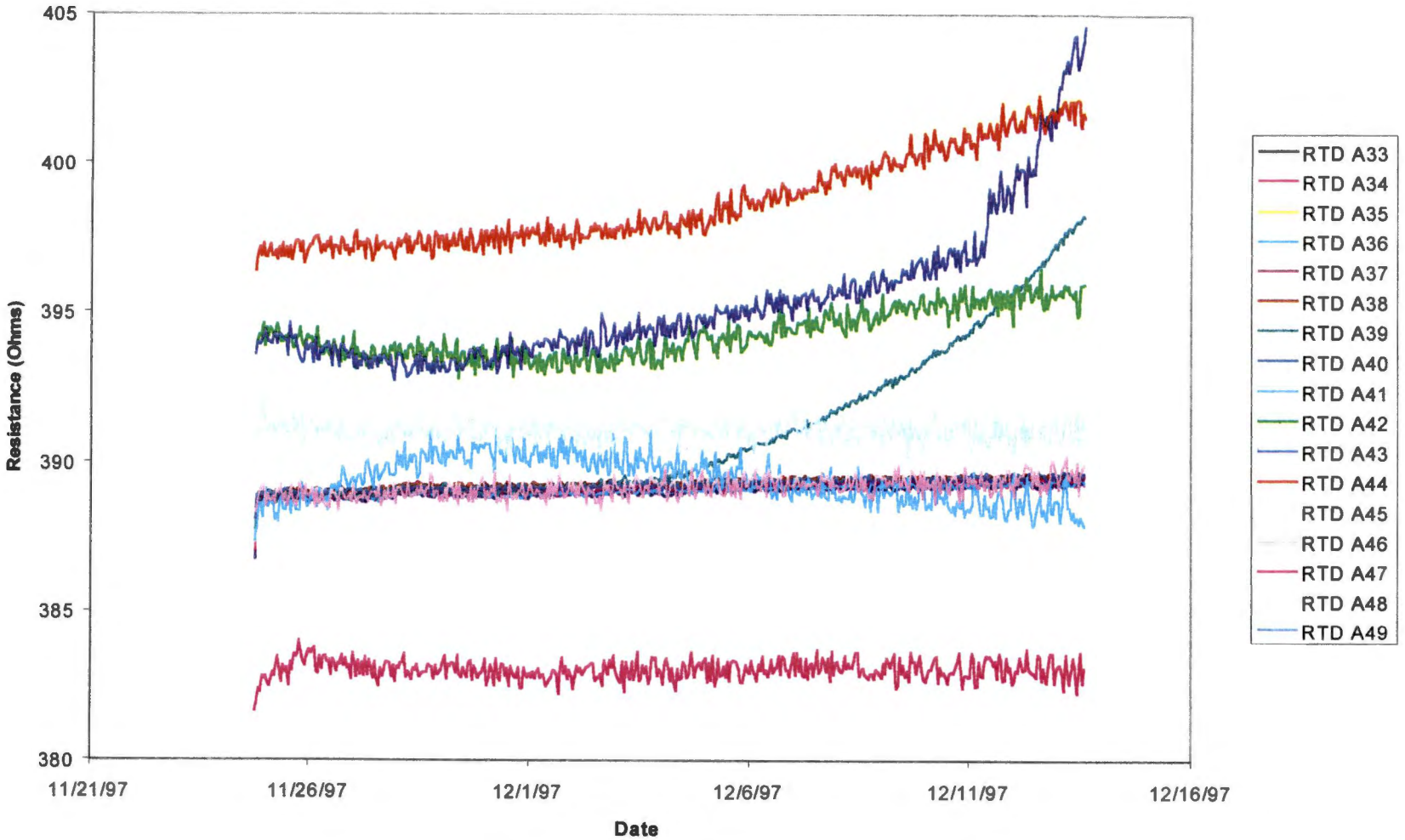


Figure A-11. Test #4 850 °C

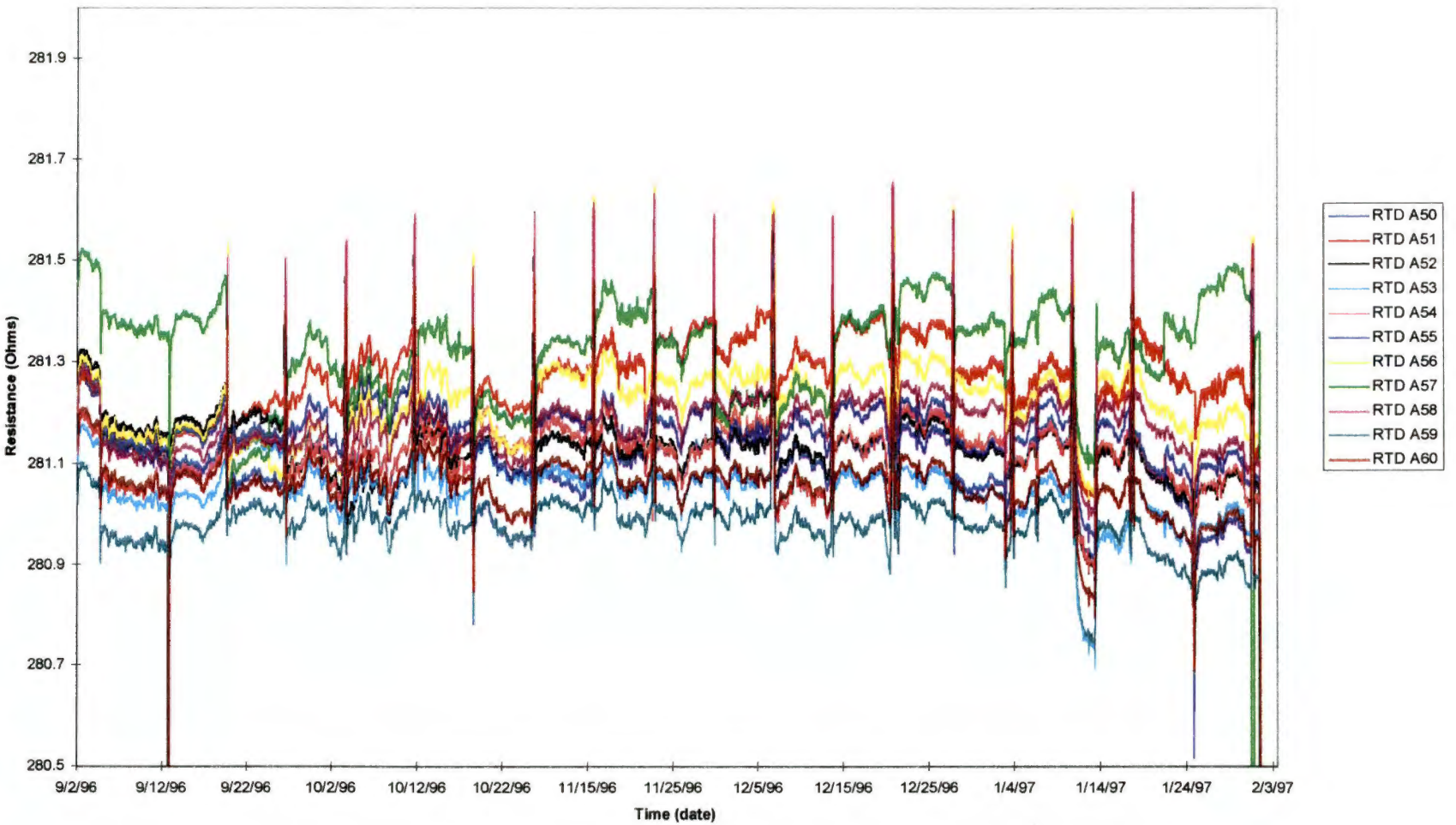


Figure A-12. Test #5 500 °C

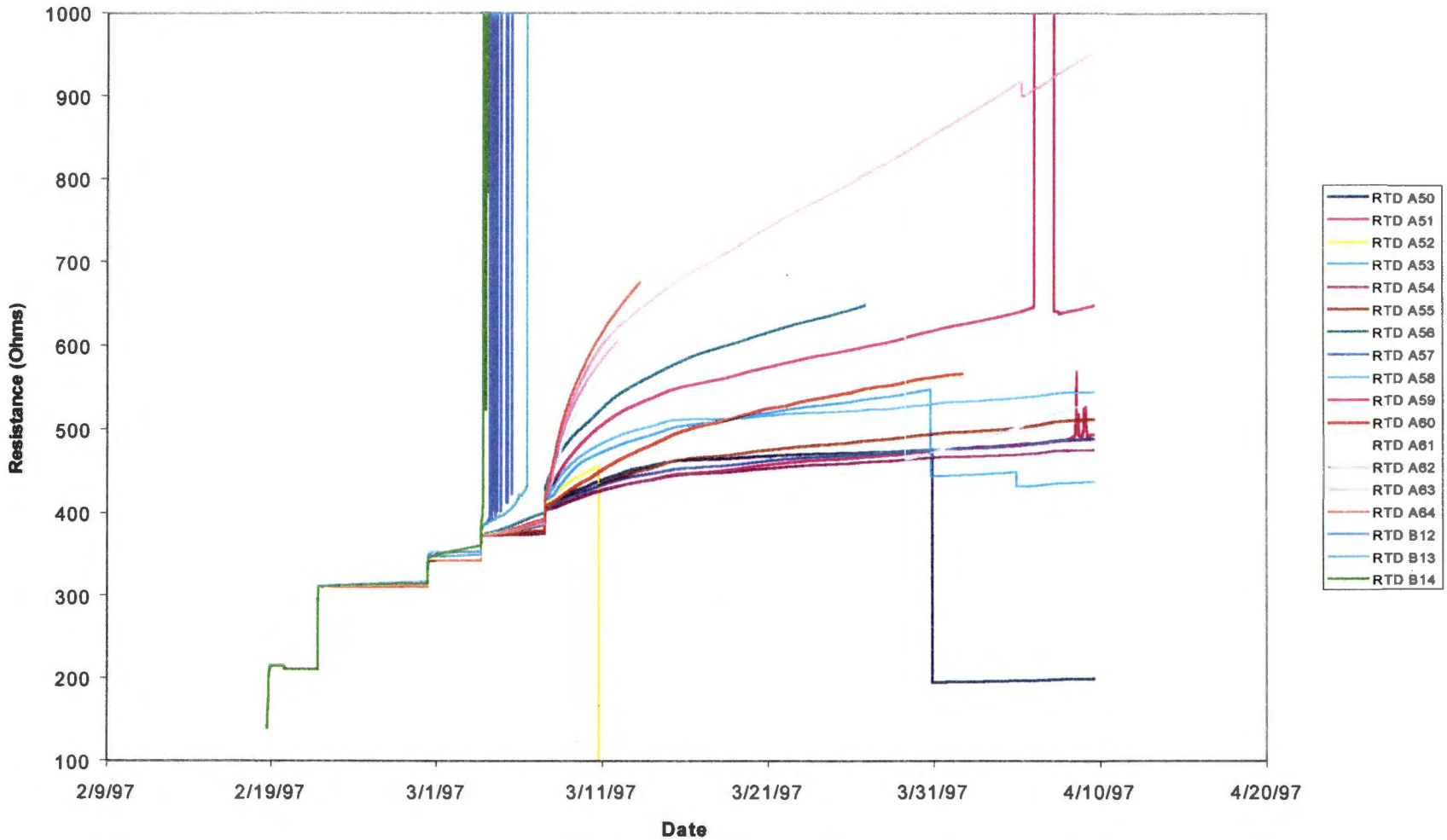


Figure A-13. Test #6 Full Plot All Temperatures

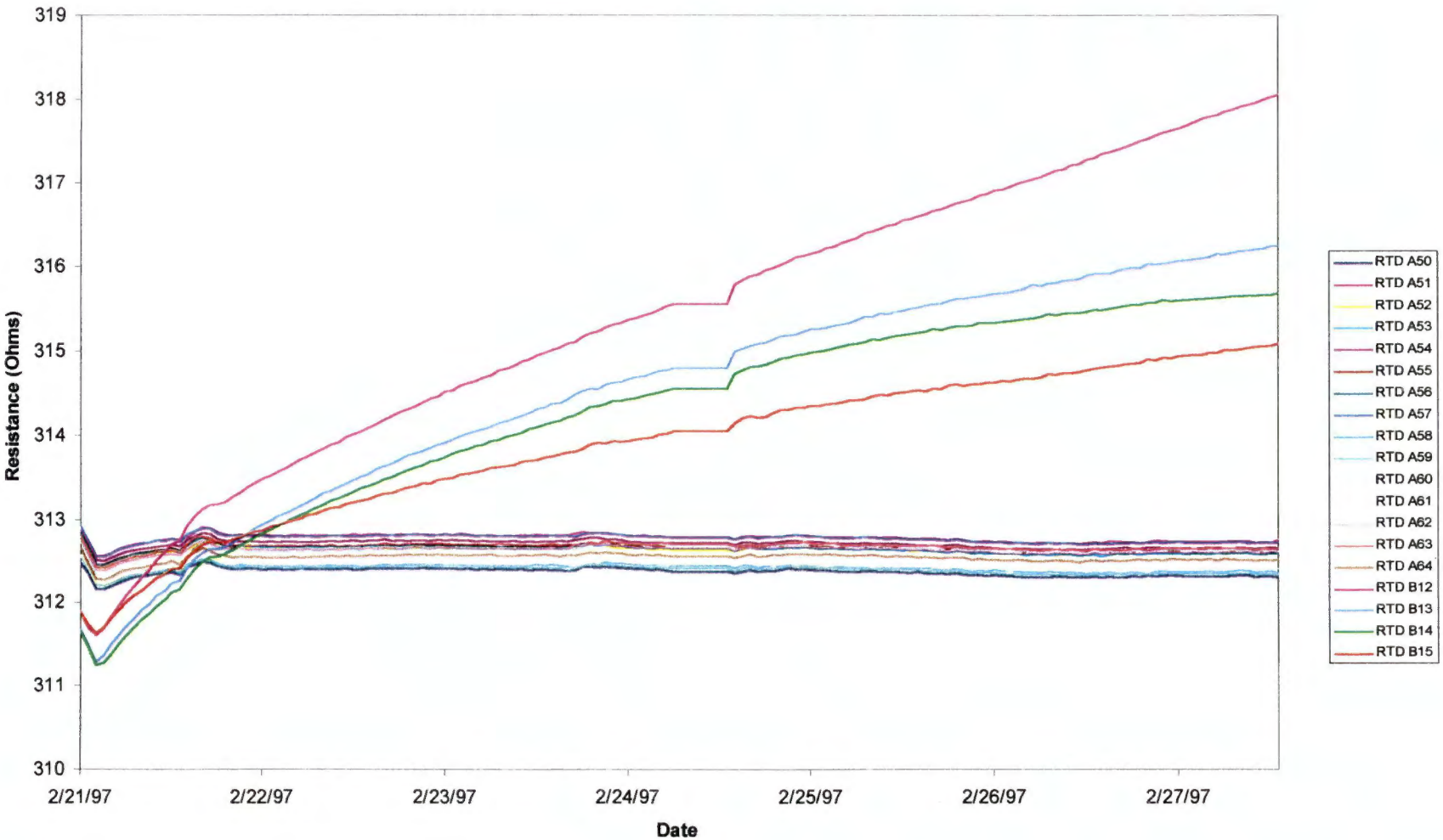


Figure A-14. Test #6 600 °C

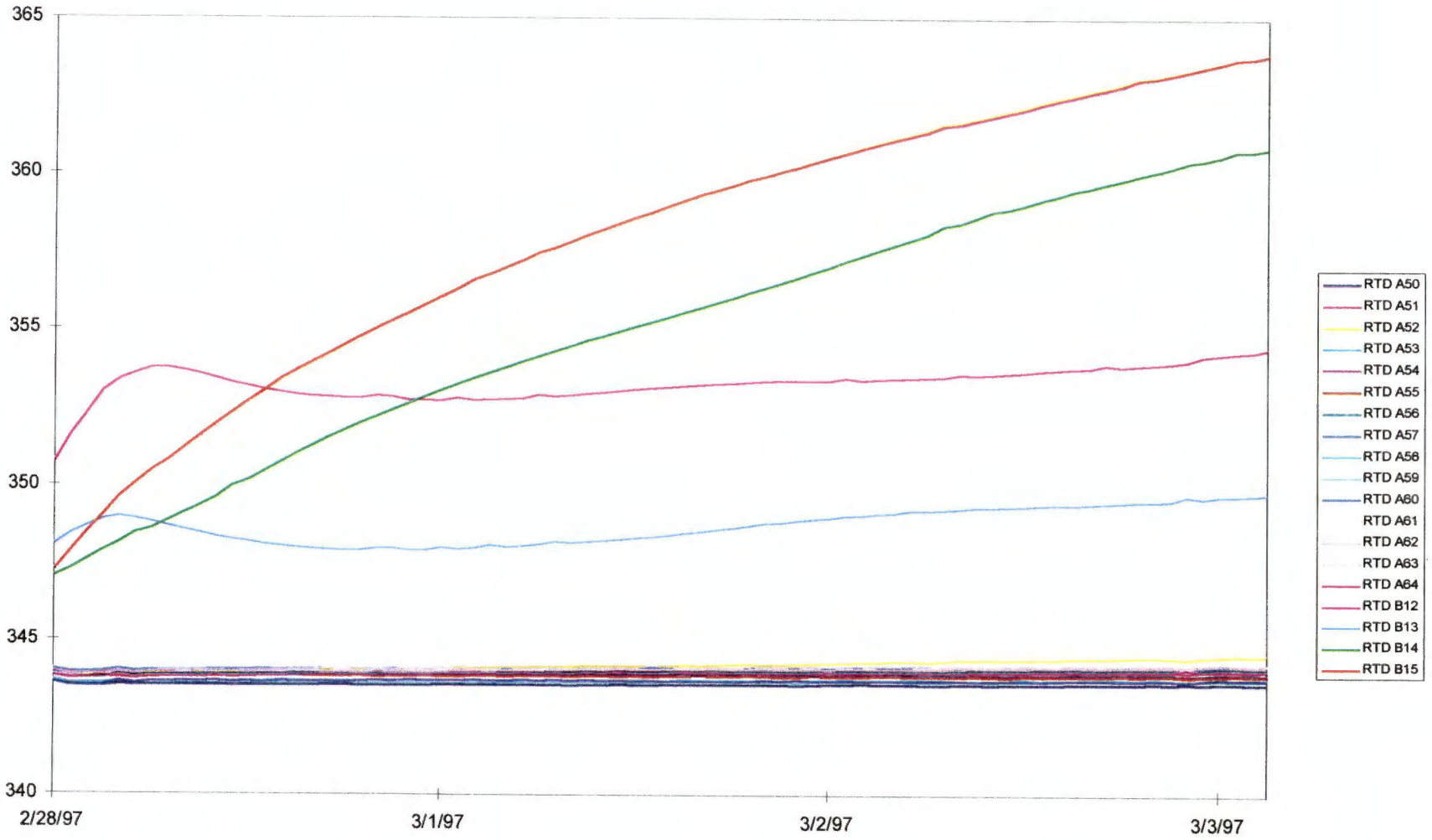


Figure A-15. Test #6 700 °C

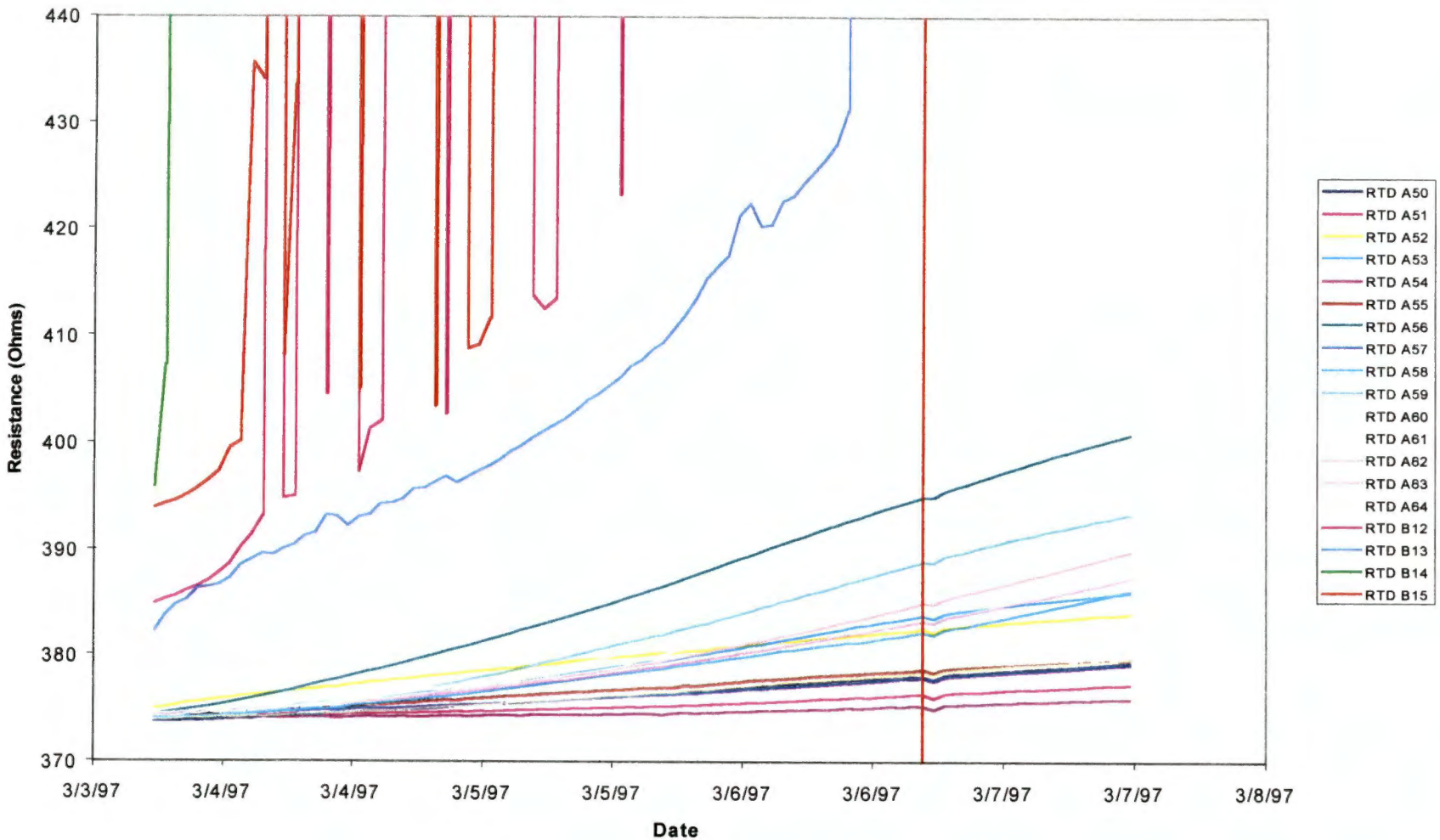


Figure A-16. Test #6 800 °C

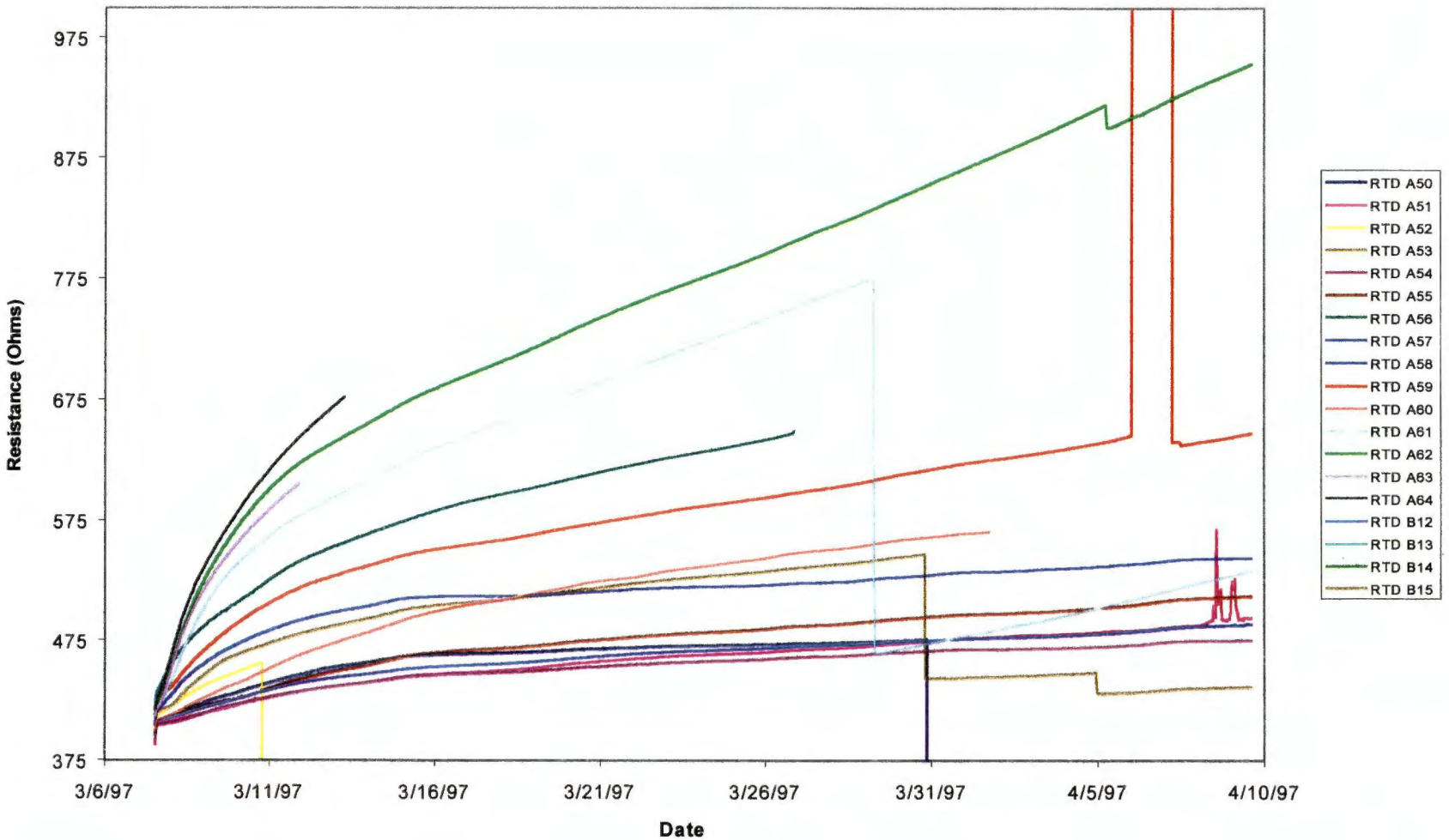


Figure A-17. Test #6 900 °C

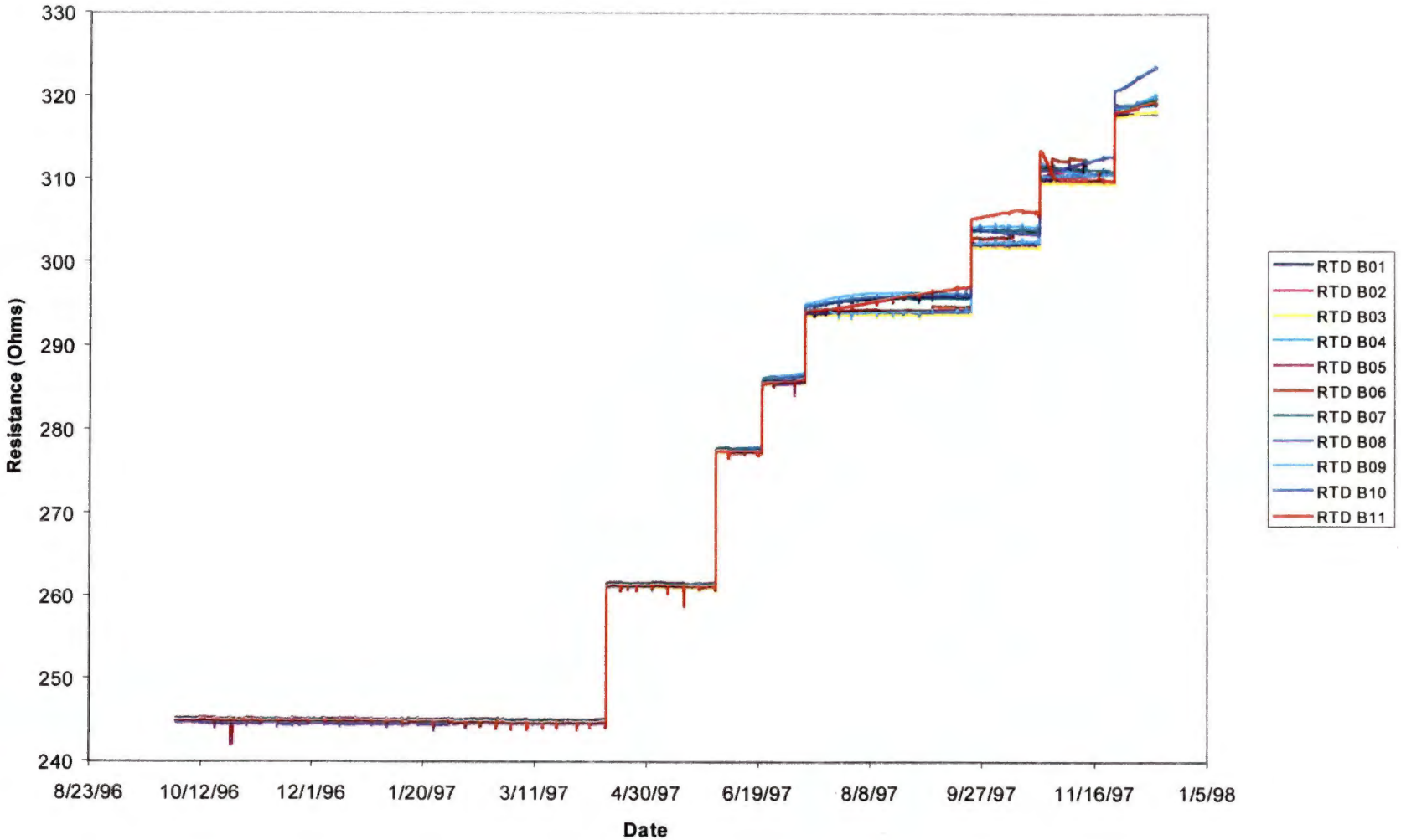


Figure A-18. Test #7 Full Plot All Temperatures

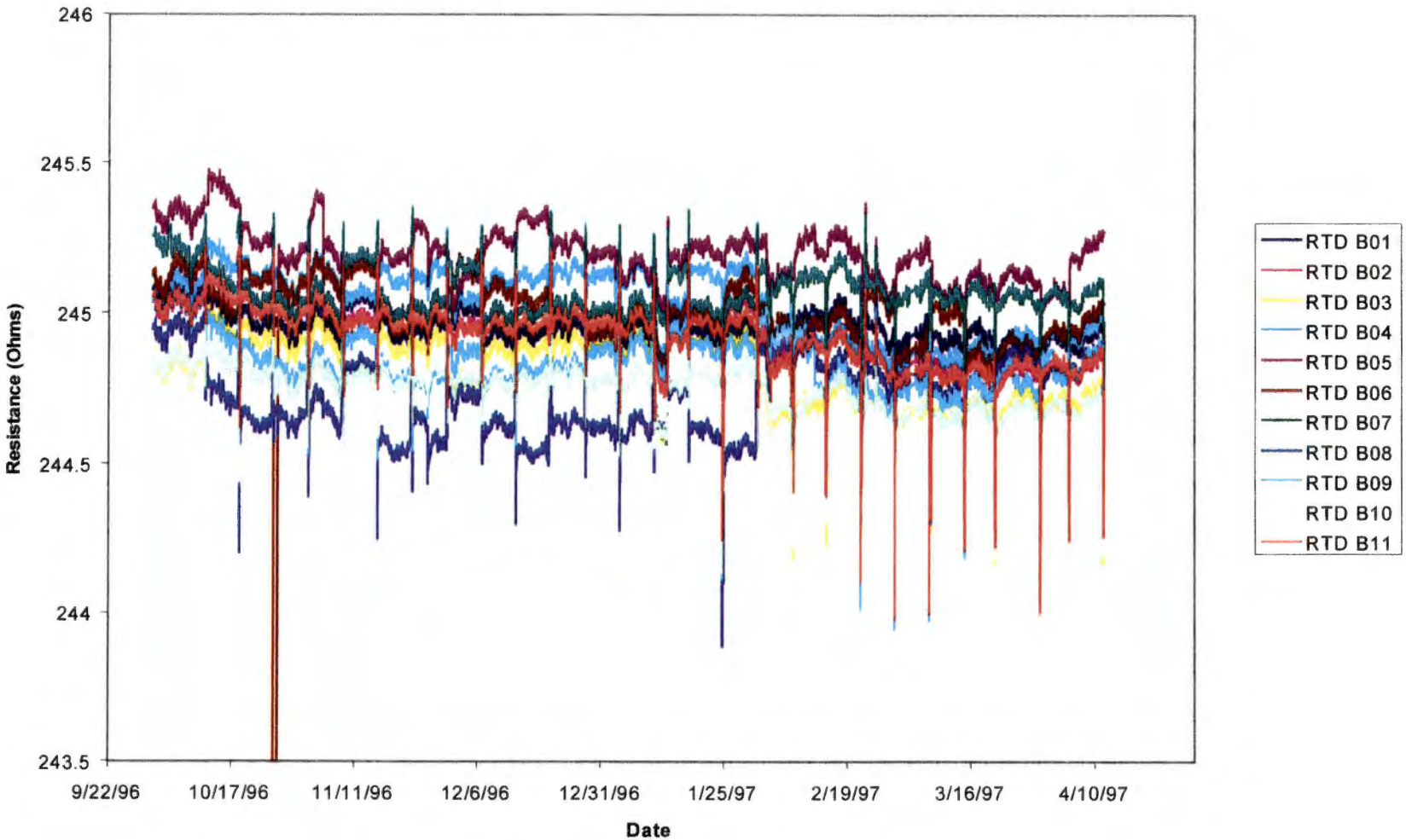


Figure A-19. Test #7 400 °C

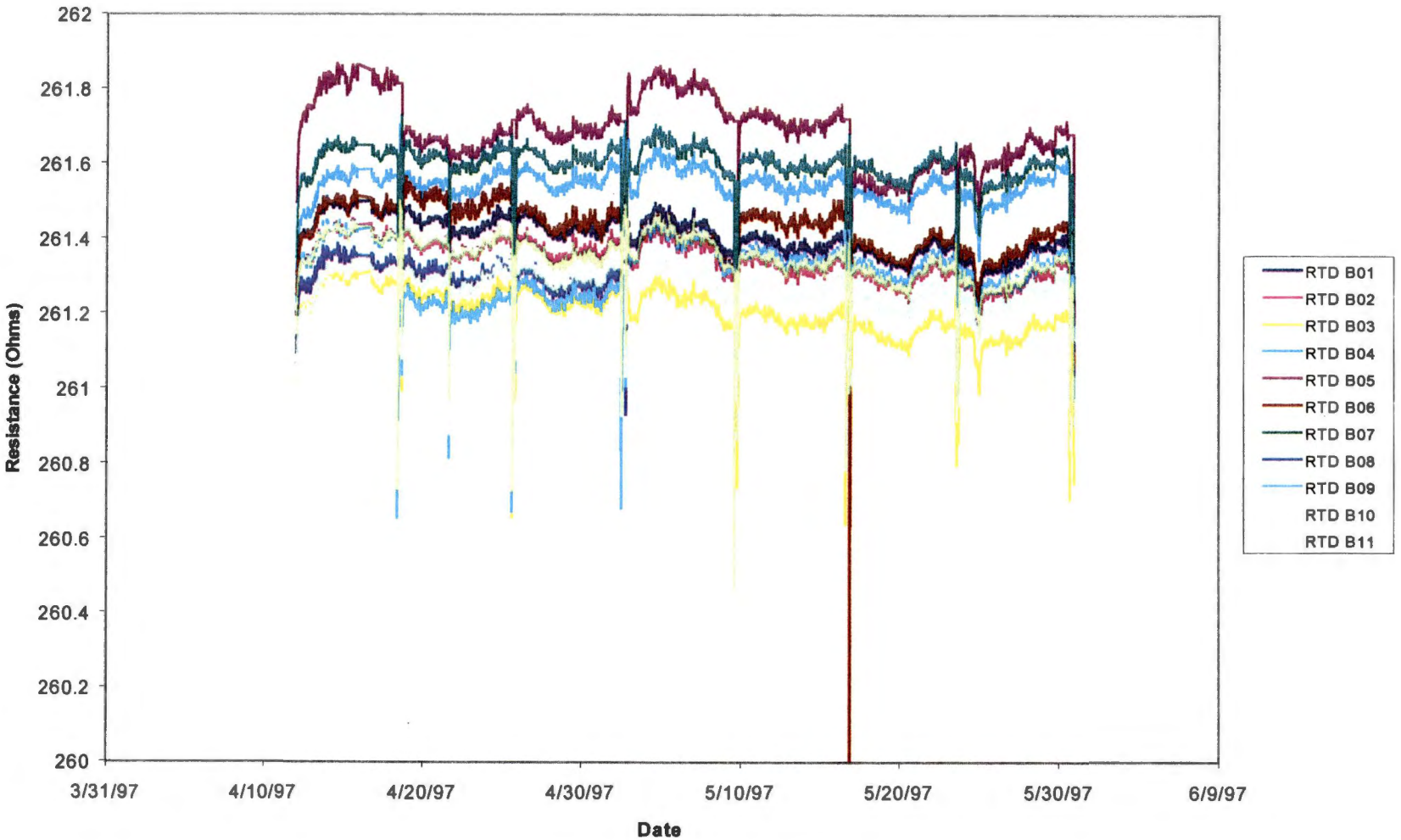


Figure A-20. Test #7 450 °C

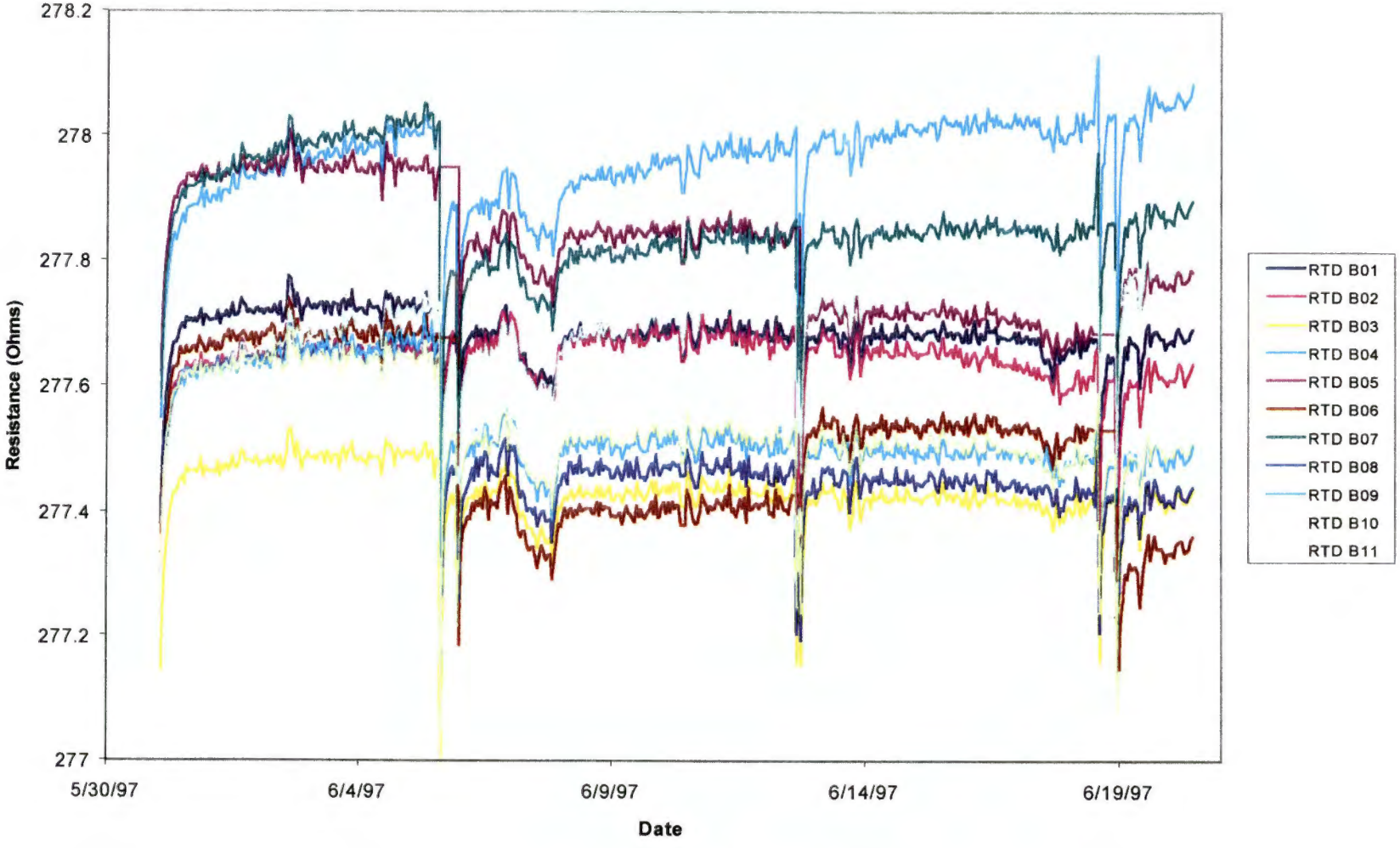


Figure A-21. Test #7 500°C

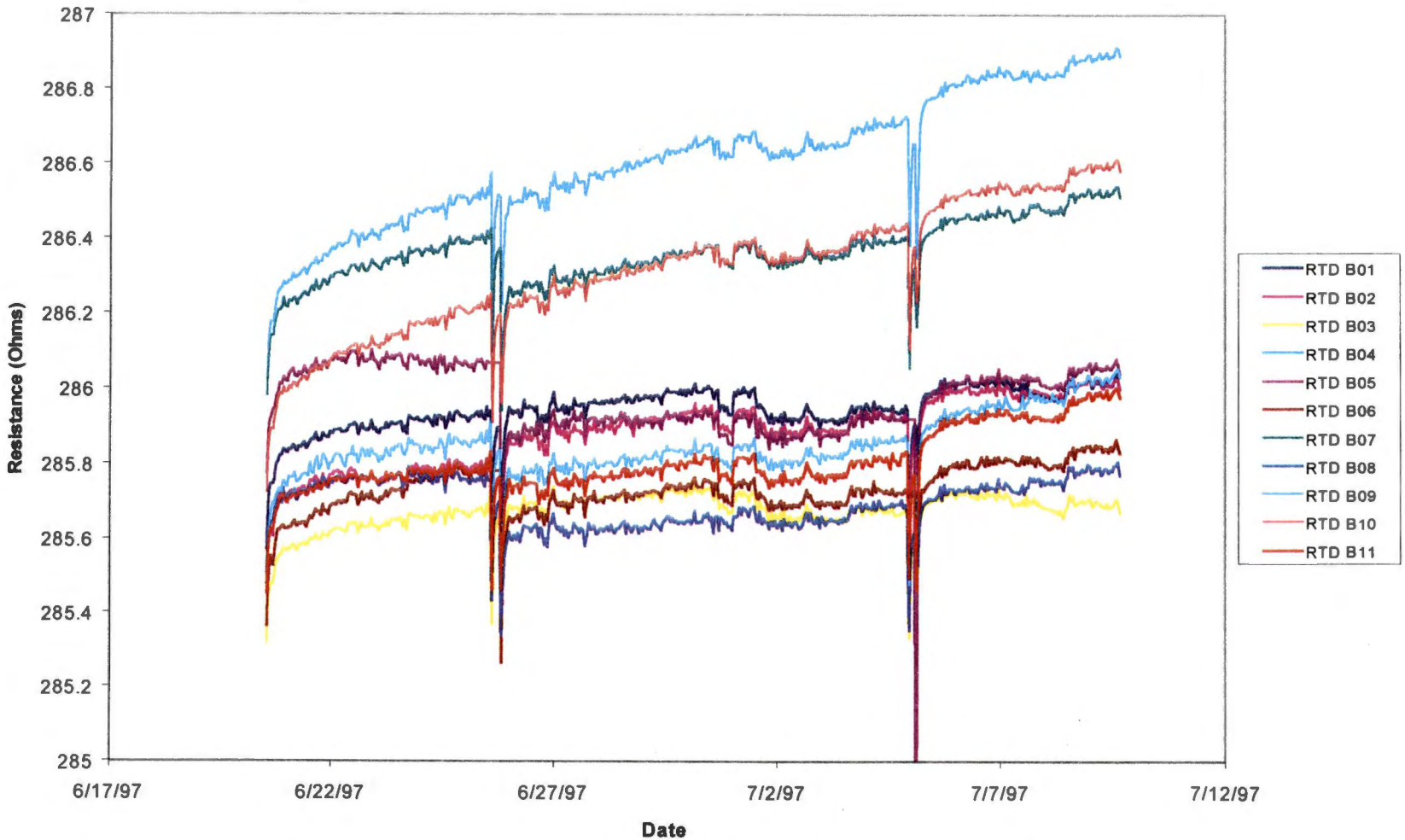


Figure A-22. Test #7 525°C

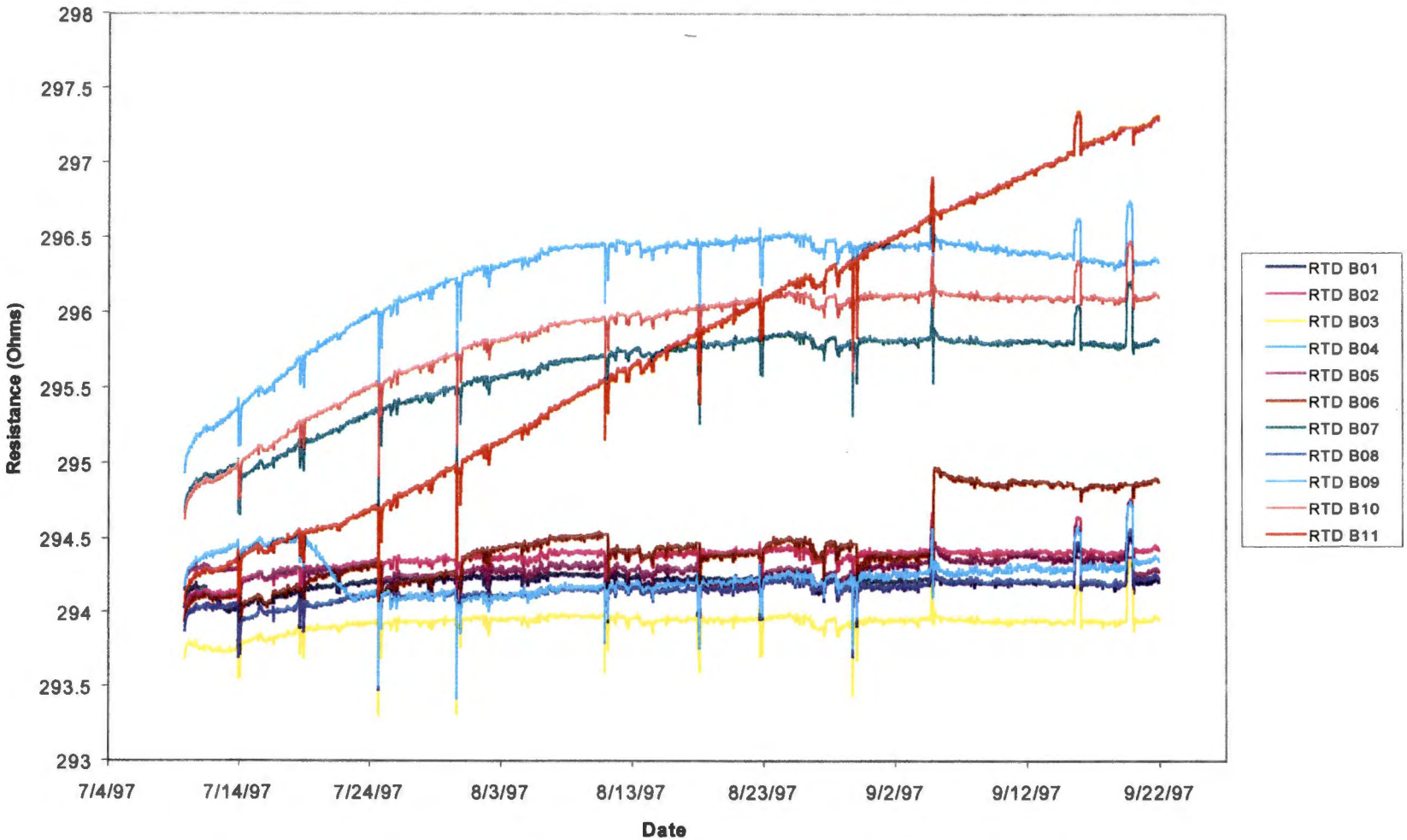


Figure A-23. Test #7 550 °C

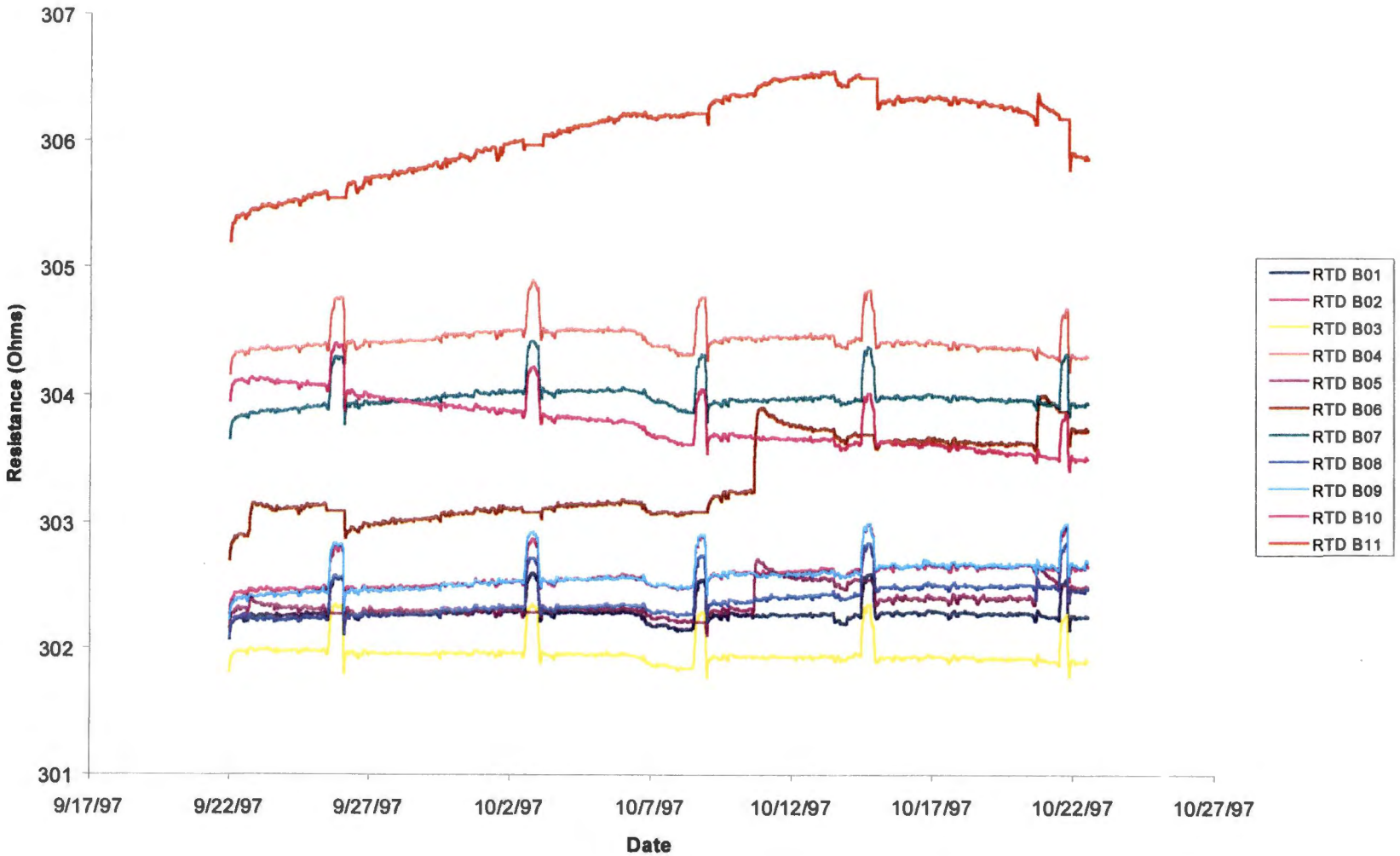


Figure A-24. Test #7 575 °C

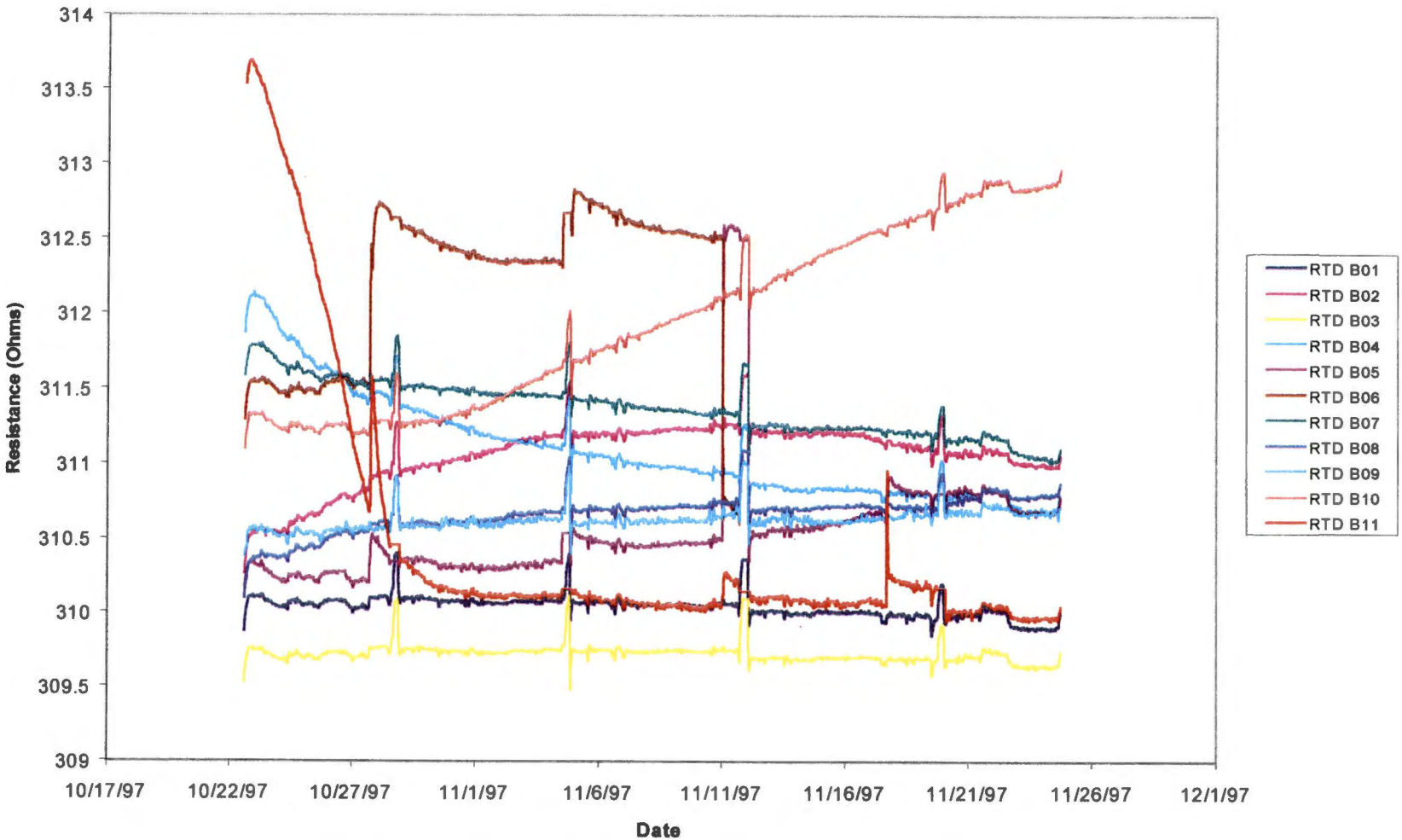


Figure A-25. Test #7 600 °C

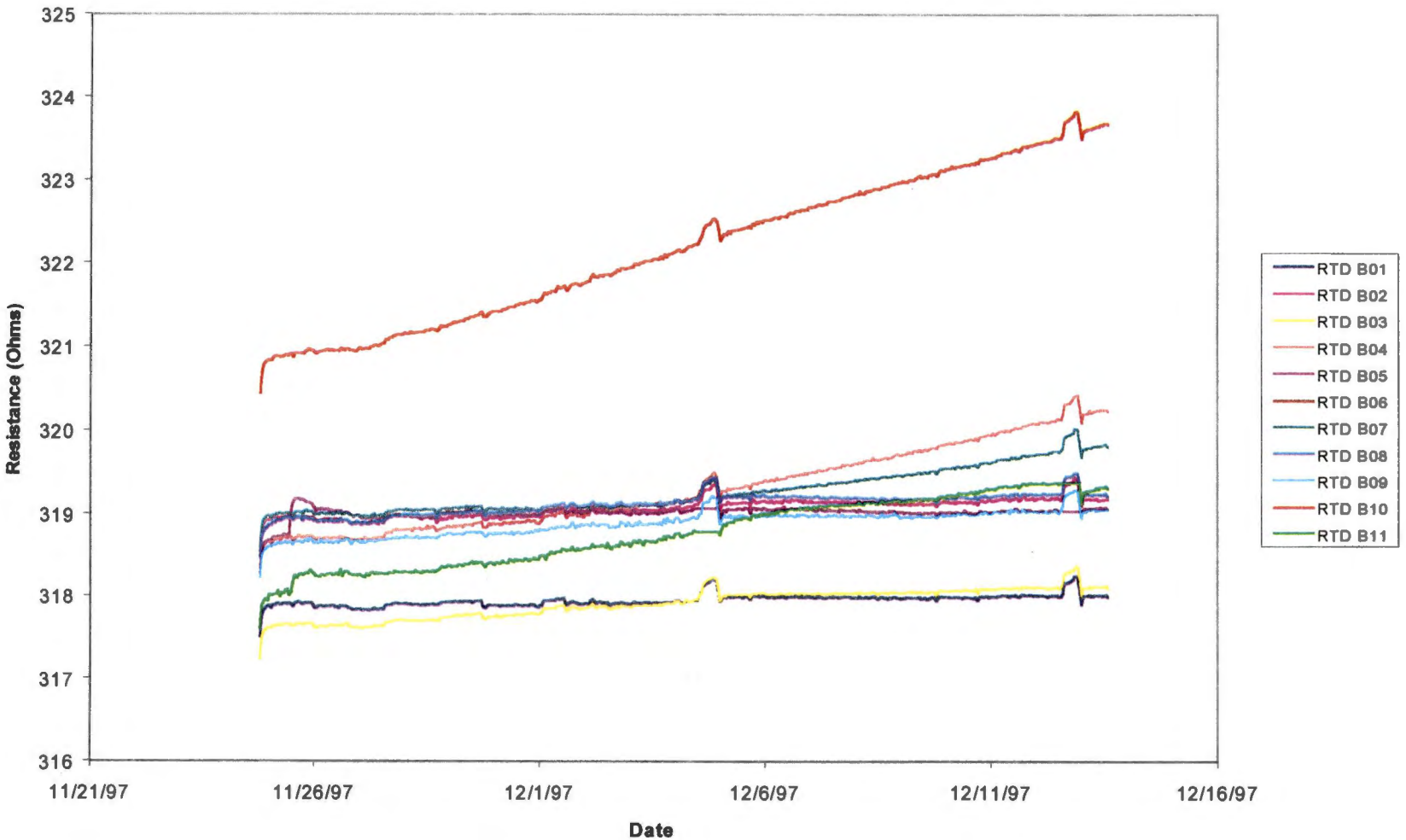


Figure A-26. Test #7 625 °C

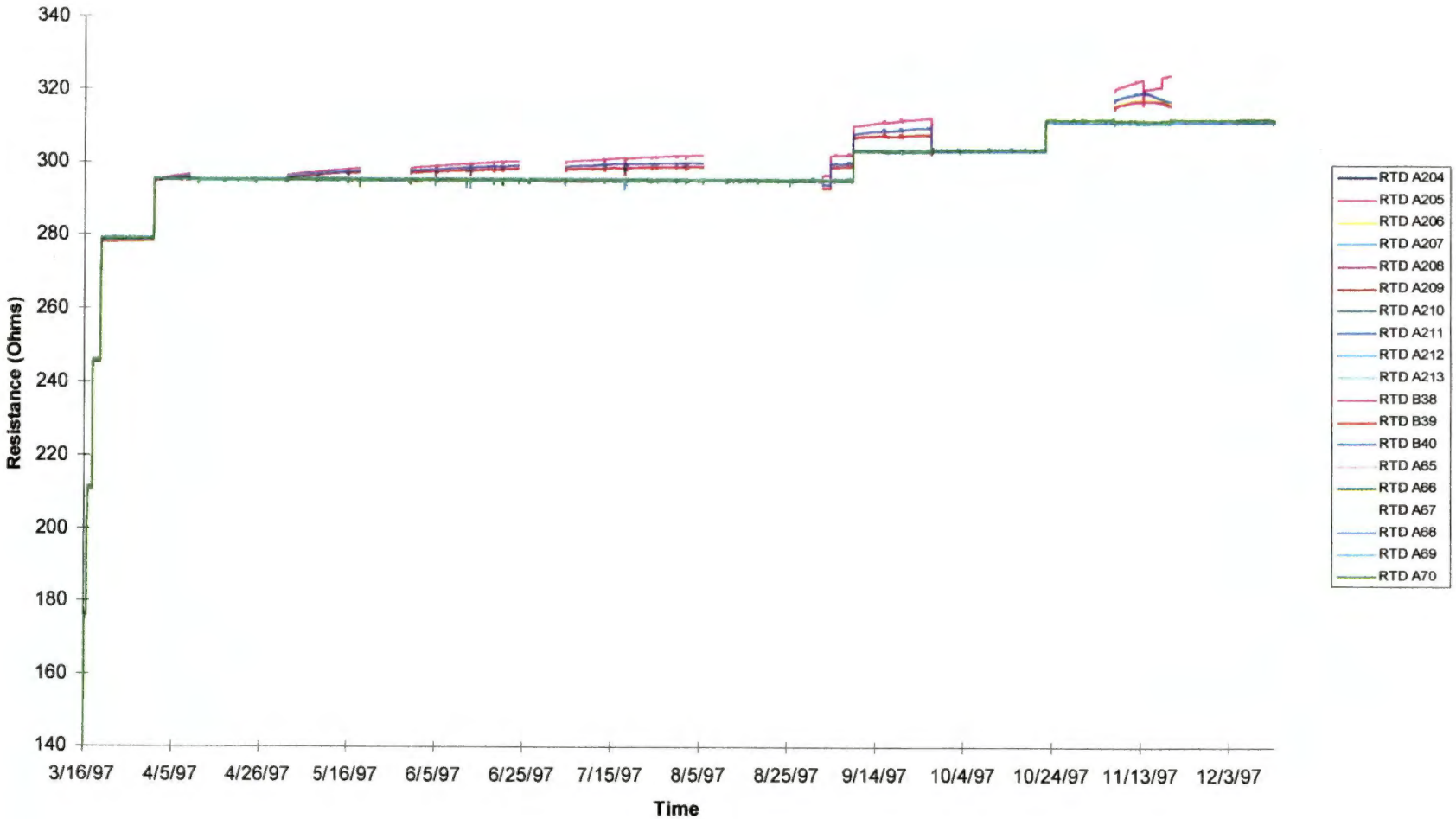


Figure A-27. Test #8 Full Plot All Temperatures

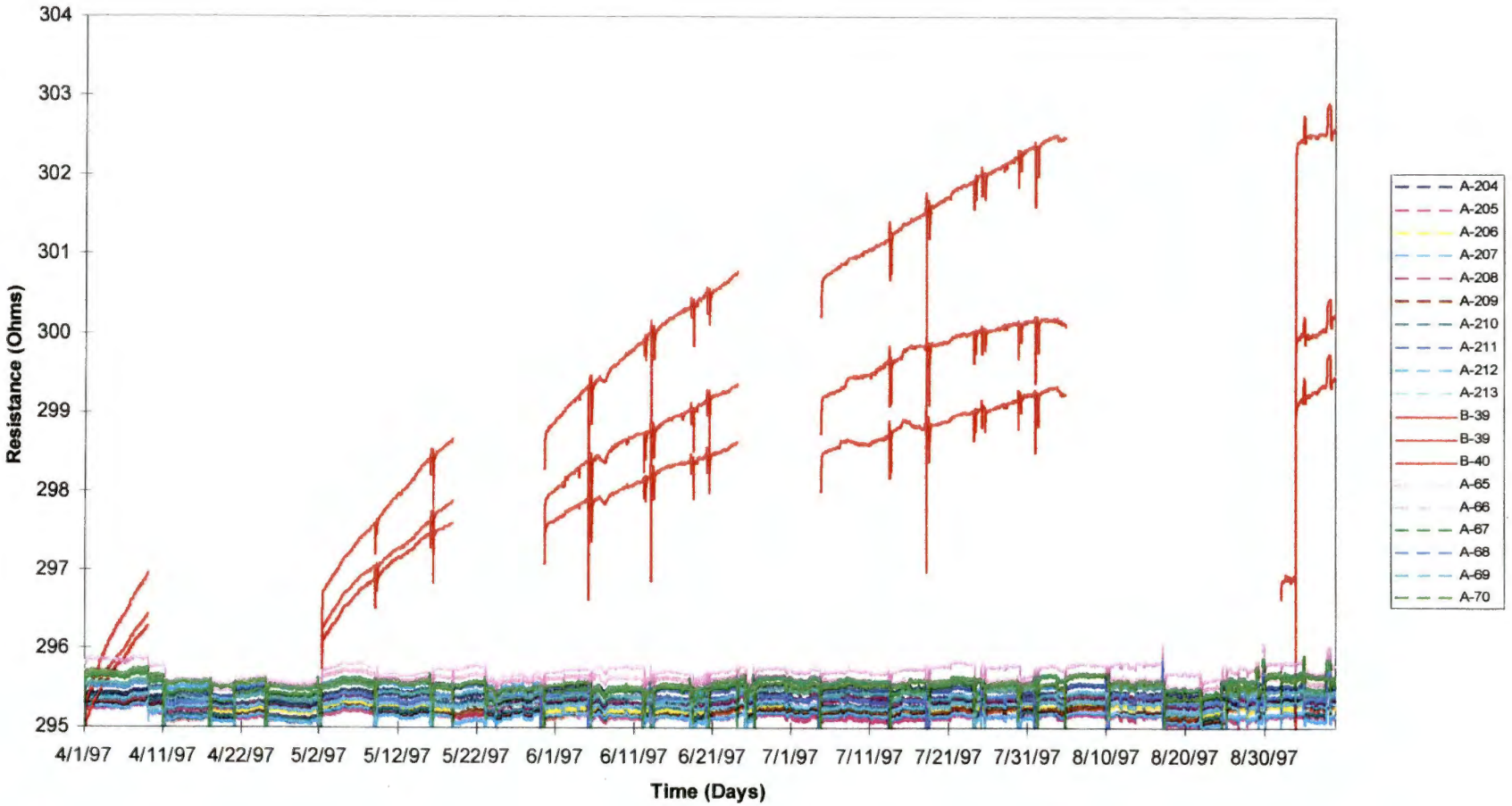


Figure A-28. Test #8 550 °C

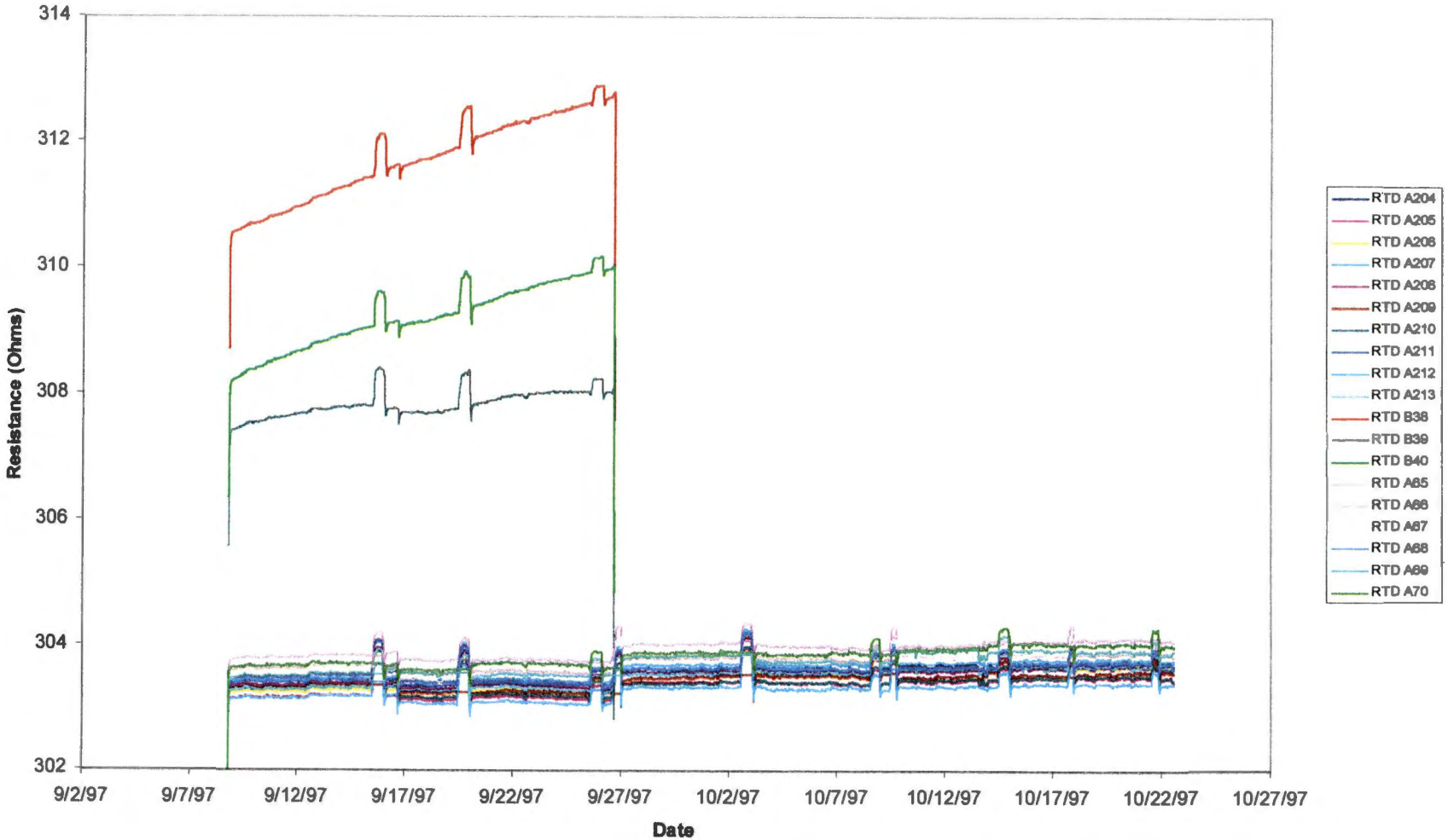


Figure A-29. Test #8 575 °C

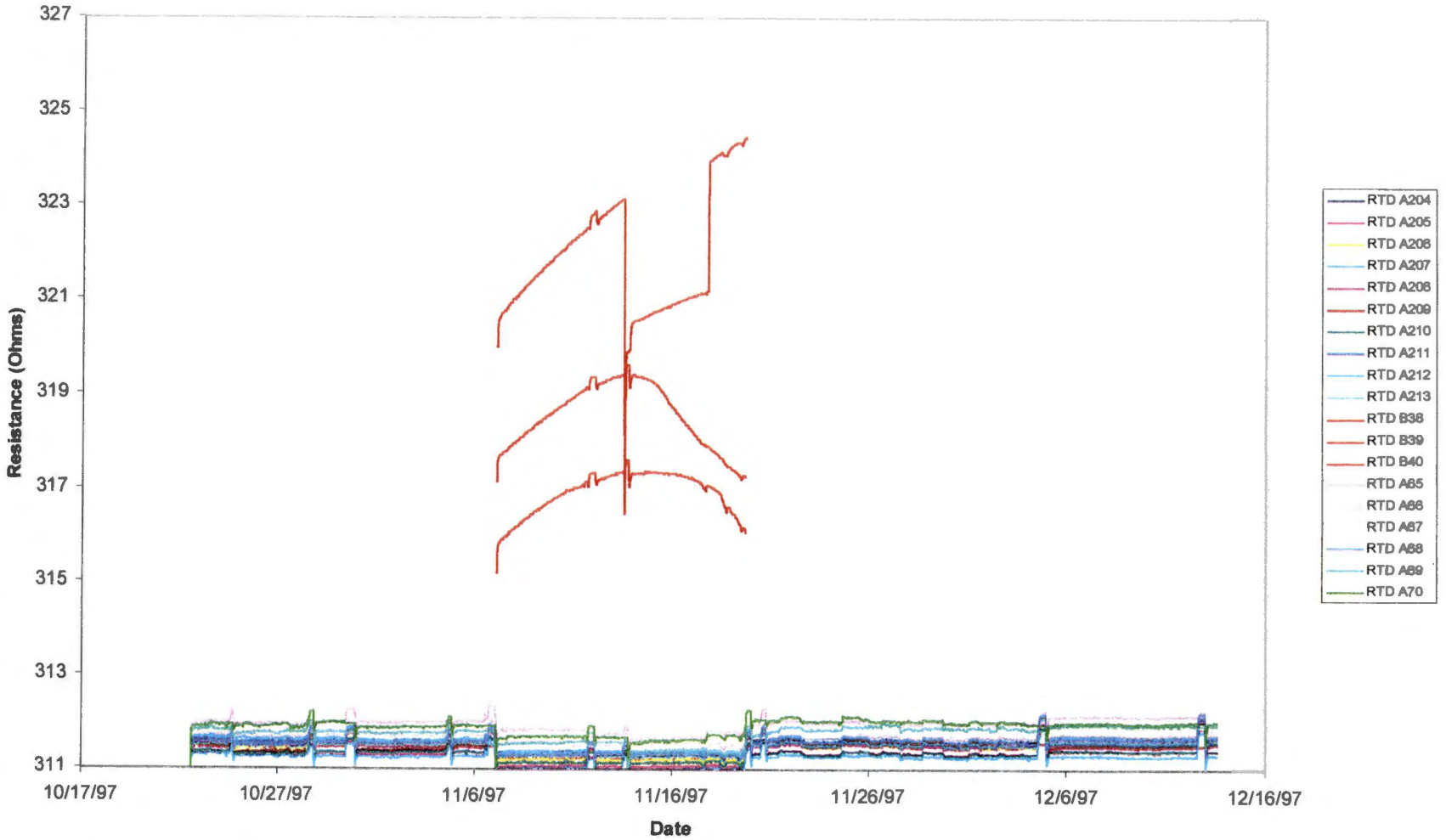


Figure A-30. Test #8 600 °C

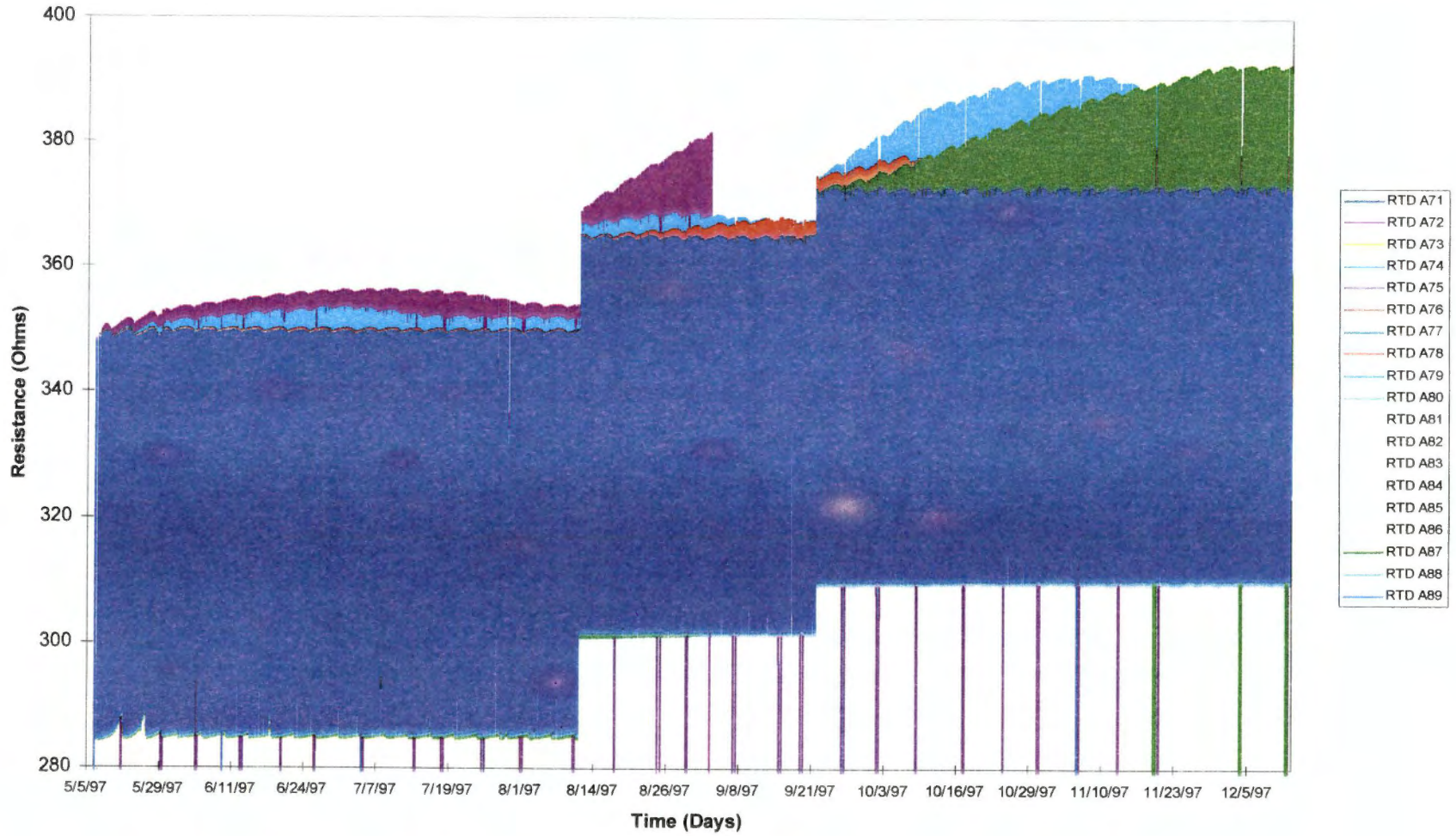


Figure A-31. Test #9 Full Plot All Temperatures

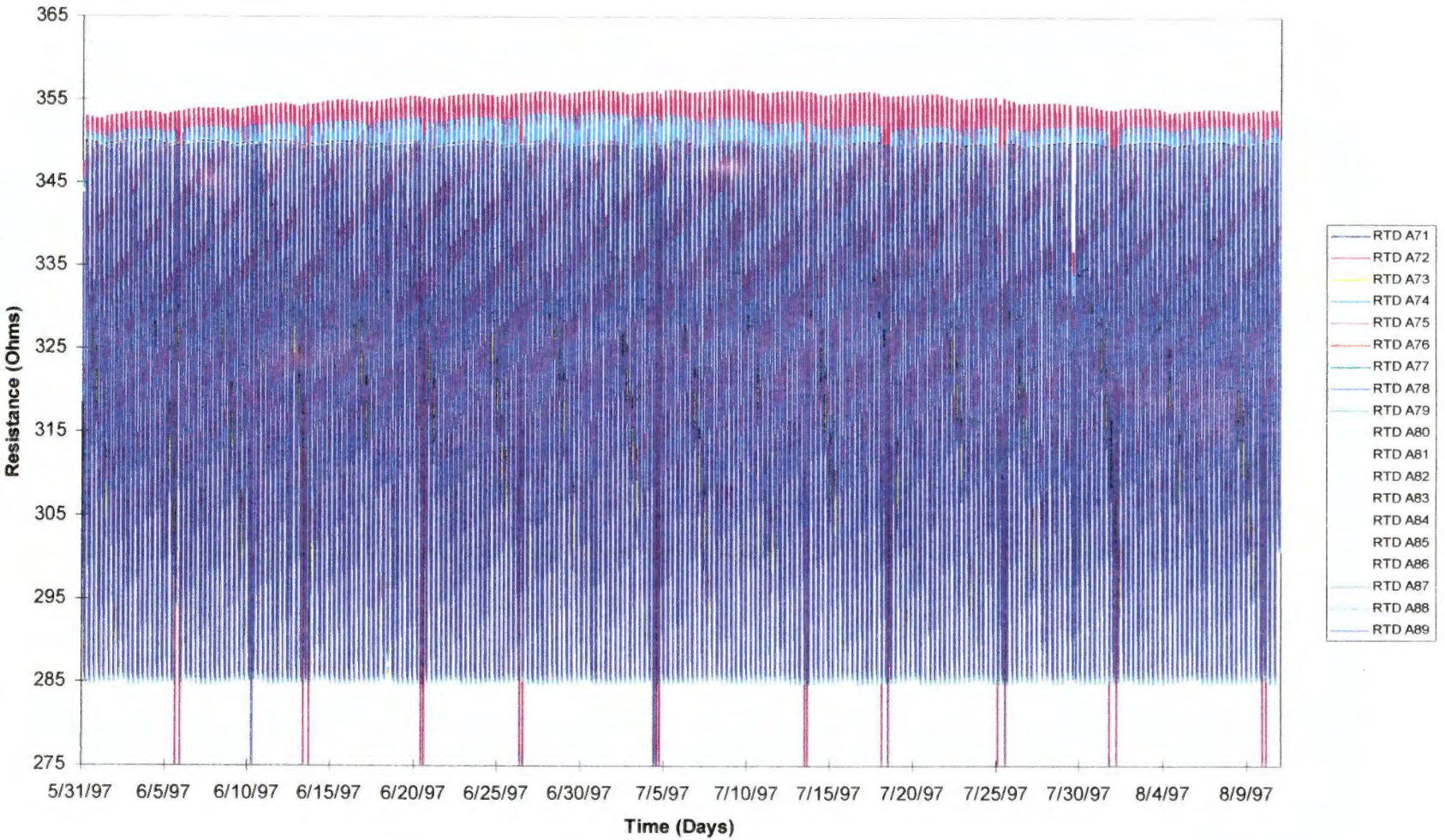


Figure A-32. Test #9 500-700 °C Thermal Cycling

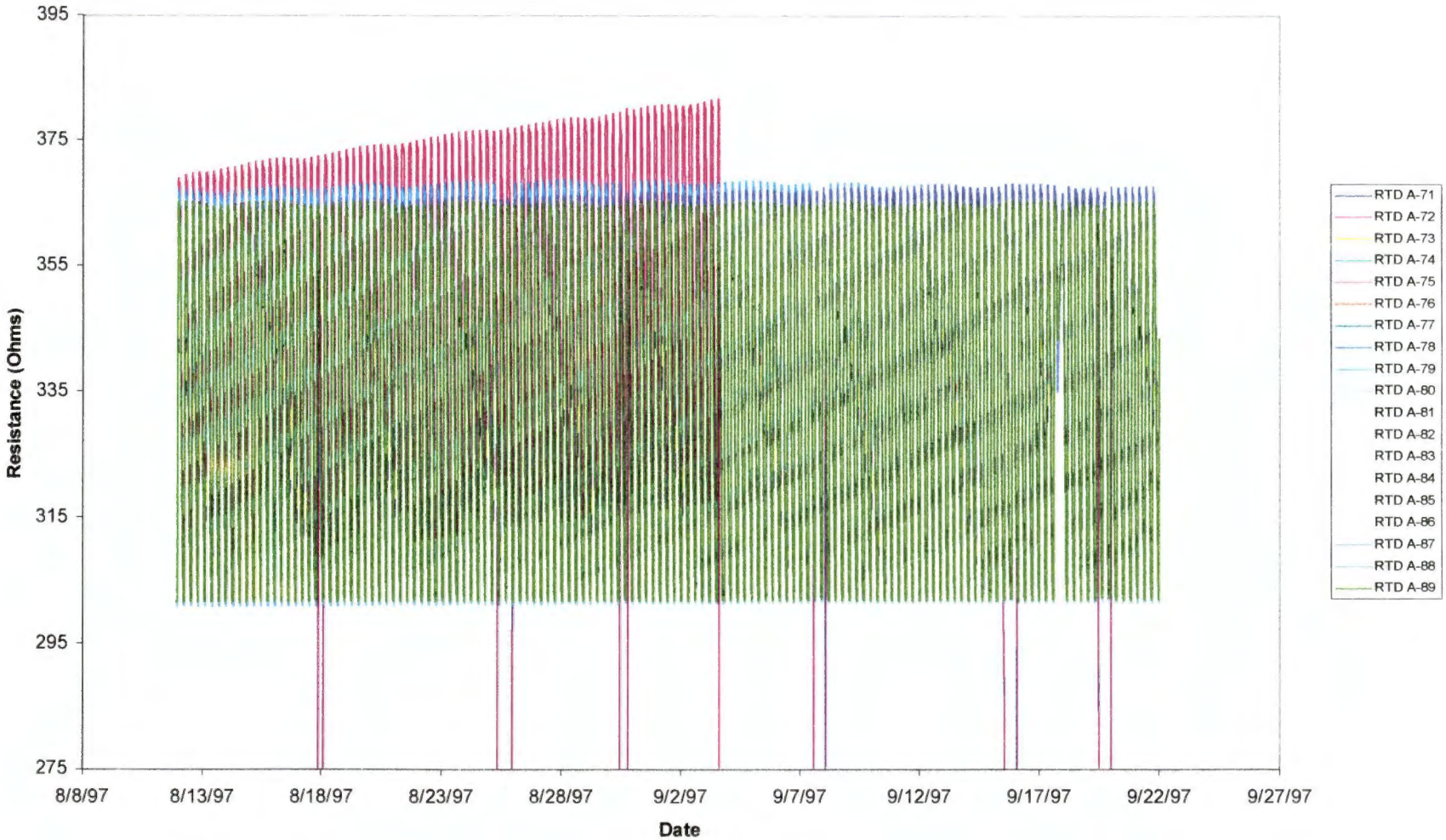


Figure A-33. Test #9 550-750 °C Thermal Cycling

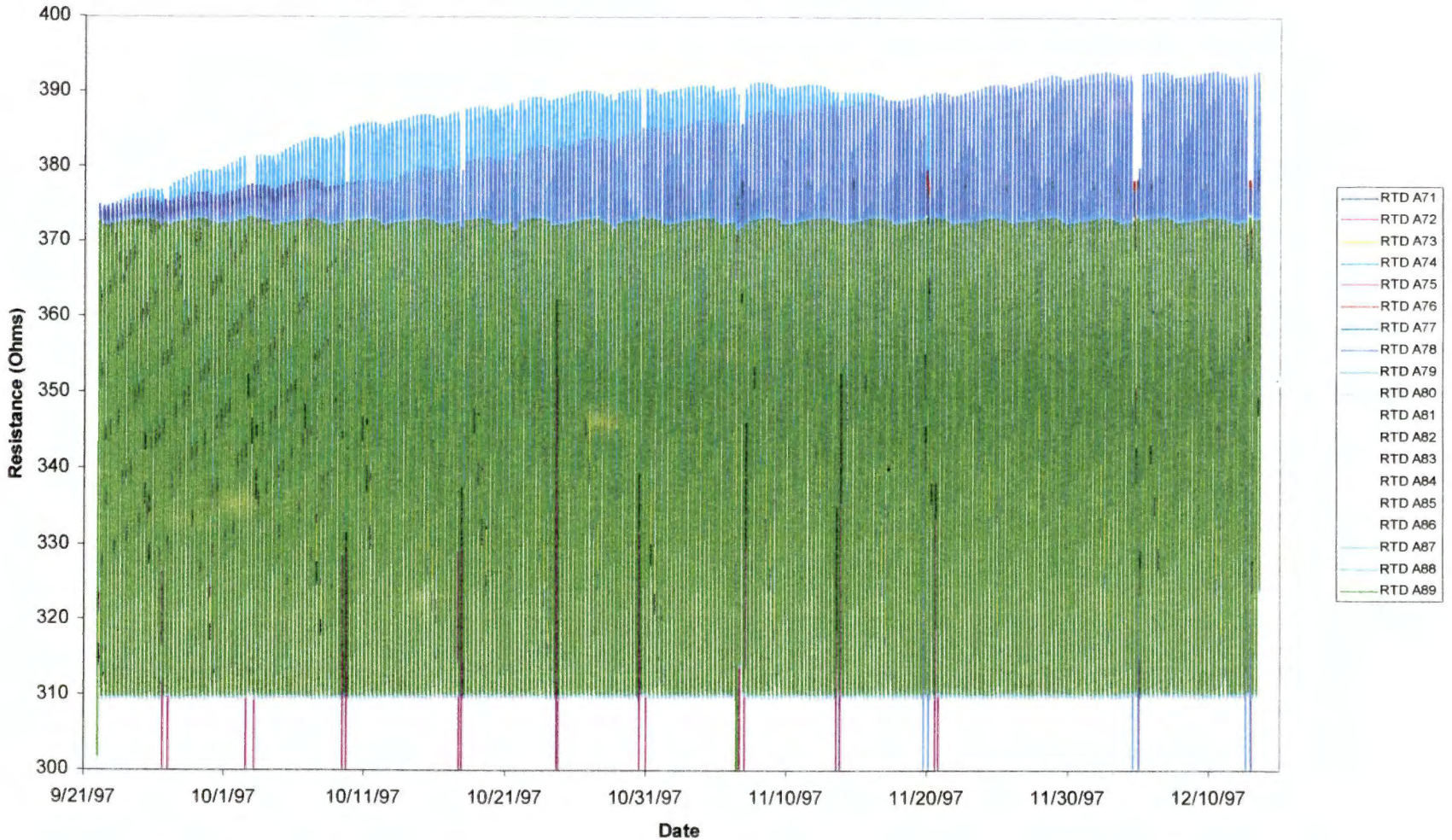


Figure A-34. Test #9 575-775 °C Thermal Cycling

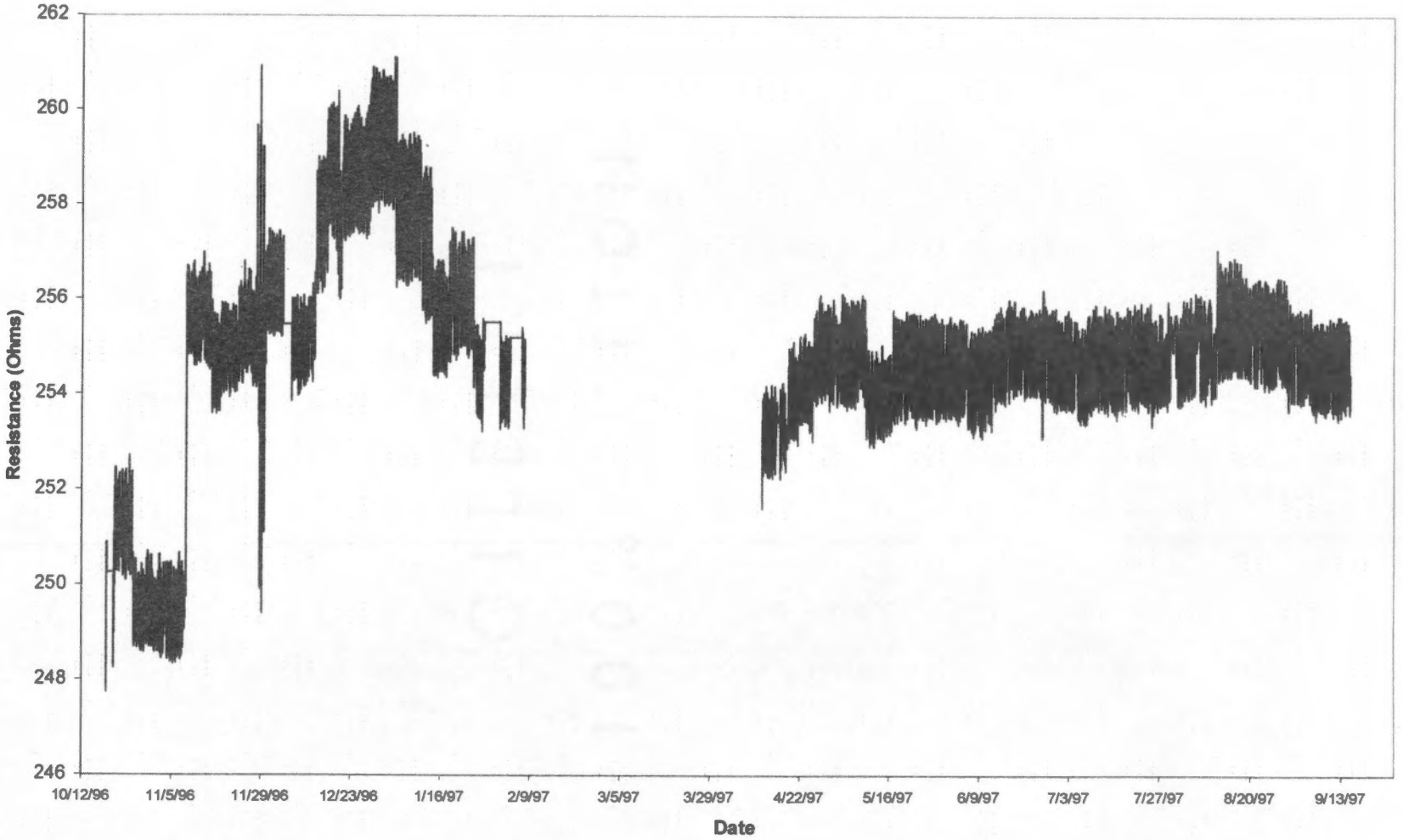


Figure A-35. Test #10 450 °C

Appendix B

Summary of weekly calibration results including Ro, alpha, delta and self heating index trend plots.

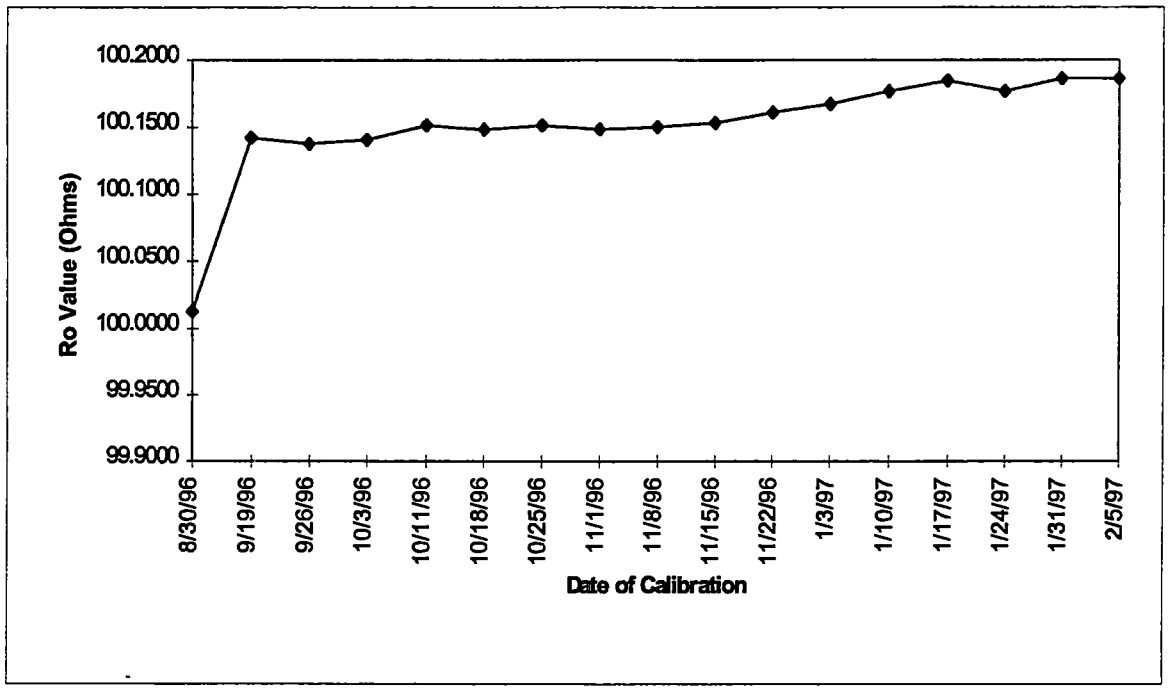


Figure B-1 RTD A-51 Ro Value Trend

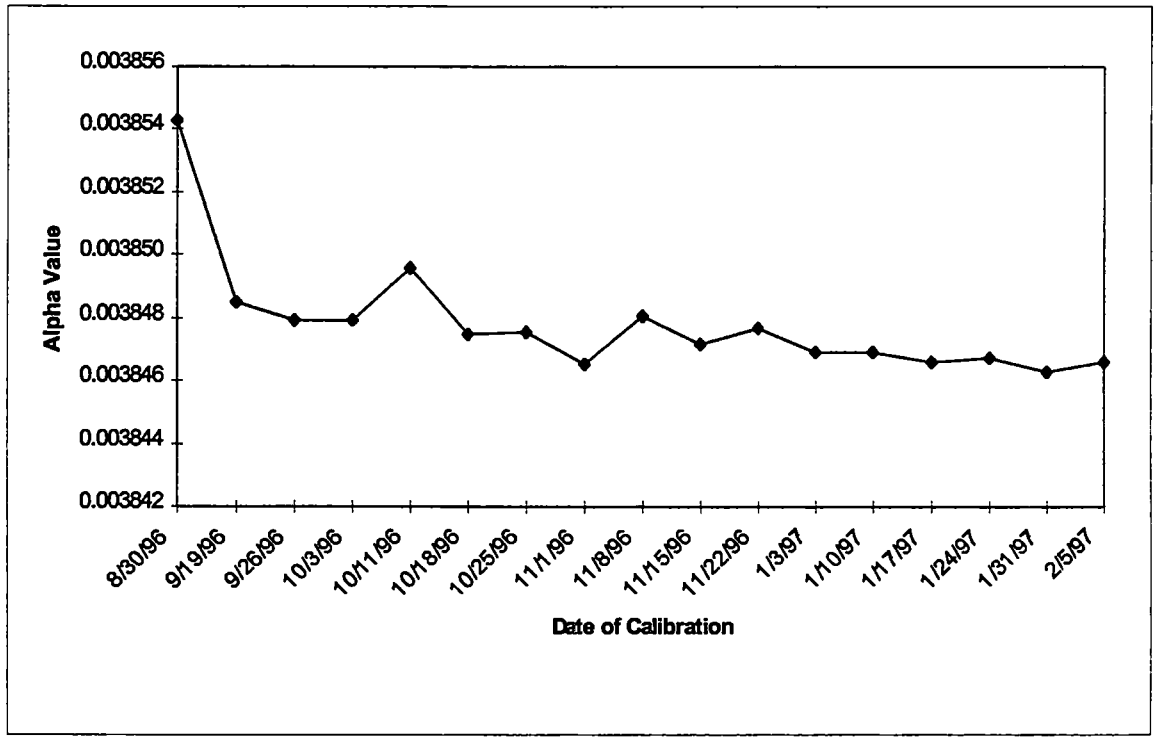


Figure B-2 RTD A-51 Alpha Value Trend

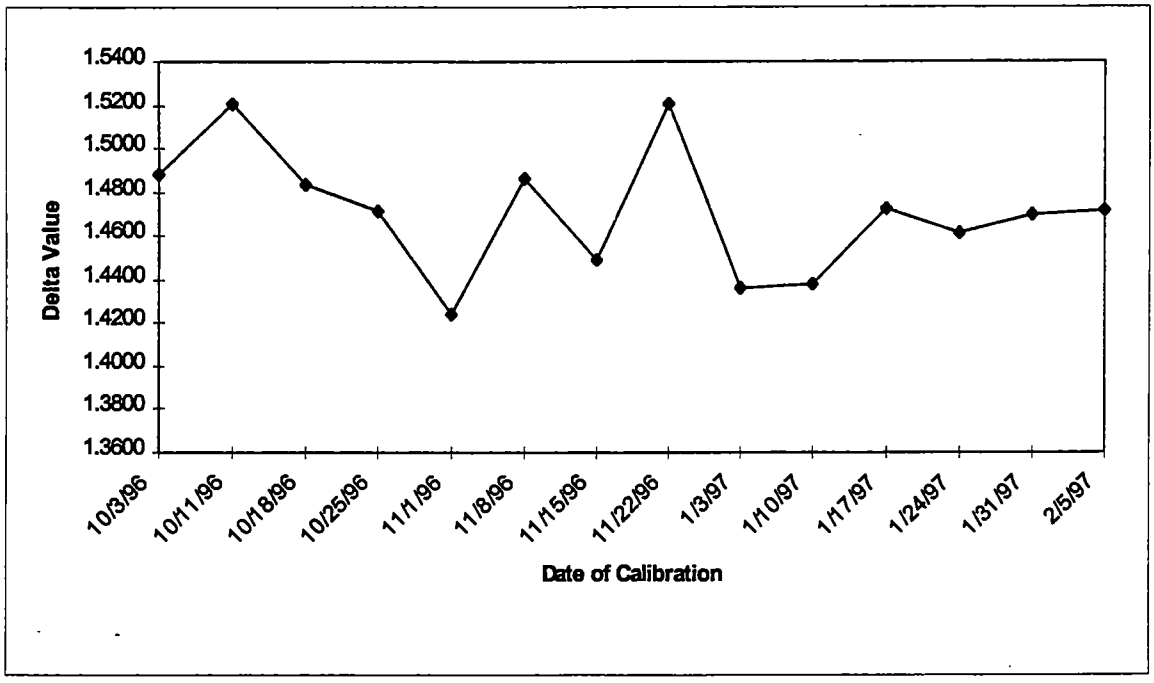


Figure B-3 RTD A-51 Delta Value Trend

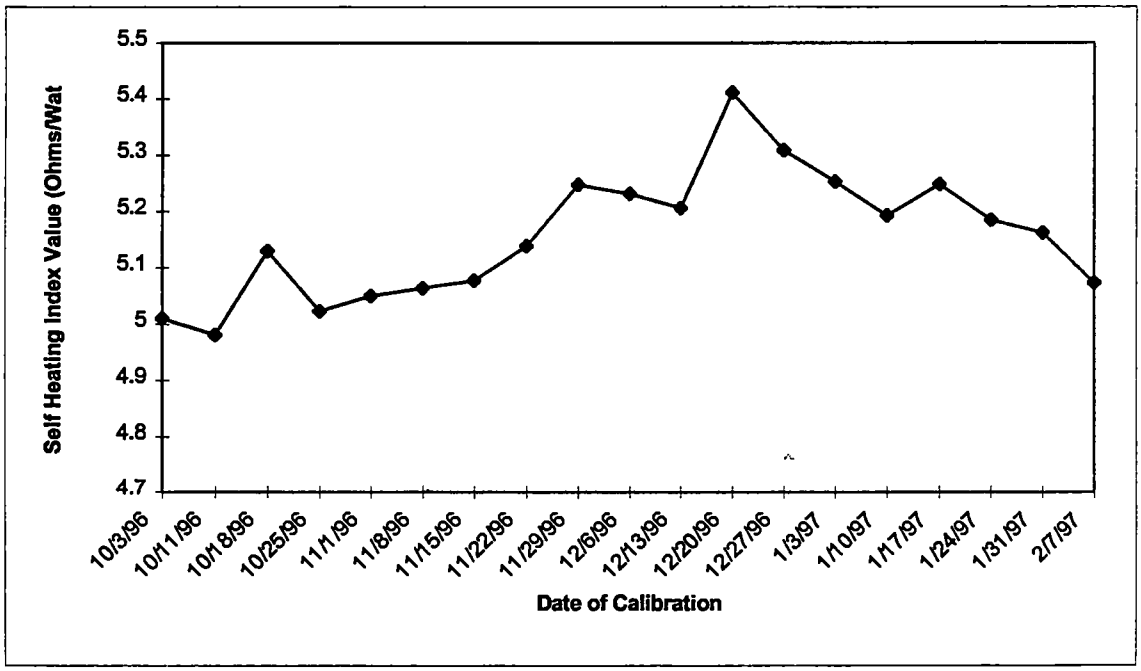


Figure B-4 RTD A-51 Self Heating Index (Ohms/Watt) Value Trend

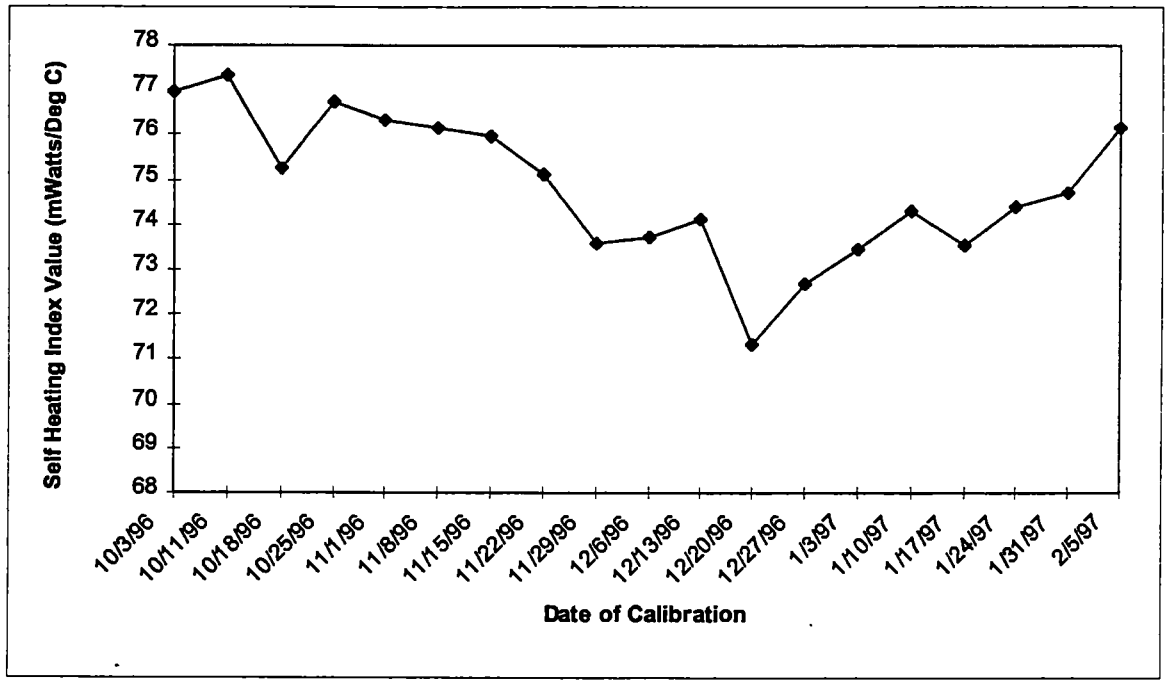


Figure B-5 RTD A-51 Self Heating Index (mWatt/°C) Value Trend

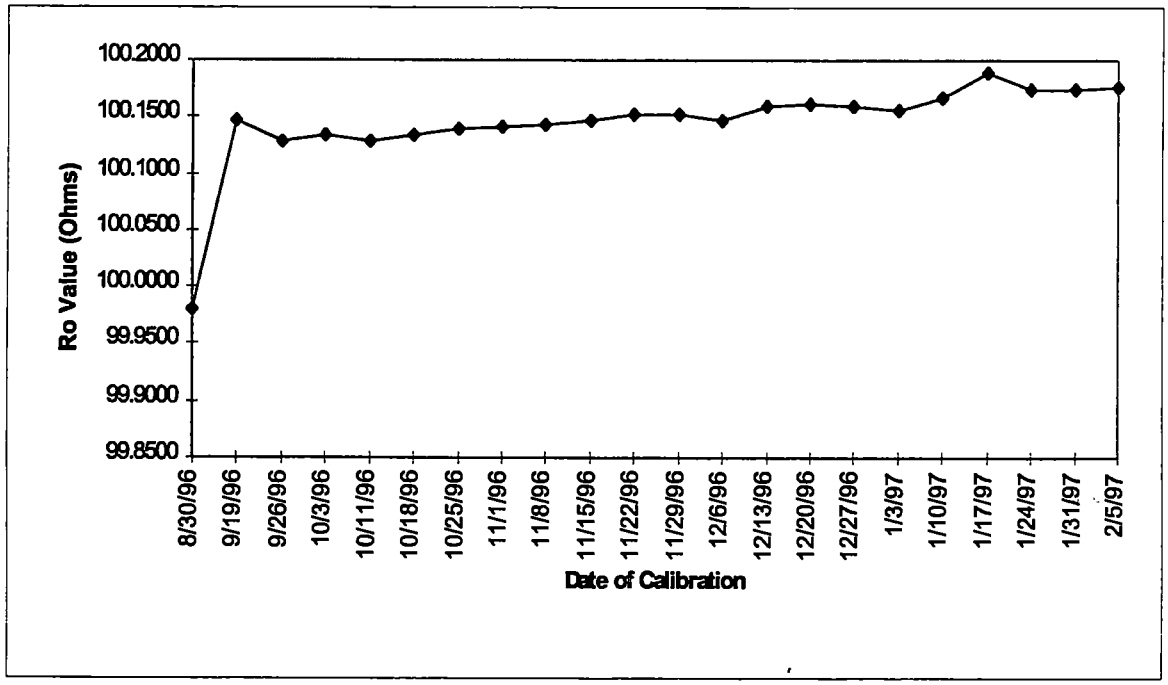


Figure B-6 RTD A-57 Ro Value Trend

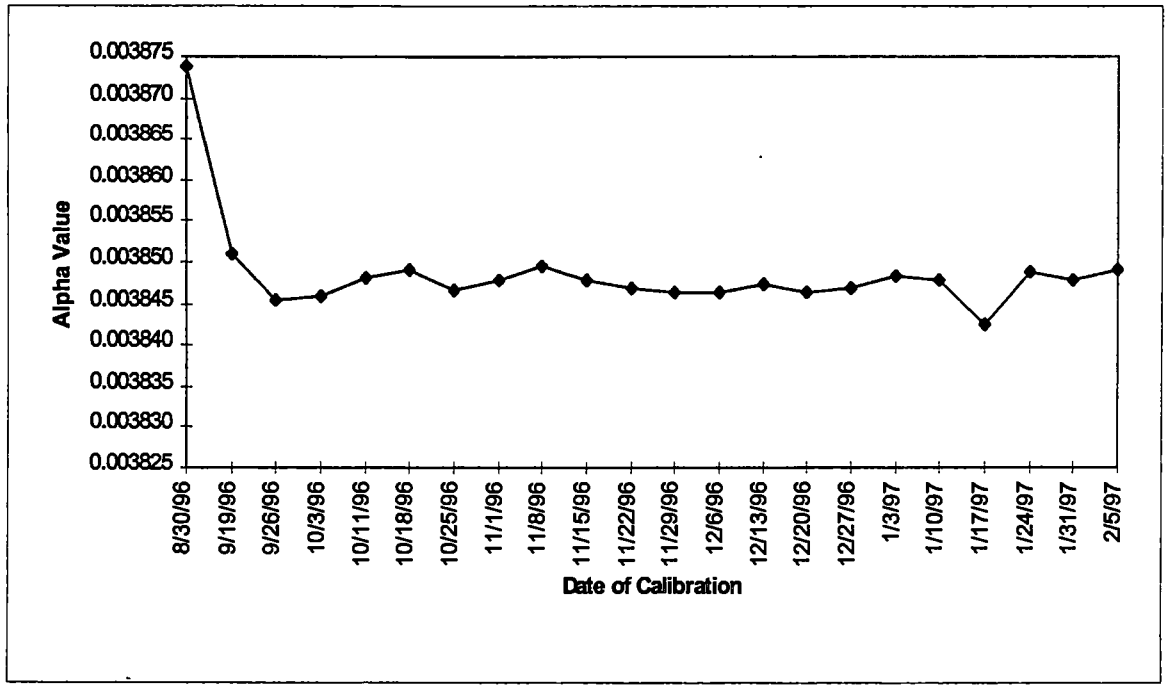


Figure B-7 RTD A-57 Alpha Value Trend

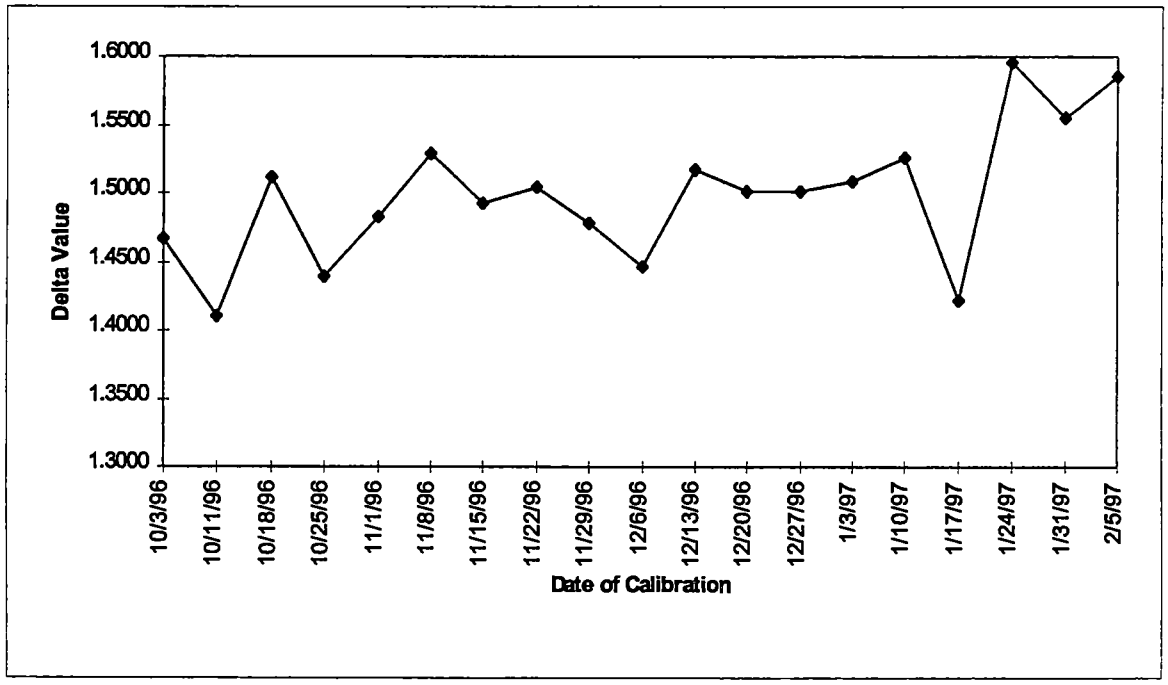


Figure B-8 RTD A-57 Delta Value Trend

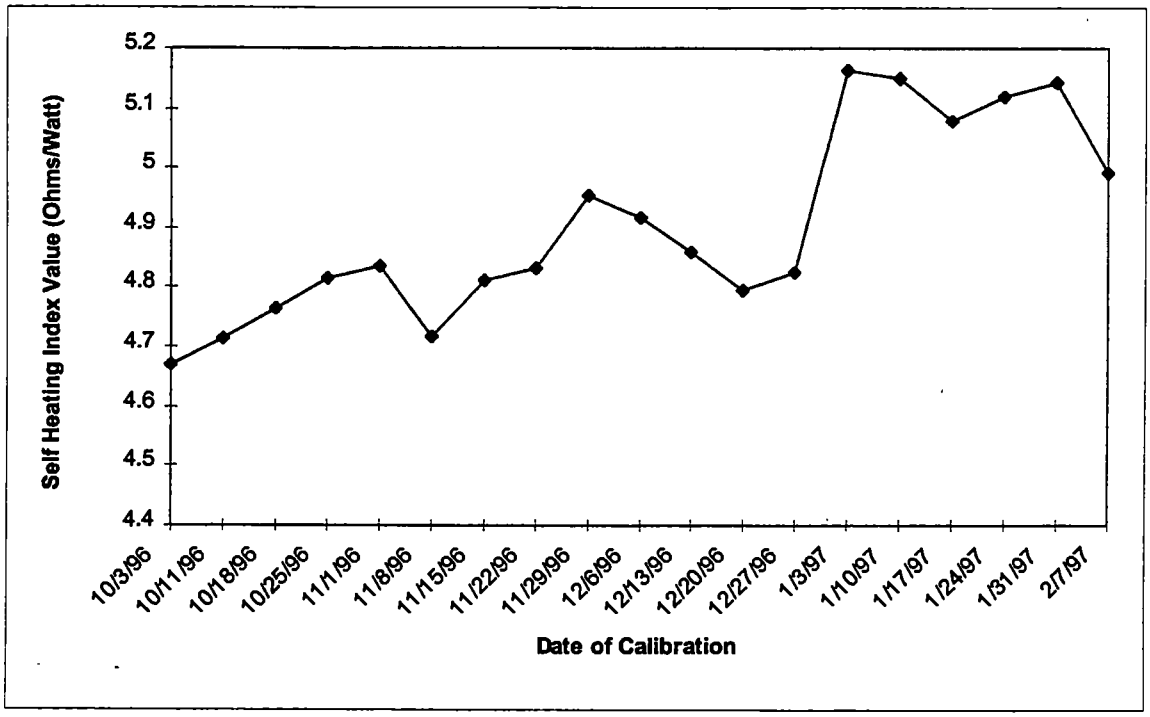


Figure B-9 RTD A-57 Self Heating Index (Ohm/Watt) Value Trend

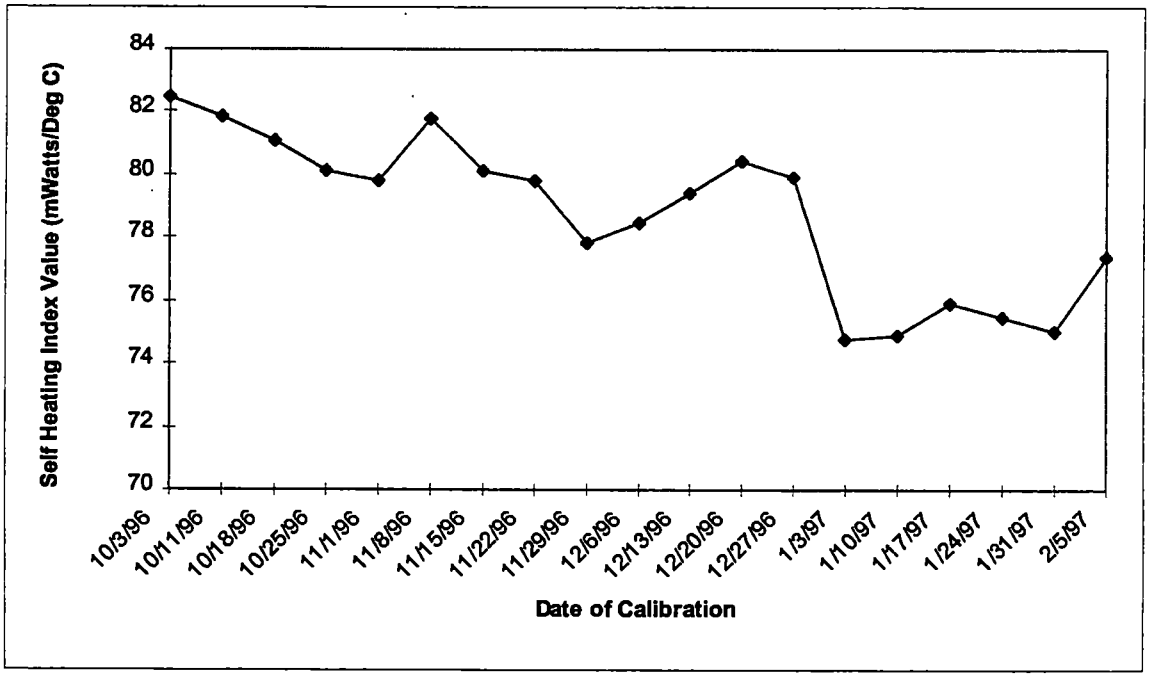


Figure B-10 RTD A-57 Self Heating Index (mWatt/°C) Value Trend

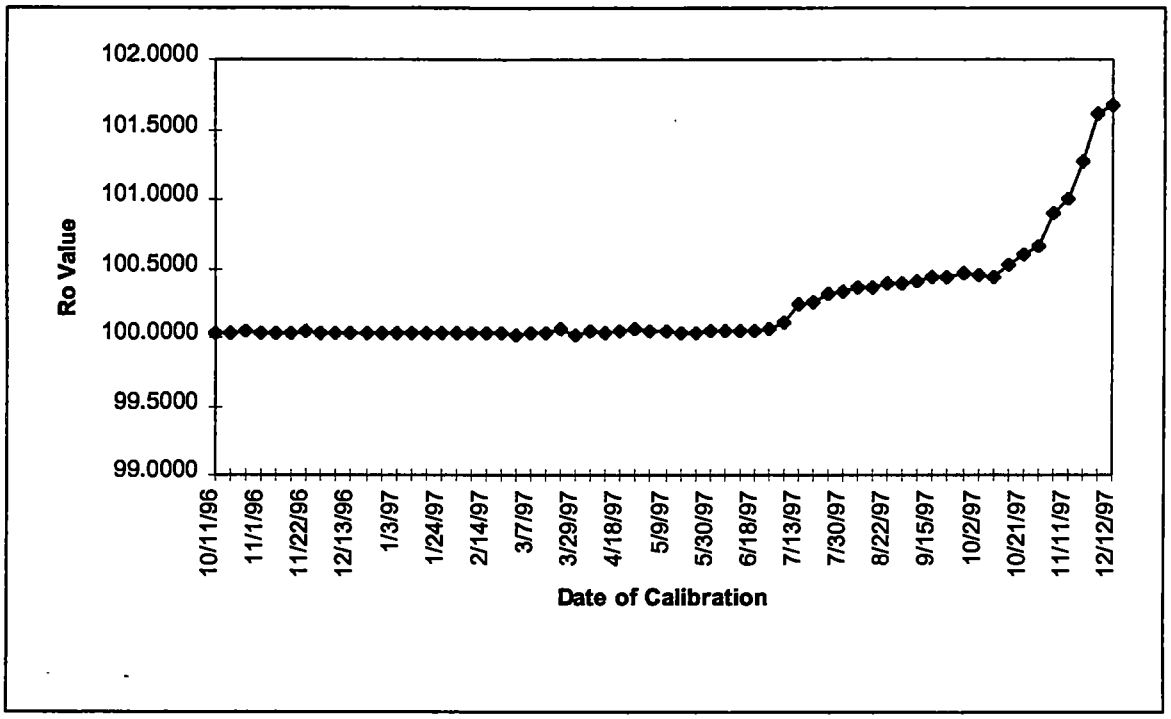


Figure B-11 RTD B-5 Ro Value Trend

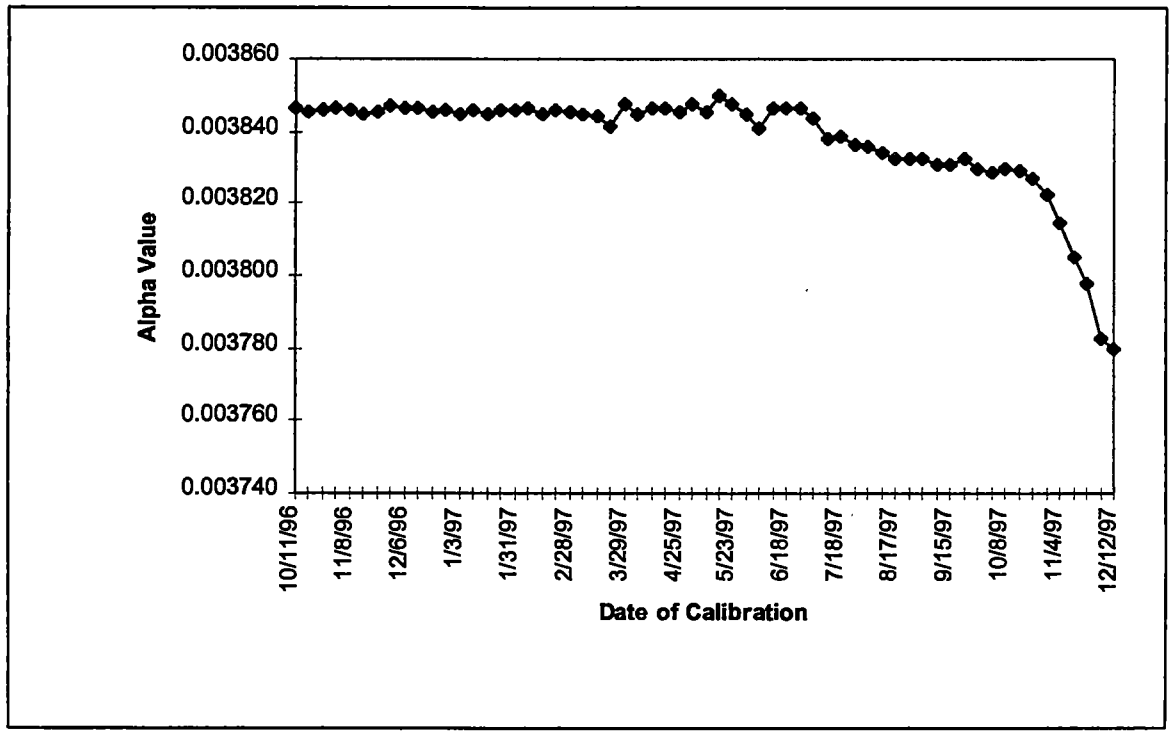


Figure B-12 RTD B-5 Alpha Value Trend

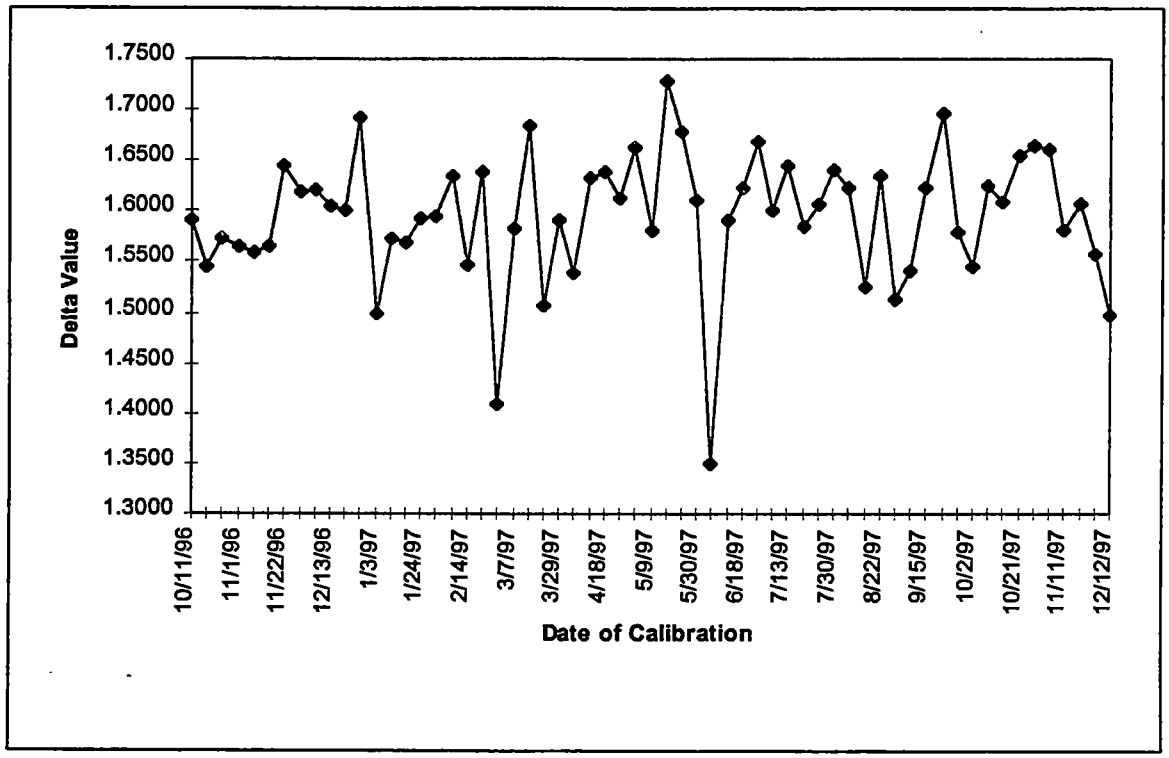


Figure B-13 RTD B-5 Delta Value Trend

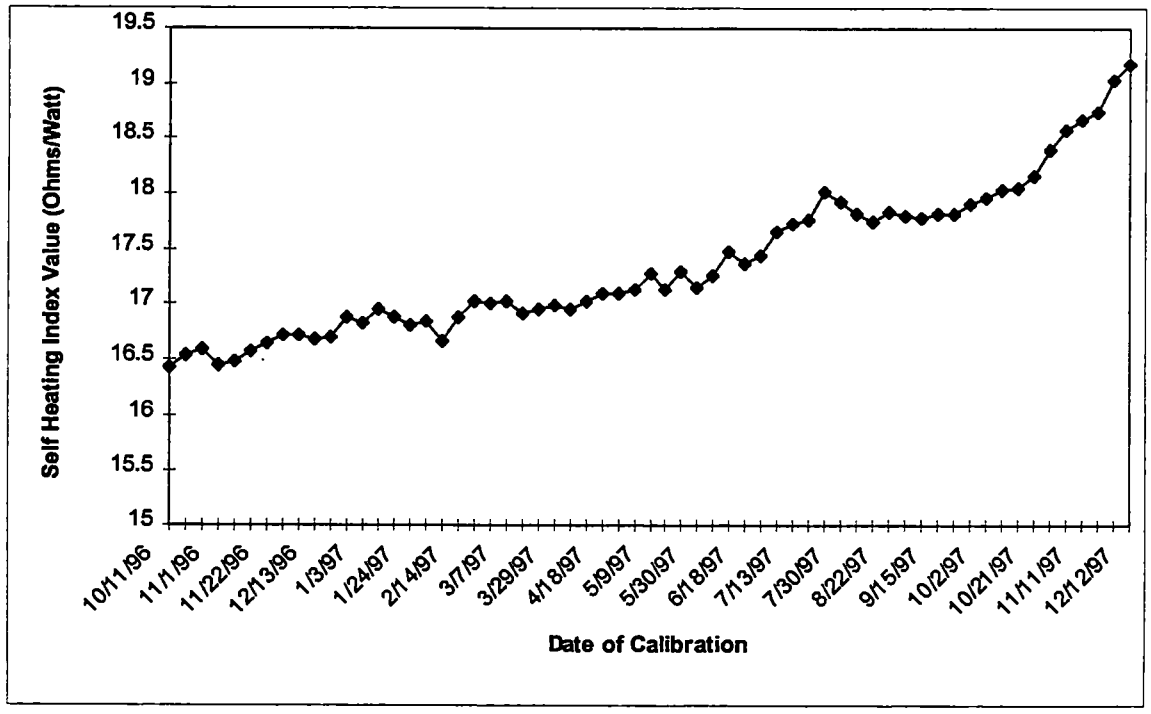


Figure B-14 RTD B-5 Self Heating Index (Ohm/Watt) Value Trend

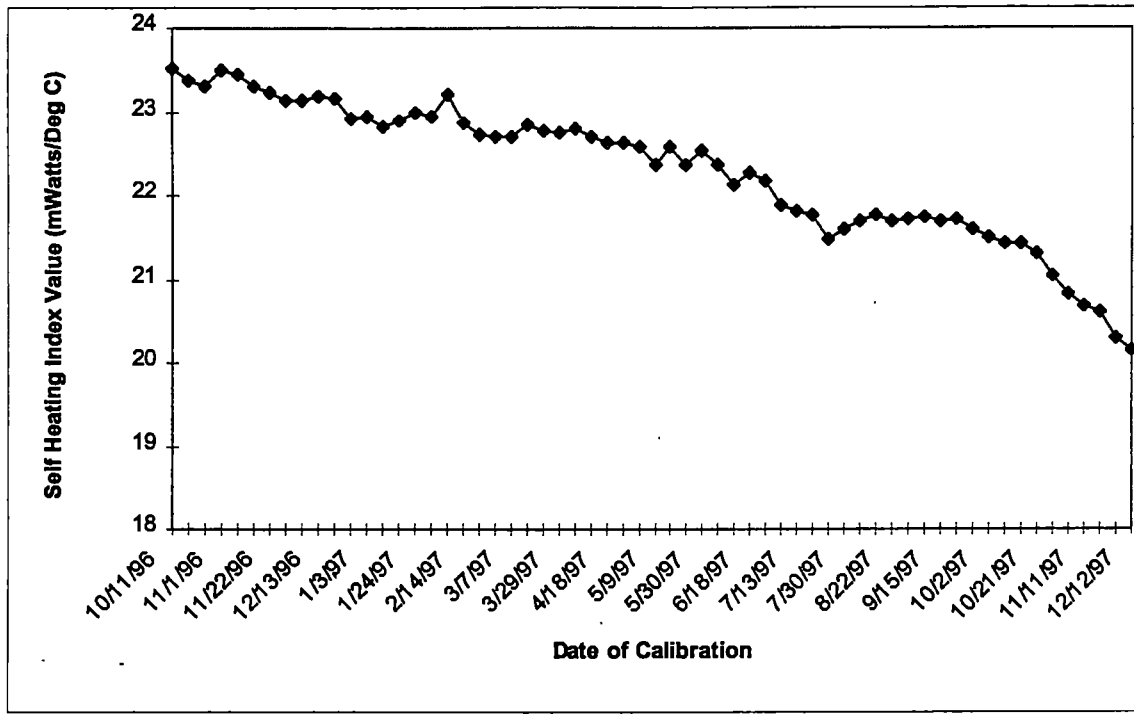


Figure B-15 RTD B-5 Self Heating Index (mWatt/°C) Value Trend

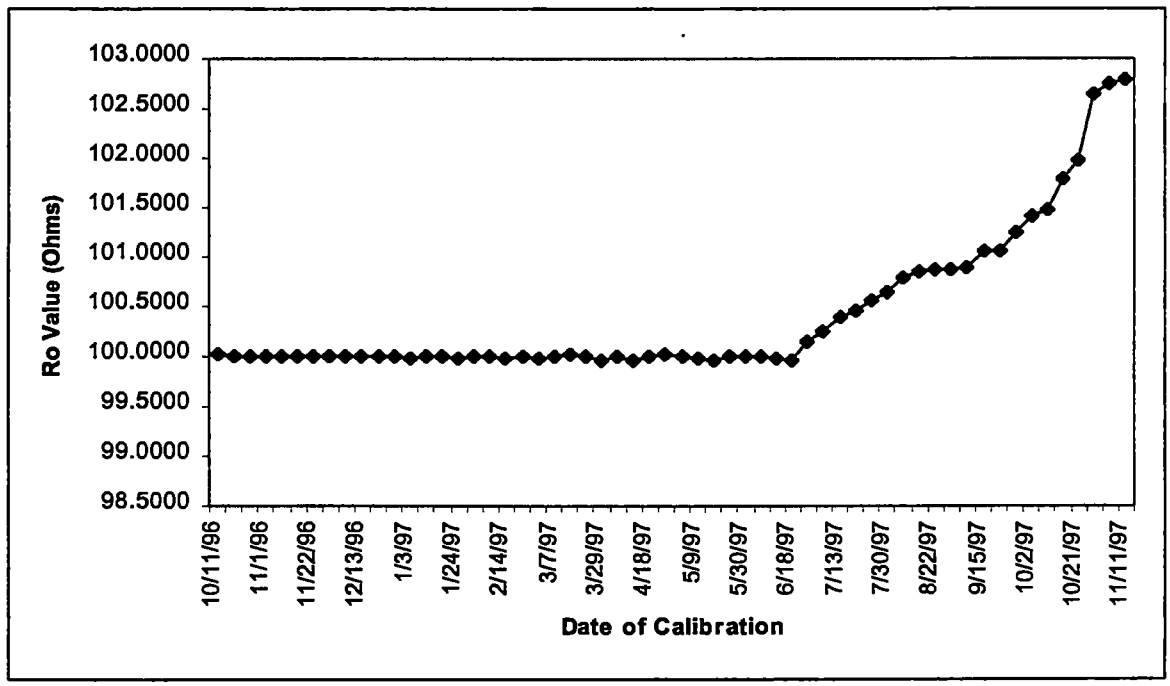


Figure B-16 RTD B-6 Ro Value Trend

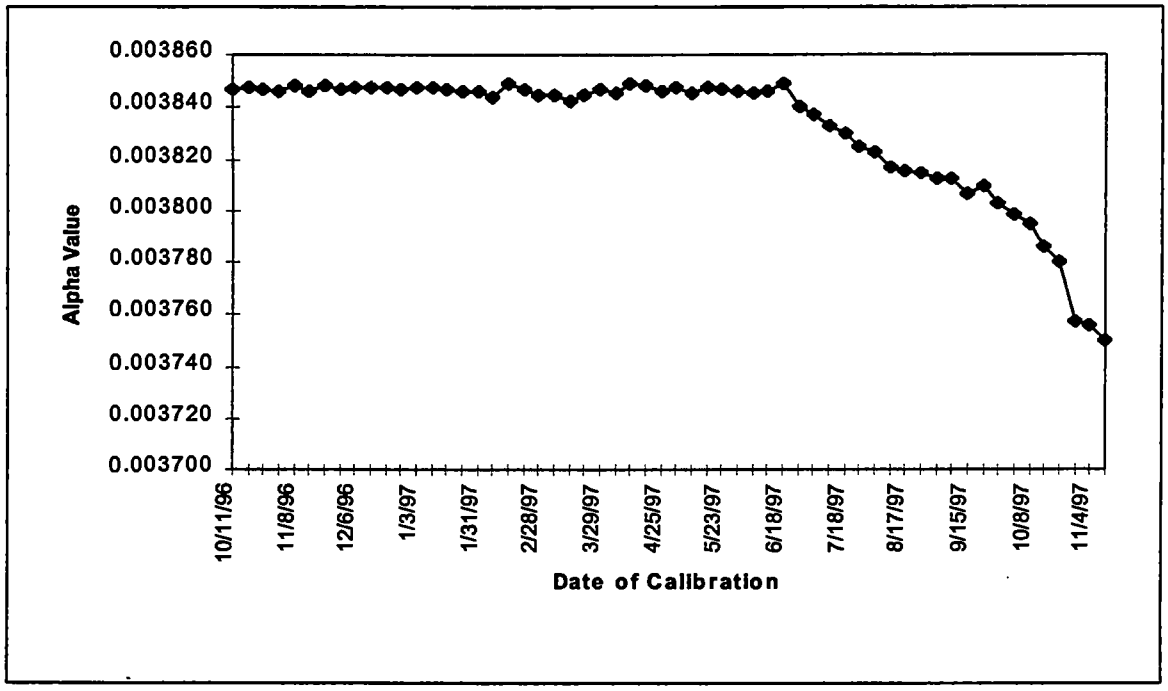


Figure B-17 RTD B-6 Alpha Value Trend

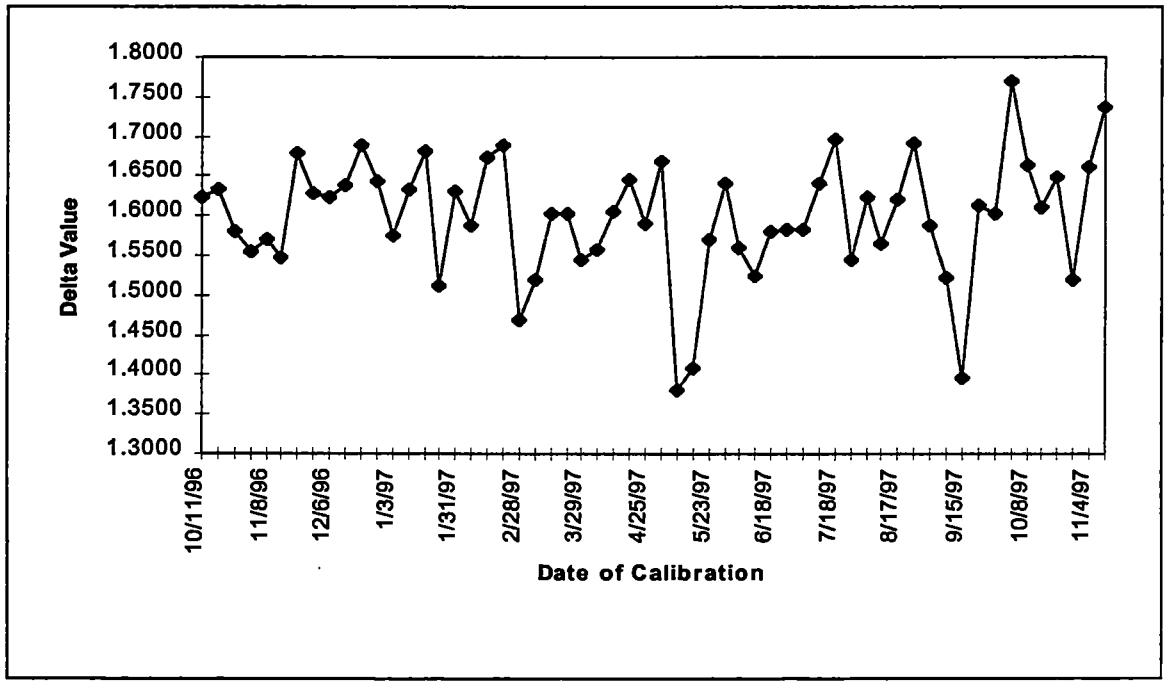


Figure B-18 RTD B-6 Delta Value Trend

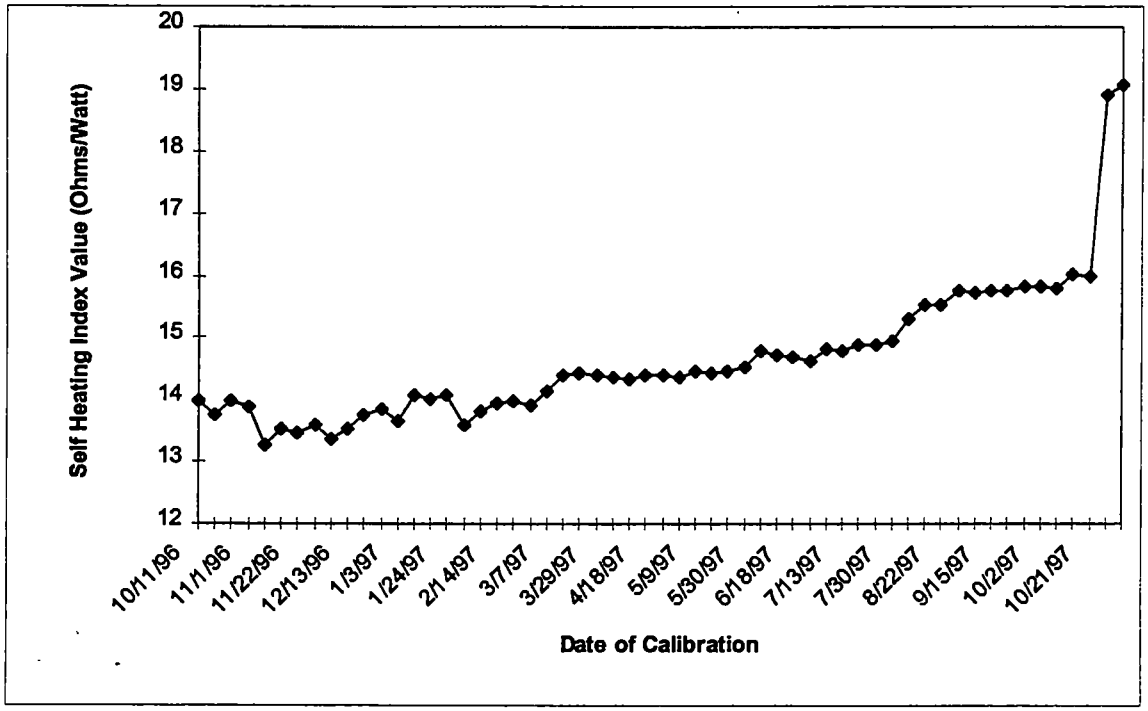


Figure B-19 RTD B-6 Self Heating Index (Ohm/Watt) Value Trend

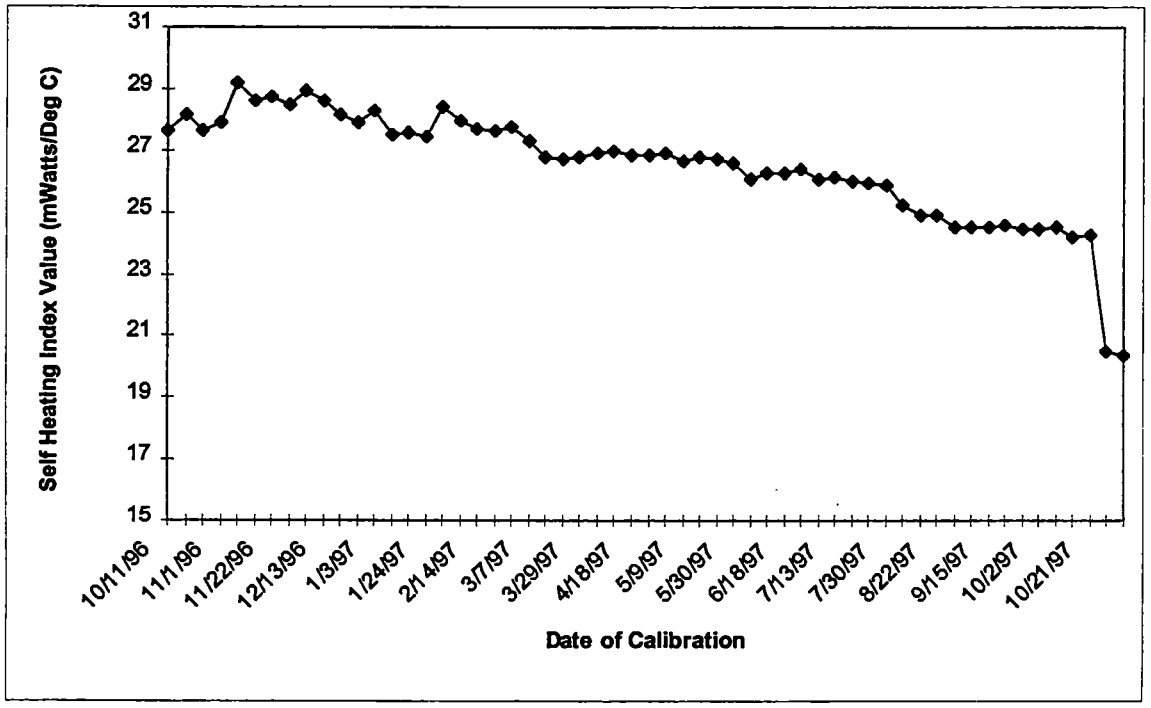


Figure B-20 RTD B-6 Self Heating Index (mWatt/°C) Value Trend

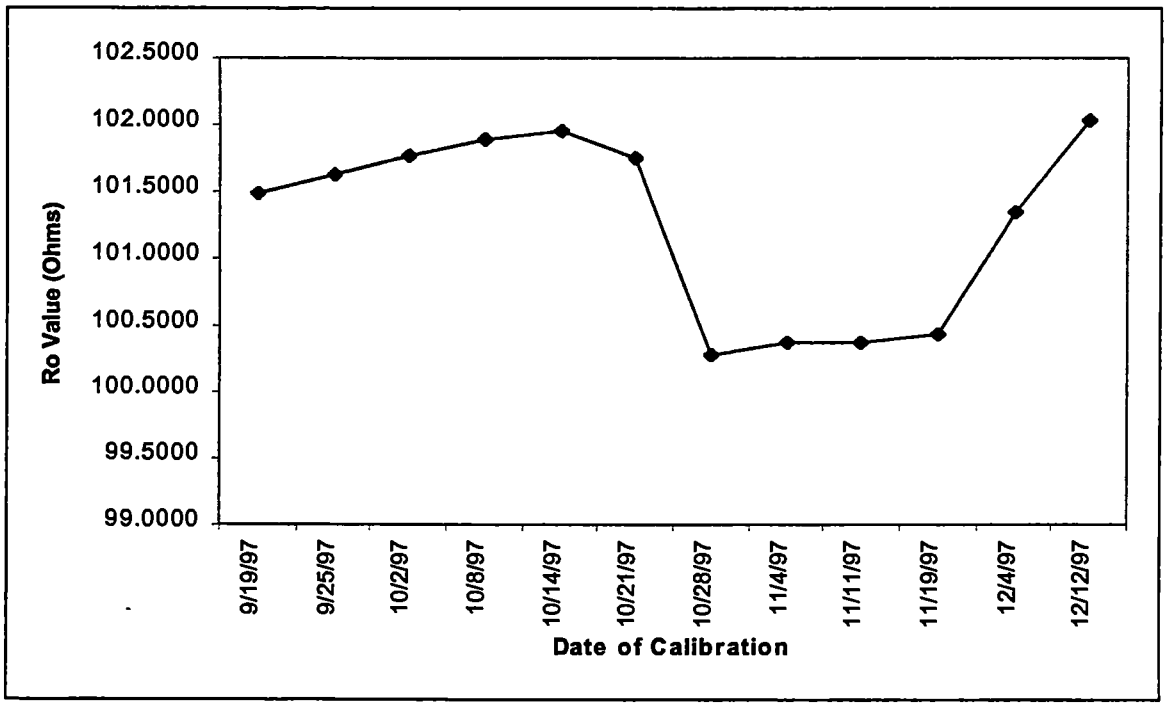


Figure B-21 RTD B-11 Ro Value Trend

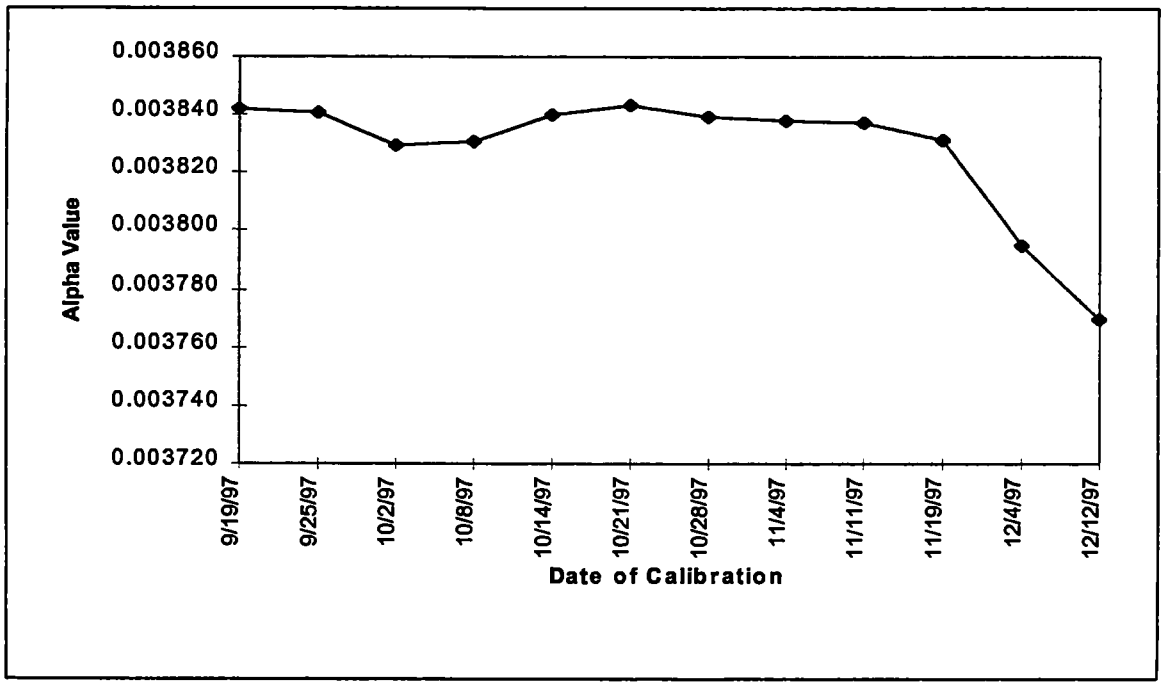


Figure B-22 RTD B-11 Alpha Value Trend

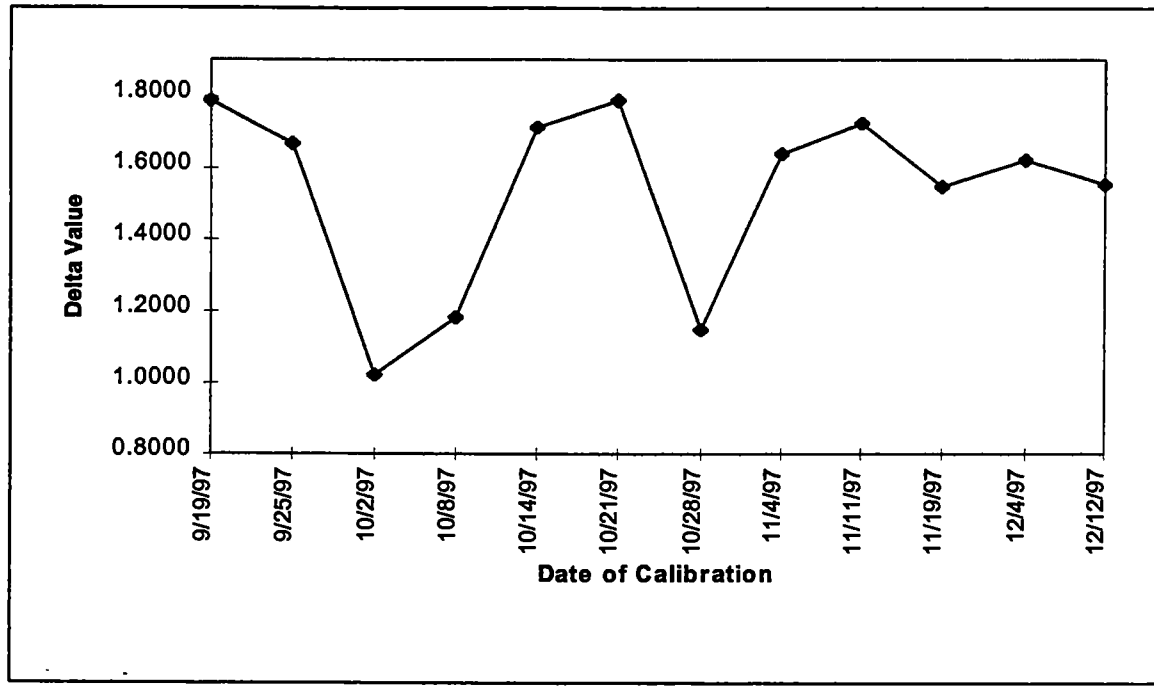


Figure B-23 RTD B-11 Delta Value Trend

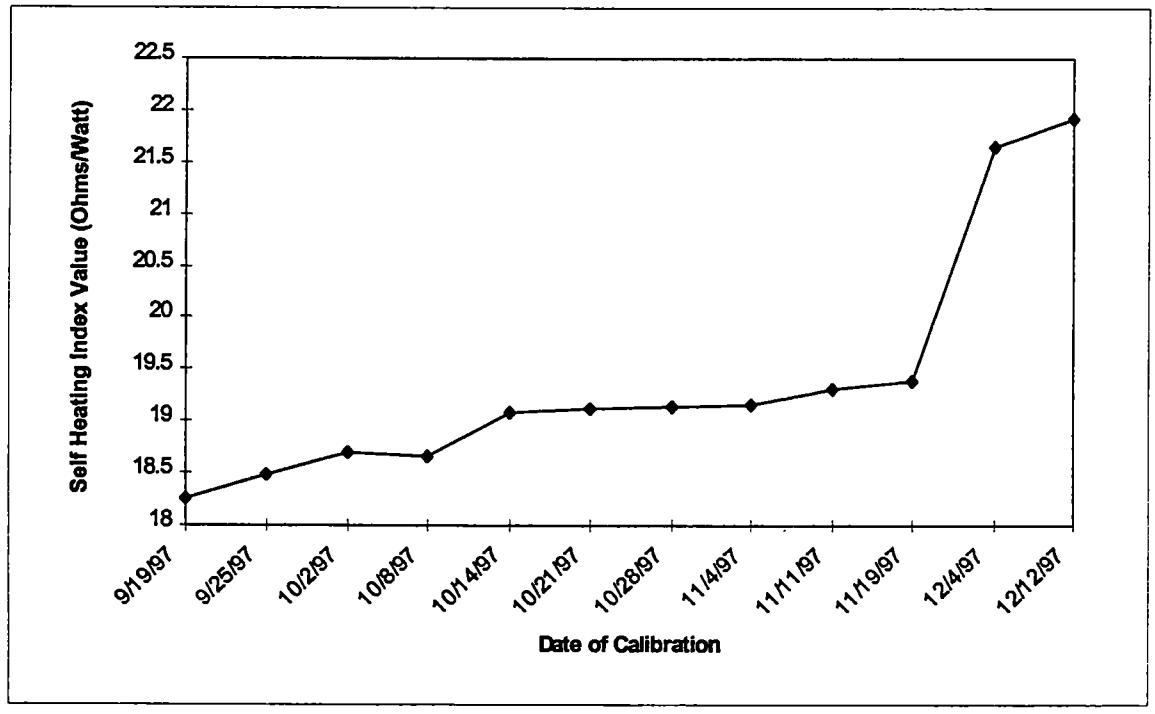


Figure B-24 RTD B-11 Self Heating Index (Ohm/Watt) Value Trend

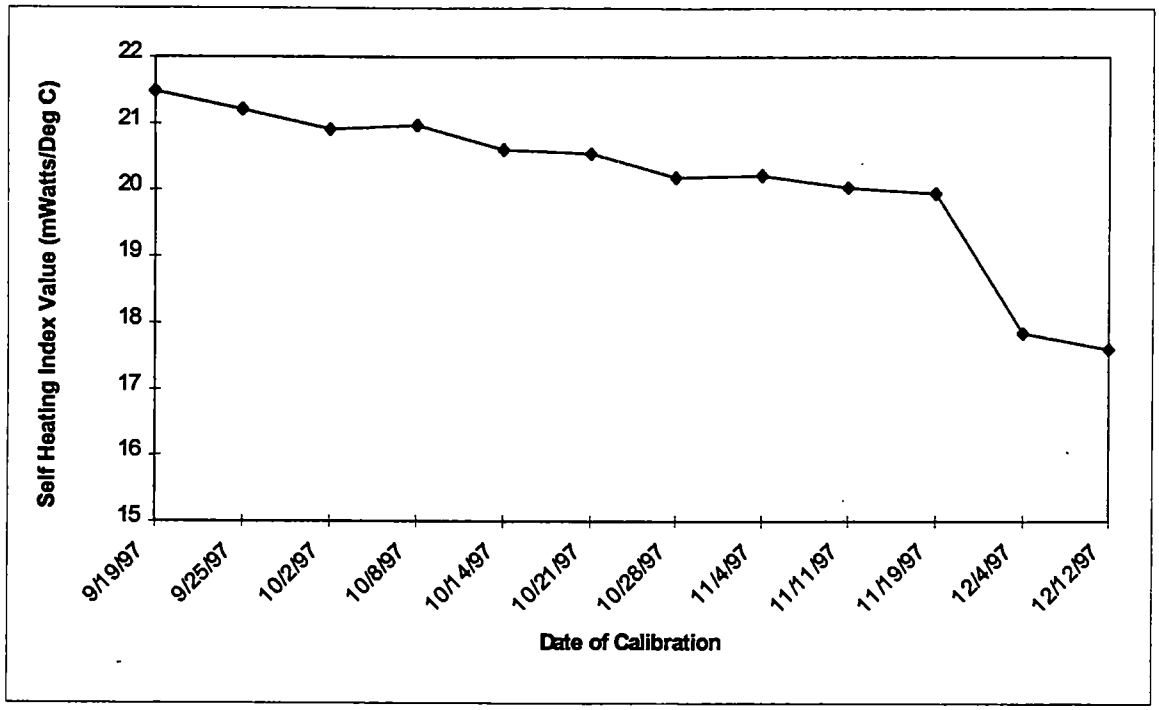


Figure B-25 RTD B-11 Self Heating Index (mWatt/°C) Value Trend

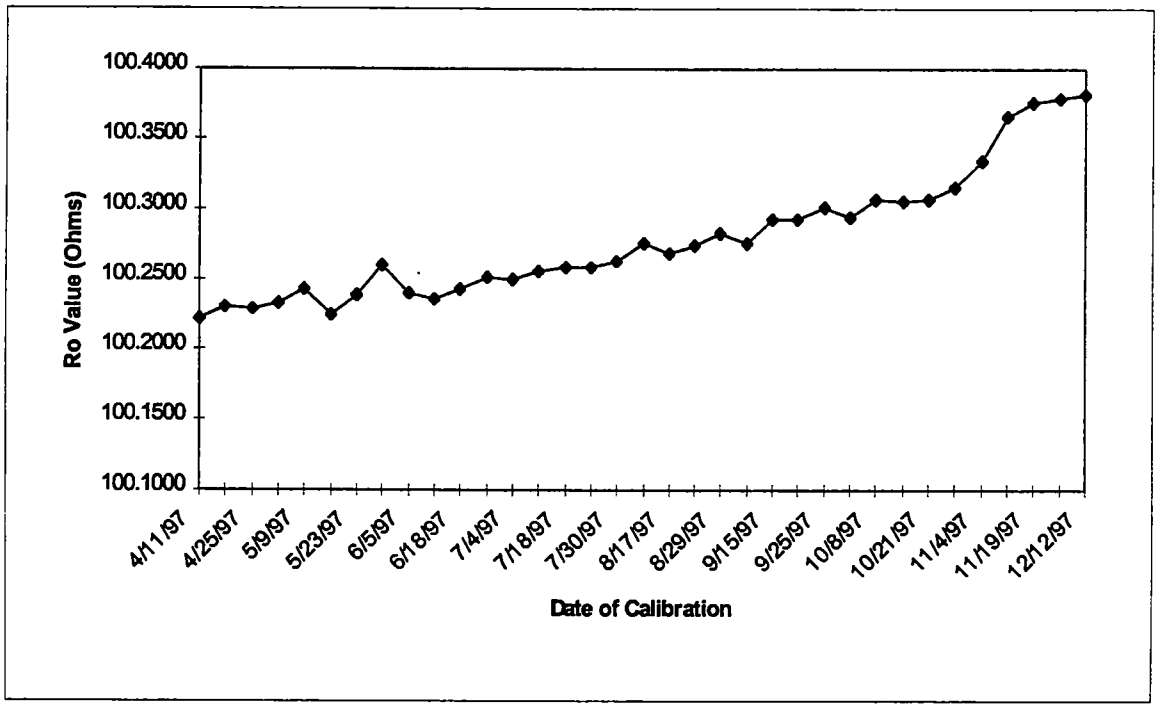


Figure B-26 RTD A-66 Ro Value Trend

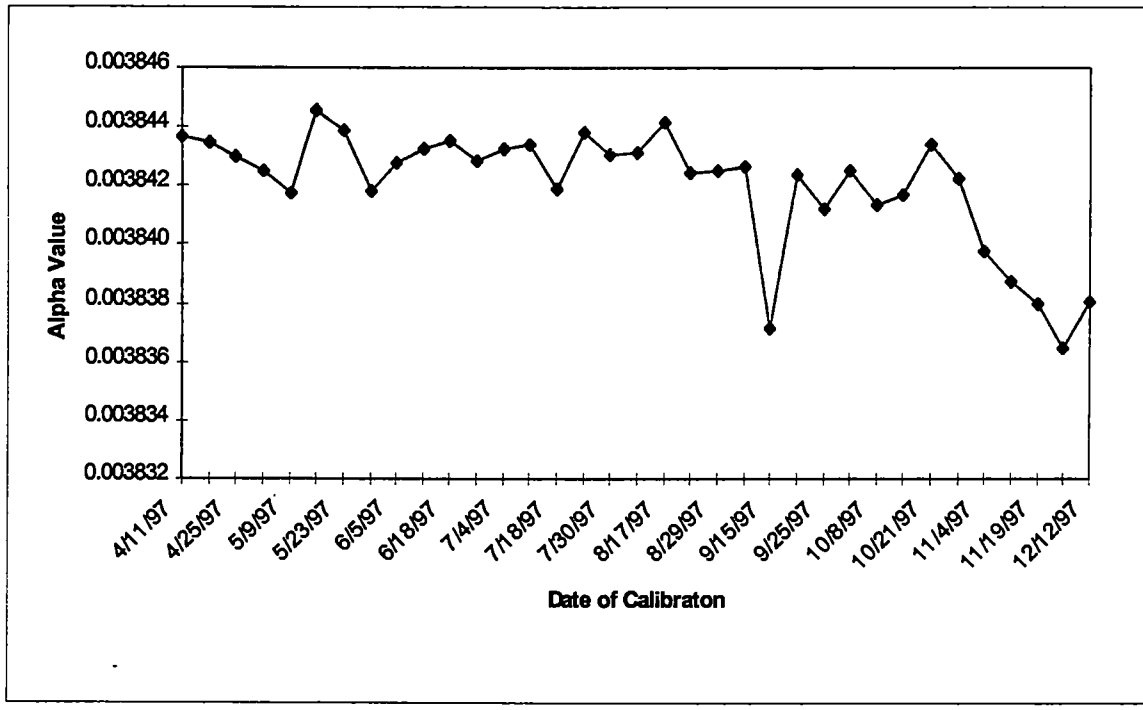


Figure B-27 RTD A-66 Alpha Value Trend

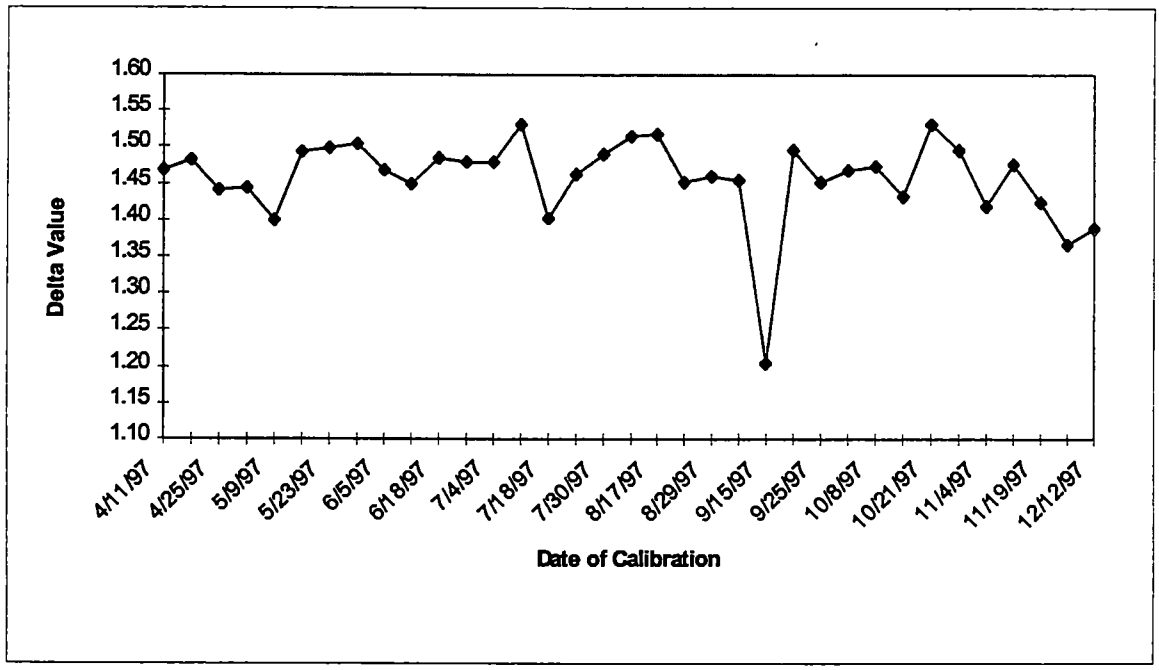


Figure B-28 RTD A-66 Delta Value Trend

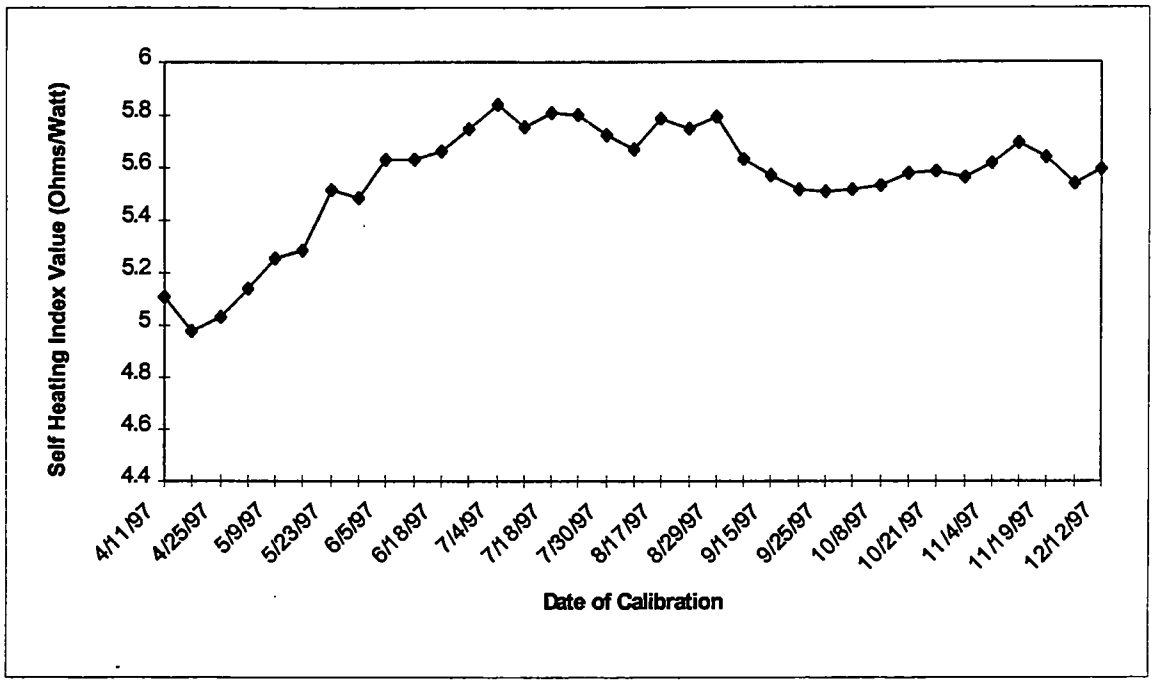


Figure B-29 RTD A-66 Self Heating Index (Ohm/Watt) Value Trend

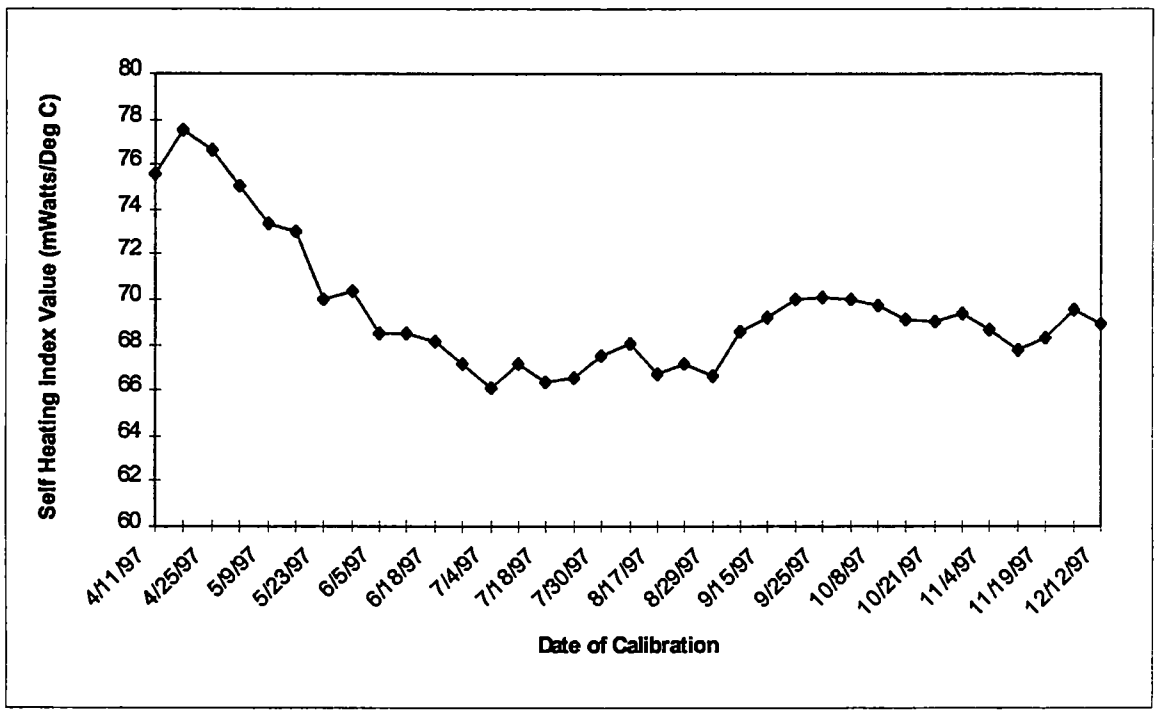


Figure B-30 RTD A-66 Self Heating Index (mWatt/°C) Value Trend

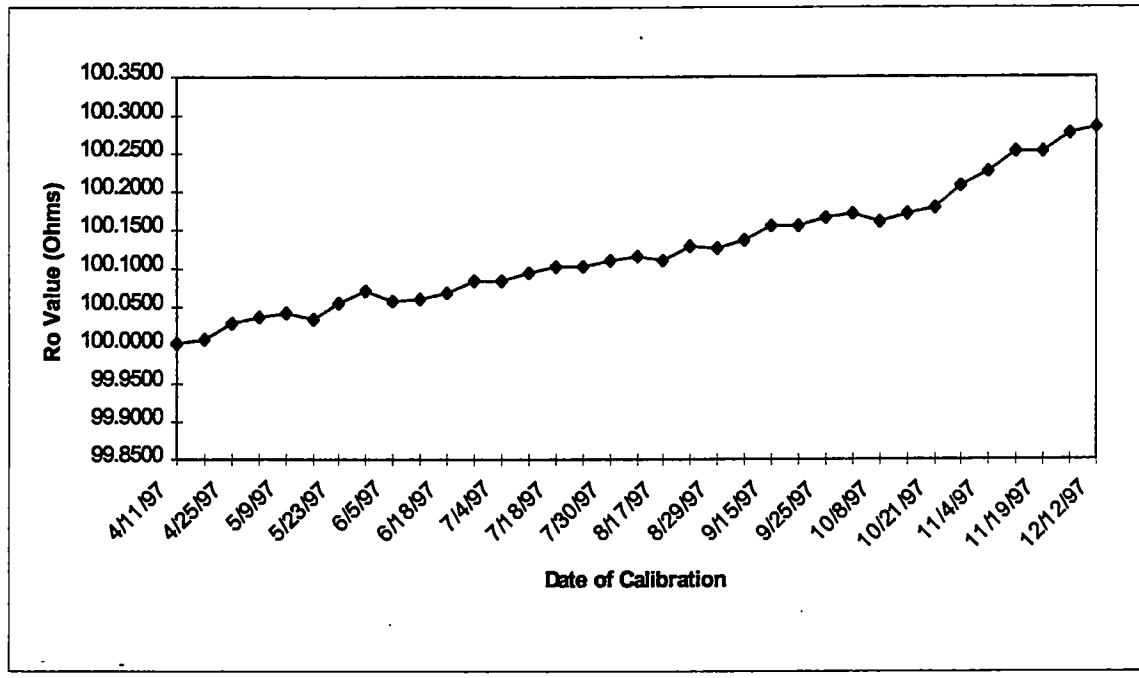


Figure B-31 RTD A-67 Ro Value Trend

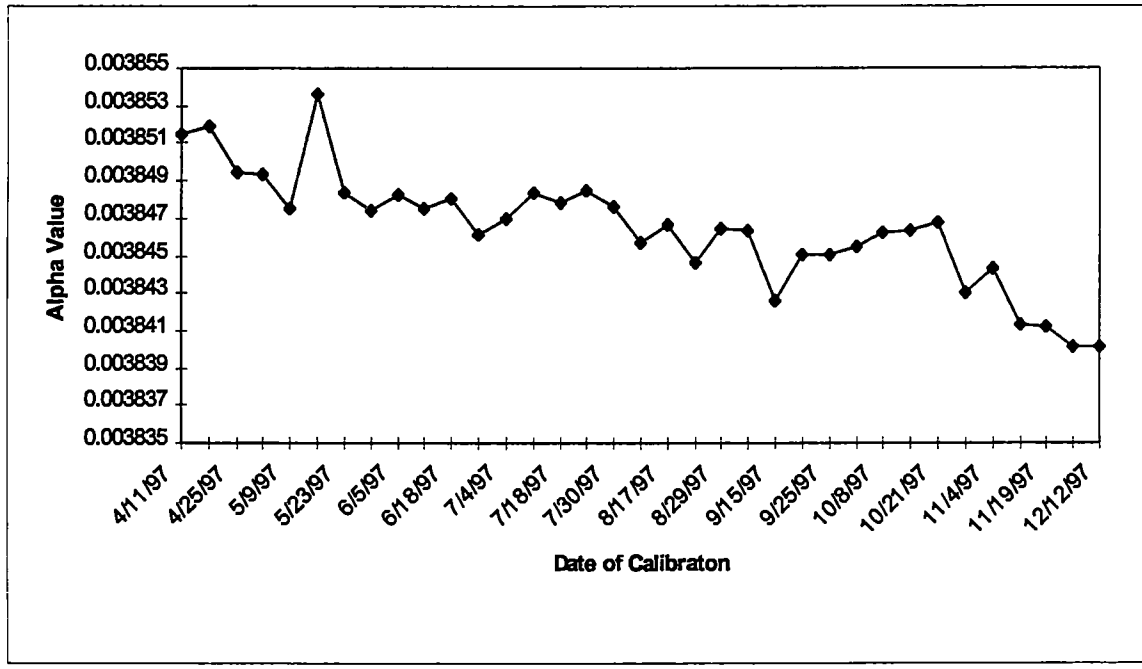


Figure B-32 RTD A-67 Alpha Value Trend

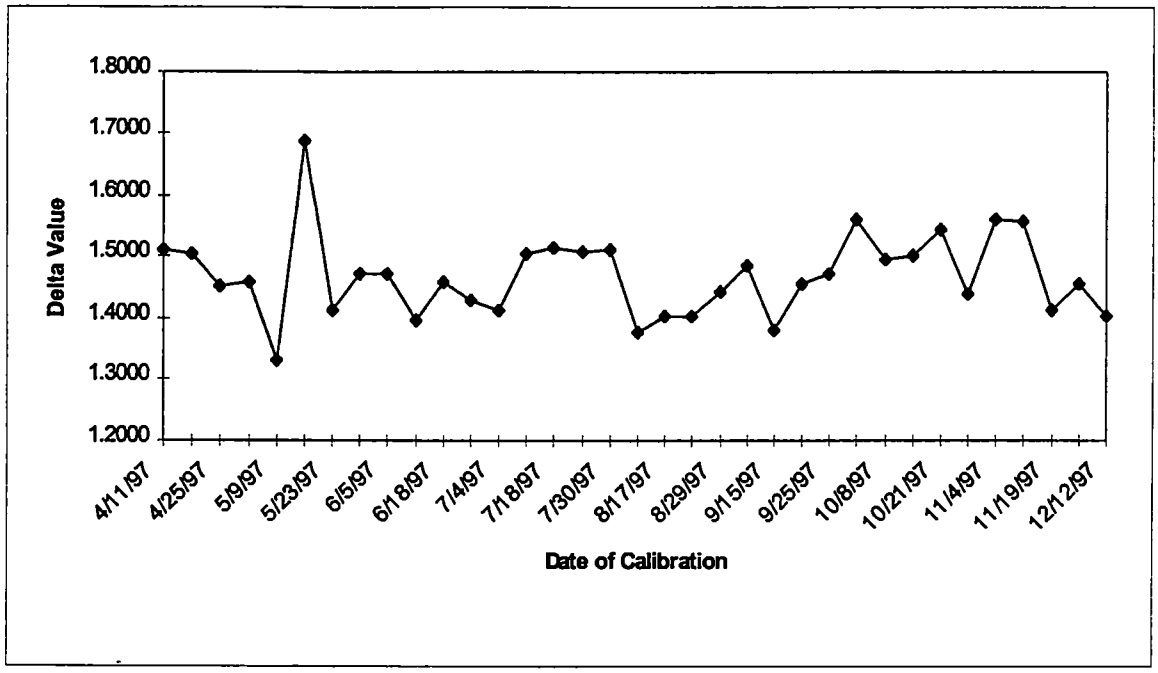


Figure B-33 RTD A-67 Delta Value Trend

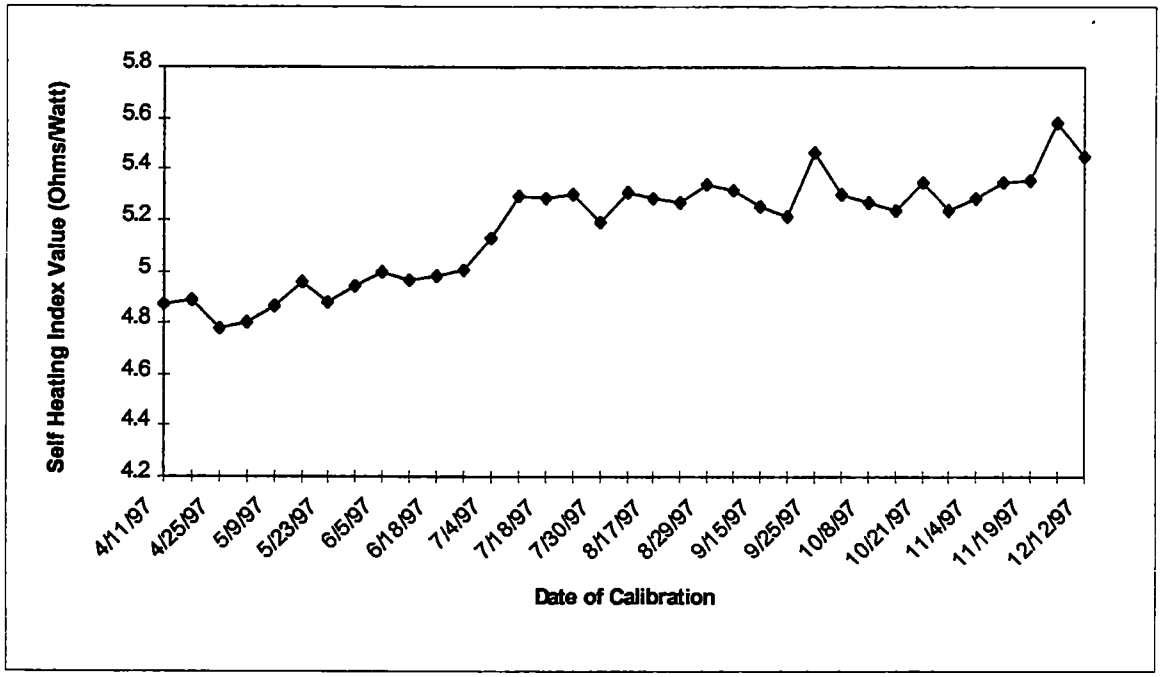


Figure B-34 RTD A-67 Self Heating Index (Ohm/Watt) Value Trend

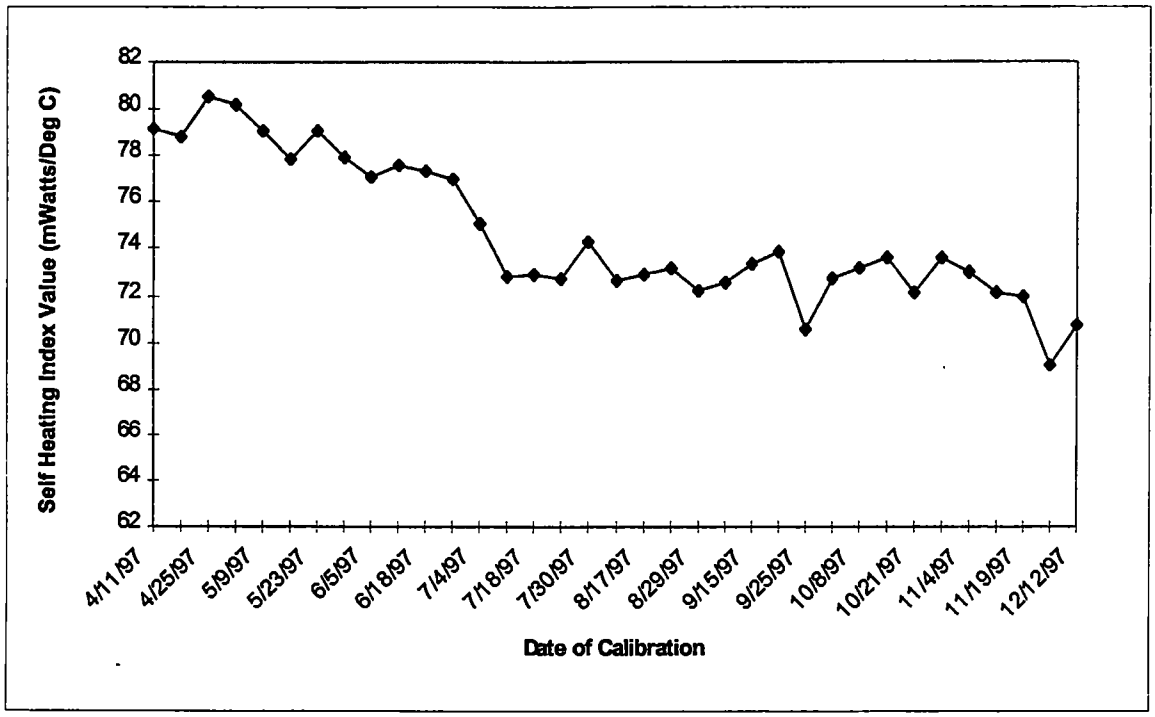


Figure B-35 RTD A-67 Self Heating Index (mWatt/°C) Value Trend

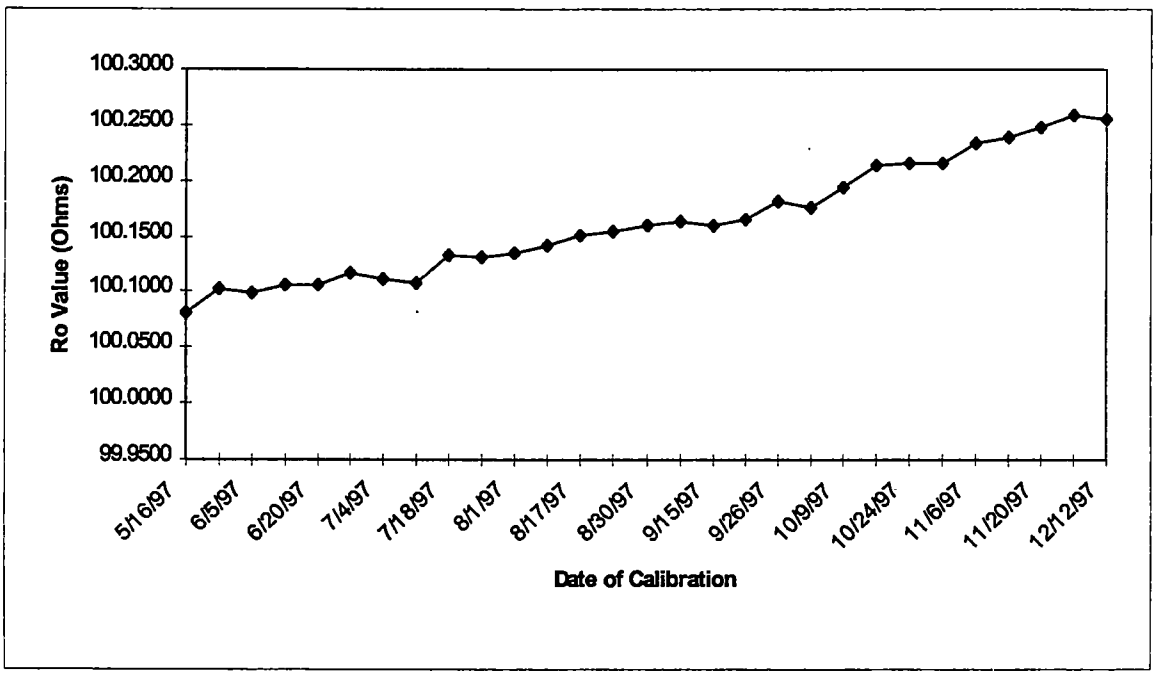


Figure B-36 RTD A-69 Ro Value Trend

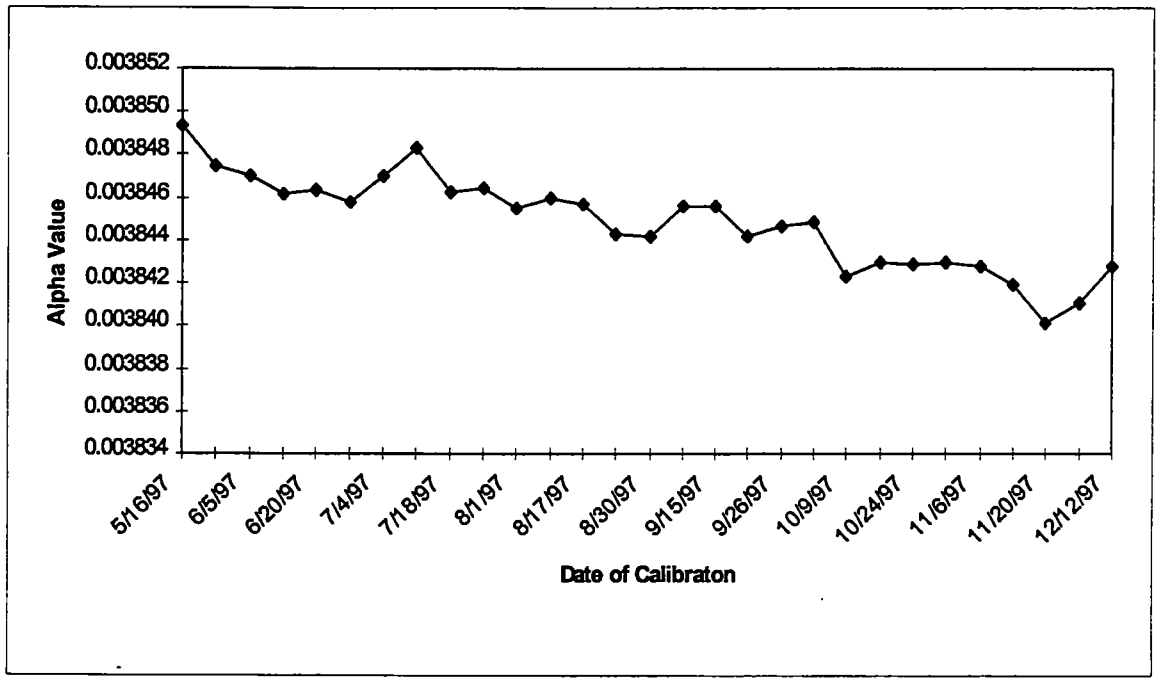


Figure B-37 RTD A-69 Alpha Value Trend

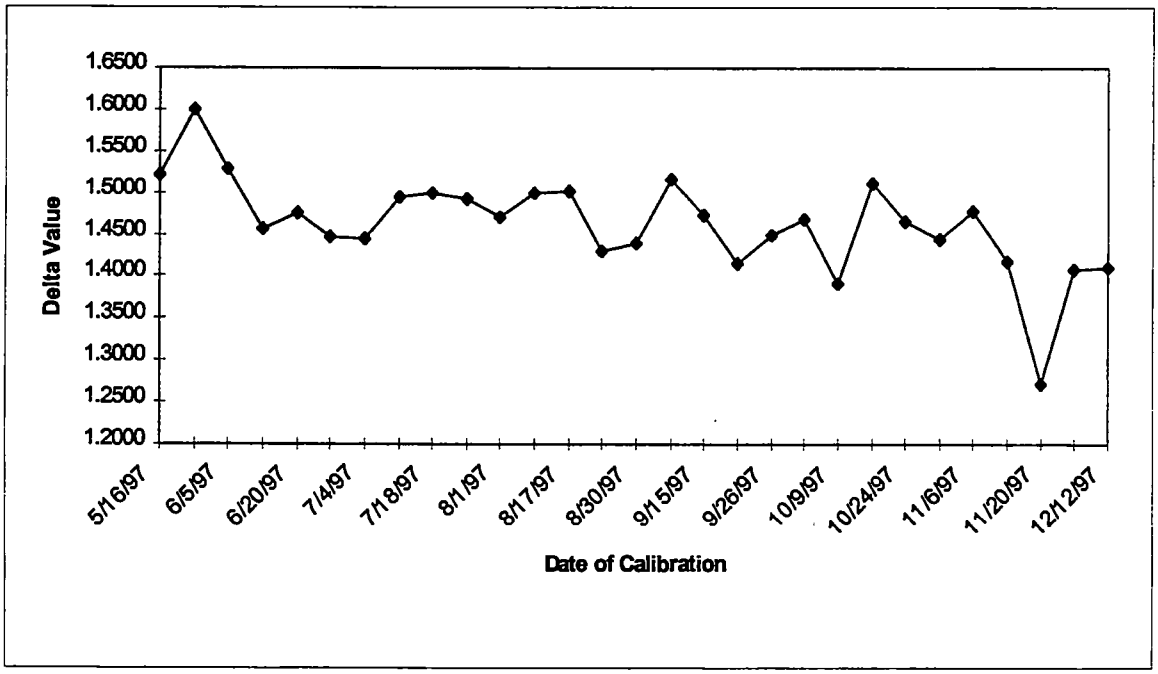


Figure B-38 RTD A-69 Delta Value Trend

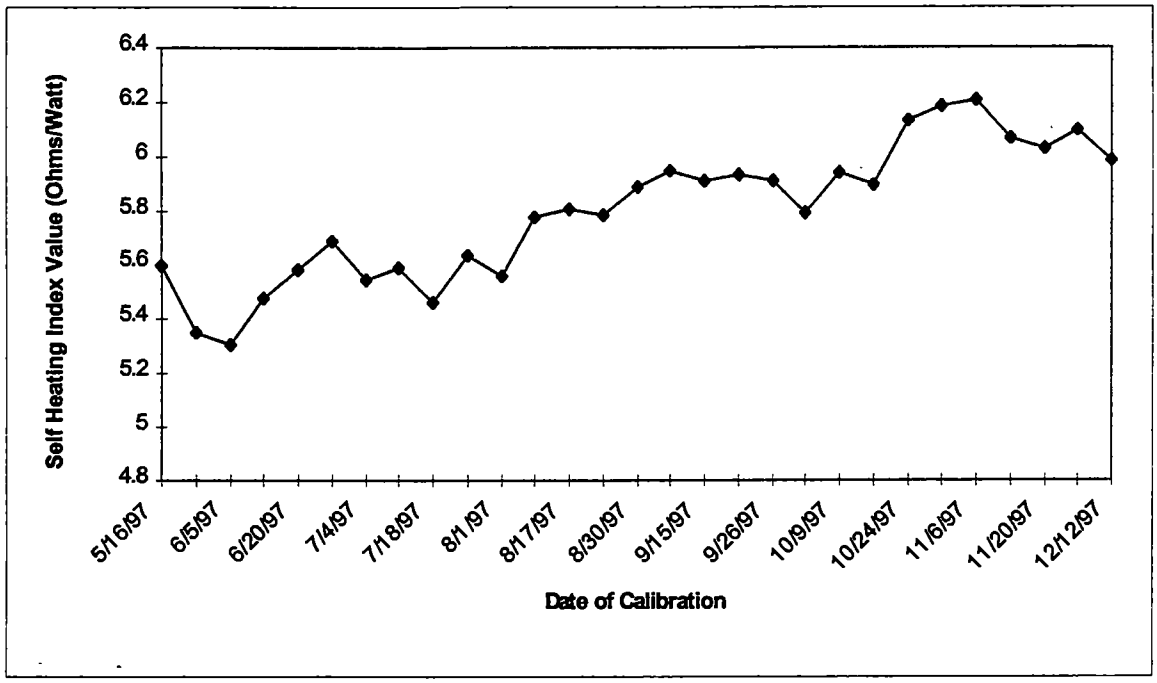


Figure B-39 RTD A-69 Self Heating Index (Ohm/Watt) Value Trend

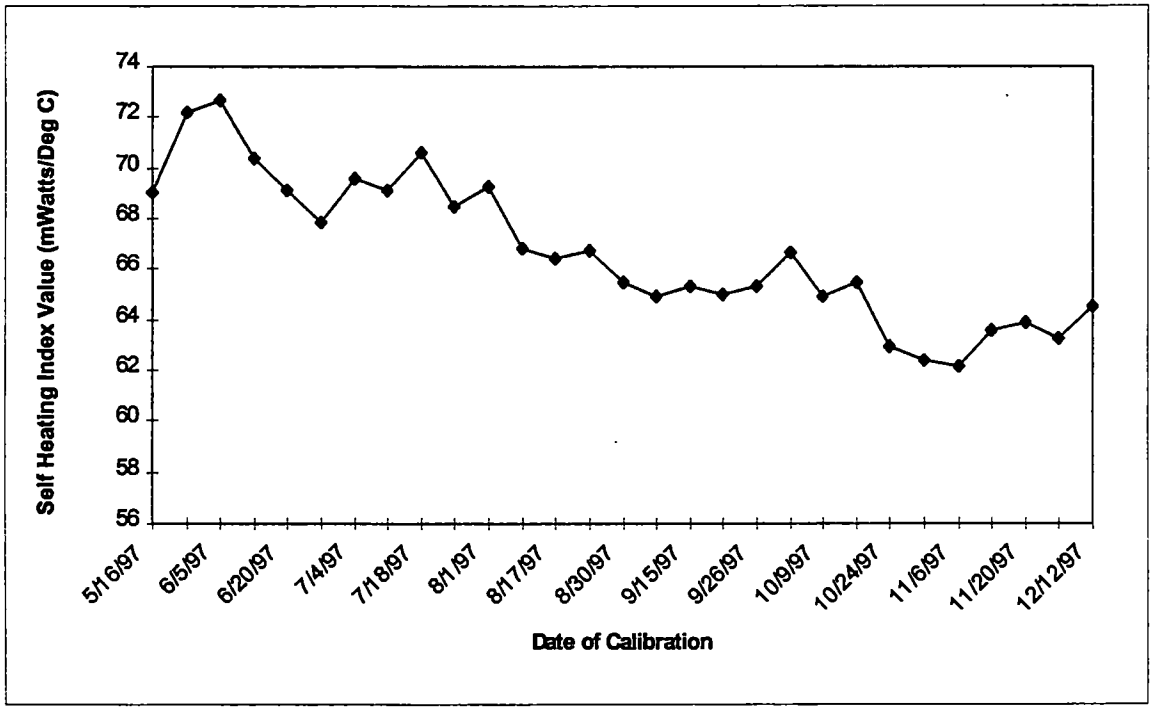


Figure B-40 RTD A-69 Self Heating Index (mWatt/°C) Value Trend

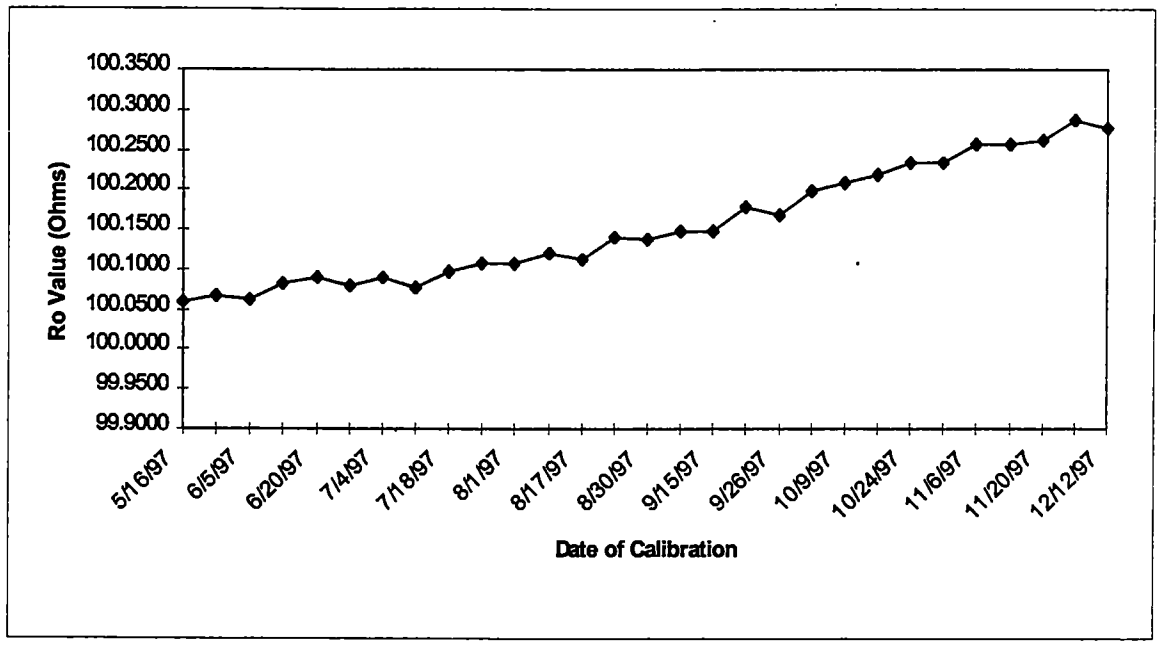


Figure B-41 RTD A-70 Ro Value Trend

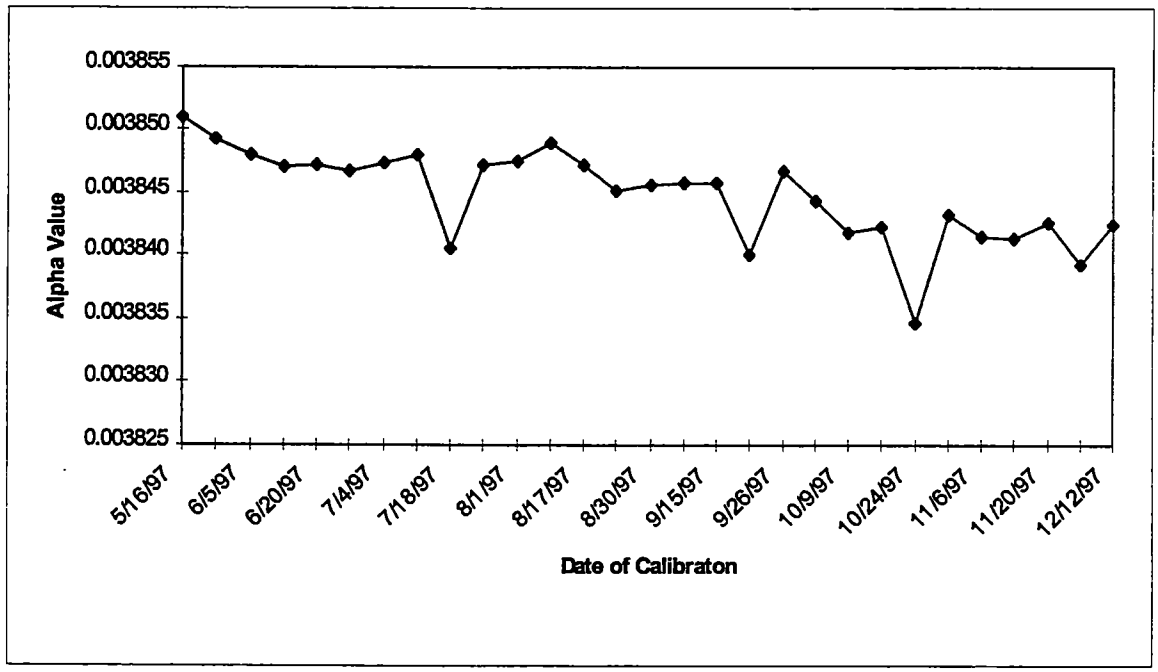


Figure B-42 RTD A-70 Alpha Value Trend

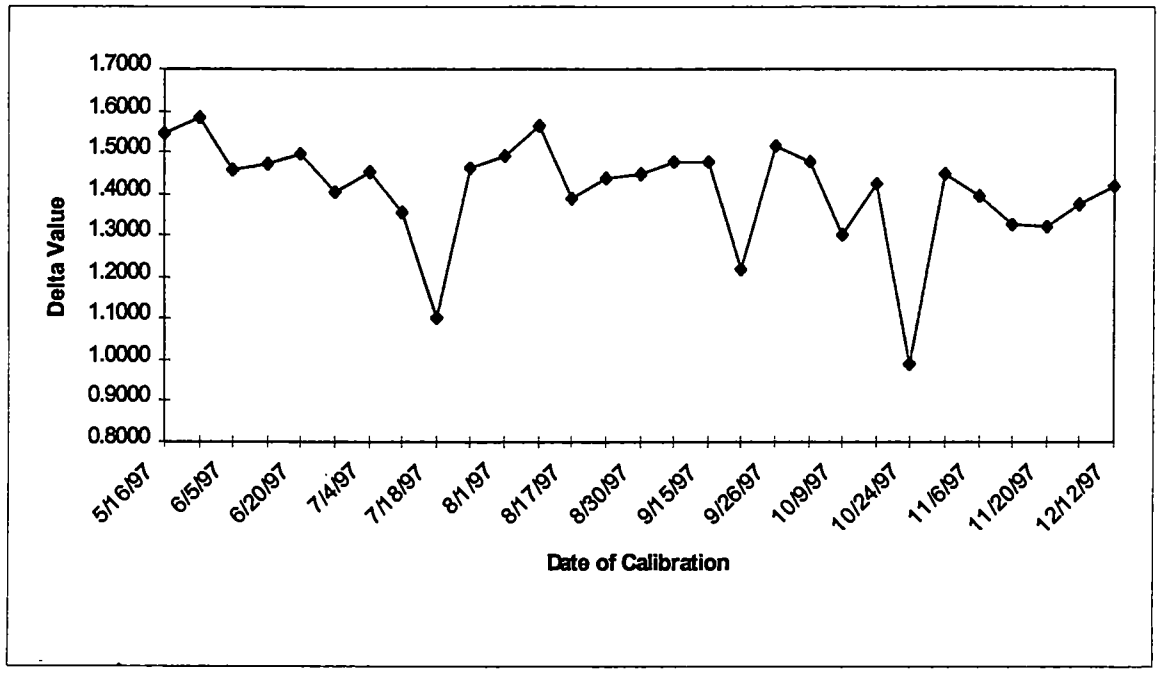


Figure B-43 RTD A-70 Delta Value Trend

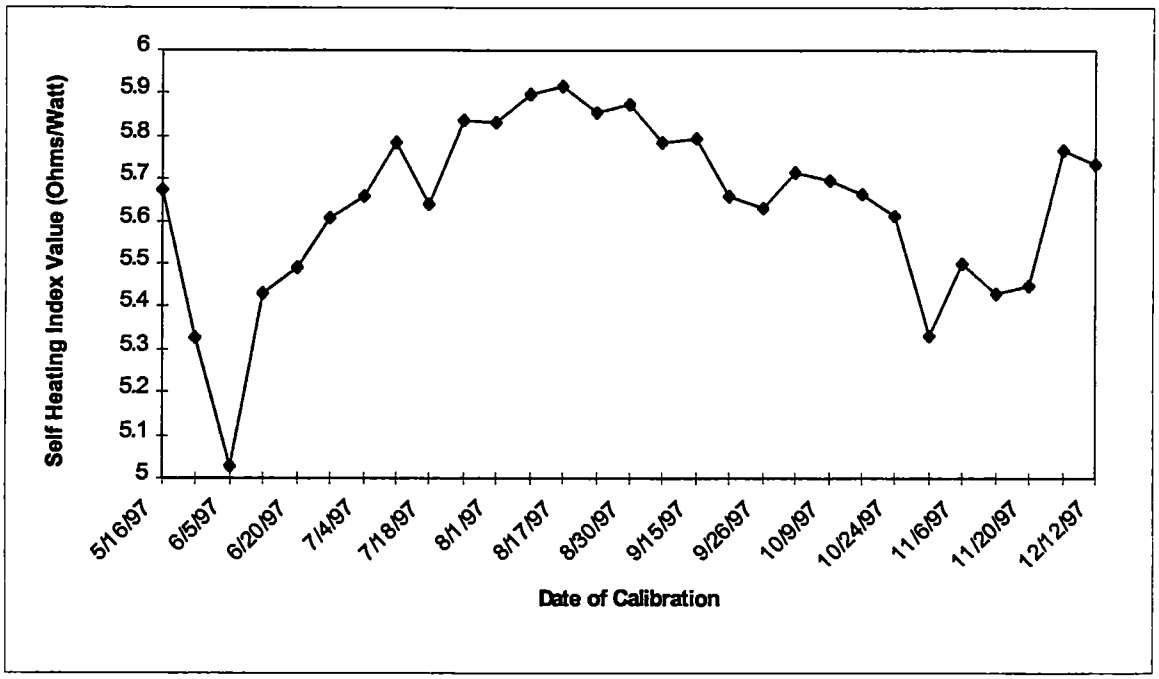


Figure B-44 RTD A-70 Self Heating Index (Ohm/Watt) Value Trend

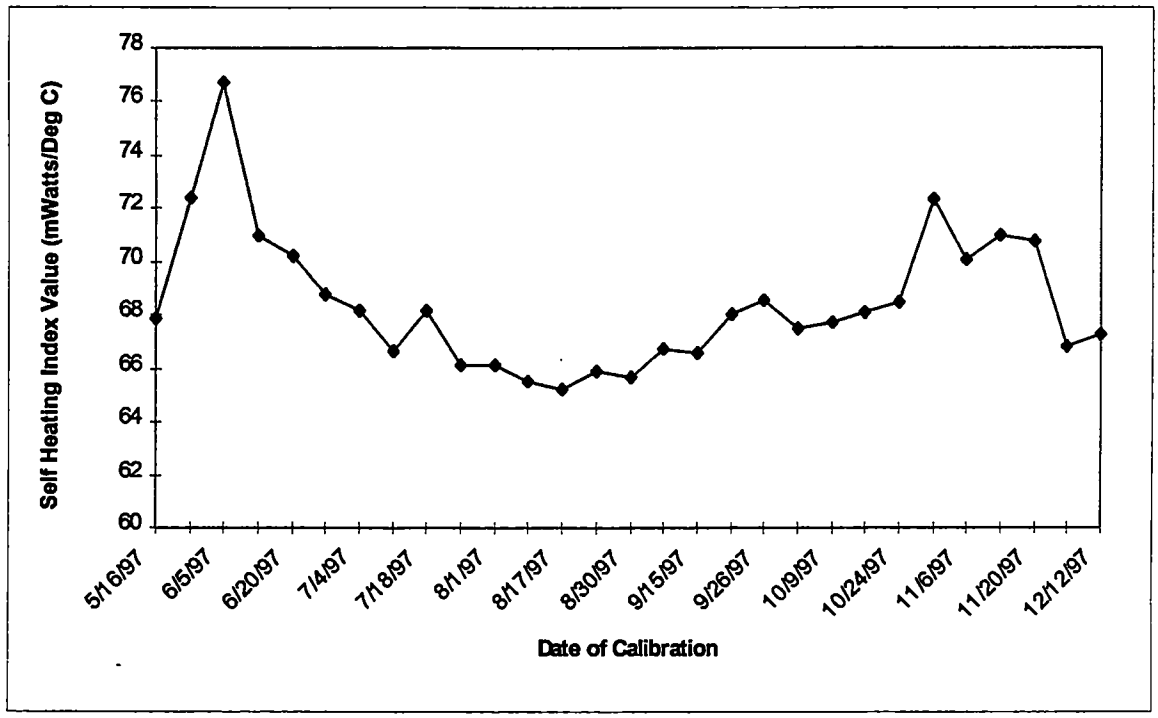


Figure B-45 RTD A-70 Self Heating Index (mWatt/°C) Value Trend

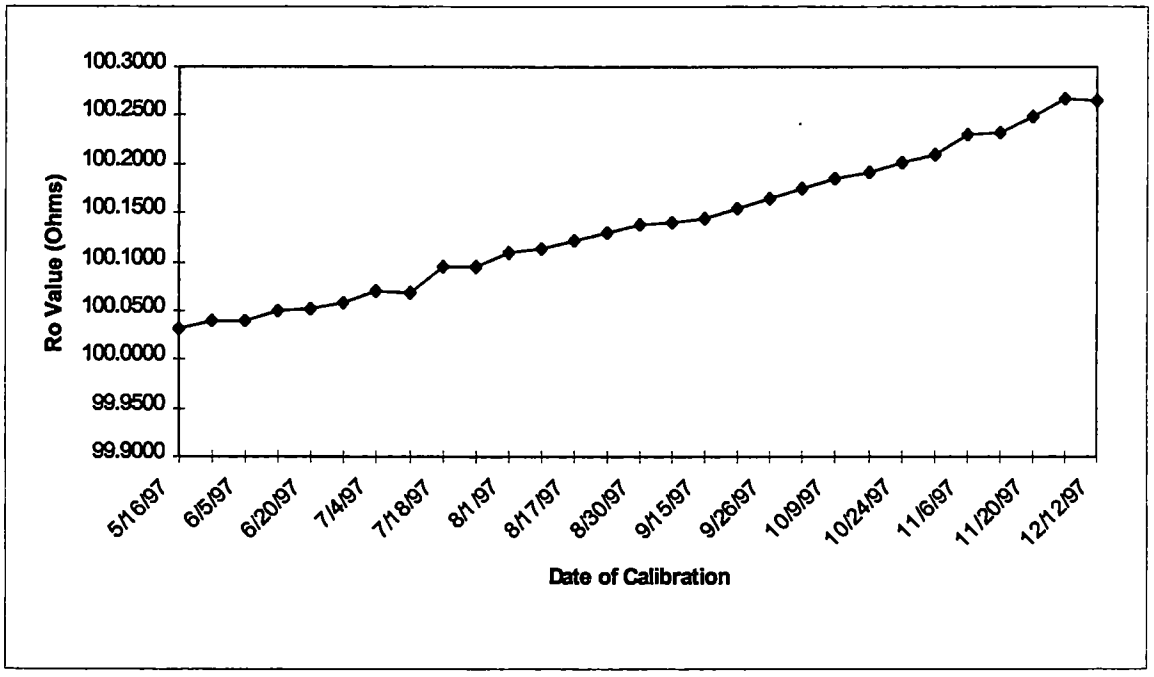


Figure B-46 RTD A-209 Ro Value Trend

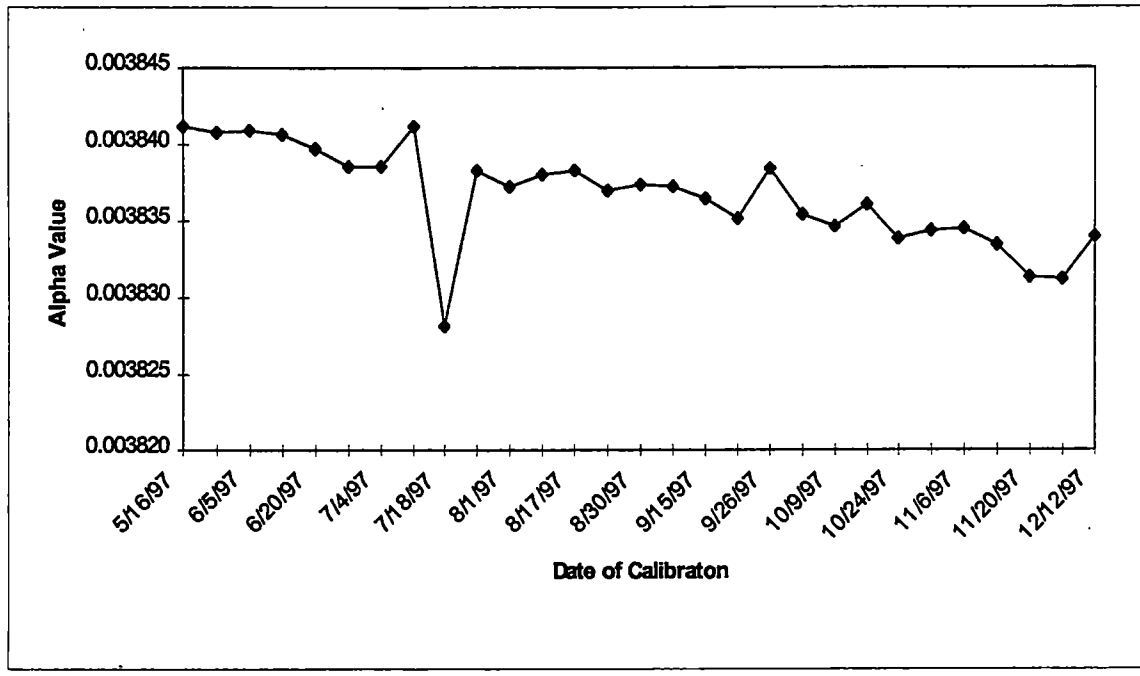


Figure B-47 RTD A-209 Alpha Value Trend

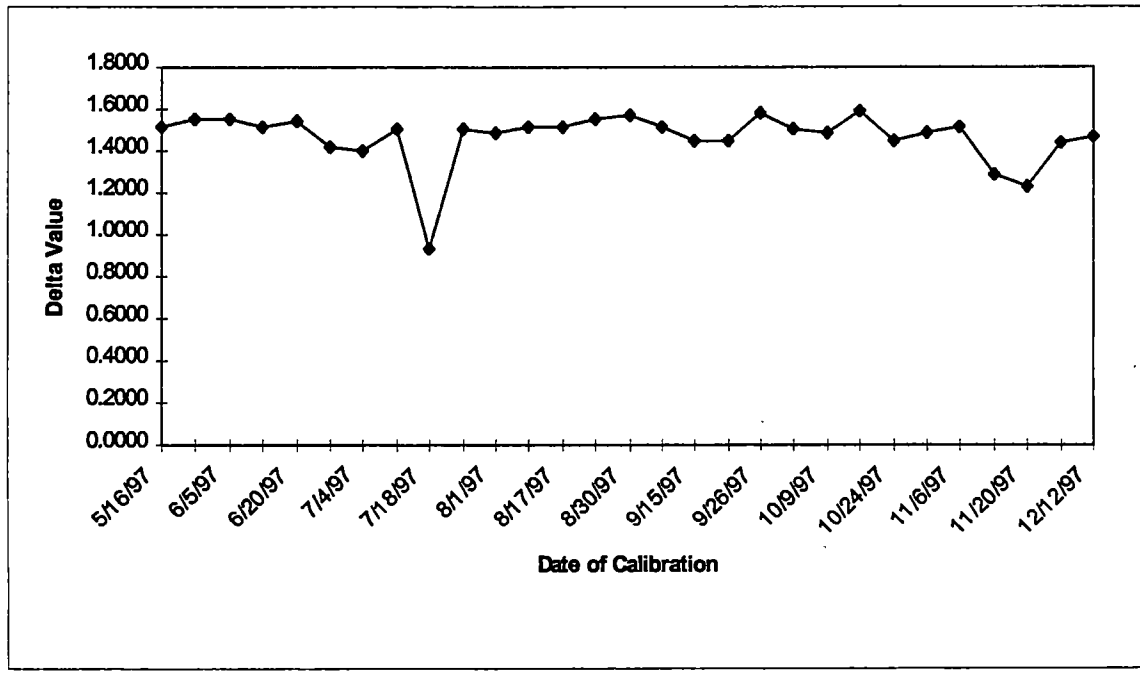


Figure B-48 RTD A-209 Delta Value Trend

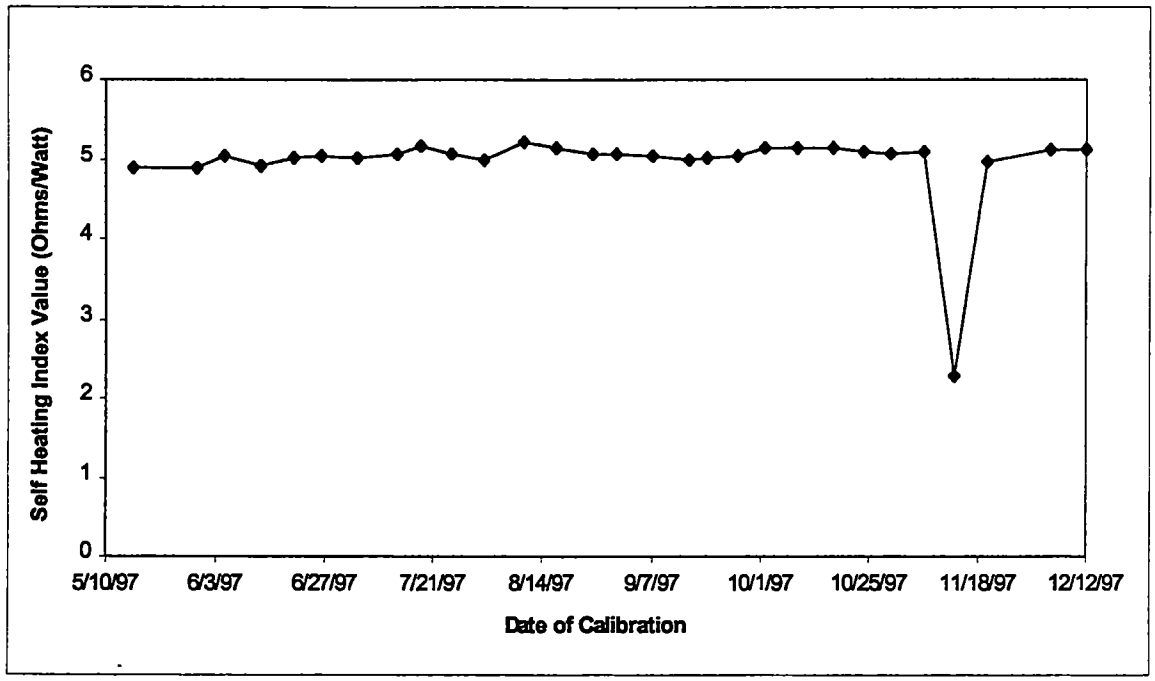


Figure B-49 RTD A-209 Self Heating Index (Ohm/Watt) Value Trend

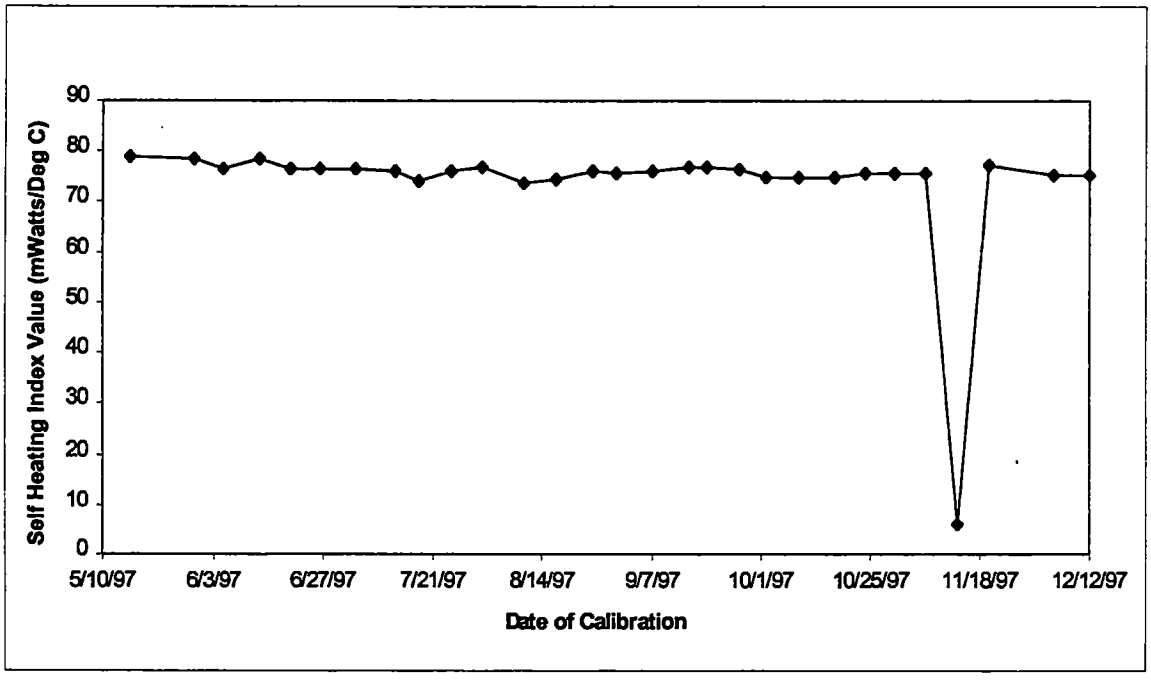


Figure B-50 RTD A-209 Self Heating Index (mWatt/°C) Value Trend

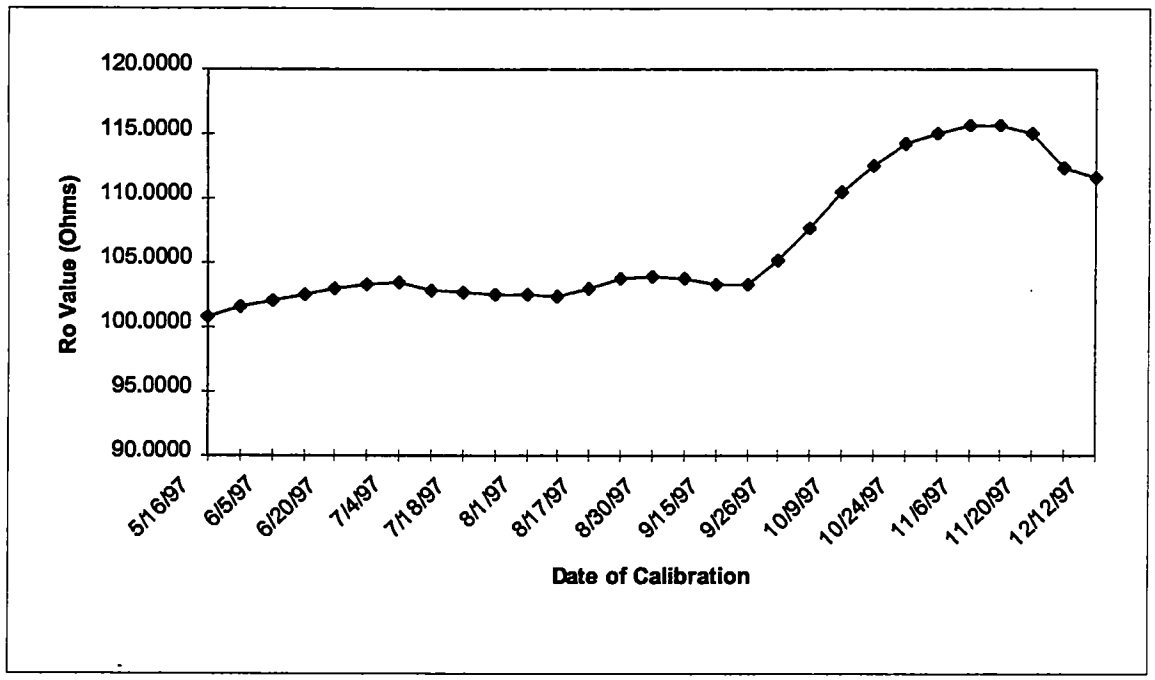


Figure B-51 RTD A-74 Ro Value Trend

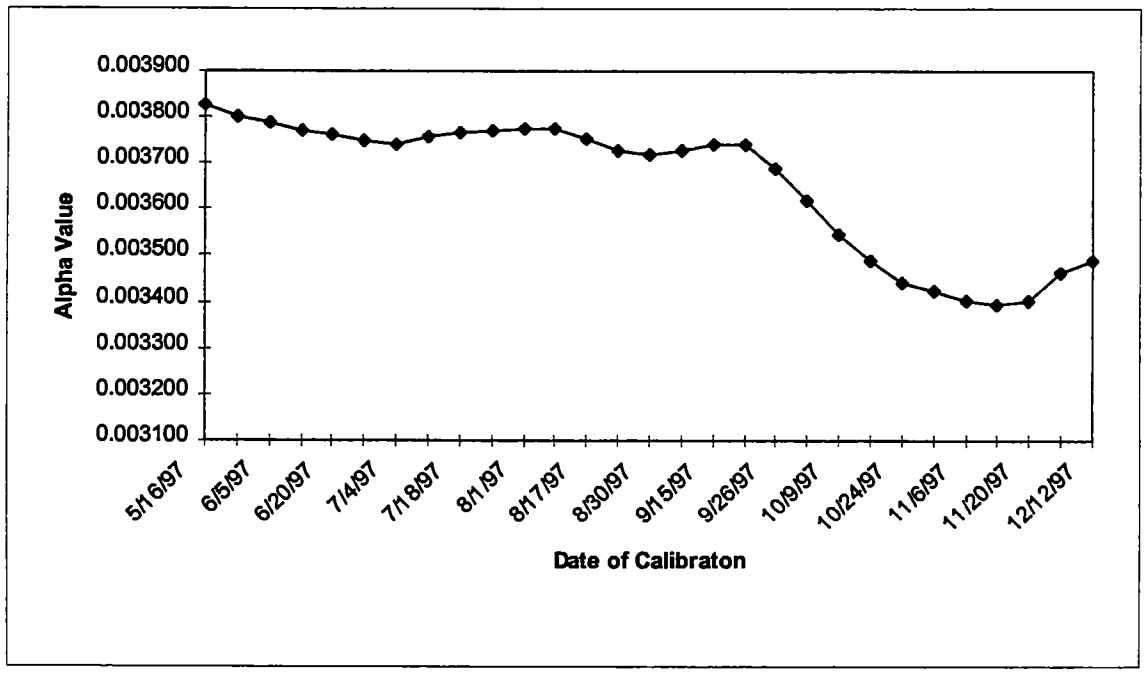


Figure B-52 RTD A-74 Alpha Value Trend

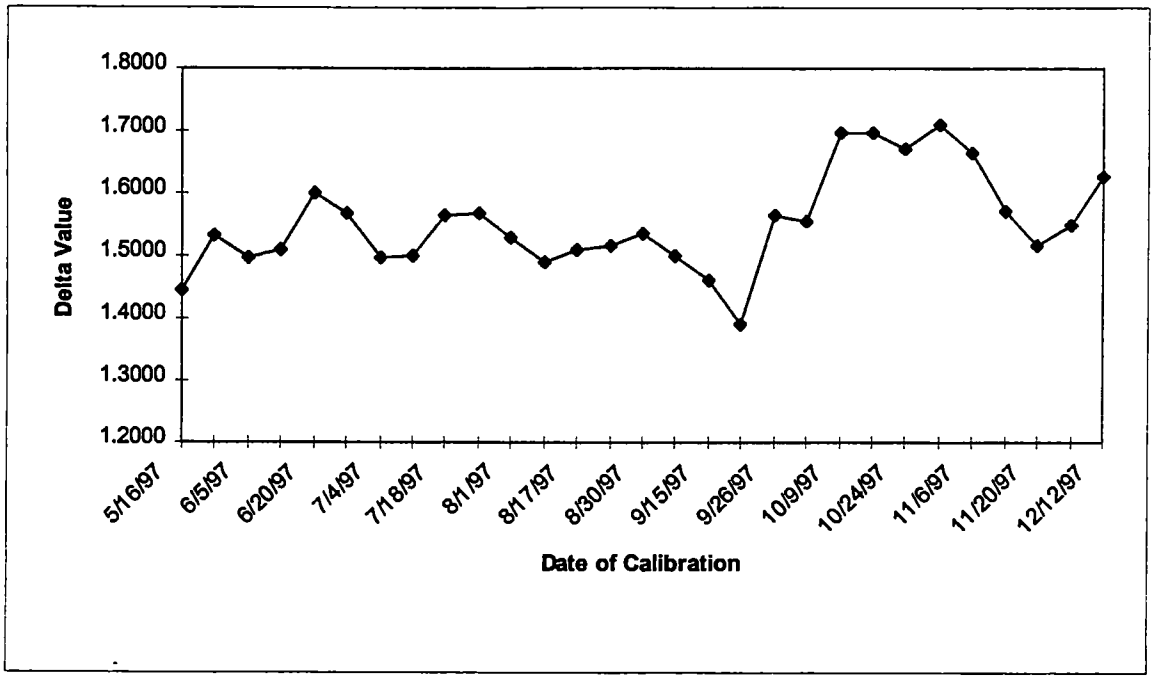


Figure B-53 RTD A-74 Delta Value Trend

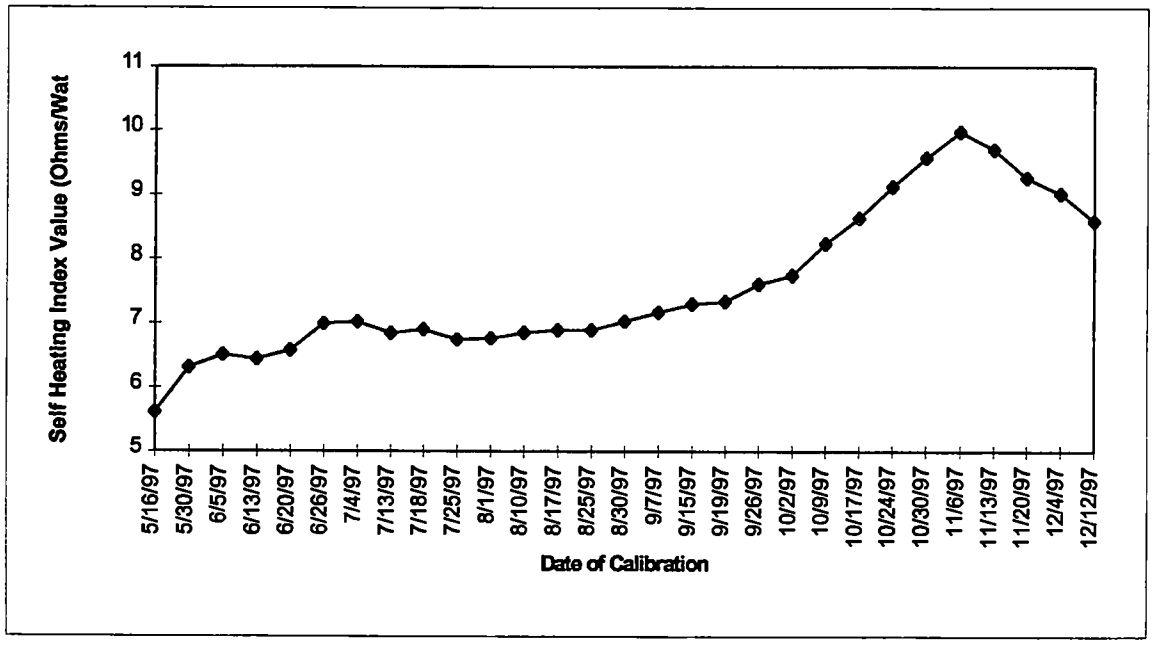


Figure B-54 RTD A-74 Self Heating Index (Ohm/Watt) Value Trend

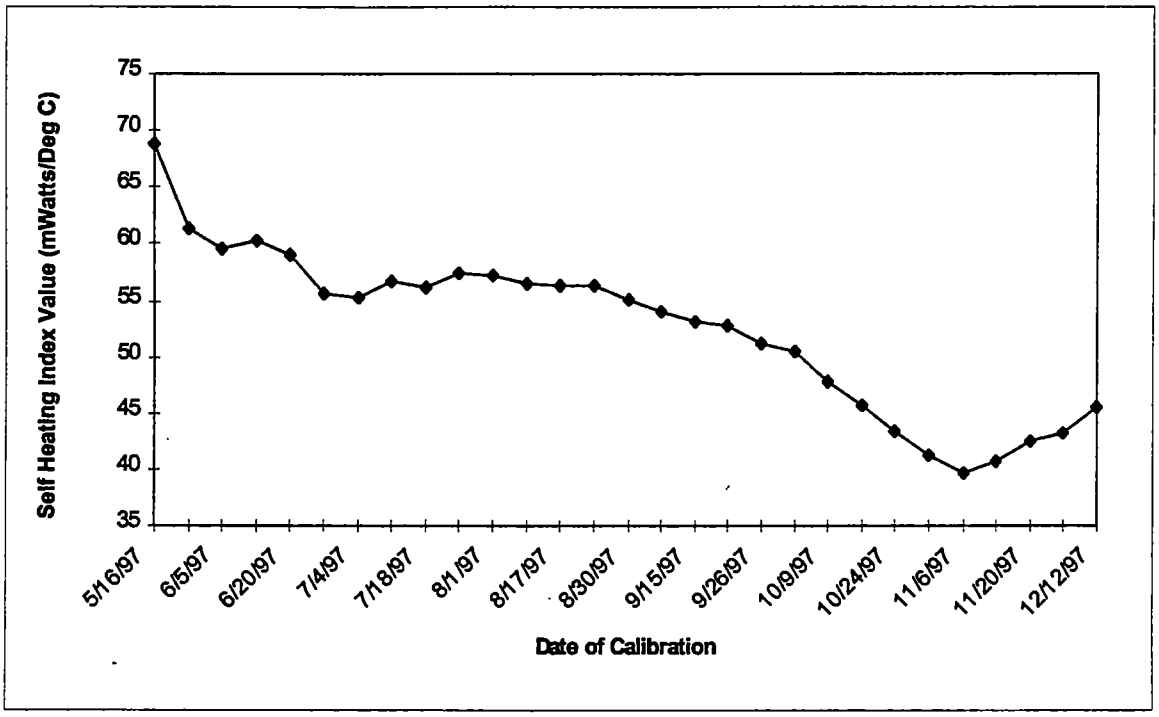


Figure B-55 RTD A-74 Self Heating Index (mWatt/°C) Value Trend

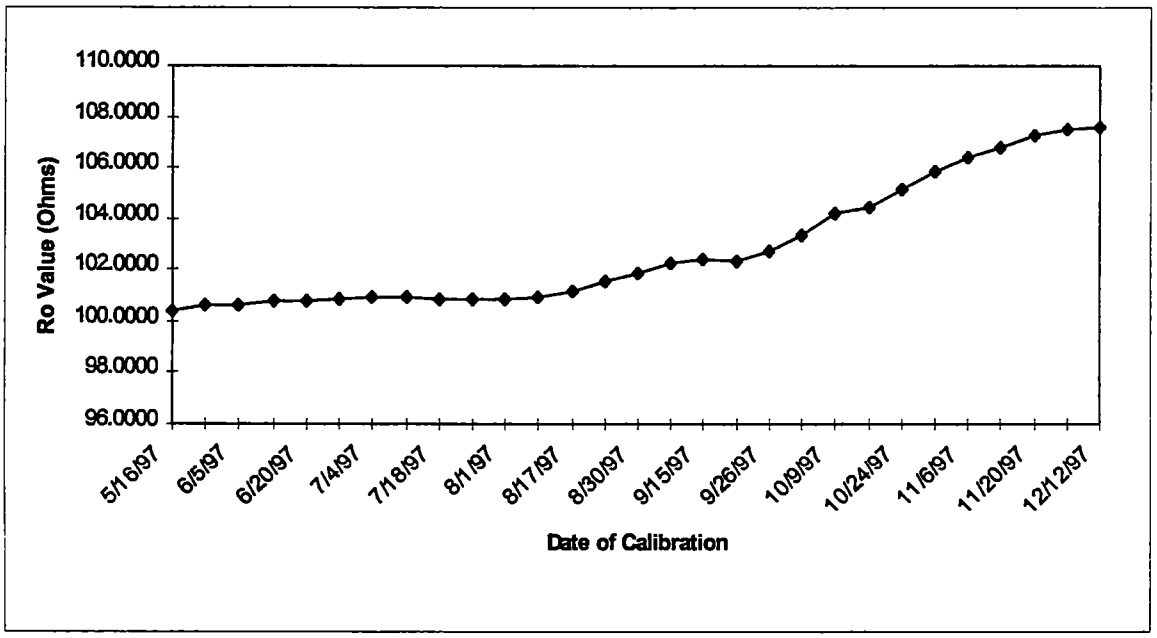


Figure B-56 RTD A-75 Ro Value Trend

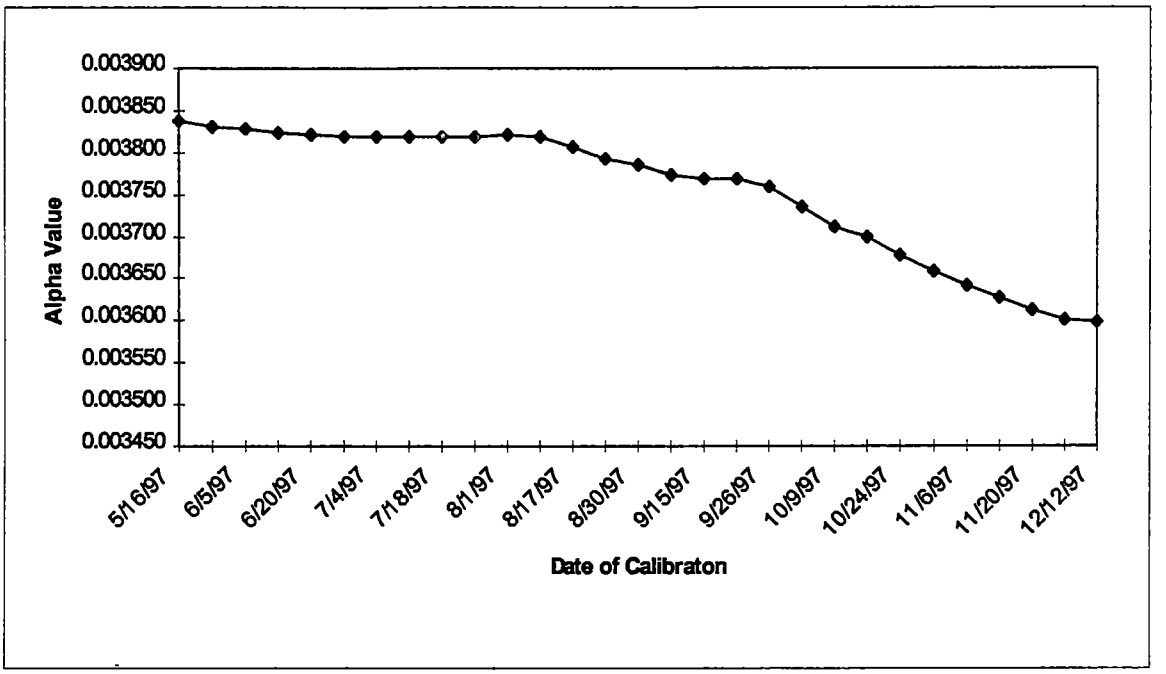


Figure B-57 RTD A-75 Alpha Value Trend

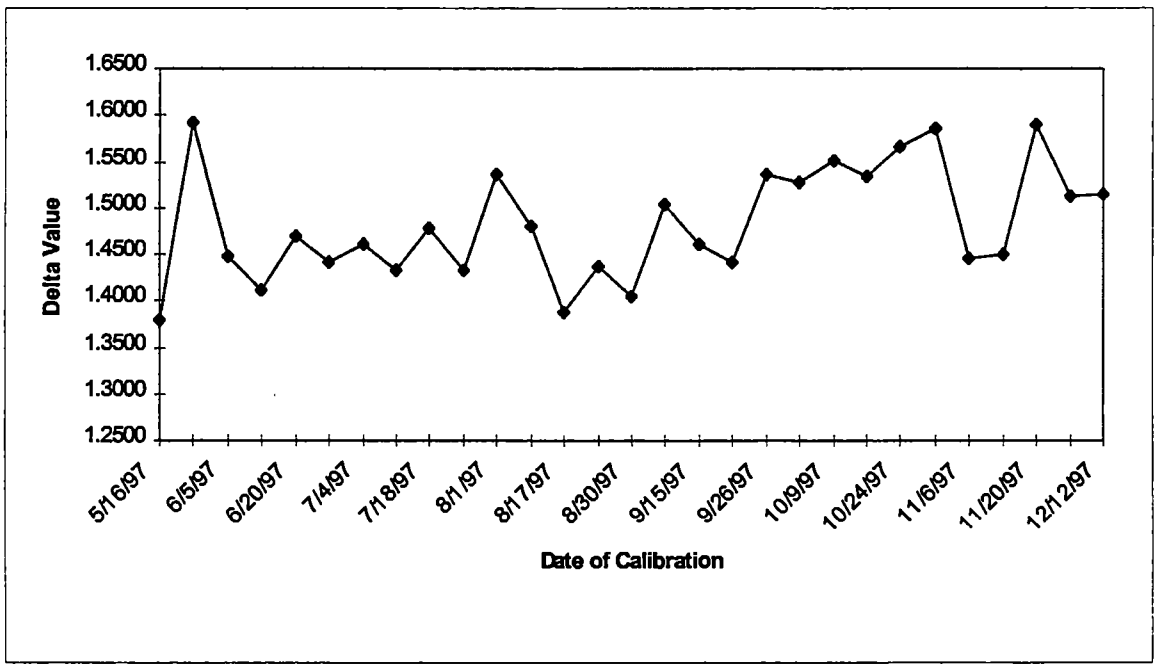


Figure B-58 RTD A-75 Delta Value Trend

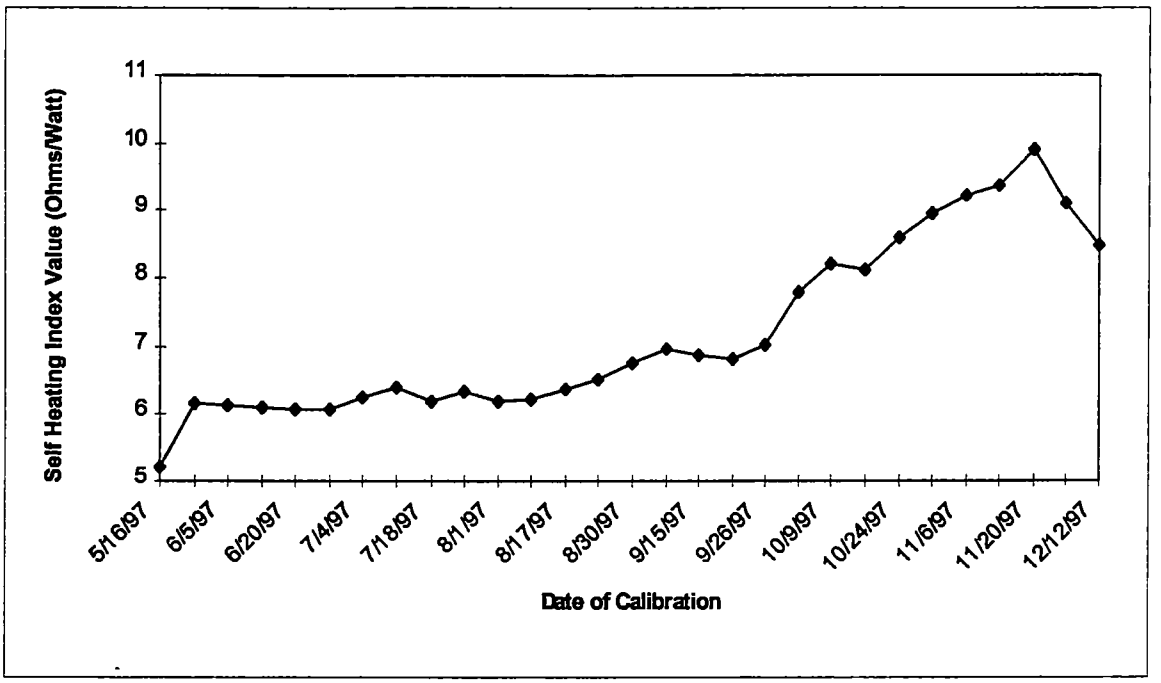


Figure B-59 RTD A-75 Self Heating Index (Ohm/Watt) Value Trend

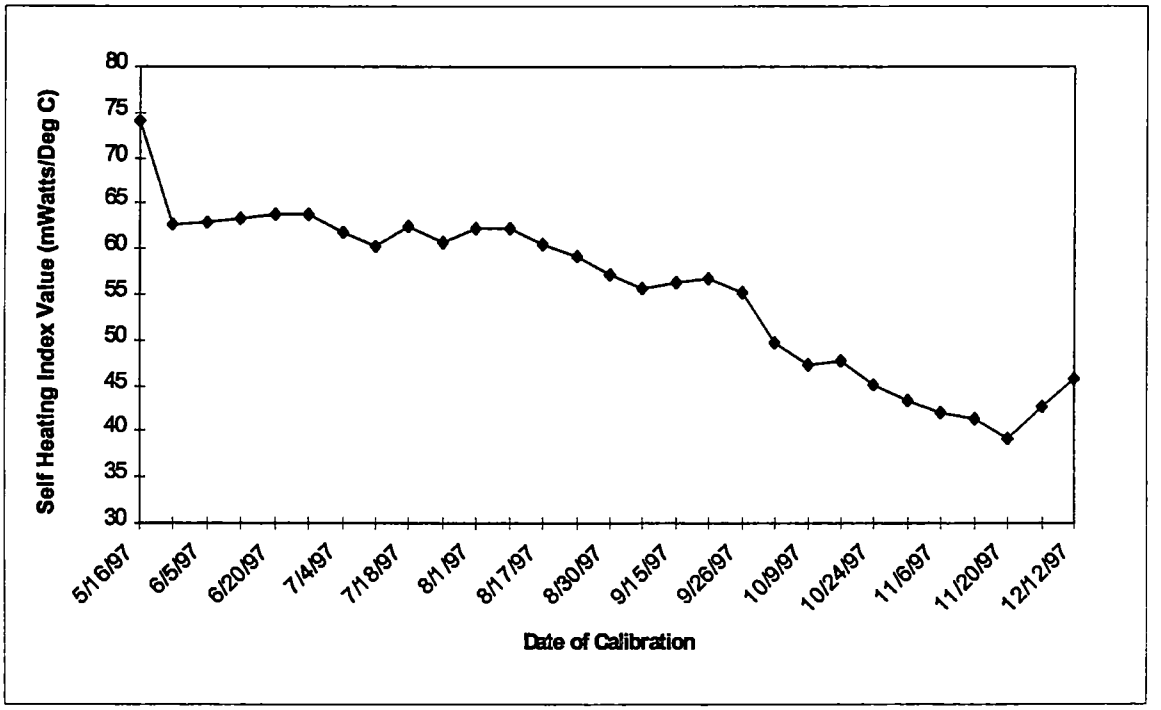


Figure B-60 RTD A-75 Self Heating Index (mWatt/°C) Value Trend

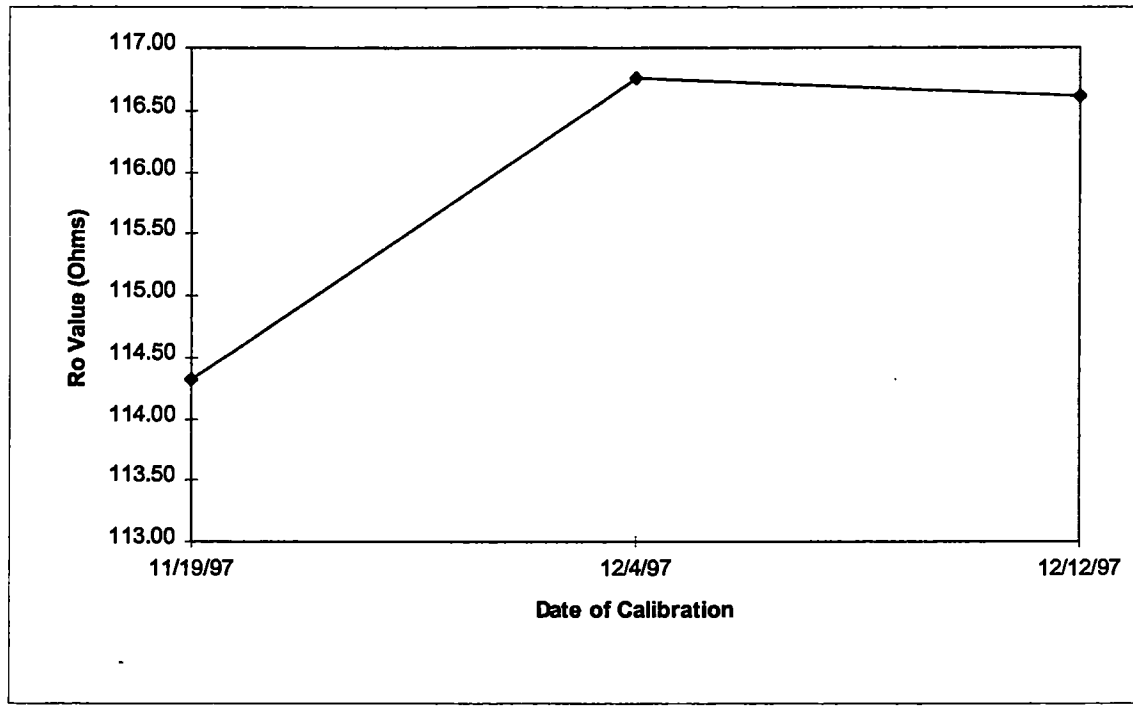


Figure B-61 RTD A-87 Ro Value Trend

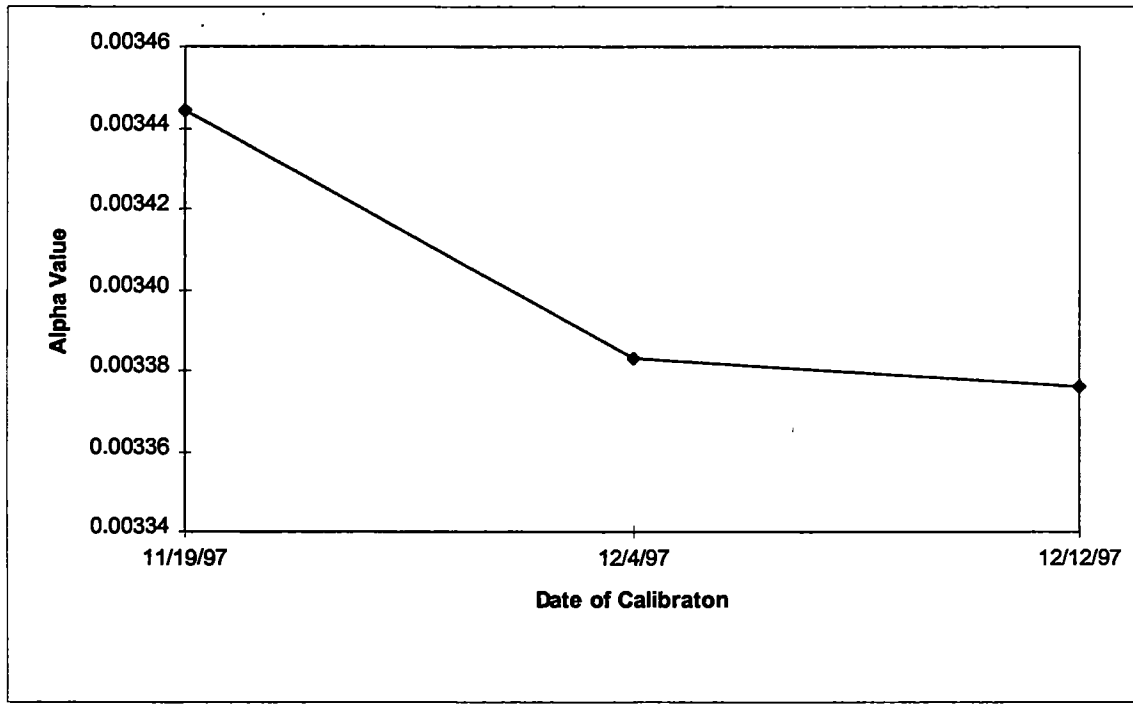


Figure B-62 RTD A-87 Alpha Value Trend

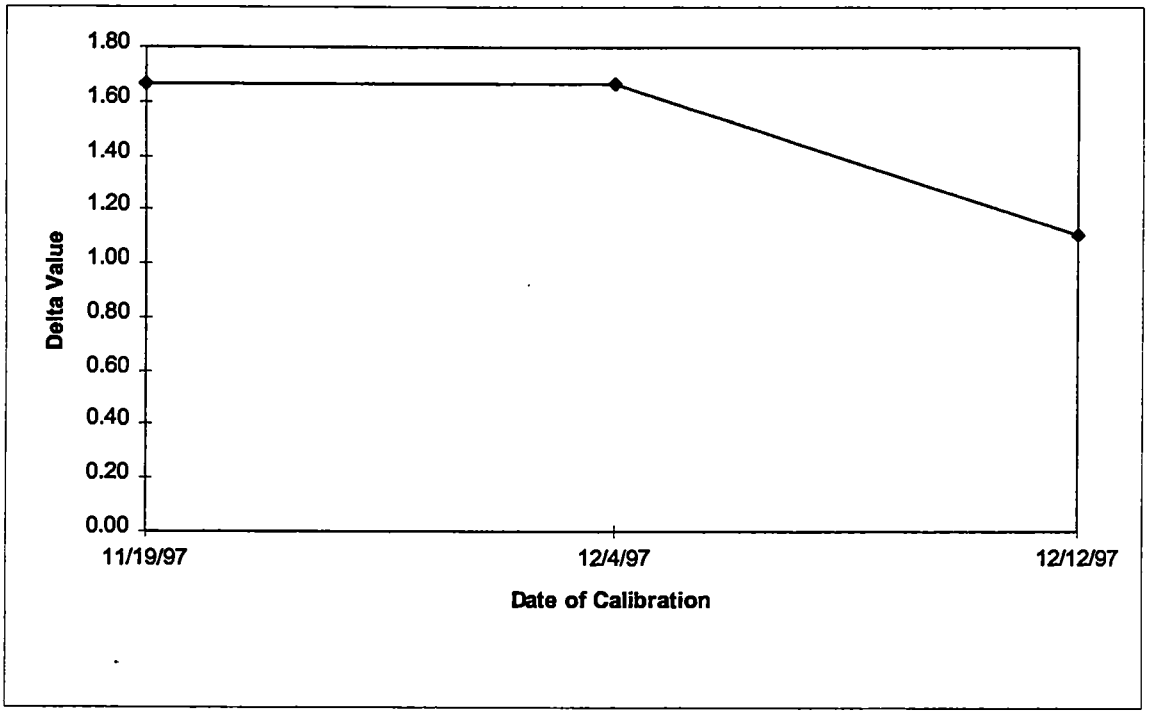


Figure B-63 RTD A-87 Delta Value Trend

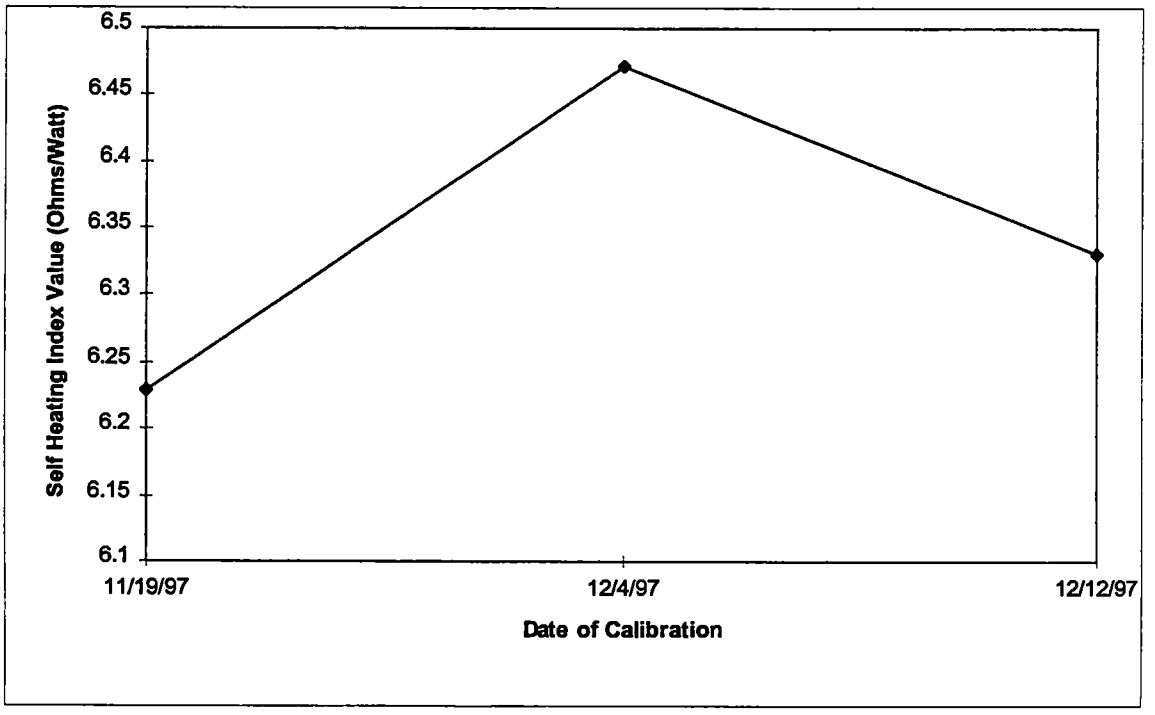


Figure B-64 RTD A-87 Self Heating Index (Ohm/Watt) Value Trend

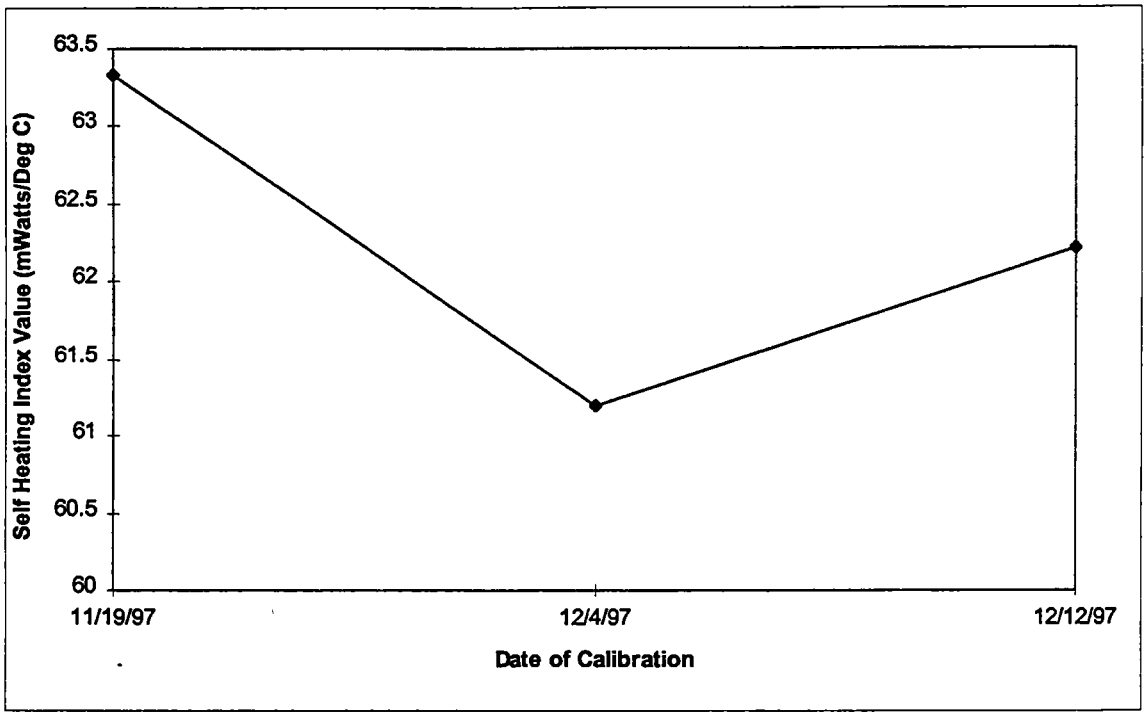


Figure B-65 RTD A-87 Self Heating Index (mWatt/°C) Value Trend

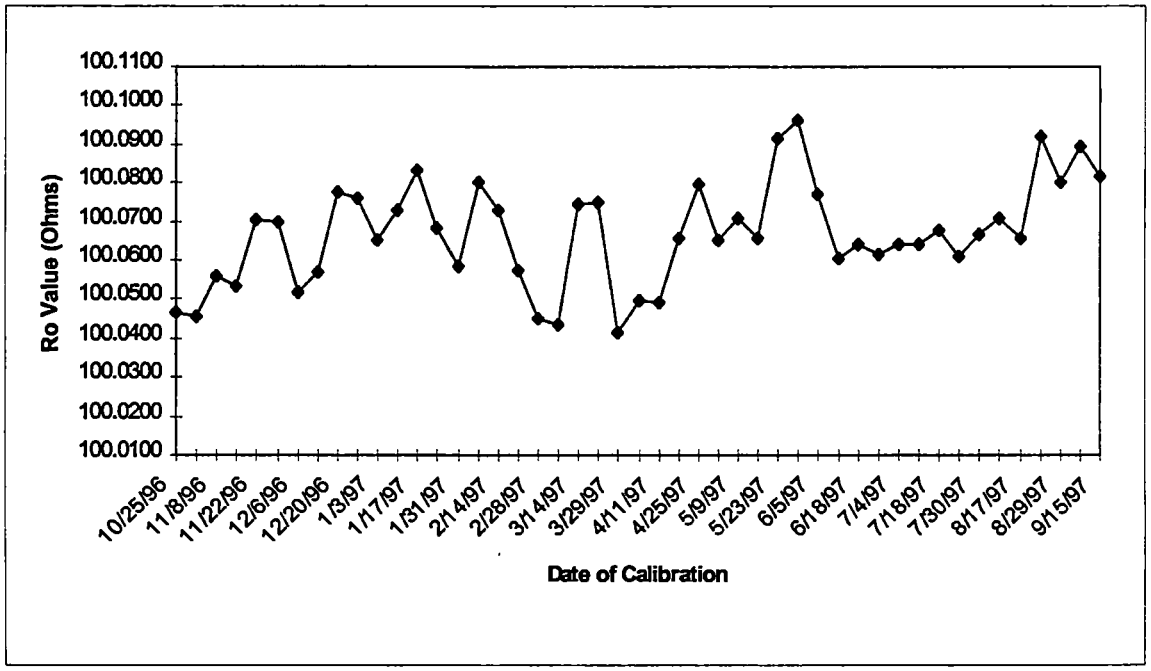


Figure B-66 RTD A-199 Ro Value Trend

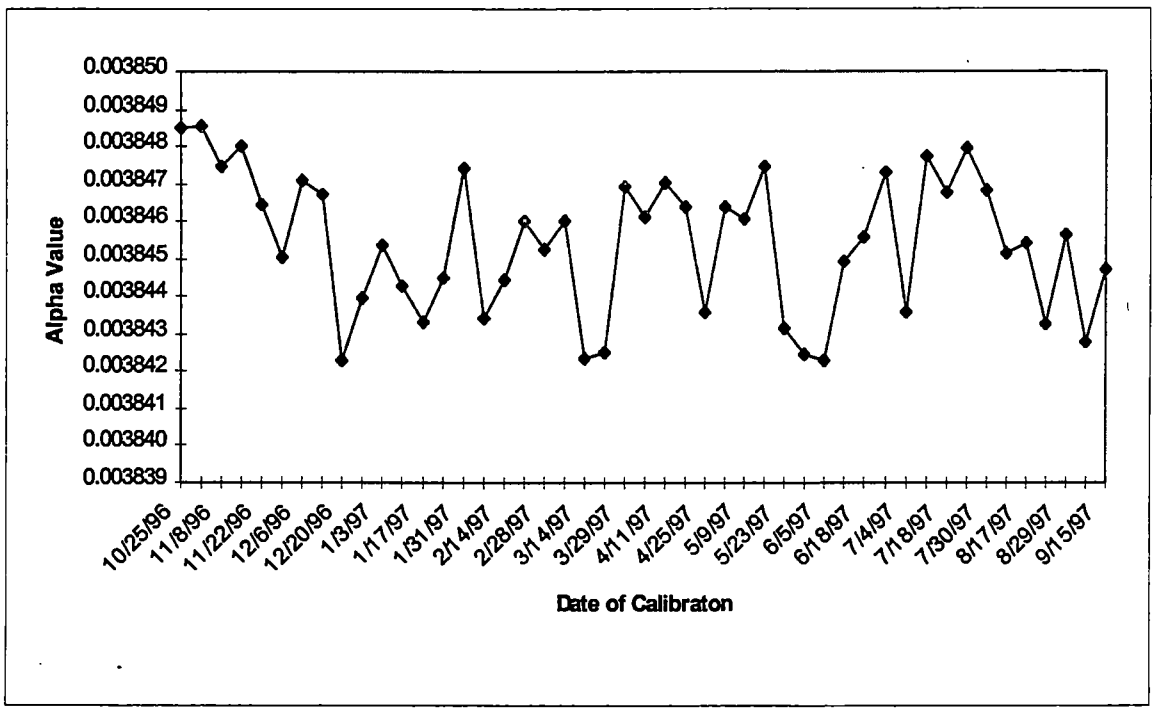


Figure B-67 RTD A-199 Alpha Value Trend

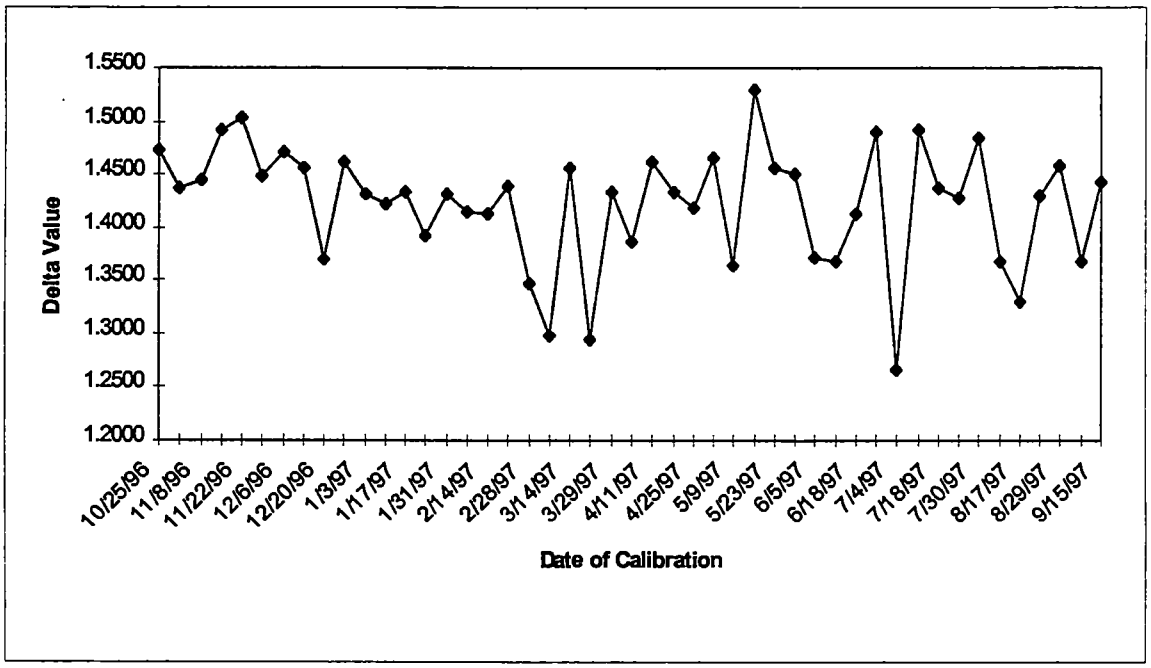


Figure B-68 RTD A-199 Delta Value Trend

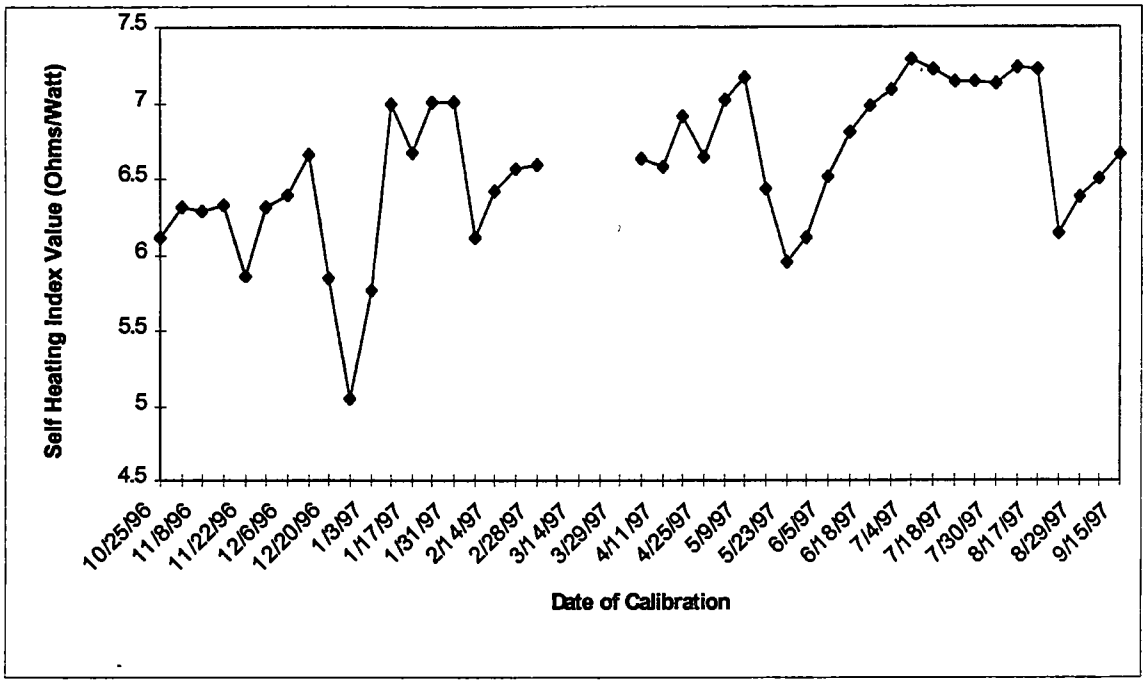


Figure B-69 RTD A-199 Self Heating Index (Ohm/Watt) Value Trend

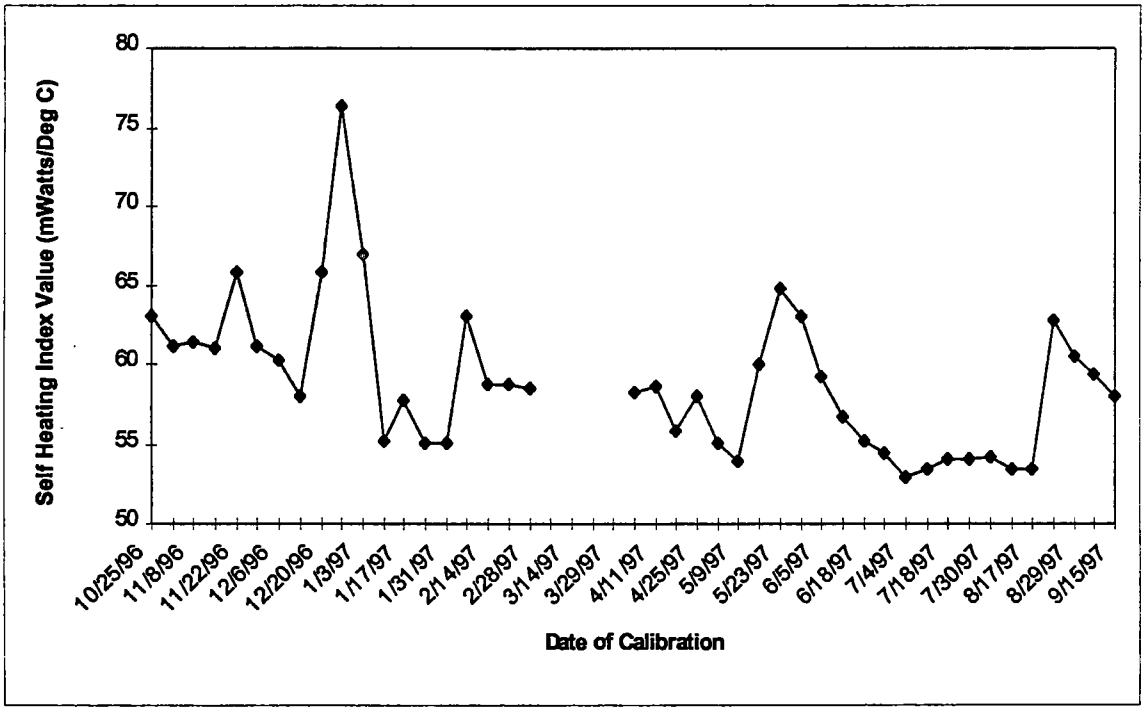


Figure B-70 RTD A-199 Self Heating Index (mWatt/°C) Value Trend

Appendix C

Tabular results of drift rate calculations.

Drift Rates Divided by Test and Temperature - Showing Test RTDs at Given Temperature

Note: Test #9 does not have a table of drift rates due to the nature of the test being thermal cycling. Due to the fact the measurements cycled, a drift rate can not be calculated in the same manner as the thermal soak tests.

Table C.1 Table of Drift Rates for Test #1 at 660 °C

RTD Number	Drift Rate in Ohms per 1000 hours
A-1	79.27356
A-2	32.96653
A-3	23.34886
A-4	30.08359
A-5	27.94653
A-6	240.7049
A-7	25.22646
A-8	36.27957

Table C.2 Table of Drift Rates for Test #2 at 660 °C

RTD Number	Drift Rate in Ohms per 1000 hours
A-9	177.1508
A-10	71.21487
A-11	42.64331
A-12	36.92105
A-13	50.21331
A-14	33.49777
A-15	28.51999
A-16	51.74904
A-17	8.433023
A-18	76.40993
A-19	12.26326
A-20	53.49401

Table C.3 Table of Drift Rates for Test #3 at 660 °C

RTD Number	Drift Rate in Ohms per 1000 hours
A-21	6.586256
A-22	7.625346
A-23	5.181206
A-24	17.59598
A-25	4.563086
A-26	5.860644
A-27	6.177914
A-28	3.736384
A-29	4.026751
A-30	6.596242
A-31	4.956107
A-32	4.118301

Table C.4 Table of Drift Rates for Test #4 at 660 °C

RTD Number	Drift Rate in Ohms per 1000 hours
A-33	0.746304
A-34	1.794313
A-35	1.725417
A-36	1.627962
A-37	1.890241
A-38	1.839484
A-39	1.654235
A-40	2.791276
A-41	1.035863
A-42	1.51708
A-43	1.382907
A-44	7.899942
A-45	2.385592
A-46	1.18156
A-47	2.309161
A-48	3.462656
A-49	2.338296

Table C.5 Table of Drift Rates for Test #4 at 700 °C

RTD Number	Drift Rate in Ohms per 1000 hours
A-33	-1.67526
A-34	-1.93453
A-35	-1.32298
A-36	-1.50688
A-37	-1.85872
A-38	0.166205
A-39	-1.36944
A-40	-0.62559
A-41	-1.81496
A-42	-0.50124
A-43	-1.12804
A-44	8.180523
A-45	0.465042
A-46	-0.23624
A-47	1.147316
A-48	1.896972
A-49	-0.17038

Table C.6 Table of Drift Rates for Test #4 at 725 °C

RTD Number	Drift Rate in Ohms per 1000 hours
A-33	1.024353
A-34	0.70965
A-35	8.906921
A-36	1.244753
A-37	1.098876
A-38	3.262222
A-39	1.356879
A-40	2.602178
A-41	-0.20282
A-42	2.499679
A-43	1.810621
A-44	19.1001
A-45	5.253973
A-46	3.452674
A-47	27.38789
A-48	38.38493
A-49	1.530778

Table C.7 Table of Drift Rates for Test #4 at 750 °C

RTD Number	Drift Rate in Ohms per 1000 hours
A-33	2.317809
A-34	2.992062
A-35	3.47297
A-36	2.668903
A-37	3.750984
A-38	4.772848
A-39	2.481503
A-40	5.014873
A-41	3.488383
A-42	9.241573
A-43	8.532566
A-44	29.83059
A-45	10.15447
A-46	6.119913
A-47	19.22083
A-48	152.383
A-49	22.44786

Table C.8 Table of Drift Rates for Test #4 at 775 °C

RTD Number	Drift Rate in Ohms per 1000 hours
A-33	6.015805
A-34	5.620071
A-35	112.7666
A-36	5.84758
A-37	6.382394
A-38	6.392477
A-39	6.387207
A-40	6.586501
A-41	120.1808
A-42	58.83766
A-43	51.81622
A-44	53.38631
A-45	55.66458
A-46	11.78363
A-47	-44.1206
A-48	233.4655
A-49	58.34656

Table C.9 Table of Drift Rates for Test #4 at 800 °C

RTD Number	Drift Rate in Ohms per 1000 hours
A-33	11.32099
A-34	11.44939
A-35	N/A
A-36	9.950108
A-37	11.05285
A-38	10.31393
A-39	9.82011
A-40	17.41773
A-41	-116.137
A-42	116.1693
A-43	107.8227
A-44	75.57096
A-45	29.15514
A-46	11.13915
A-47	-42.4361
A-48	N/A
A-49	N/A

Table C.10 Table of Drift Rates for Test #4 at 850 °C

RTD Number	Drift Rate in Ohms per 1000 hours
A-33	31.84885
A-34	34.84442
A-35	N/A
A-36	34.55474
A-37	45.92033
A-38	32.82872
A-39	422.9434
A-40	35.11454
A-41	431.2641
A-42	118.153
A-43	361.8464
A-44	266.2501
A-45	-3.32281
A-46	38.89192
A-47	2.043241
A-48	N/A
A-49	N/A

Table C.11 Table of Drift Rates for Test #5 at 500 °C

RTD Number	Drift Rate in Ohms per 1000 hours
A-50	-0.27228
A-51	0.71625
A-52	-0.44056
A-53	-0.52307
A-54	-0.02547
A-55	-0.24252
A-56	0.574217
A-57	0.551577
A-58	0.363136
A-59	-0.30411
A-60	-0.39397

Table C.12 Table of Drift Rates for Test #6 at 600 °C

RTD Number	Drift Rate in Ohms per 1000 hours
A-50	-12.2084
A-51	-10.5329
A-52	-5.8645
A-53	-13.0808
A-54	-11.4311
A-55	-11.0526
A-56	-12.5229
A-57	-11.086
A-58	-8.53035
A-59	-11.6706
A-60	-8.07348
A-61	8.930809
A-62	-2.92089
A-63	-1.93495
A-64	-0.85068
B-12	871.9976
B-13	666.2936
B-14	600.0363
B-15	437.0402

Table C.13 Table of Drift Rates for Test #6 at 700 °C

RTD Number	Drift Rate in Ohms per 1000 hours
A-50	28.77462
A-51	15.07779
A-52	216.6071
A-53	30.92014
A-54	14.9157
A-55	18.59113
A-56	92.65252
A-57	56.33183
A-58	42.91273
A-59	49.39774
A-60	30.40151
A-61	98.51798
A-62	107.0736
A-63	84.18689
A-64	79.92722
B-12	362.0633
B-13	611.109
B-14	4187.96
B-15	4448.594

Table C.14 Table of Drift Rates for Test #6 at 800 °C

RTD Number	Drift Rate in Ohms per 1000 hours
A-50	1533.283
A-51	842.8744
A-52	2363.472
A-53	3420.589
A-54	506.9851
A-55	1557.827
A-56	7440.524
A-57	1318.487
A-58	3203.751
A-59	5646.397
A-60	1645.551
A-61	4508.531
A-62	4207.918
A-63	3490.58
A-64	5044.543
B-12	18811.48
B-13	16140.28
B-14	270118.6
B-15	85813.85

Table C.15 Table of Drift Rates for Test #6 at 900 °C

RTD Number	Drift Rate in Ohms per 1000 hours
A-50	2193.091
A-51	2224.419
A-52	14281.14
A-53	4388.491
A-54	1721.875
A-55	2629.364
A-56	9067.976
A-57	1915.588
A-58	2281.661
A-59	5713.096
A-60	5778.265
A-61	13282.87
A-62	13482.1
A-63	41545.23
A-64	41344.56
B-12	N/A
B-13	N/A
B-14	N/A
B-15	N/A

Table C.16 Table of Drift Rates for Test #7 at 400 °C

RTD Number	Drift Rate in Ohms per 1000 hours
B-1	-0.57065
B-2	-1.41888
B-3	-1.39782
B-4	-1.62708
B-5	-0.60079
B-6	-0.90492
B-7	-0.33495
B-8	0.431349
B-9	-0.77565
B-10	-0.93946
B-11	-1.42483

Table C.17 Table of Drift Rates for Test #7 at 450 °C

RTD Number	Drift Rate in Ohms per 1000 hours
B-1	-2.70591
B-2	-2.76451
B-3	-3.0564
B-4	-0.51406
B-5	-3.1992
B-6	-2.71333
B-7	-0.91841
B-8	-0.0297
B-9	0.517638
B-10	-1.25372
B-11	-2.42016

Table C.18 Table of Drift Rates for Test #7 at 500 °C

RTD Number	Drift Rate in Ohms per 1000 hours
B-1	-2.33787
B-2	-1.09352
B-3	-3.32078
B-4	6.801399
B-5	-14.0612
B-6	-11.1226
B-7	-5.38722
B-8	-12.2438
B-9	-8.85199
B-10	7.889087
B-11	-7.97883

Table C.19 Table of Drift Rates for Test #7 at 525 °C

RTD Number	Drift Rate in Ohms per 1000 hours
B-1	7.279539
B-2	15.05961
B-3	4.416431
B-4	29.53071
B-5	-2.83723
B-6	6.997615
B-7	11.46299
B-8	0.971125
B-9	10.38955
B-10	29.20498
B-11	11.7774

Table C.20 Table of Drift Rates for Test #7 at 550 °C

RTD Number	Drift Rate in Ohms per 1000 hours
B-1	1.319233
B-2	3.100791
B-3	1.892649
B-4	12.96072
B-5	1.184741
B-6	10.4879
B-7	12.24996
B-8	3.1547
B-9	0.603621
B-10	15.56257
B-11	43.82912

Table C.21 Table of Drift Rates for Test #7 at 575 °C

RTD Number	Drift Rate in Ohms per 1000 hours
B-1	0.356461
B-2	7.829854
B-3	-2.14289
B-4	-1.17513
B-5	7.520678
B-6	30.62797
B-7	1.760428
B-8	10.22177
B-9	9.060827
B-10	-20.1625
B-11	30.1958

Table C.22 Table of Drift Rates for Test #7 at 600 °C

RTD Number	Drift Rate in Ohms per 1000 hours
B-1	-4.19495
B-2	12.66419
B-3	-1.61001
B-4	-33.3538
B-5	20.75715
B-6	41.09793
B-7	-17.5019
B-8	10.24985
B-9	4.434294
B-10	59.91383
B-11	-62.6722

Table C.23 Table of Drift Rates for Test #7 at 625 °C

RTD Number	Drift Rate in Ohms per 1000 hours
B-1	9.652951
B-2	17.54318
B-3	31.38716
B-4	89.0889
B-5	5.607552
B-6	N/A
B-7	45.80849
B-8	20.79397
B-9	25.21706
B-10	163.1784
B-11	75.08592

Table C.24 Table of Drift Rates for Test #8 at 550 °C

RTD Number	Drift Rate in Ohms per 1000 hours
A-65	-0.15524
A-66	0.556919
A-67	0.603604
A-68	-0.16362
A-69	-0.14886
A-70	-0.14164
A-204	0.143438
A-205	-0.27997
A-206	-0.16208
A-207	-0.42975
A-208	0.538915
A-209	0.486089
A-210	0.195737
A-211	0.127859
A-212	-0.10452
A-213	0.046001
B-38	41.111
B-39	19.29173
B-40	25.42197

Table C.25 Table of Drift Rates for Test #8 at 575 °C

RTD Number	Drift Rate in Ohms per 1000 hours
A-65	7.698588
A-66	8.769452
A-67	9.568115
A-68	9.54812
A-69	12.23251
A-70	10.96251
A-204	9.527847
A-205	9.393152
A-206	11.5099
A-207	9.646638
A-208	8.548716
A-209	8.32594
A-210	6.660947
A-211	6.642894
A-212	7.350595
A-213	10.70823
B-38	128.1397
B-39	32.25996
B-40	98.54232

Table C.26 Table of Drift Rates for Test #8 at 600 °C

RTD Number	Drift Rate in Ohms per 1000 hours
A-65	0.914104
A-66	3.843785
A-67	2.843471
A-68	3.47245
A-69	4.72346
A-70	3.507035
A-204	3.011178
A-205	2.764765
A-206	3.114249
A-207	3.430558
A-208	2.121447
A-209	3.6727
A-210	1.833229
A-211	0.859782
A-212	1.880668
A-213	3.027877
B-38	133.9467
B-39	243.3451
B-40	286.7735

Table C.27 Table of Drift Rates for Test #10 at 450 °C

RTD Number	Drift Rate in Ohms per 1000 hours
A-199	0.813803

Table C.28 Table of Drift Rates for Test #8 at 550 °C RTDs B-38, B-39 and B-40

RTD Number	Drift Rate in Ohms per 1000 hours
B-38	213.7627
	117.5676
	75.94166
	60.32069
	974.1649
B-39	158.7108
	88.84103
	37.72699
	26.16418
	1034.413
B-40	146.2374
	91.2074
	59.44268
	30.77656
	1003.729

Drift Rates Divided by Temperature - Showing All RTDs at Given Temperature

Table C.29 Table of Drift Rates for Temperature 400 °C

RTD Number	Test Number	Drift Rate in Ohms per 1000 hours
B-1	7	-0.57065
B-2	7	-1.41888
B-3	7	-1.39782
B-4	7	-1.62708
B-5	7	-0.60079
B-6	7	-0.90492
B-7	7	-0.33495
B-8	7	0.431349
B-9	7	-0.77565
B-10	7	-0.93946
B-11	7	-1.42483
Average =		-0.86943

Table C.30 Table of Drift Rates for Temperature 450 °C

RTD Number	Test Number	Drift Rate in Ohms per 1000 hours
B-1	7	-2.70591
B-2	7	-2.76451
B-3	7	-3.0564
B-4	7	-0.51406
B-5	7	-3.1992
B-6	7	-2.71333
B-7	7	-0.91841
B-8	7	-0.0297
B-9	7	0.517638
B-10	7	-1.25372
B-11	7	-2.42016
A-199	10	0.813803
Average =		-1.52033

Table C.31 Table of Drift Rates for Temperature 500 °C

RTD Number	Test Number	Drift Rate in Ohms per 1000 hours
B-1	7	-2.33787
B-2	7	-1.09352
B-3	7	-3.32078
B-4	7	6.801399
B-5	7	-14.0612
B-6	7	-11.1226
B-7	7	-5.38722
B-8	7	-12.2438
B-9	7	-8.85199
B-10	7	7.889087
B-11	7	-7.97883
A-50	5	-0.27228
A-51	5	0.71625
A-52	5	-0.44056
A-53	5	-0.52307
A-54	5	-0.02547
A-55	5	-0.24252
A-56	5	0.574217
A-57	5	0.551577
A-58	5	0.363136
A-59	5	-0.30411
A-60	5	-0.39397
Average =		-2.35019

Table C.32 Table of Drift Rates for Temperature 525 °C

RTD Number	Text Number	Drift Rate in Ohms per 1000 hours
B-1	7	7.279539
B-2	7	15.05961
B-3	7	4.416431
B-4	7	29.53071
B-5	7	-2.83723
B-6	7	6.997615
B-7	7	11.46299
B-8	7	0.971125
B-9	7	10.38955
B-10	7	29.20498
B-11	7	11.7774
Average =		11.2957

Table C.33 Table of Drift Rates for Temperature 550 °C

RTD Number	Text Number	Drift Rate in Ohms per 1000 hours
B-1	7	1.319233
B-2	7	3.100791
B-3	7	1.892649
B-4	7	12.96072
B-5	7	1.184741
B-6	7	10.4879
B-7	7	12.24996
B-8	7	3.1547
B-9	7	0.603621
B-10	7	15.56257
B-11	7	43.82912
A-65	8	-0.15524
A-66	8	0.556919
A-67	8	0.603604
A-68	8	-0.16362
A-69	8	-0.14886
A-70	8	-0.14164
A-204	8	0.143438
A-205	8	-0.27997
A-206	8	-0.16208
A-207	8	-0.42975
A-208	8	0.538915
A-209	8	0.486089
A-210	8	0.195737
A-211	8	0.127859
A-212	8	-0.10452
A-213	8	0.046001
B-38	8	41.111
B-39	8	19.29173
B-40	8	25.42197
Average =		6.442786

Table C.34 Table of Drift Rates for Temperature 575 °C

RTD Number	Text Number	Drift Rate in Ohms per 1000 hours
B-1	7	0.356461
B-2	7	7.829854
B-3	7	-2.14289
B-4	7	-1.17513
B-5	7	7.520678
B-6	7	30.62797
B-7	7	1.760428
B-8	7	10.22177
B-9	7	9.060827
B-10	7	-20.1625
B-11	7	30.1958
A-65	8	7.698588
A-66	8	8.769452
A-67	8	9.568115
A-68	8	9.54812
A-69	8	12.23251
A-70	8	10.96251
A-204	8	9.527847
A-205	8	9.393152
A-206	8	11.5099
A-207	8	9.646638
A-208	8	8.548716
A-209	8	8.32594
A-210	8	6.660947
A-211	8	6.642894
A-212	8	7.350595
A-213	8	10.70823
B-38	8	128.1397
B-39	8	32.25996
B-40	8	98.54232
Average =		16.00431

Table C.35 Table of Drift Rates for Temperature 600 °C

RTD Number	Text Number	Drift Rate in Ohms per 1000 hours
A-50	6	-12.2084
A-51	6	-10.5329
A-52	6	-5.8645
A-53	6	-13.0808
A-54	6	-11.4311
A-55	6	-11.0526
A-56	6	-12.5229
A-57	6	-11.086
A-58	6	-8.53035
A-59	6	-11.6706
A-60	6	-8.07348
A-61	6	8.930809
A-62	6	-2.92089
A-63	6	-1.93495
A-64	6	-0.85068
B-12	6	871.9976
B-13	6	666.2936
B-14	6	600.0363
B-15	6	437.0402
B-1	7	-4.19495
B-2	7	12.66419
B-3	7	-1.61001
B-4	7	-33.3538
B-5	7	20.75715
B-6	7	41.09793
B-7	7	-17.5019
B-8	7	10.24985
B-9	7	4.434294
B-10	7	59.91383
B-11	7	-62.6722
A-65	8	0.914104
A-66	8	3.843785
A-67	8	2.843471
A-68	8	3.47245
A-69	8	4.72346
A-70	8	3.507035
A-204	8	3.011178
A-205	8	2.764765

RTD Number	Text Number	Drift Rate in Ohms per 1000 hours
A-206	8	3.114249
A-207	8	3.430558
A-208	8	2.121447
A-209	8	3.6727
A-210	8	1.833229
A-211	8	0.859782
A-212	8	1.880668
A-213	8	3.027877
B-38	8	133.9467
B-39	8	243.3451
B-40	8	286.7735
Average =		65.33487

Table C.36 Table of Drift Rates for Temperature 625 °C

RTD Number	Text Number	Drift Rate in Ohms per 1000 hours
B-1	7	9.652951
B-2	7	17.54318
B-3	7	31.38716
B-4	7	89.0889
B-5	7	5.607552
B-6	7	N/A
B-7	7	45.80849
B-8	7	20.79397
B-9	7	25.21706
B-10	7	163.1784
B-11	7	75.08592
Average =		48.33636

Table C.37 Table of Drift Rates for Temperature 660 °C

RTD Number	Text Number	Drift Rate in Ohms per 1000 hours
A-1	1	79.27356
A-2	1	32.96653
A-3	1	23.34886
A-4	1	30.08359
A-5	1	27.94653
A-6	1	240.7049
A-7	1	25.22646
A-8	1	36.27957
A-9	2	177.1508
A-10	2	71.21487
A-11	2	42.64331
A-12	2	36.92105
A-13	2	50.21331
A-14	2	33.49777
A-15	2	28.51999
A-16	2	51.74904
A-17	2	8.433023
A-18	2	76.40993
A-19	2	12.26326
A-20	2	53.49401
A-21	3	6.586256
A-22	3	7.625346
A-23	3	5.181206
A-24	3	17.59598
A-25	3	4.563086
A-26	3	5.860644
A-27	3	6.177914
A-28	3	3.736384
A-29	3	4.026751
A-30	3	6.596242
A-31	3	4.956107
A-32	3	4.118301
A-33	4	0.746304
A-34	4	1.794313
A-35	4	1.725417
A-36	4	1.627962
A-37	4	1.890241
A-38	4	1.839484

RTD Number	Text Number	Drift Rate in Ohms per 1000 hours
A-39	4	1.654235
A-40	4	2.791276
A-41	4	1.035863
A-42	4	1.51708
A-43	4	1.382907
A-44	4	7.899942
A-45	4	2.385592
A-46	4	1.18156
A-47	4	2.309161
A-48	4	3.462656
A-49	4	2.338296
Average =		25.57034

Table C.38 Table of Drift Rates for Temperature 700 °C

RTD Number	Text Number	Drift Rate in Ohms per 1000 hours
A-33	4	-1.67526
A-34	4	-1.93453
A-35	4	-1.32298
A-36	4	-1.50688
A-37	4	-1.85872
A-38	4	0.166205
A-39	4	-1.36944
A-40	4	-0.62559
A-41	4	-1.81496
A-42	4	-0.50124
A-43	4	-1.12804
A-44	4	8.180523
A-45	4	0.465042
A-46	4	-0.23624
A-47	4	1.147316
A-48	4	1.896972
A-49	4	-0.17038
A-50	6	28.77462
A-51	6	15.07779
A-52	6	216.6071
A-53	6	30.92014
A-54	6	14.9157
A-55	6	18.59113
A-56	6	92.65252
A-57	6	56.33183
A-58	6	42.91273
A-59	6	49.39774
A-60	6	30.40151
A-61	6	98.51798
A-62	6	107.0736
A-63	6	84.18689
A-64	6	79.92722
B-12	6	362.0633
B-13	6	611.109
B-14	6	4187.96
B-15	6	4448.594
Average =		293.7146

Table C.39 Table of Drift Rates for Temperature 725 °C

RTD Number	Text Number	Drift Rate in Ohms per 1000 hours
A-33	4	1.024353
A-34	4	0.70965
A-35	4	8.906921
A-36	4	1.244753
A-37	4	1.098876
A-38	4	3.262222
A-39	4	1.356879
A-40	4	2.602178
A-41	4	-0.20282
A-42	4	2.499679
A-43	4	1.810621
A-44	4	19.1001
A-45	4	5.253973
A-46	4	3.452674
A-47	4	27.38789
A-48	4	38.38493
A-49	4	1.530778
Average =		7.024921

Table C.40 Table of Drift Rates for Temperature 750 °C

RTD Number	Text Number	Drift Rate in Ohms per 1000 hours
A-33	4	2.317809
A-34	4	2.992062
A-35	4	3.47297
A-36	4	2.668903
A-37	4	3.750984
A-38	4	4.772848
A-39	4	2.481503
A-40	4	5.014873
A-41	4	3.488383
A-42	4	9.241573
A-43	4	8.532566
A-44	4	29.83059
A-45	4	10.15447
A-46	4	6.119913
A-47	4	19.22083
A-48	4	152.383
A-49	4	22.44786
Average =		16.9936

Table C.41 Table of Drift Rates for Temperature 775 °C

RTD Number	Text Number	Drift Rate in Ohms per 1000 hours
A-33	4	6.015805
A-34	4	5.620071
A-35	4	112.7666
A-36	4	5.84758
A-37	4	6.382394
A-38	4	6.392477
A-39	4	6.387207
A-40	4	6.586501
A-41	4	120.1808
A-42	4	58.83766
A-43	4	51.81622
A-44	4	53.38631
A-45	4	55.66458
A-46	4	11.78363
A-47	4	-44.1206
A-48	4	233.4655
A-49	4	58.34656
Average =		44.4329

Table C.42 Table of Drift Rates for Temperature 800 °C

RTD Number	Text Number	Drift Rate in Ohms per 1000 hours
A-33	4	11.32099
A-34	4	11.44939
A-35	4	N/A
A-36	4	9.950108
A-37	4	11.05285
A-38	4	10.31393
A-39	4	9.82011
A-40	4	17.41773
A-41	4	-116.137
A-42	4	116.1693
A-43	4	107.8227
A-44	4	75.57096
A-45	4	29.15514
A-46	4	11.13915
A-47	4	-42.4361
A-48	4	N/A
A-49	4	N/A
A-50	6	1533.283
A-51	6	842.8744
A-52	6	2363.472
A-53	6	3420.589
A-54	6	506.9851
A-55	6	1557.827
A-56	6	7440.524
A-57	6	1318.487
A-58	6	3203.751
A-59	6	5646.397
A-60	6	1645.551
A-61	6	4508.531
A-62	6	4207.918
A-63	6	3490.58
A-64	6	5044.543
B-12	6	18811.48
B-13	6	16140.28
B-14	6	270118.6
B-15	6	85813.85
Average =		13269.03

Table C.43 Table of Drift Rates for Temperature 850 °C

RTD Number	Text Number	Drift Rate in Ohms per 1000 hours
A-33	4	31.84885
A-34	4	34.84442
A-35	4	N/A
A-36	4	34.55474
A-37	4	45.92033
A-38	4	32.82872
A-39	4	422.9434
A-40	4	35.11454
A-41	4	431.2641
A-42	4	118.153
A-43	4	361.8464
A-44	4	266.2501
A-45	4	-3.32281
A-46	4	38.89192
A-47	4	2.043241
A-48	4	N/A
A-49	4	N/A
Average =		132.3701

Table C.44 Table of Drift Rates for Temperature 900 °C

RTD Number	Text Number	Drift Rate in Ohms per 1000 hours
A-50	6	2193.091
A-51	6	2224.419
A-52	6	14281.14
A-53	6	4388.491
A-54	6	1721.875
A-55	6	2629.364
A-56	6	9067.976
A-57	6	1915.588
A-58	6	2281.661
A-59	6	5713.096
A-60	6	5778.265
A-61	6	13282.87
A-62	6	13482.1
A-63	6	41545.23
A-64	6	41344.56
B-12	6	N/A
B-13	6	N/A
B-14	6	N/A
B-15	6	N/A
Average =		10789.98

Drift Rates Divided by Test - Showing All Temperatures for each RTD

Table C.45 Table of Drift Rates for Test #1 all Temperatures

RTD Number	Drift Rate in Ohms per 1000 hours
Temperature	660
A-1	79.27356
A-2	32.96653
A-3	23.34886
A-4	30.08359
A-5	27.94653
A-6	240.7049
A-7	25.22646
A-8	36.27957

Table C.46 Table of Drift Rates for Test #2 all Temperatures

RTD Number	Drift Rate in Ohms per 1000 hours
Temperature	660
A-9	177.1508
A-10	71.21487
A-11	42.64331
A-12	36.92105
A-13	50.21331
A-14	33.49777
A-15	28.51999
A-16	51.74904
A-17	8.433023
A-18	76.40993
A-19	12.26326
A-20	53.49401

Table C.47 Table of Drift Rates for Test #3 all Temperatures

RTD Number	Drift Rate in Ohms per 1000 hours
Temperature	660
A-21	6.586256
A-22	7.625346
A-23	5.181206
A-24	17.59598
A-25	4.563086
A-26	5.860644
A-27	6.177914
A-28	3.736384
A-29	4.026751
A-30	6.596242
A-31	4.956107
A-32	4.118301

Table C.48 Table of Drift Rates for Test #4 all Temperatures

RTD #	Drift Rate in Ohms per 1000 hours	Drift Rate in Ohms per 1000 hours	Drift Rate in Ohms per 1000 hours	Drift Rate in Ohms per 1000 hours	Drift Rate in Ohms per 1000 hours	Drift Rate in Ohms per 1000 hours	Drift Rate in Ohms per 1000 hours
Temp	660	700	725	750	775	800	850
A-33	0.746304	-1.67526	1.024353	2.317809	6.015805	11.32099	31.84885
A-34	1.794313	-1.93453	0.70965	2.992062	5.620071	11.44939	34.84442
A-35	1.725417	-1.32298	8.906921	3.47297	112.7666	N/A	N/A
A-36	1.627962	-1.50688	1.244753	2.668903	5.84758	9.950108	34.55474
A-37	1.890241	-1.85872	1.098876	3.750984	6.382394	11.05285	45.92033
A-38	1.839484	0.166205	3.262222	4.772848	6.392477	10.31393	32.82872
A-39	1.654235	-1.36944	1.356879	2.481503	6.387207	9.82011	422.9434
A-40	2.791276	-0.62559	2.602178	5.014873	6.586501	17.41773	35.11454
A-41	1.035863	-1.81496	-0.20282	3.488383	120.1808	-116.137	431.2641
A-42	1.51708	-0.50124	2.499679	9.241573	58.83766	116.1693	118.153
A-43	1.382907	-1.12804	1.810621	8.532566	51.81622	107.8227	361.8464
A-44	7.899942	8.180523	19.1001	29.83059	53.38631	75.57096	266.2501
A-45	2.385592	0.465042	5.253973	10.15447	55.66458	29.15514	-3.32281
A-46	1.18156	-0.23624	3.452674	6.119913	11.78363	11.13915	38.89192
A-47	2.309161	1.147316	27.38789	19.22083	-44.1206	-42.4361	2.043241
A-48	3.462656	1.896972	38.38493	152.383	233.4655	N/A	N/A
A-49	2.338296	-0.17038	1.530778	22.44786	58.34656	N/A	N/A

Table C.49 Table of Drift Rates for Test #5 all Temperatures

RTD Number	Drift Rate in Ohms per 1000 hours
Temperature	500
A-50	-0.27228
A-51	0.71625
A-52	-0.44056
A-53	-0.52307
A-54	-0.02547
A-55	-0.24252
A-56	0.574217
A-57	0.551577
A-58	0.363136
A-59	-0.30411
A-60	-0.39397

Table C.50 Table of Drift Rates for Test #6 all Temperatures

RTD Number	Drift Rate in Ohms per 1000 hours	Drift Rate in Ohms per 1000 hours	Drift Rate in Ohms per 1000 hours	Drift Rate in Ohms per 1000 hours
Temperature	600	700	800	900
A-50	-12.2084	28.77462	1533.283	2193.091
A-51	-10.5329	15.07779	842.8744	2224.419
A-52	-5.8645	216.6071	2363.472	14281.14
A-53	-13.0808	30.92014	3420.589	4388.491
A-54	-11.4311	14.9157	506.9851	1721.875
A-55	-11.0526	18.59113	1557.827	2629.364
A-56	-12.5229	92.65252	7440.524	9067.976
A-57	-11.086	56.33183	1318.487	1915.588
A-58	-8.53035	42.91273	3203.751	2281.661
A-59	-11.6706	49.39774	5646.397	5713.096
A-60	-8.07348	30.40151	1645.551	5778.265
A-61	8.930809	98.51798	4508.531	13282.87
A-62	-2.92089	107.0736	4207.918	13482.1
A-63	-1.93495	84.18689	3490.58	41545.23
A-64	-0.85068	79.92722	5044.543	41344.56
B-12	871.9976	362.0633	18811.48	N/A
B-13	666.2936	611.109	16140.28	N/A
B-14	600.0363	4187.96	270118.6	N/A
B-15	437.0402	4448.594	85813.85	N/A

Table C.51 Table of Drift Rates for Test #7 all Temperatures

RTD #	Drift Rate in Ohms per 1000 hrs	Drift Rate in Ohms per 1000 hrs	Drift Rate in Ohms per 1000 hrs	Drift Rate in Ohms per 1000 hrs	Drift Rate in Ohms per 1000 hrs	Drift Rate in Ohms per 1000 hrs	Drift Rate in Ohms per 1000 hrs	Drift Rate in Ohms per 1000 hrs
Temp	400	450	500	525	550	575	600	625
B-1	-0.57065	-2.70591	-2.33787	7.279539	1.319233	0.356461	-4.19495	9.652951
B-2	-1.41888	-2.76451	-1.09352	15.05961	3.100791	7.829854	12.66419	17.54318
B-3	-1.39782	-3.0564	-3.32078	4.416431	1.892649	-2.14289	-1.61001	31.38716
B-4	-1.62708	-0.51406	6.801399	29.53071	12.96072	-1.17513	-33.3538	89.0889
B-5	-0.60079	-3.1992	-14.0612	-2.83723	1.184741	7.520678	20.75715	5.607552
B-6	-0.90492	-2.71333	-11.1226	6.997615	10.4879	30.62797	41.09793	N/A
B-7	-0.33495	-0.91841	-5.38722	11.46299	12.24996	1.760428	-17.5019	45.80849
B-8	0.431349	-0.0297	-12.2438	0.971125	3.1547	10.22177	10.24985	20.79397
B-9	-0.77565	0.517638	-8.85199	10.38955	0.603621	9.060827	4.434294	25.21706
B-10	-0.93946	-1.25372	7.889087	29.20498	15.56257	-20.1625	59.91383	163.1784
B-11	-1.42483	-2.42016	-7.97883	11.7774	43.82912	30.1958	-62.6722	75.08592

Table C.52 Table of Drift Rates for Test #8 all Temperatures

RTD Number	Drift Rate in Ohms Per 1000 hours	Drift Rate in Ohms per 1000 hours	Drift Rate in Ohms per 1000 hours
Temperature	550	575	600
A-65	-0.15524	7.698588	0.914104
A-66	0.556919	8.769452	3.843785
A-67	0.603604	9.568115	2.843471
A-68	-0.16362	9.54812	3.47245
A-69	-0.14886	12.23251	4.72346
A-70	-0.14164	10.96251	3.507035
A-204	0.143438	9.527847	3.011178
A-205	-0.27997	9.393152	2.764765
A-206	-0.16208	11.5099	3.114249
A-207	-0.42975	9.646638	3.430558
A-208	0.538915	8.548716	2.121447
A-209	0.486089	8.32594	3.6727
A-210	0.195737	6.660947	1.833229
A-211	0.127859	6.642894	0.859782
A-212	-0.10452	7.350595	1.880668
A-213	0.046001	10.70823	3.027877
B-38	41.111	128.1397	133.9467
B-39	19.29173	32.25996	243.3451
B-40	25.42197	98.54232	286.7735

Table C.53 Table of Drift Rates for Test #8b all Temperatures

RTD Number	Drift Rate in Ohms per 1000 hours	Drift Rate in Ohms per 1000 hours	Drift Rate in Ohms per 1000 hours	Drift Rate in Ohms per 1000 hours	Drift Rate in Ohms per 1000 hours
Temperature	550-1	550-2	550-3	550-4	550-5
B-38	213.7627	117.5676	75.94166	60.32069	974.1649
B-39	158.7108	88.84103	37.72699	26.16418	1034.413
B-40	146.2374	91.2074	59.44268	30.77656	1003.729

Table C.54 Table of Drift Rates for Test #10 all Temperatures

RTD Number	Drift Rate in Ohms per 1000 hours
Temperature	450
A-199	0.813803

Appendix D

Linear fit of Alpha and Self Heating Index results for all RTDs.

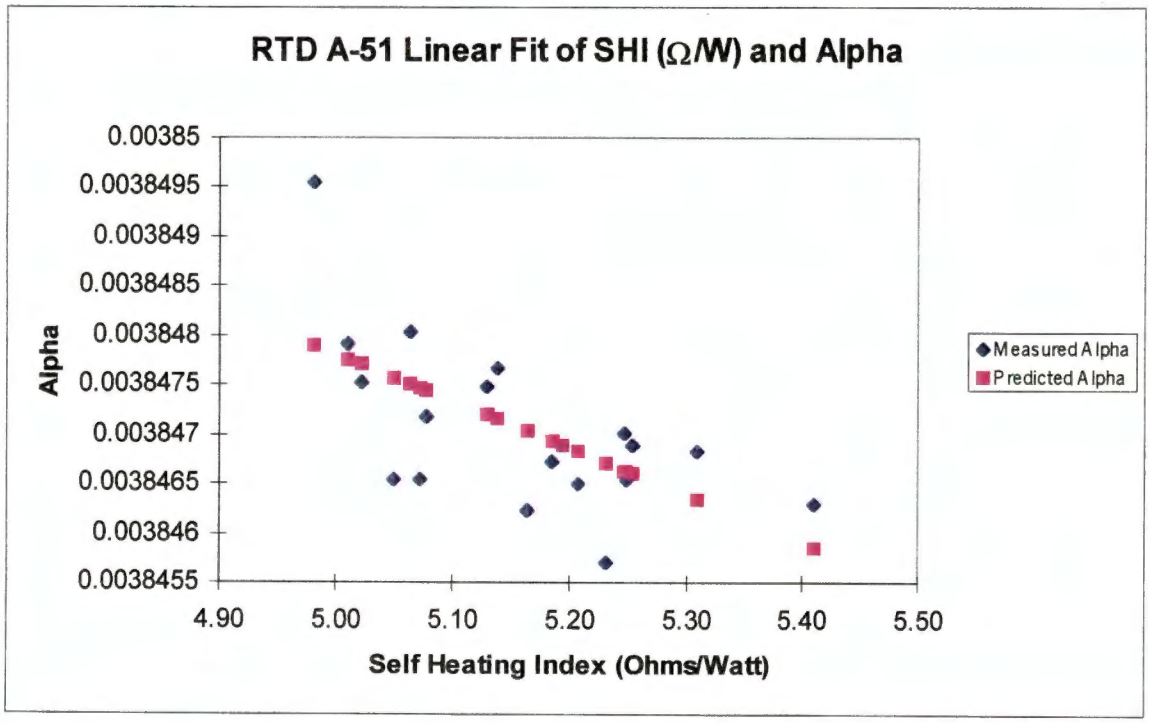


Figure D-1. Self Heating Index (Ω/W) versus Alpha Plot with Fitted Line for RTD A-51

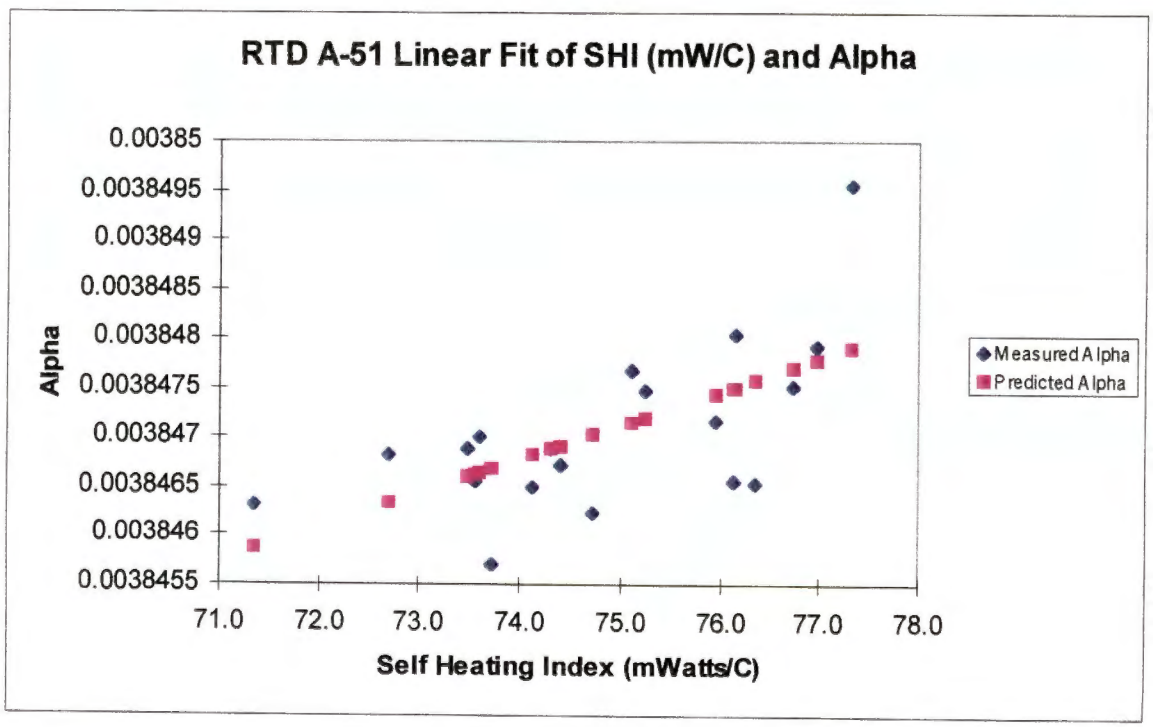


Figure D-2. Self Heating Index (mW/C) versus Alpha Plot with Fitted Line for RTD A-51

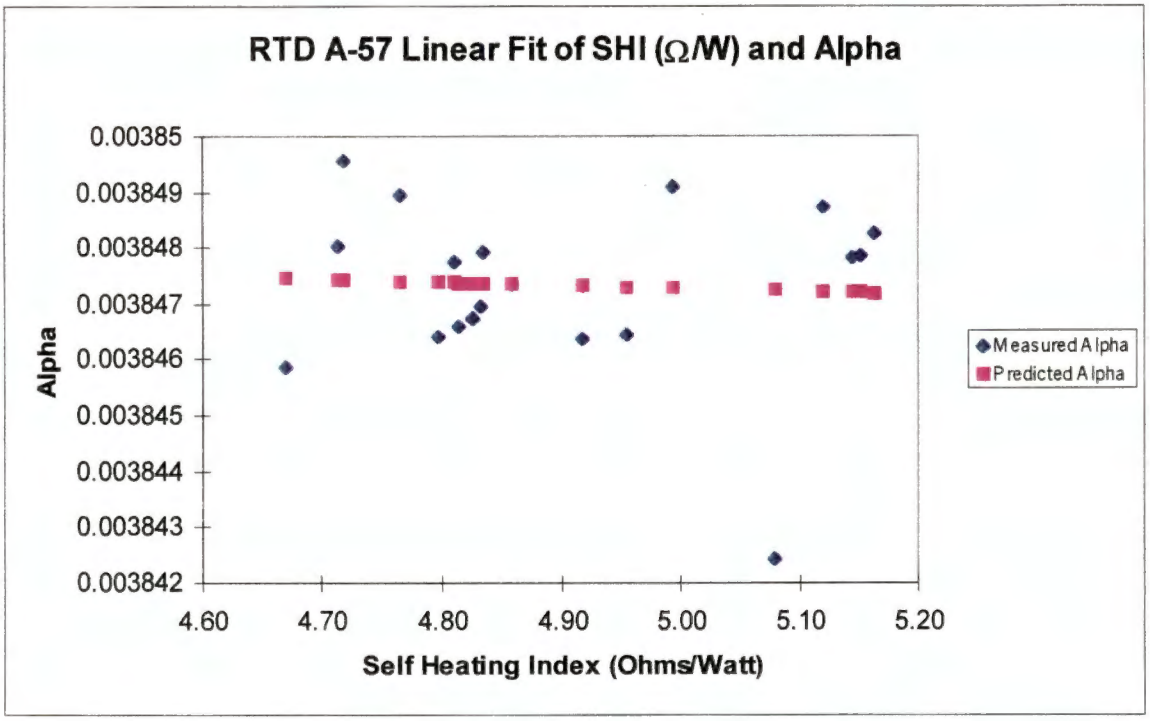


Figure D-3. Self Heating Index (Ω/W) versus Alpha Plot with Fitted Line for RTD A-57

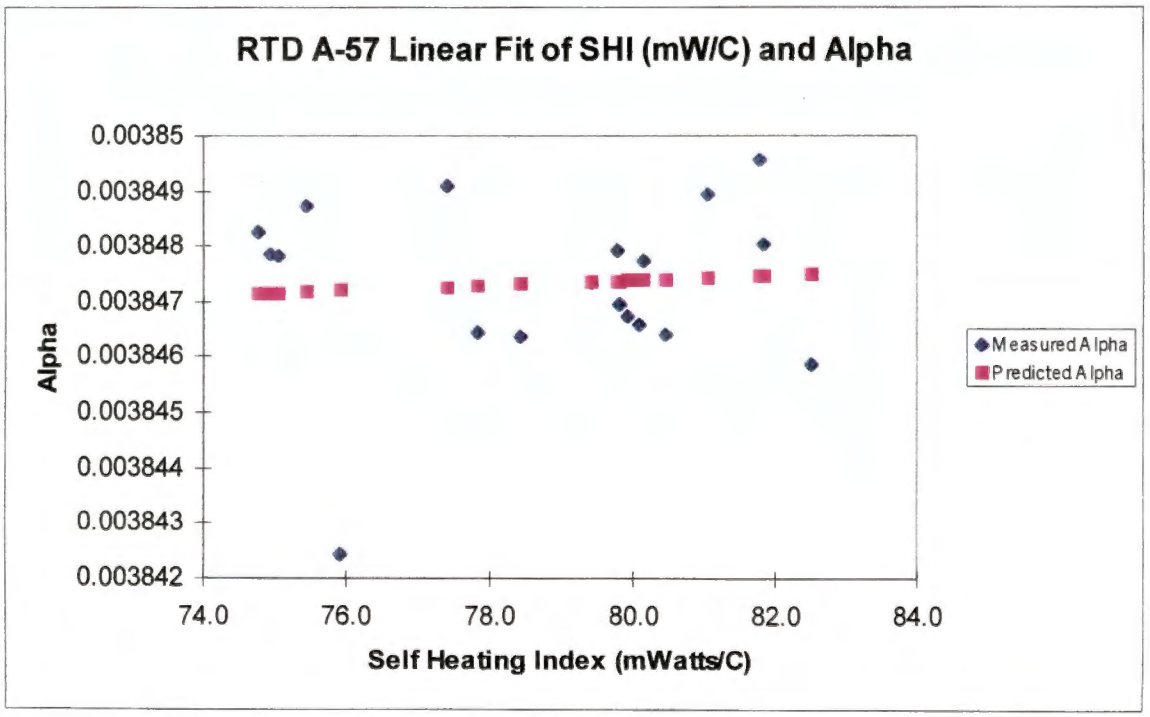


Figure D-4. Self Heating Index (mW/C) versus Alpha Plot with Fitted Line for RTD A-57

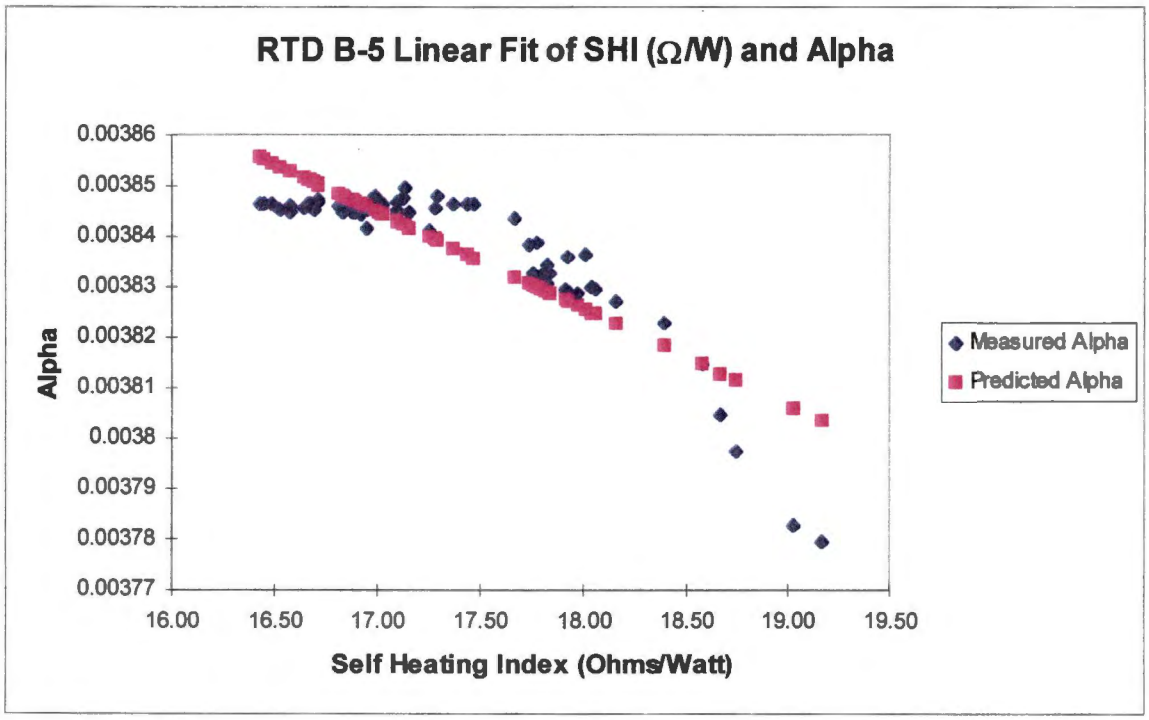


Figure D-5. Self Heating Index (Ω/W) versus Alpha Plot with Fitted Line for RTD B-5

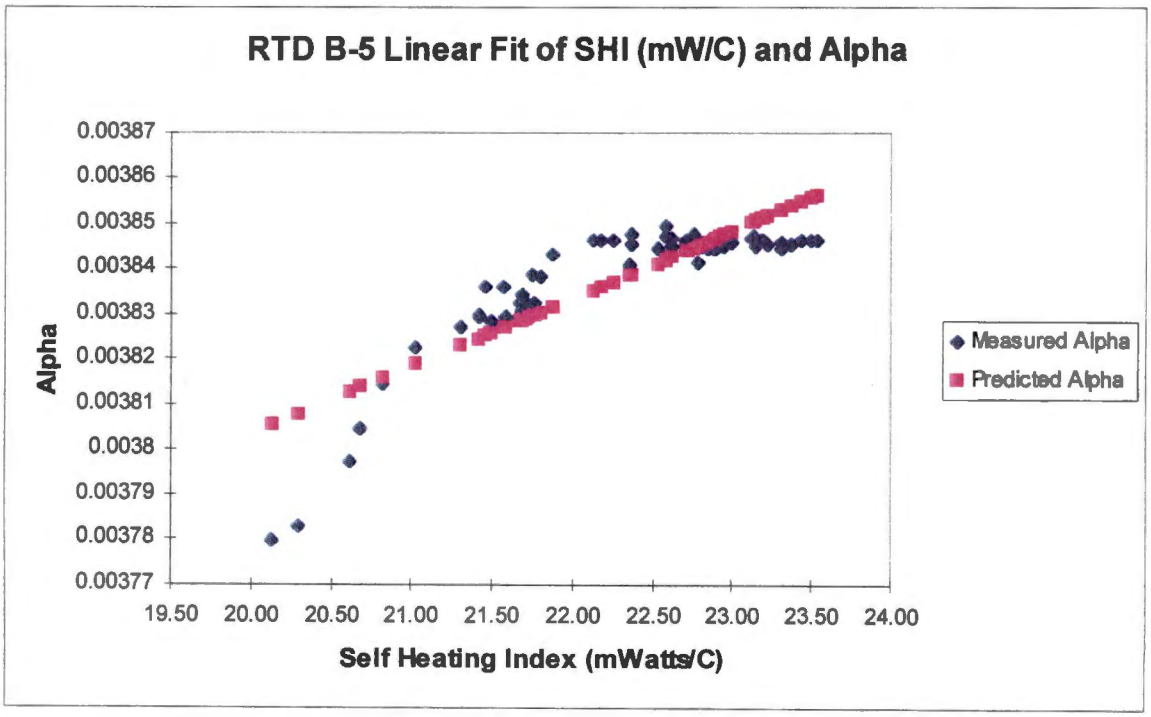


Figure D-6. Self Heating Index (mW/C) versus Alpha Plot with Fitted Line for RTD B-5

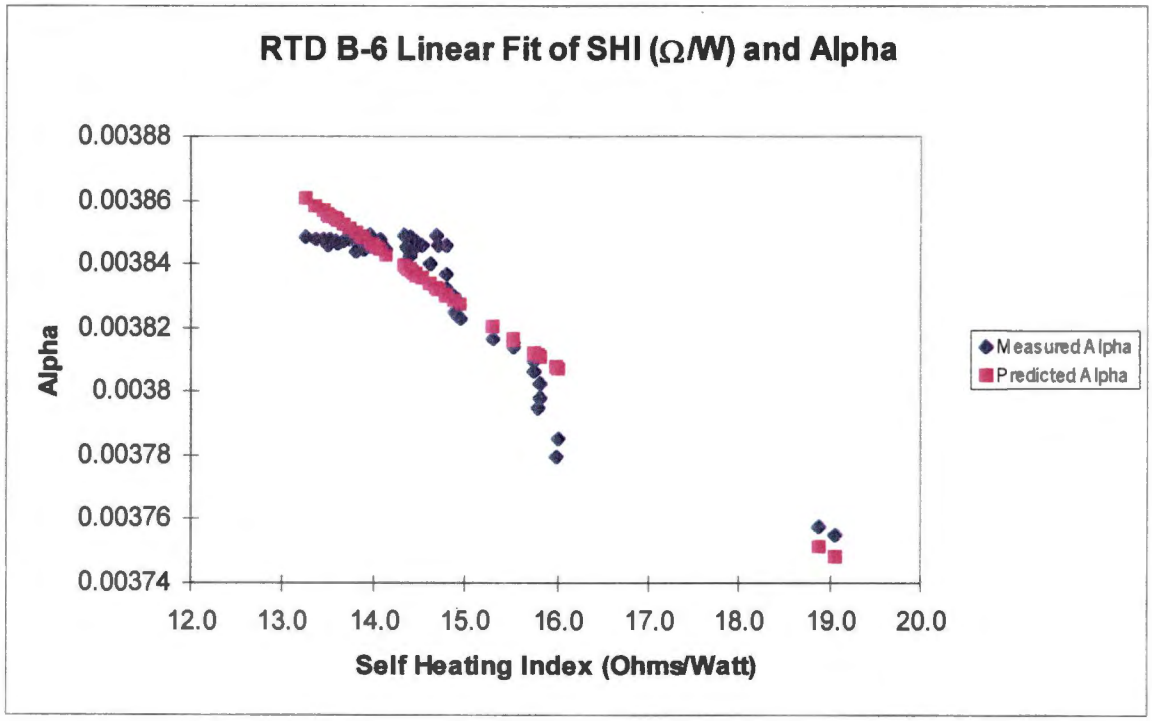


Figure D-7. Self Heating Index (Ω/W) versus Alpha Plot with Fitted Line for RTD B-6

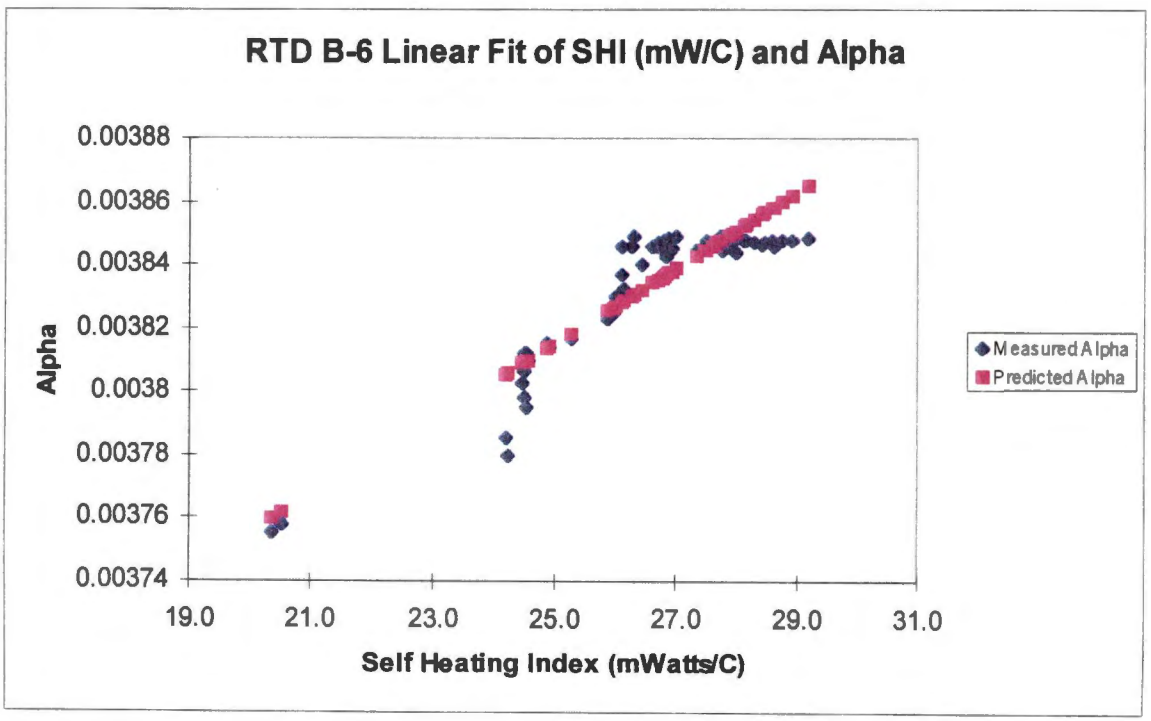


Figure D-8. Self Heating Index (mW/C) versus Alpha Plot with Fitted Line for RTD B-6

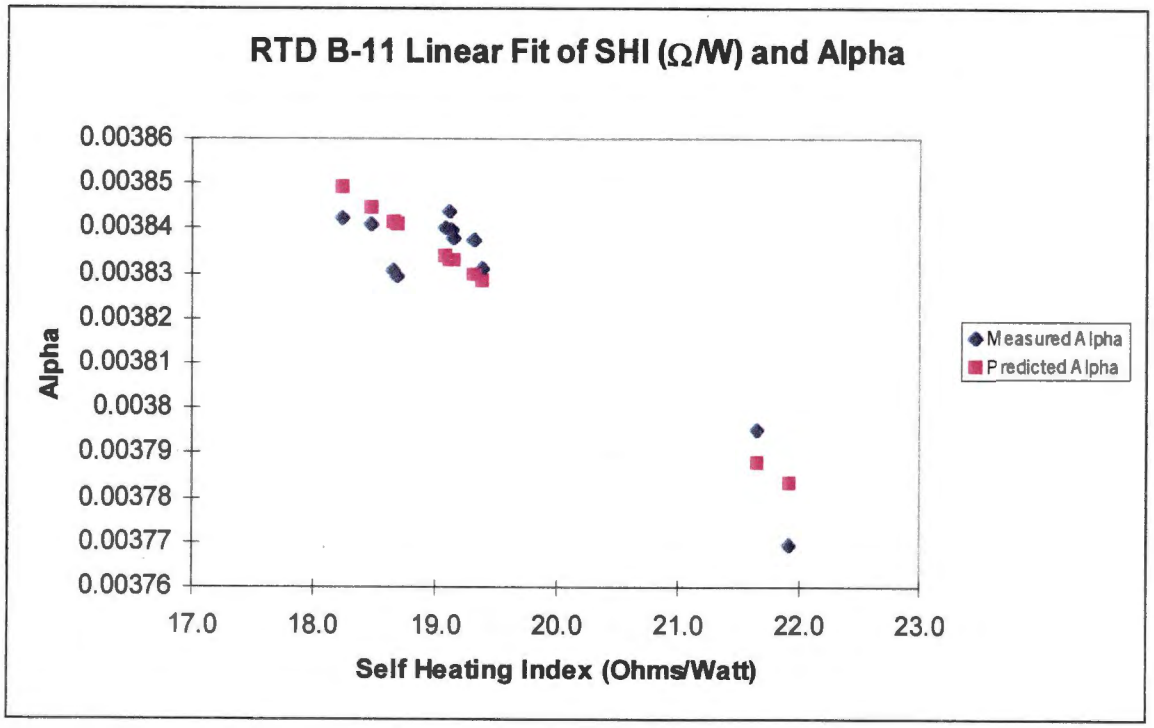


Figure D-9. Self Heating Index (Ω/W) versus Alpha Plot with Fitted Line for RTD B-11

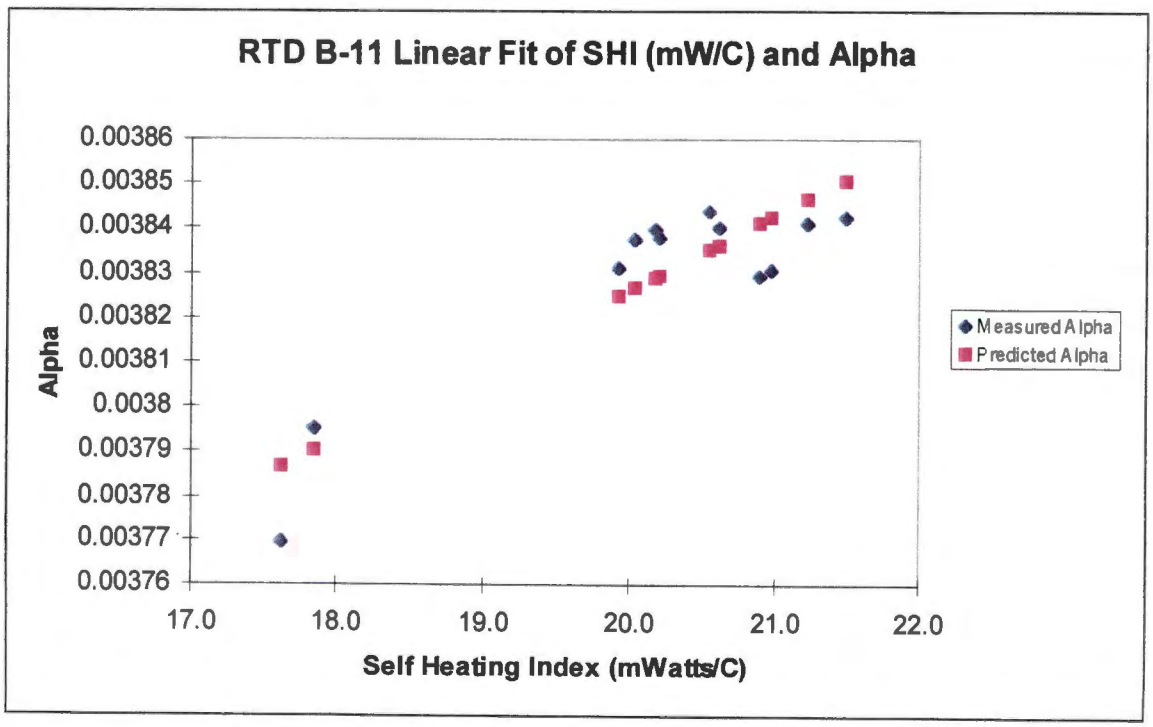


Figure D-10. Self Heating Index (mW/C) versus Alpha Plot with Fitted Line for RTD B-11

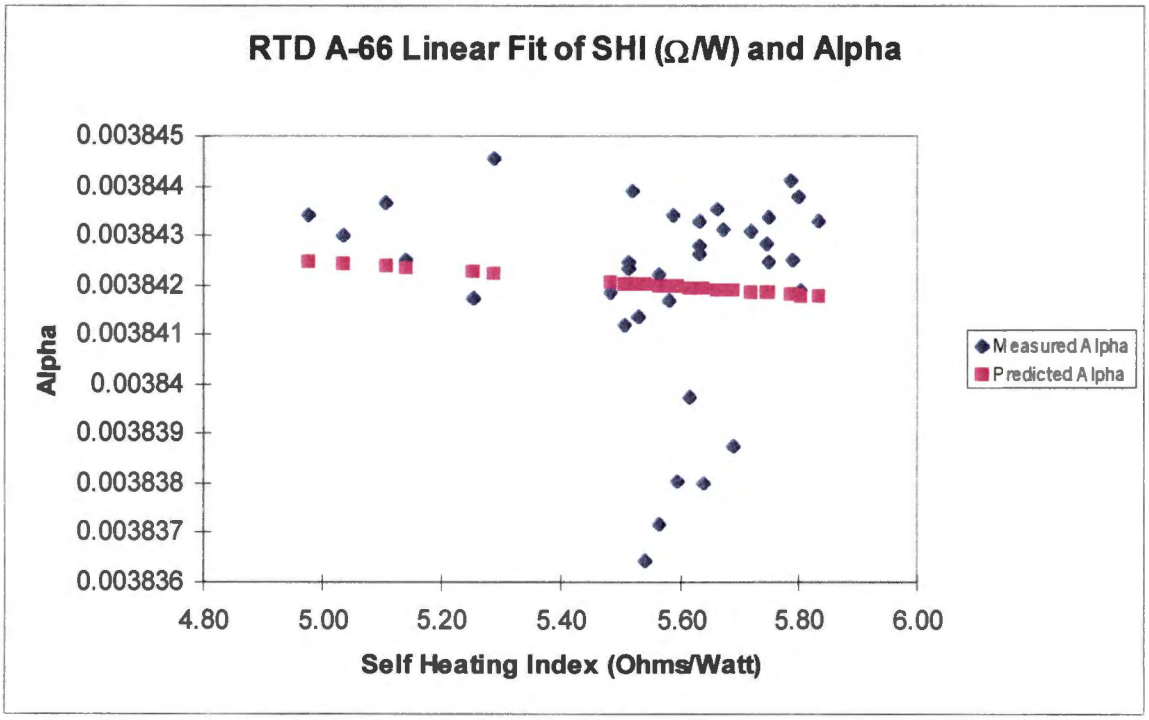


Figure D-11. Self Heating Index (Ω/W) versus Alpha Plot with Fitted Line for RTD A-66

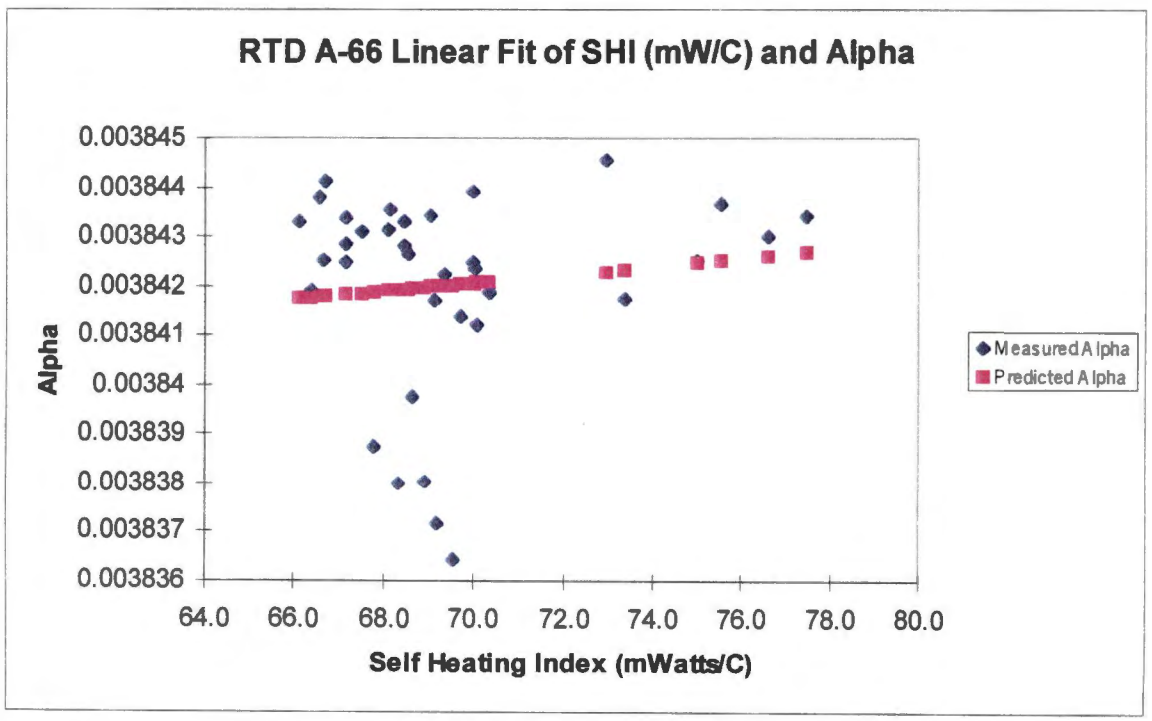


Figure D-12. Self Heating Index (mW/C) versus Alpha Plot with Fitted Line for RTD A-66

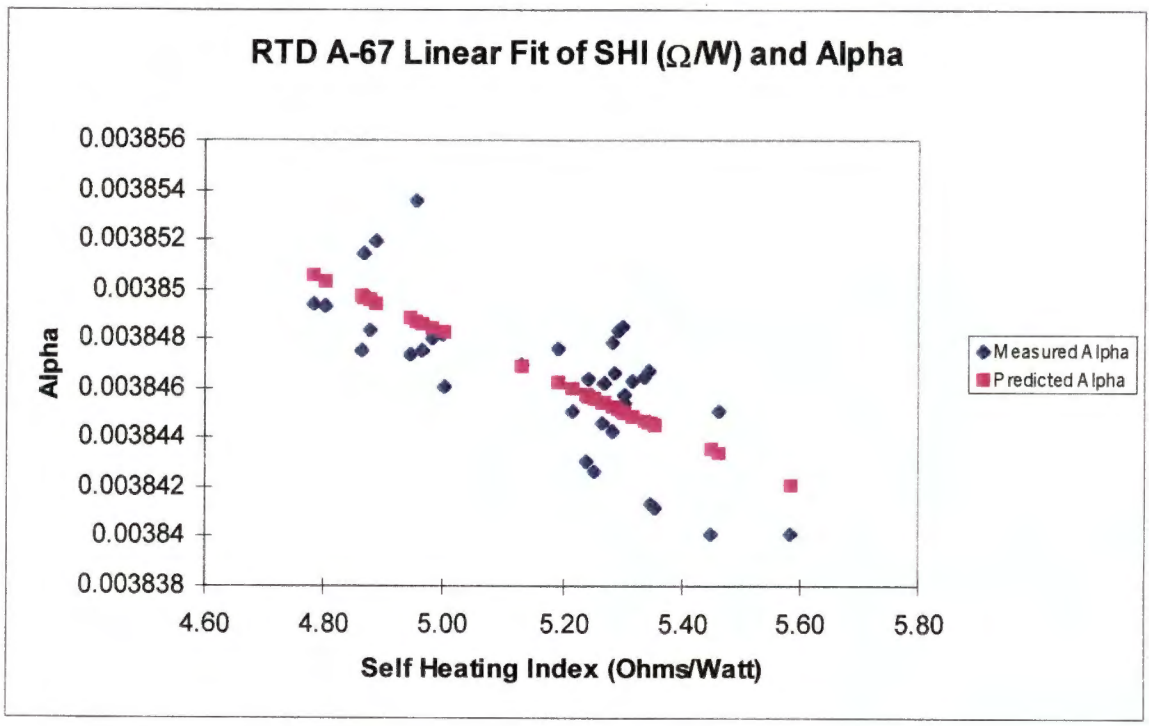


Figure D-13. Self Heating Index (Ω/W) versus Alpha Plot with Fitted Line for RTD A-67

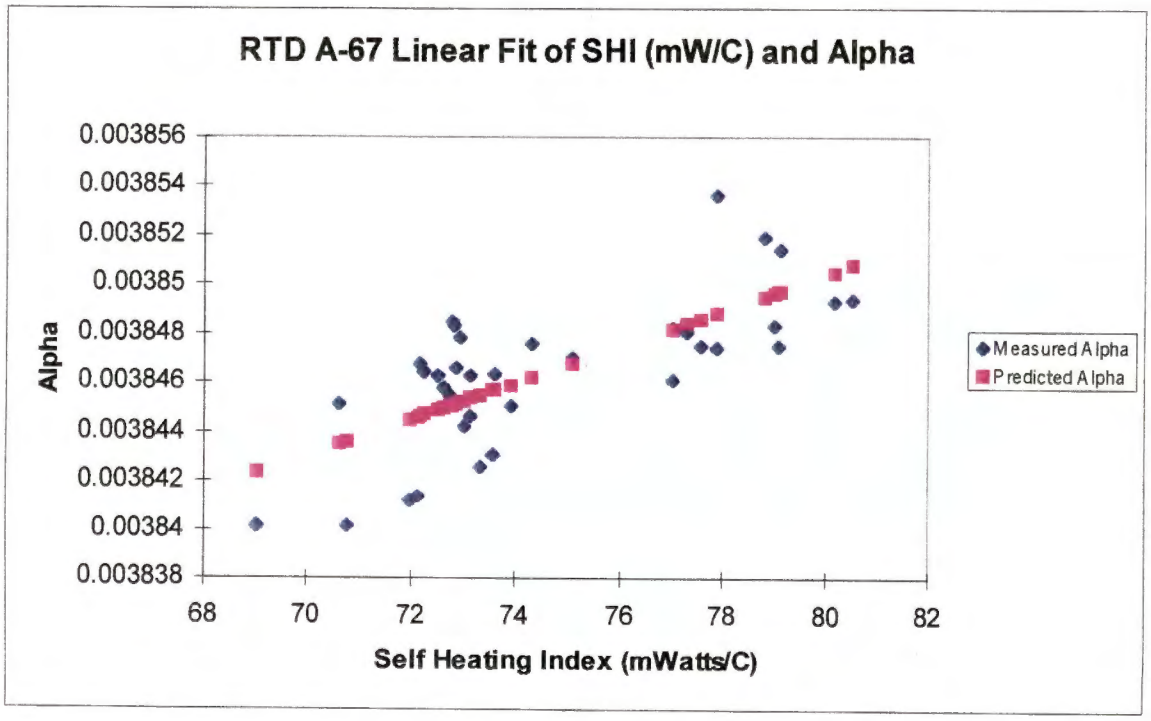


Figure D-14. Self Heating Index (mW/C) versus Alpha Plot with Fitted Line for RTD A-67

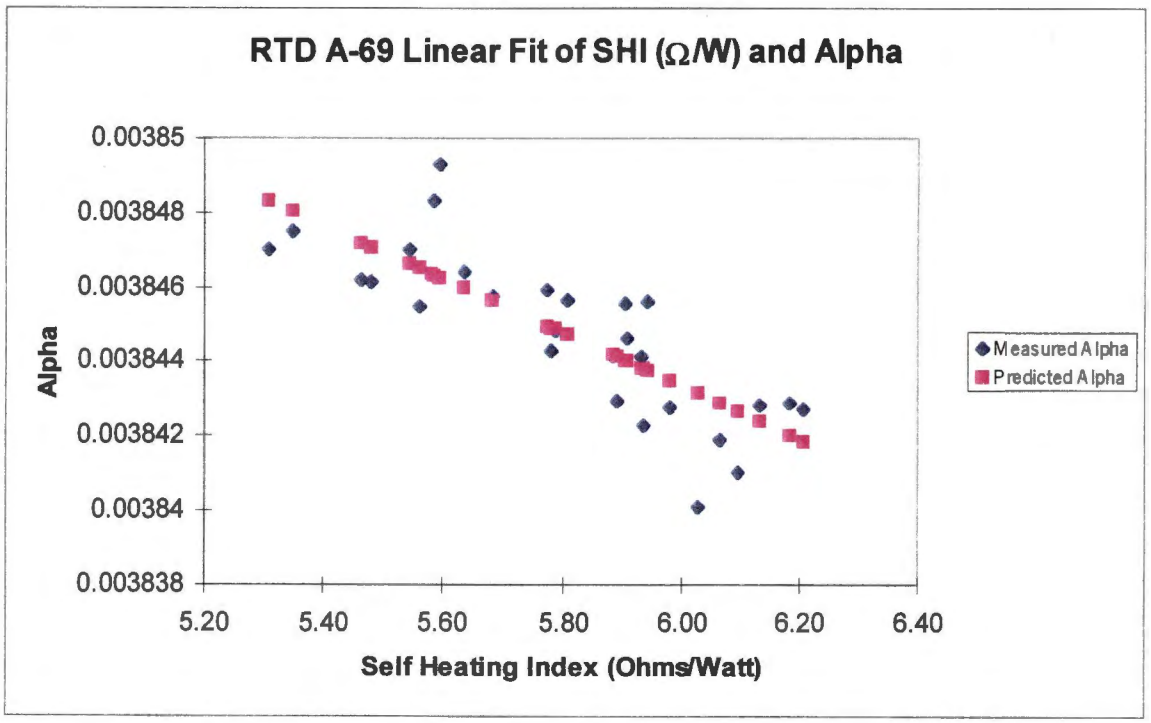


Figure D-15. Self Heating Index (Ω/W) versus Alpha Plot with Fitted Line for RTD A-69

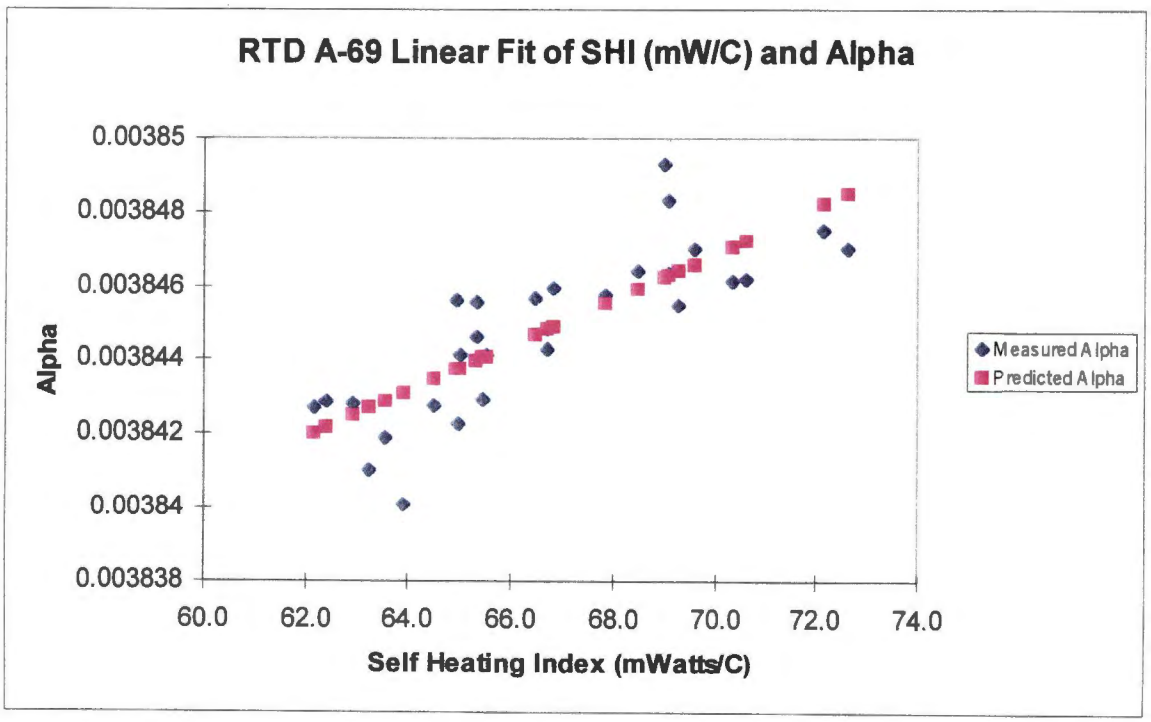


Figure D-16. Self Heating Index (mW/C) versus Alpha Plot with Fitted Line for RTD A-69

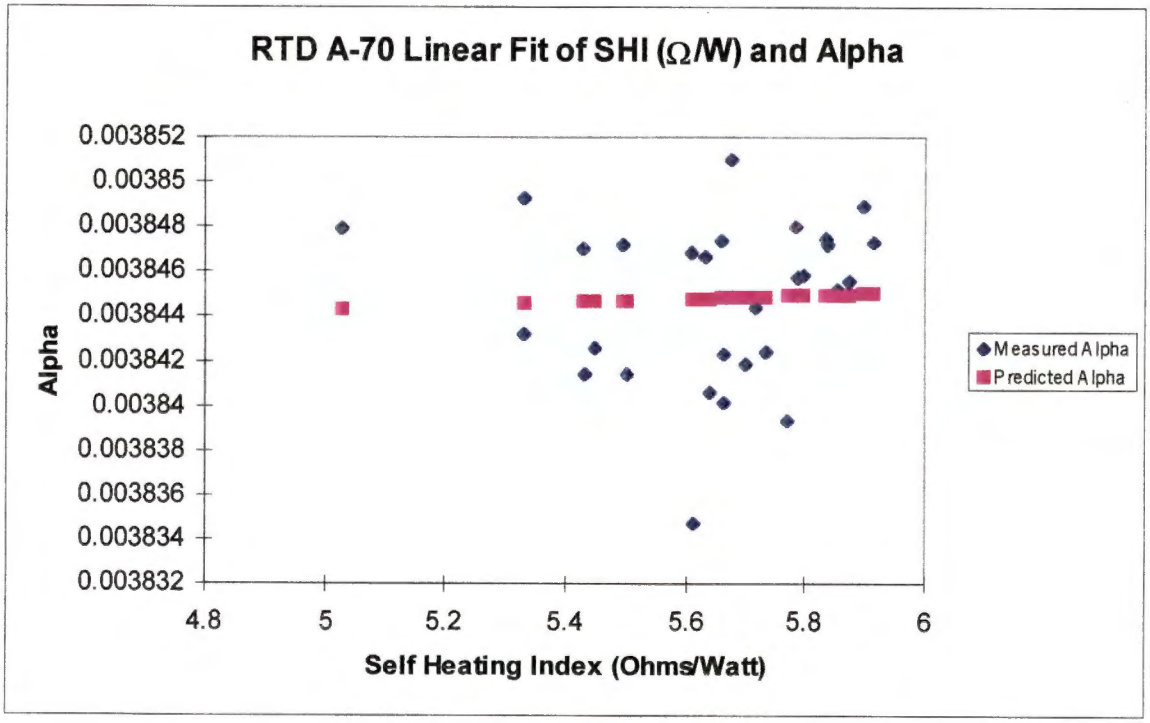


Figure D-17. Self Heating Index (Ω/W) versus Alpha Plot with Fitted Line for RTD A-70

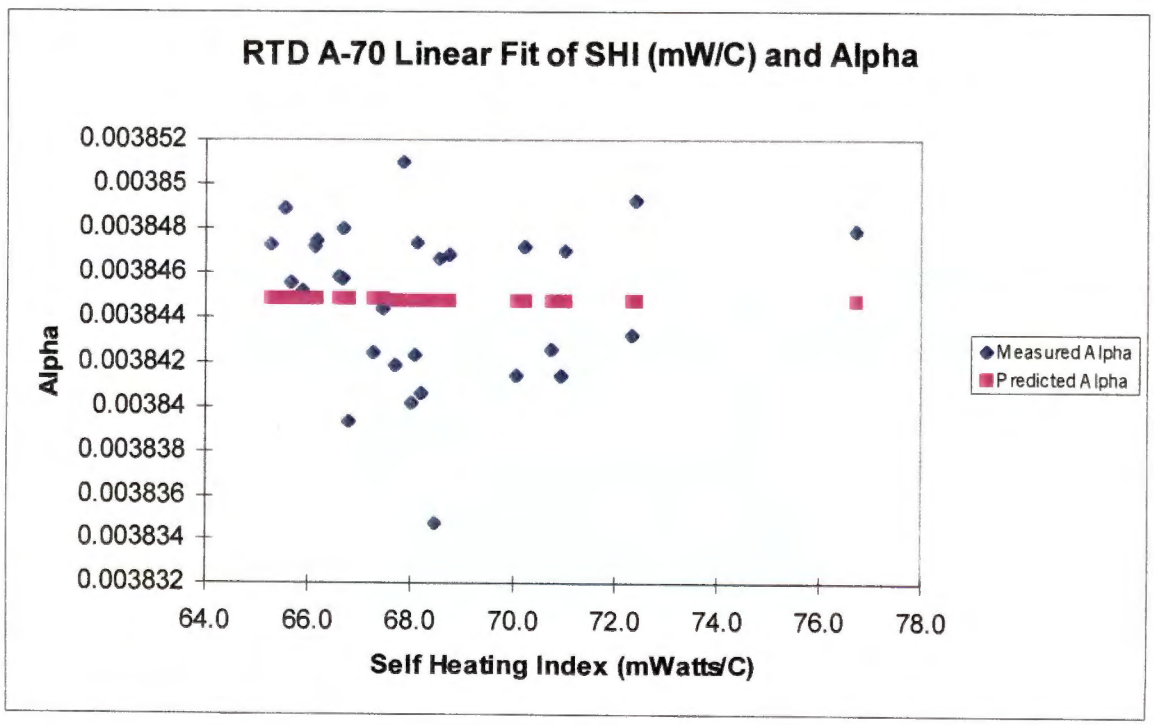


Figure D-18. Self Heating Index (mW/C) versus Alpha Plot with Fitted Line for RTD A-70

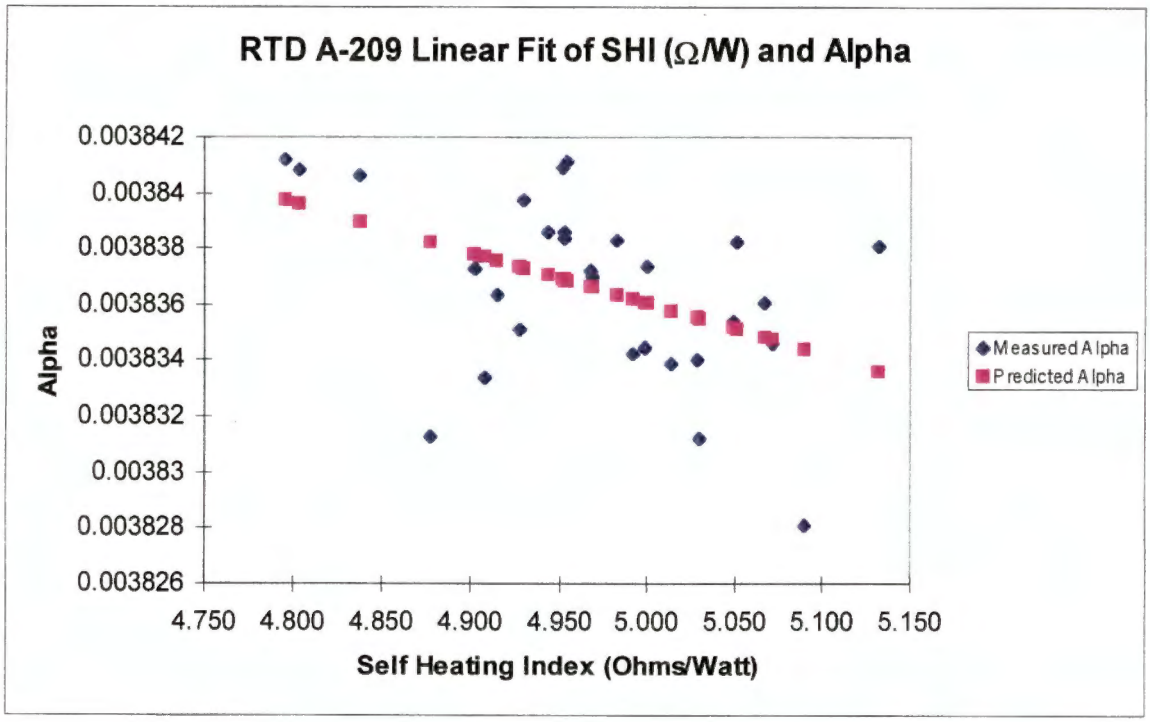


Figure D-19. Self Heating Index (Ω/W) versus Alpha Plot with Fitted Line for RTD A-209

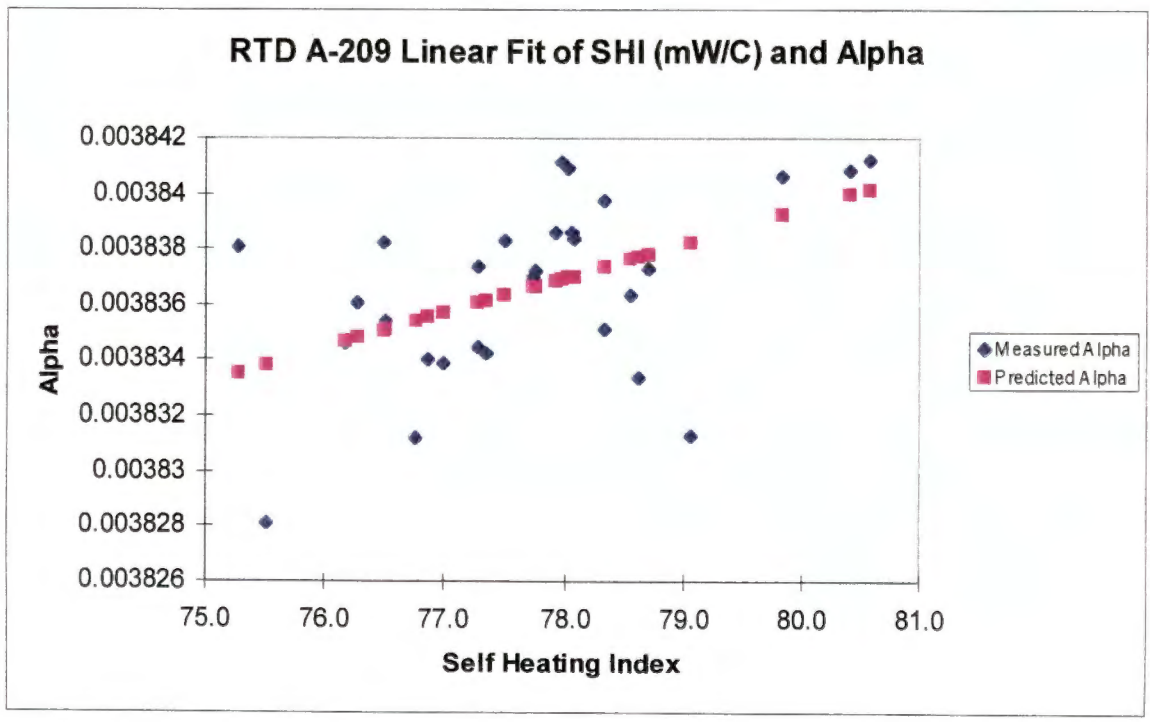


Figure D-20. Self Heating Index (mW/C) versus Alpha Plot with Fitted Line for RTD A-209

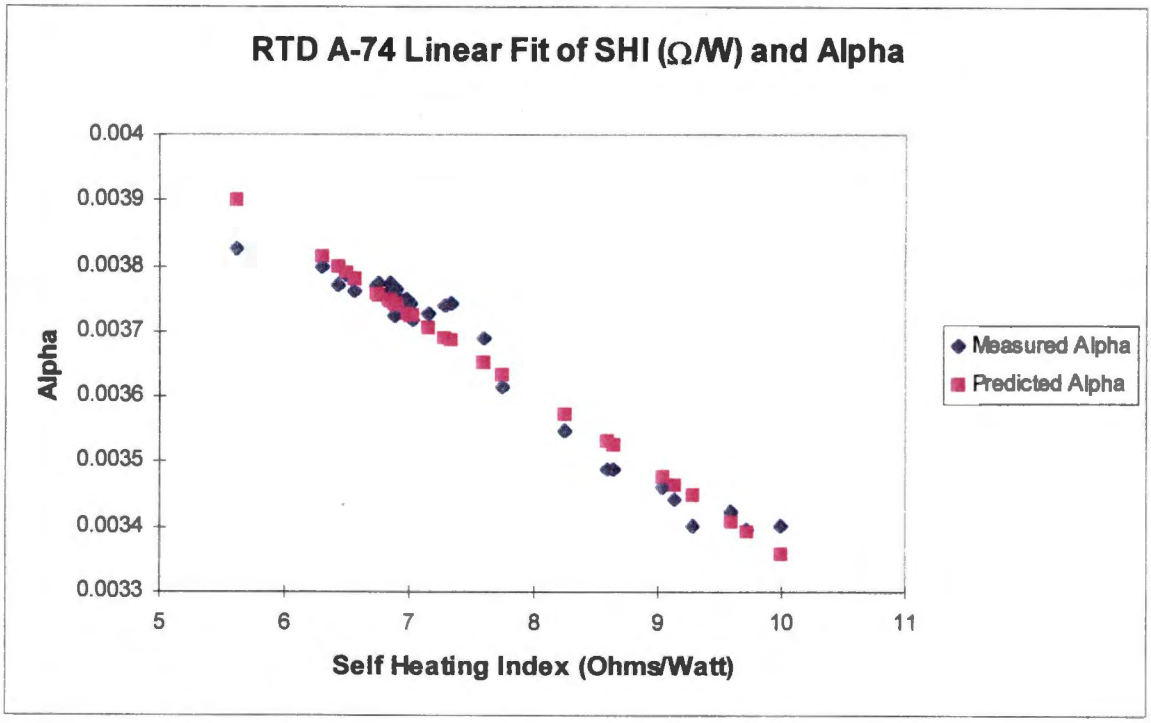


Figure D-21. Self Heating Index (Ω/W) versus Alpha Plot with Fitted Line for RTD A-74

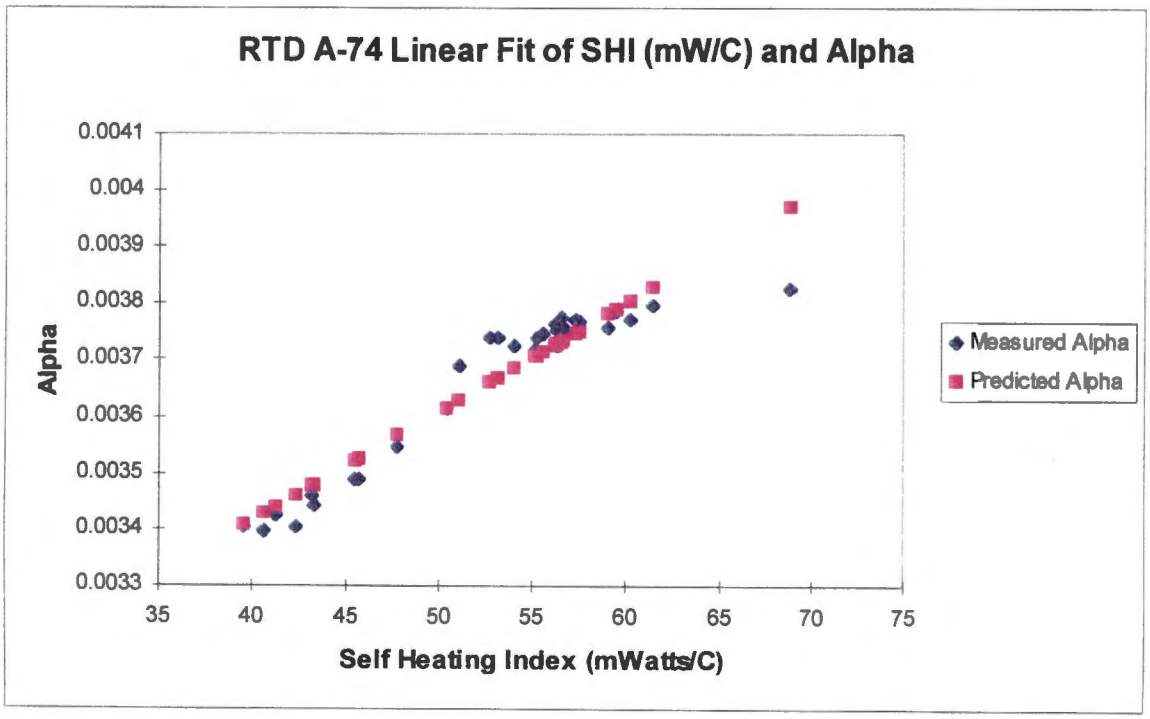


Figure D-22. Self Heating Index (mW/C) versus Alpha Plot with Fitted Line for RTD A-74

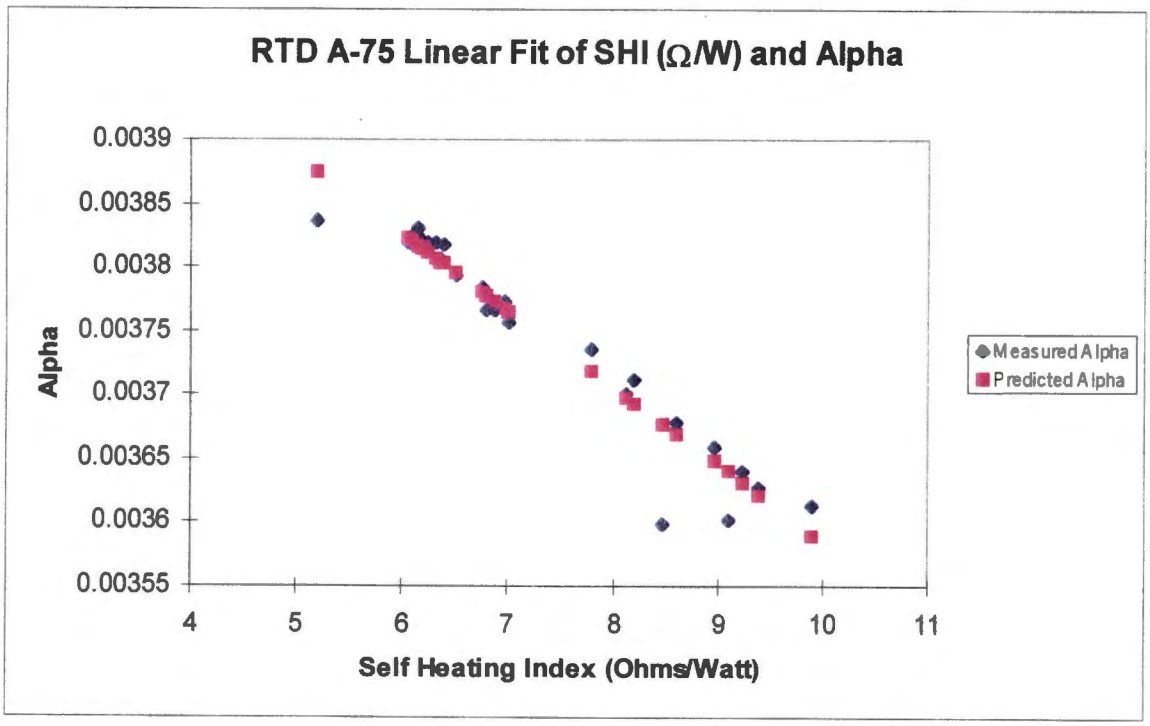


Figure D-23. Self Heating Index (Ω/W) versus Alpha Plot with Fitted Line for RTD A-75

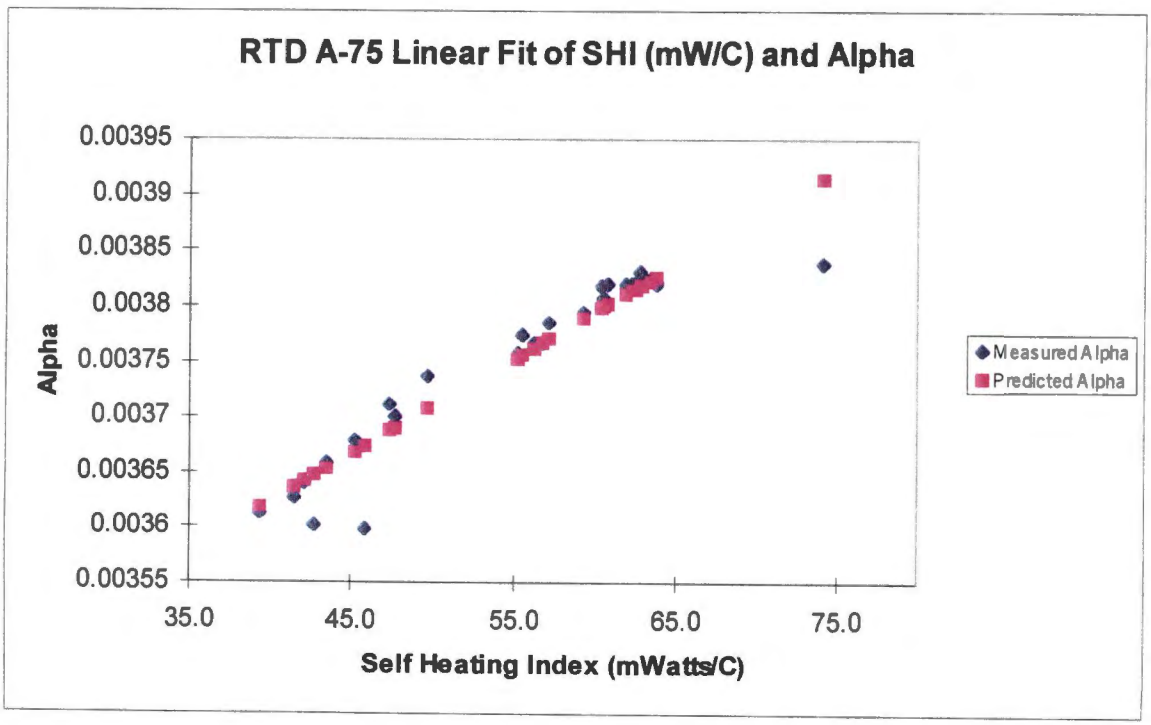


Figure D-24. Self Heating Index (mW/C) versus Alpha Plot with Fitted Line for RTD A-75

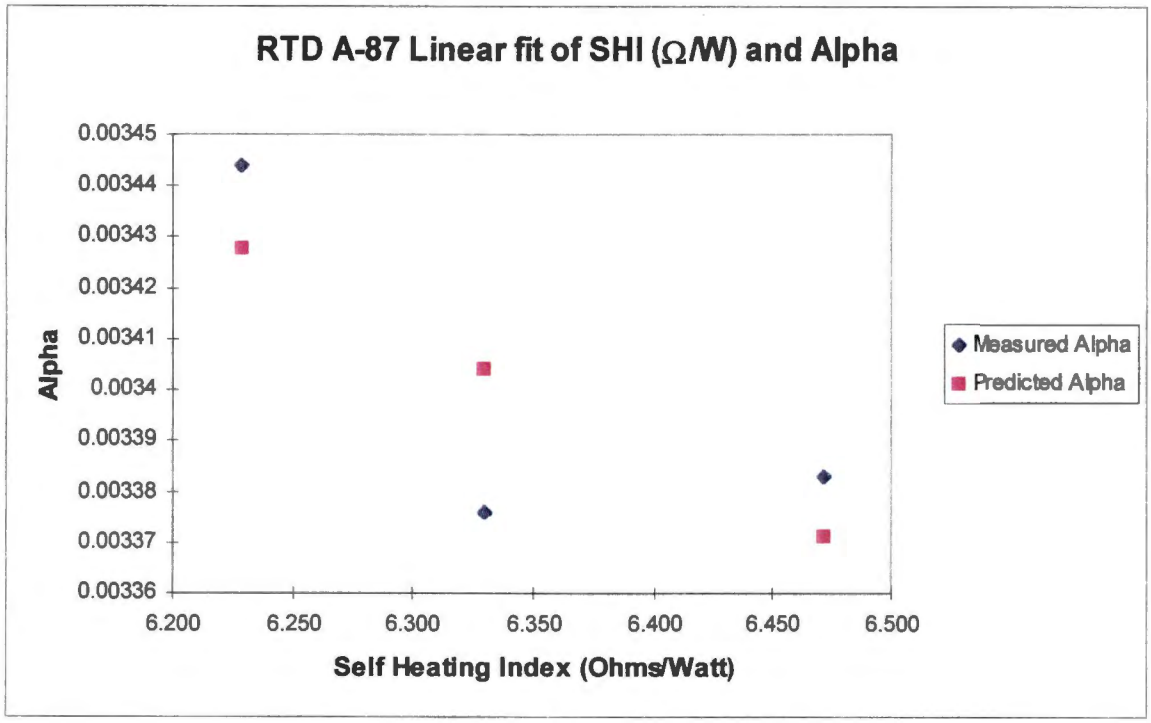


Figure D-25. Self Heating Index (Ω/W) versus Alpha Plot with Fitted Line for RTD A-87

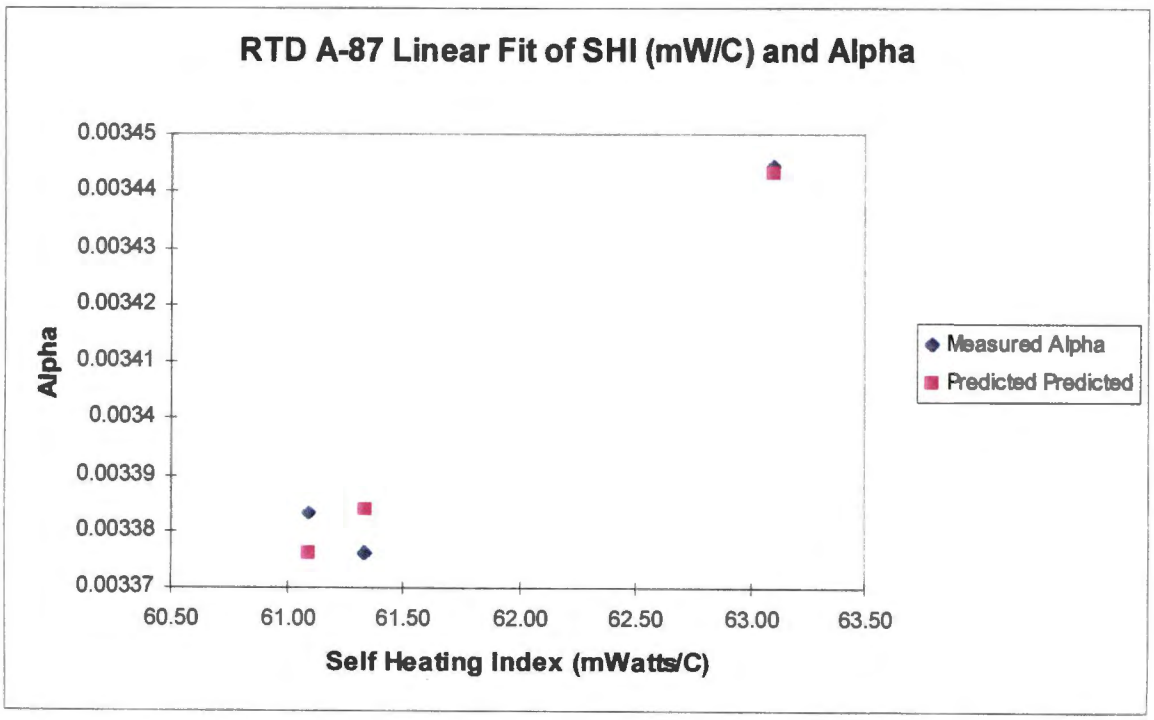


Figure D-26. Self Heating Index (mW/C) versus Alpha Plot with Fitted Line for RTD A-87

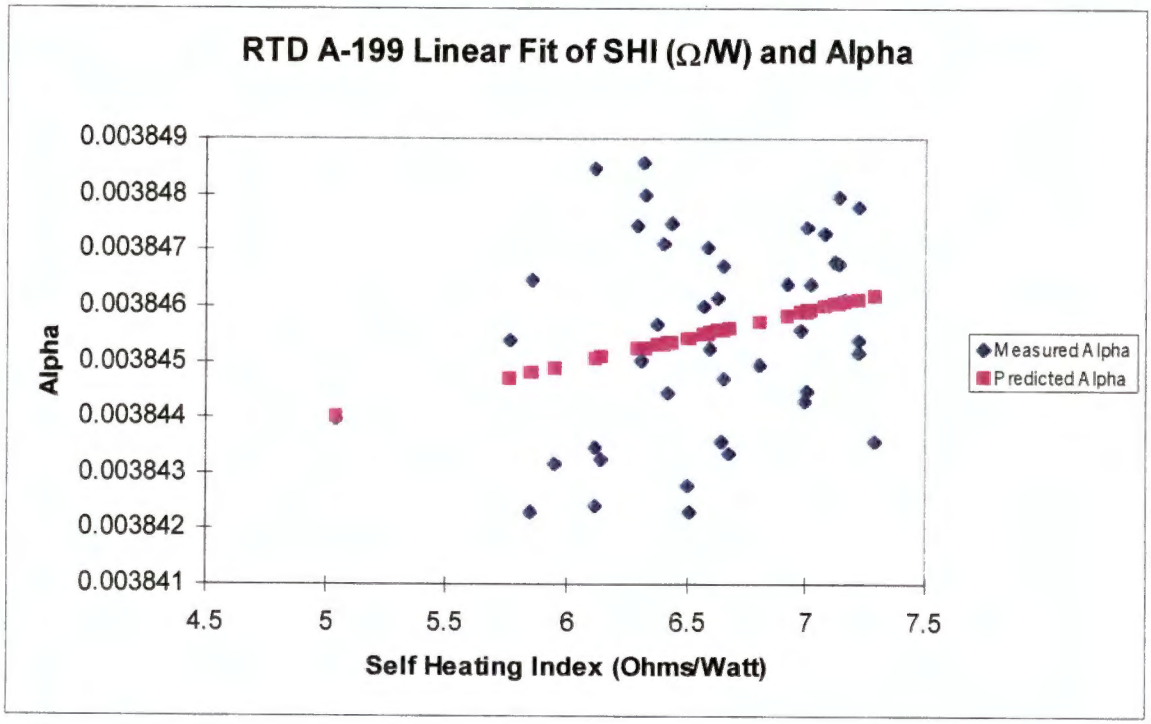


Figure D-27. Self Heating Index (Ω/W) versus Alpha Plot with Fitted Line for RTD A-199

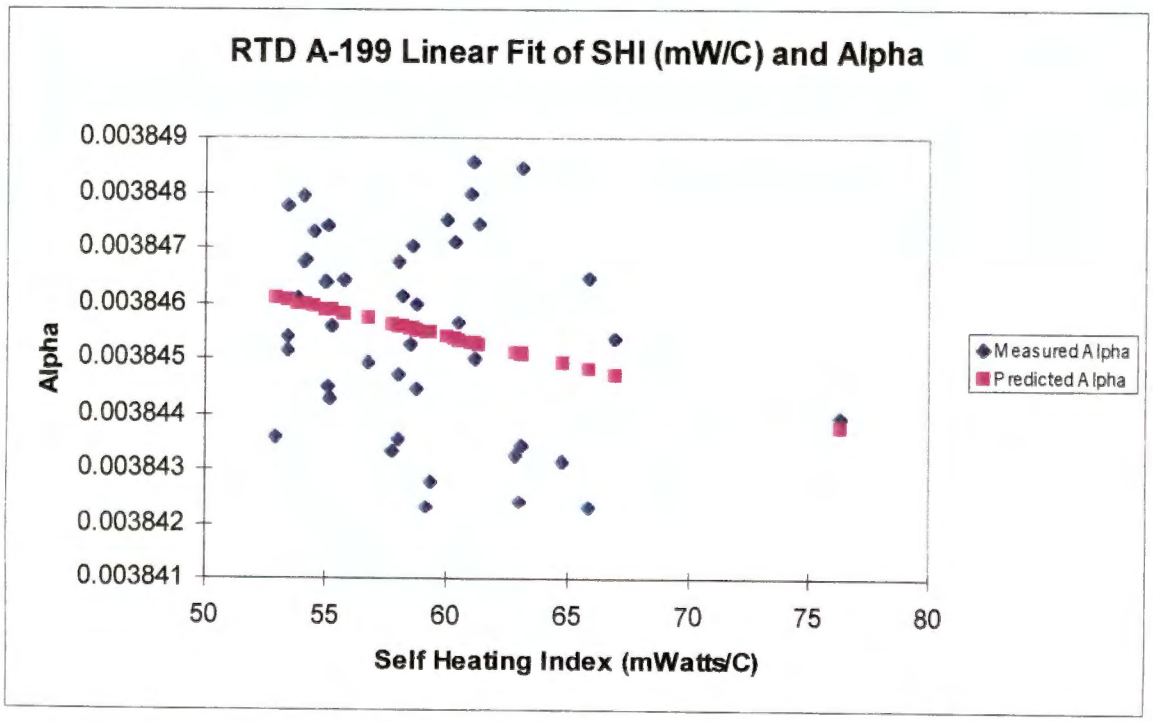


Figure D-28. Self Heating Index (mW/C) versus Alpha Plot with Fitted Line for RTD A-199

VITA

Anne Elizabeth Robinson-Silber grew up in Knoxville Tennessee where she attended Knoxville Central High School and graduated with honors in May of 1992. Upon completion of her high school education, she attended the University of Tennessee Knoxville pursuing a Bachelor's Degree in Nuclear Engineering and completed in May of 1996. Following further with her education she completed coursework and research requirements for a Master's Degree in Nuclear Engineering in December of 1997. At this time she accepted a position in industry with the Tennessee Valley Authority at their Sequoyah Nuclear Power Plant, outside Chattanooga, Tennessee. She is currently a Licensing Engineer at Sequoyah and is living with her husband Brian in Chattanooga. Upon completion of her Master's Thesis in January of 1999 she has completed all of the requirements for her Master's Degree in Nuclear Engineering which will be confirmed in May 1999.